April 2019

The Potential of Marine Microbes, Flora and Fauna in Drug Discovery

Santana Alexa Lavonia Thomas
University of South Florida, tanat1989@gmail.com

The Potential of Marine Fauna, Flora and Microbes in Drug Discovery

by

Santana Alexa Lavonia Thomas

A dissertation submitted in partial fulfillment
of the requirements for the degree of
Doctor of Philosophy in Chemistry
Department of Chemistry
College of Arts & Sciences
University of South Florida

Major Professor: Bill J. Baker, Ph. D.
Juan Del Valle, Ph. D.
Lindsey Shaw, Ph. D.
X. Michael Shi, Ph. D.

Date of Approval:
March 27, 2019

Keywords: Endophytic fungi, epigenetics, keikipukalide, bathyptilone, enbepenone, scotianone, Ntera-2, octocoral, Antarctica

DEDICATION

This dissertation is dedicated to the phenomenal women responsible for the individual I am today. To Mammy, you are the epitome of a strong woman and for this I will always have you as an exemplary woman to follow. To Mommy, words cannot express how much I appreciate your love and endeavoring support throughout this journey and my entire life. I value the contributions both of you made to my life and with this small token I would like to say thank you.

"Here's to strong women.
May we know them.
May we be them.
May we raise them."

- Unknown

ACKNOWLEDGEMENTS

In life we encounter fear and doubt for numerous reasons and sometimes it requires another person to shed light on the potential we possess to overcome and succeed. This beacon of light came in the form of my mentor, Father Cioffi. Father Cioffi, it would be impossible to count the many ways you have contributed to my educational journey and life itself. Thank you for your inspiring me to pursue my full potential. Dr. Bill Baker, I cannot thank you enough for your mentorship and the continuous support of my PhD. journey over the past four years. I am grateful that I had the opportunity to be under your guidance. Thank you for being patient with me as I developed throughout this journey.

I extend my sincerest gratitude to my lab mates during my PhD journey. Silvia and Ally words would not suffice how much I appreciate your support. Thank you for always offering words of encouragement and advice in time of need. They were always timely and made a significant impact in my studies. Thank you for being my awesome friends and scientists. Matt, one of the best story-teller, thank you for the well-illustrated stories that brightened my days. Thank you for words of advice and your encouragement. Nicole, I cannot express how grateful I am to experience your selflessness and kind heart towards me or anyone you encounter. You are a ray of sunshine and I hope that you continue to light up the world. You are an amazing scientist and an awesome woman. Thank you for always going over and beyond even its lending me your own mom (Barb). To all the

members of the Baker lab, I am grateful to have shared space with all of you. Thank you for the encouragement when hope didn't seem to exist. Thanks for the therapeutic walks and sharing in the long rants about science and the stresses of graduate school.

Victoria D., Victoria M. and Nikki thank you for trusting my guidance and mentorship. It was a privilege to witness the potential each one of you is exhibited, I am proud of the dedication and determination that you each portrayed. You made my journey easier and for that I would like to extend my gratitude.

To my committee members, Dr. Del Valle, Dr. Shi, Dr. Shaw and Dr. Teng, thank you for your advisement and assistance during this PhD journey.

I am extremely grateful to my support group especially my friends I have met along the way. They have unknowingly inspired me to always put forth my best. They are always in celebratory mode for any milestone I have accomplished. Thank you Lynelle, Lynette and Antonique for being my emotional supporters and biggest cheerleaders. Thank you Lateasha for always reminding me to persevere through all obstacles.

Finally, I would like to extend my gratitude to my family, especially my aunts and uncles for always being there when I am in need. Your text messages, calls and visits are always appreciated.

"Don't be afraid. Be focused. Be determined. Be hopeful. Be empowered."
-Michelle Obama

TABLE OF CONTENTS

LIST OF TABLES

LIST OF FIGURES

LIST OF SCHEMES

LIST OF ABBREVIATIONS

%	out of 100
$[\alpha]^{25}_{D}$	optical rotation at 25 degrees Celsius using a Sodium lamp
°	degree
^{13}C	Carbon-13
1D	one dimensional
^{1}H	Hydrogen-1
2D	two-dimensional
3D	three-dimensional
A549	adenocarcinomic human alveolar epithelial cells
acetyl CoA	acetyl coenzyme A
$AgNO_3$	Silver Nitrate
AgOAc	Silver Acetate
Ara-C	cytosine arabinoside
Br	Bromine
br s	broad singlet
C	Carbon
CCl_4	carbon tetrachloride
$CDCl_3$	deuterated chloroform
CH	methine
CH_2	methylene
CH_2Cl_2	methylene dichloride
CH_3	methyl
COSY	Correlated Spectroscopy
D-Ala	D-alanyl-D-alanine
DBU	1,8-Diazabicyclo [5.4.0] undec-7-ene
dd	doublet of doublets
ddd	doublet of doublet of doublets
DEPT	distortionless enhancement of polarization transfer
DHA	dihydroartemisinin
DNA	deoxyribonucleic acid
DNMT	deoxyribonucleic acid methyl transferase
DNMTi	deoxyribonucleic acid methyl transferase inhibitors
E	entgegen (opposite)
EIMS	electron ionization mass spectrometry
ESIMS	electrospray ionization mass spectrometry

ESKAPE	*Enterococcus faecium, Staphylococcus aureus, Klebsiella pneumoniae, Acinetobacter baumannii, Pseudomonas aeruginosa, Enterobacter* species
EtOAc	ethyl acetate
g	grams
gHSQCAD	heteronuclear single quantum coherence using pulsed-field gradients with adiabatic coupling
H	Hydrogen
H+/K+ ATPase	Hydrogen potassium adenosine triphosphatase
H_2	methylene
H_2O	water
H_3	methyl
HAT	histone acetyl transferase
HDAC	histone deacetyltransferase
HeLa	Henrietta Lacks cervical cancer cell lines
HMBC	Heteronuclear Multiple Bond Correlation
HMQC	Heteronuclear Multiple Quantum Correlation
HOAc	Acetic acid
HPLC	High Performance Liquid Chromatography
Hsp90	Heat Shock Protein 90
hv	high voltage
Hz	Hertz
IC_{50}	Concentration at 50% inhibition
LC/MS	Liquid chromatography mass spectrometry
m	multiplet
MeOH	methanol
mg	milligrams
MHz	Megahertz
MiaPaca-2	human pancreatic cancer cell line
mL	milliliters
MM2	
MPLC	medium pressure liquid chromatography
MRSA	methicillin-resistant *Staphylococcus aureus*
MS/MS	Tandem mass spectrometry
mTOR	mechanistic target of rapamycin
n	unbranched or linear
Na+/K+ ATPase	sodium potassium adenosine triphosphatase
ng	nanogram
NMBS	
NMR	nuclear magnetic resonance
NOESY	nuclear overhauser effect spectroscopy
NP	normal phase
NT2	Ntera-2

O	oxygen
P_2O_5	Phosphorus pentoxide
PKC	protein kinase C
pyridine-d5	deuterated pyridine
q	quartet
R	rectus (right)
R/V	Research vessel
RNA	Ribonucleic Acid
ROV	remotely operated vehicle
RP	reversed phase
RSA	regulator of spindle assembly
s	singlet
S	sinister (left)
SCUBA	self-contained underwater breathing apparatus
SDA	sabouraud dextrose agar
sp.	species (singular)
sp^2	a sigma and 2 pi orbitals hybrid
sp^3	a sigma and 3 pi orbitals hybrid
spp.	species (plural)
t	triplet
td	triplet of doublets
THF	tetrahydrofuran
U2OS	osteosarcoma
Z	zusammen (together)
δ	change in position (organic structures and NMR)
δ_C	Carbon NMR shifts
δ_H	Proton NMR shifts
µg	micrograms
µM	micromolar

Abstract

Natural products are chemical compounds synthesized by a living organism. These compounds have been utilized by humans from ancient times to the present for their pharmacological and biological activities. Terrestrial organisms are considered a lucrative source of bioactive compounds and chemical diversity. Within the past 60 years, the marine environment has presented its potential as a validated source for structural diversity and biologically active compounds. Technology has given access from shallow waters down to the abyssal plane for exploration and investigation of the inhabitants. Marine organisms have displayed their benefits in the pharmaceutical industry with the approval of several marine-derived drugs active against various diseases.

This dissertation presents the potential of marine microbes, flora, and fauna specifically fungal endophytes, red alga and corals in drug discovery. Chapter 2 describes the isolation of secondary metabolites from endophytic fungi by manipulation of their epigenome. As a continuation of a screening project, prioritization of the extracts of the fungal endophytes was necessary for further chemical investigation based on the significant biological activity against two free-living amoebas; *Naegleria fowleri* and *Acanthamoeba* sp. Bioassay-guided isolation and mass-directed fractionation were the two methods utilized in the isolation of compounds — several known mycotoxins isolated with known biological activities against the amoeba. With repetition of isolating known compounds, mass-directed fractionation facilitated the pursuit of new compounds from

bioactive extracts. A new compound was successfully isolated and is currently awaiting biological activity against *N. fowleri*. Chapter 3 demonstrates the ecological importance of secondary metabolites from the Antarctic red alga, *Delisea pulchra.* A suite of polyhalogenated polyketides was isolated and described. Five of the metabolites were previously described in the literature isolated from *Delisea* sp. and a new natural product isolated, previously reported as a synthetic precursor. The activity of these natural products as antibiotics is due to the structural similarities of a bacterial enzyme inhibitor. In Chapter 4, Antarctic corals collected from depths starting deeper than 800 m. The first coral described, afforded seven new and known diterpenes in which their structure elucidation is detailed. Varying biological activity against the parasite *Leishmania donovani* was found from these furanocembranes. Another suite of diterpenes was isolated from a second Antarctic coral *Anthoptilum* sp. These compounds are structurally related to briarane diterpenes with modifications leading to three new compounds. The fourth compound isolated presented a newly reported scaffold. These compounds tested against several biological targets; discovering one of the diterpenes significantly active against an induced neuronal cell assay called Ntera-2. A third coral was chemically investigated producing two halogenated sesquiterpenes. The structures were elucidated using one- and two- dimensional NMR analysis, HRESIMS, and x-ray crystallography. This scaffold is common in terrestrial sources as well as another marine source. These compounds were tested against various disease targets in which one of the compounds were discovered to be moderately active against the bacterium *Mycobacterium tuberculosis*. This dissertation demonstrates the pharmaceutical potential of natural products from marine organisms.

CHAPTER ONE:

THE ESSENCE OF NATURAL PRODUCTS

1.1 Introduction to natural products

1.1.1 Defining natural products

All living organisms, producers and consumers, require energy for metabolic processes needed to synthesize metabolites. These organic compounds called metabolites are vital for various cellular functions. The “building blocks of nature” is a term often used to describe primary metabolites comprised of carbohydrates, lipids, proteins, and nucleic acids necessary for growth, survival, and reproduction. Secondary metabolites are end products of biological pathways derived from the primary building blocks.[1] Secondary metabolites, also called natural products, are not essential for the survival of the organism but have specialized ecological functions. All living organisms produce natural products, but they are specific to an organism’s ecological demands. Natural products allow organisms to avoid predation; compete for nutrients and space; and confer protection against infection.[2,3] Without natural products, the organism would not have the ability to persist in a competitive environment.

1.1.2 Metabolic Pathways Leading to Natural Products

Biosynthetic (metabolic) pathways lead to multiple classes of natural products. These pathways are extension of the primary metabolic process called photosynthesis or glycogenesis. Photosynthesis provides four metabolic intermediates: erythrose-4-phosphate, phosphoenolpyruvate, pyruvate, and 3-phosphoglycerate.[4] Each of the intermediates rely on a cascade of specific enzymes under tight regulation to establish a metabolic pathway. Figure 1.1 displays a scheme of the principle biosynthetic pathways which leads to the formation of natural products.[5] Carbon dioxide and nitrogen molecules are manipulated by specialized enzymes – unique to each organism – to create diverse classes of natural products.[5] Polyketides, terpenes, nonribosomal peptides and alkaloids are some of the core classes of natural products.

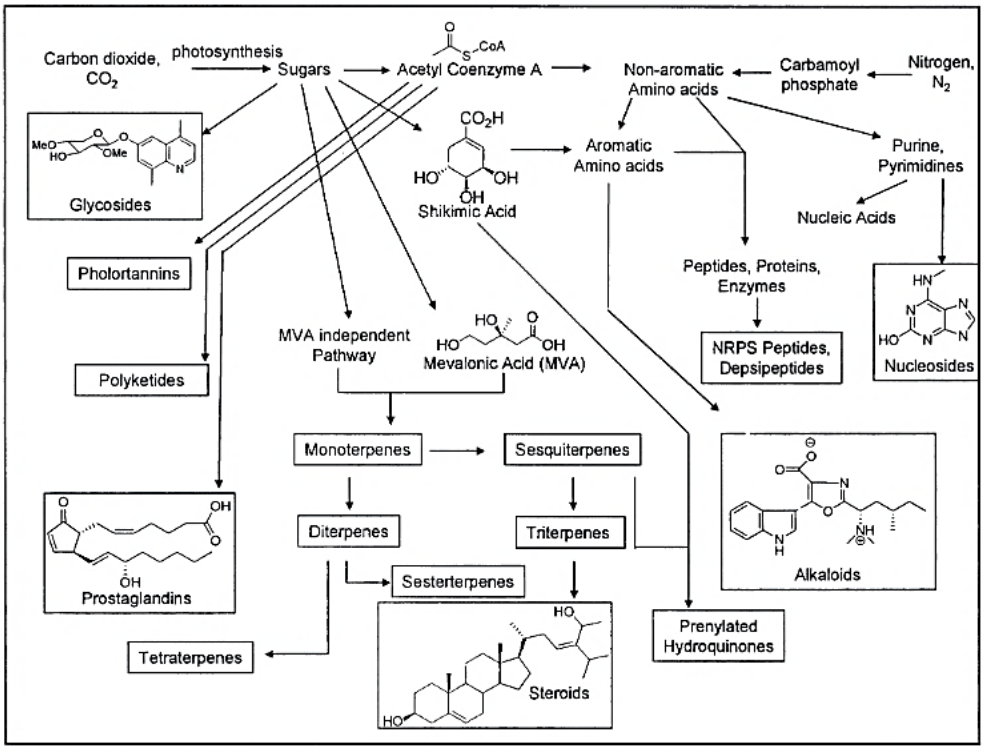

Figure 1.1 Scheme of principle secondary metabolic pathways in plants [5]

Acetyl coenzyme A (acetyl CoA), derived from pyruvate, is the starting material for multiple secondary metabolic processes including the family of complex enzymes called polyketide synthases (PKSs).[4] These enzymes form polymers of acetyl CoA to construct polyketides. Diversity among polyketides structure partially results from the three classes of PKSs.[6,7] Type I PKSs entail two subgroups, iterative and modular. The iterative PKS formulates polyketides through repetitive use of cyclic domains; however, the modular type I PKS do not reuse domains.[6] Type I usually produces polyoxygenated aliphatic compounds including macrolides.[7,8] Type II contains monofunctional proteins clumped together; and, type III PKSs distinctively lacks the acyl carrier protein found in others. Bacteria are the only organisms that possess type II PKSs, but type III PKSs exist in plants, bacteria, and fungi.[7] PKSs form these polyketones in a 1,2- head-to-tail Claisen-type condensation between thioesters and malonyl-derived extender units.[8]

Polyketides are diverse in structure and often bear biomedical significance, including antibiotic, anti-cancer, and antifungal activity.[6] Polyketides encompass a wide range of substances such as xanthones, quinones, flavonoids, and phenols. These natural products are highly oxygenated compounds, often containing macrocyclic lactones and cyclic ethers. An example of therapeutic polyketide is the macrolide isolated from a marine organism called palmerolide A (**1.1**), which is presumed a product of type I polyketide synthases (PKSs), and exhibits selective nanomolar activity against melanoma.[9]

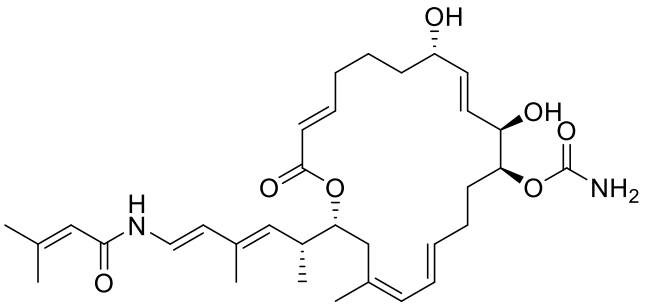

1.1

The acetate metabolism also contributes to the malonic and mevalonic acid pathway. The mevalonic acid or the mevalonic independent pathway drives the production of dimethylallylpyrophosphate (DMAPP) and its isomer isopentyl pyrophosphate (IPP) to produce terpenes – the largest group of natural products. [10] The common structural feature of terpenes is a C_5 (isoprene) unit. The precursor of this biosynthetic pathway was difficult to assign because naturally occurring C_5 acids and aldehydes were plausible.[11] However, radiolabeled precursor studies determined that the 3*R* enantiomer of mevalonic acid (MVA) is the precursor of the isoprene unit.[11] Phosphorylation of MVA, followed by decarboxylation and dehydration, results in the C_5 unit, isopentenyl pyrophosphate (IPP).[11] When IPP isomerizes it forms dimethylallyl pyrophosphate (DMAPP).[11] Figure 1.2 describes the elongation of the C_5 unit into several classes of terpenes. The smallest unit of terpenes is a C_5 unit (2-methyl-1,3-butadiene), called hemiterpene, is formed by the loss of the pyrophosphate group from DMAPP. The C_5 chain grows into the geranyl (C_{10}) and farnesyl (C_{15}) units through head-to-tail condensation. Further IPP condensation of the farnesyl unit yields geranylgeranyl (C_{20}) pyrophosphate (GGPP). These units are the precursors for mono-, sesqui- and di-terpenes. Squalene, a C30 unit, forms from the condensation of two farnesyl units. The same applies to the C_{40} unit and GGPP.

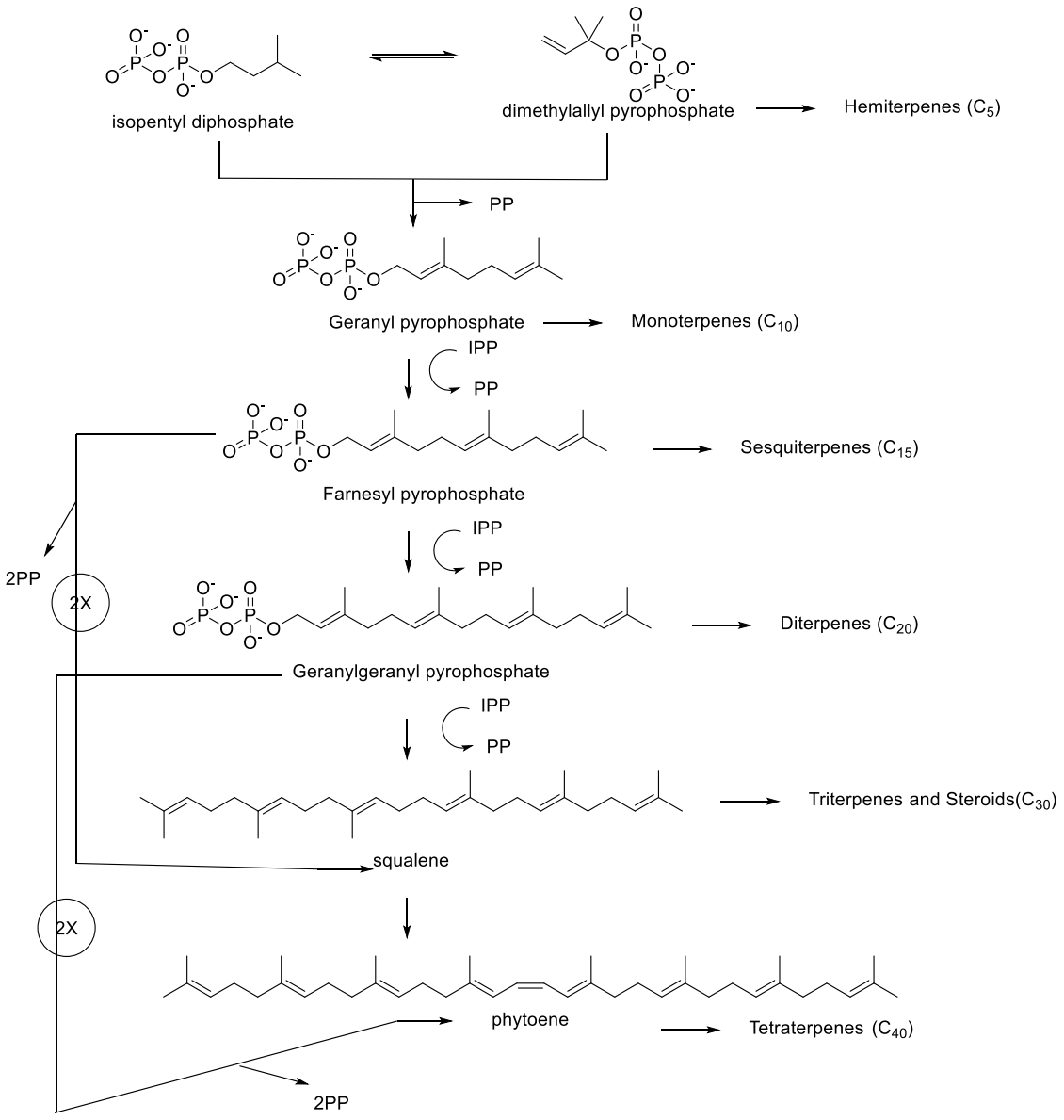

Figure 1.2 The major subclasses of terpenoids biosynthesized from IPP.[12]

Nitrogen also contributes to the metabolic pathways of secondary metabolism specifically those derived from amino acid precursors. Alkaloids are the largest and most interesting group of compounds synthesized through an amino acid precursor. The definition of an alkaloid is a "cyclic compound containing nitrogen in a negatively oxidized state with limited distribution in living organisms."[13] The broad distribution of these compounds is evident among organisms in both terrestrial and aquatic environments.

Plants were considered a prominent source of alkaloids and exploited for these structurally diverse metabolites.[13] Recently, isolation of alkaloids from animals, insects, marine organisms, and microorganisms has increased.[14] It is proposed that the production of these compounds are essential for various ecological roles targeting a variety of receptors. As a result, multiple biosynthetic pathways produce diverse alkaloid structures.[15,16]

Due to enzymatic pathways, complex structures contain specific stereochemical configurations. An excellent depiction of the complex nature of the alkaloid metabolites is morphine. This compound was first isolated for its anti-inflammatory properties in the 19th century from the opium poppy, *Papaver somniferum.*[12] The first isolate of the alkaloid class structure elucidation was not successful until 1952, almost 150 years after its isolation.[13] Along with limited technology, the four stereocenters within this compound created difficulties in the structure elucidation.[12] Since the discovery of this alkaloid in 1805, more than 12,000 alkaloids were isolated and described.[12,13]

The complexity, along with the pharmacological activities affiliated with alkaloids, drove attention to the biosynthesis and the enzymes involved.[13] Monoterpenoid indole, benzylisoquinoline, and tropane alkaloids are three groups that gained medicinal interests.[17] An alkaloid antibiotic, berberine, was initially isolated from *Geoffroya jamaicensis*. It belongs to the benzylisoquinoline class with the first fully described alkaloid biosynthetic pathway. The amino acid (L)-tyrosine undergoes 11 transformations by ten specific enzymes to produce a compound with nine quaternary centers. The genes involved in this pathway have been identified and characterized to describe the multiple changes such as reduction, oxidation, and cyclization. (S)-norcoclaurine synthase (NCS)

condenses dopamine to 4-hydroxyphenylacetaldehyde to (S)-norcoclaurine followed by a series of reactions to convert (S)-norcoclaurine to berberine. The berberine bridge enzyme (BBE) constructs a tetracyclic ring from (S)-reticuline and other enzymes subsequently oxidize and reduces functionalities to form berberine. (Figure 1.3).[18]

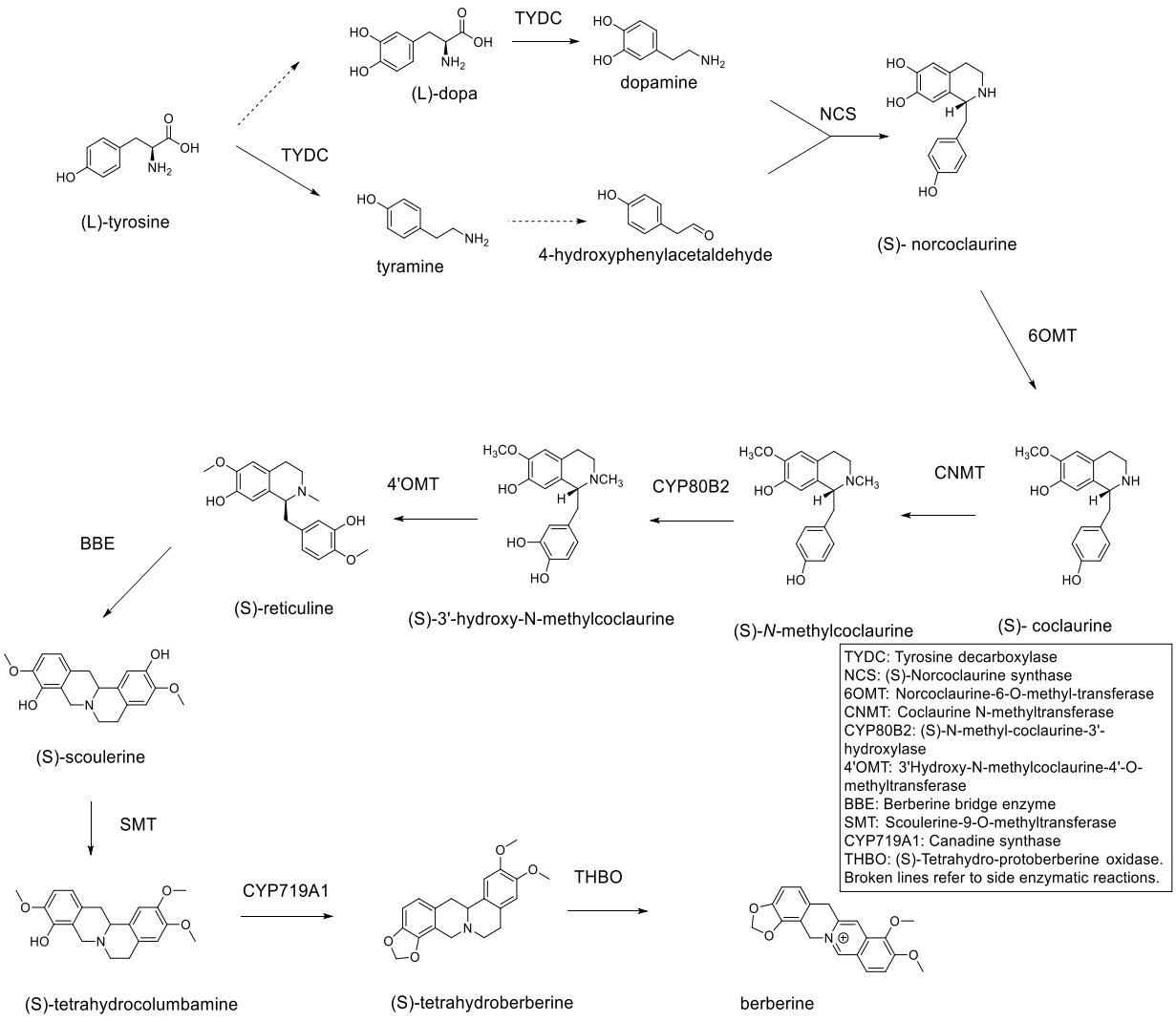

Figure 1.3 The first complete alkaloid biosynthetic pathway. (Reproduced from Yamada et al[18])

As described, the biosynthetic pathways between classes of secondary metabolites can differ tremendously. Precursors, enzymes, and mechanisms are a few differences among metabolic pathways. Secondary metabolites are specific in functions as they are created to target specific receptors in nature — internal and external factors

direct metabolic mechanisms. The efficiency of an organism determines if it survives in a hostile environment or environmental change. Therefore, biological evolution contributes to the diversity of natural products.

1.1.3 Evolution and Natural Products Chemistry

To fully understand the evolution of natural products, a brief insight into taxonomic classifications is necessary. Traditional taxonomy categorizes organisms based on morphological and molecular properties. These properties arranged in a hierarchy of relatedness, known as the phylogenetic tree, where related organisms appear close together. Domain, kingdom, phylum, class, order, family, genus, and species are the taxonomic ranks used to construct this hierarchy. Figure 1.4 displays the three domains of life: Bacteria, Archaea and Eukaryota.[19] The bacterial domain encompasses microscopic organisms that lack structural compartments within the cell, such as a nucleus or organelle.[19] Archaea are also unicellular prokaryotes with complex RNA polymerases present, distinguishing it from the bacterial domain.[19] Eukaryota, unlike archaea and bacteria, has enclosed intracellular compartments and can exist as uni- or multi-cellular organisms.[19]

The phylogenetic tree portrays all organisms stemming from a common ancestor that diversified throughout evolution to create the complex relationship.[19] Evolution is responsible for the diversity and complexity developed from simple unicellular organism to complex multicellular organisms. Diversity and specificity in secondary metabolites can also account as response to evolutionary pressure.[19] Simpler organisms can adjust to changes in the environment in a shorter time frame compared to the higher complex organisms. Evolution of receptors resulting in the resistance to chemical cues in simpler

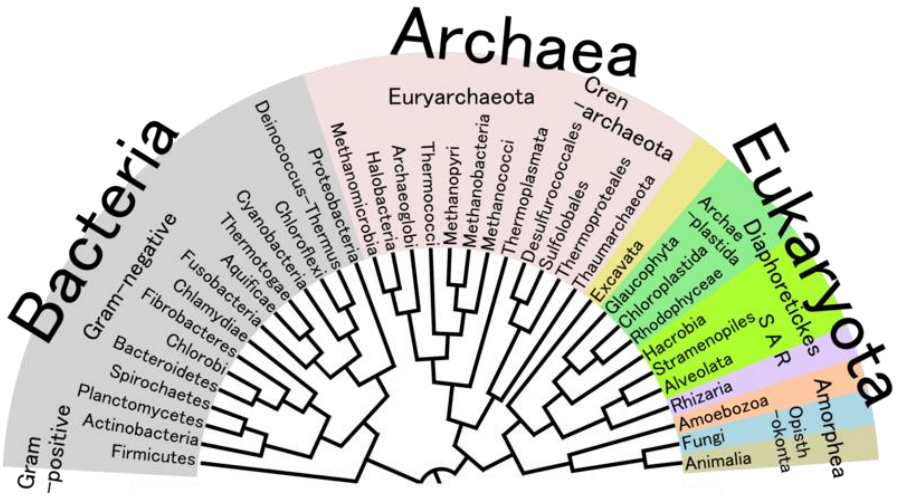

Figure 1.4 Phylogenetic Tree of Life[20]

organisms like bacteria demands the co-evolution of natural products from complex organisms.[21] Therefore, secondary metabolites are manipulated on accounts of biological evolution.

The production of vancomycin (**1.2**) is an excellent example of this ecological evolution. This peptide was initially isolated from an actinomycete and displayed bactericidal activity against *Staphylococcus aureus.*[22] This antibiotic binds strongly to a specific sequence of peptides ending with D-Ala D-Ala. These peptides are on the cell wall of bacteria such as *S. aureus.*[23] Vancomycin is deemed a product of biosynthetic pathway evolution, as the linear precursor exhibits antagonistic properties and weak binding to the vancomycin receptor.[22] The enzymatic activity led to the formation of the cross-linked cyclic peptide with potent antibiotic activity (Figure 1.5).[22]

1.1.4 Secondary Metabolites as Nature's Unspoken Language

Ecological constraints, biological regulation, co-existence, and co-evolution are factors responsible for the production of natural products.[2] Chemical ecology is a

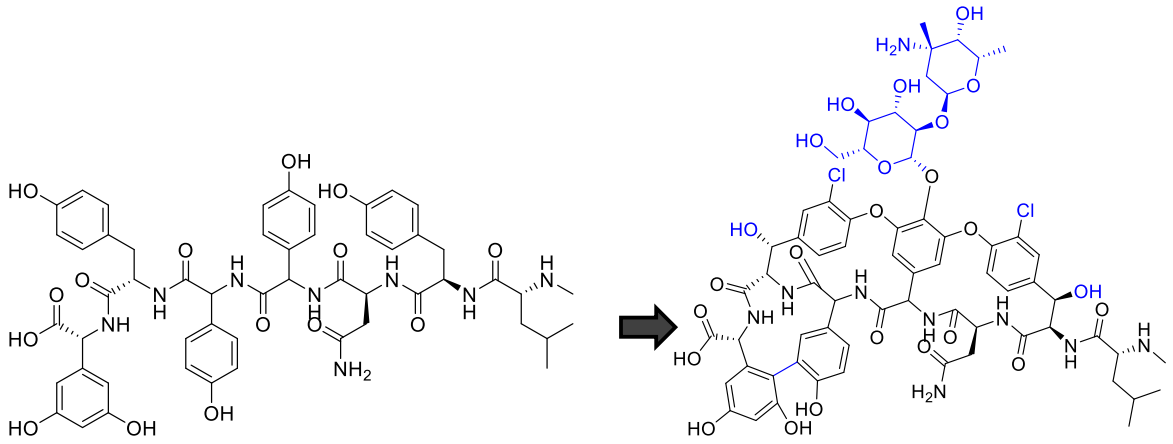

1.2

Figure 1.5 Example of metabolic evolution. Linear peptide sequence cyclized to form the glycopeptide, vancomycin. Blue indicates the differences.[23]

multidisciplinary field that studies the functionalities of these specialized metabolites and the manner in which they offer an advantage to their producing organism.Terrestrial ecosystems have extensive studies in comparison to their marine counterparts. However, marine chemical ecology shows considerable growth with research in predator-prey relations, competitive interactions, settlement cues, and defense mechanisms against microbial infections.[24,25]

The cardenolides present an example of adaptation as a mechanism of ecological evolution. Early studies of the monarch butterfly failed to detect cardenolides, but observation of the butterfly years later showed otherwise. After noticing that this insect was continually feeding on the milkweed plants, ecologists eventually discovered that these butterflies sequestered the cardenolides that are poisonous to their larvae.[26]

Cardenolides belong to a suite of toxic compounds characterized as steroid aglycones. The presence of a five-membered lactone ring distinguishes the cardenolides from the structurally related bufadienolides.[27] Both compounds are derived from the same sterol precursor but are subjected to two different biosynthetic pathway (pregane and

norcholanic pathways) to result in a bufadienolide of cardenolide (Figure 1.6). Steroids with a δ-valerolactone subunit are often produced by mammals and amphibians, while plants usually produce the related cardenolides. These lactone-bearing steroids are well studied and can be fatal at high doses by causing cardiac arrest. Oswald Schmiedeberg isolated the first cardenolide from the foxglove plant,[27] and later found in the milkweed *Asclepias curassavica* as a toxin for its lepidopteran predator.[10]

A similar ecological example of evolution exists in the marine environment. *Plocamium cartilagineum* is a chemically defended marine alga that produces polyhalogenated monoterpenes.[28] Amphipods are mesograzers that usually feed on marine algae for nutrition. However, mesograzers do not consume *P. cartilagineum* excluding the amphipod *Paradexamine fissicauda*. Studies of this predator-prey relationship led to the discovery that this amphipod not only consumes the chemically defended macroalgae but also sequesters the chemistry of this alga for its defense against its predators, as the chemical toxins are a deterrent to amphipod predators.[29]

Understanding the chemical interactions between organisms can be fruitful if applied to drug discovery. As described above, secondary metabolites are produced as a form of communication within their environment, whether its chemistry is used as a feeding deterrent as displayed in the cardenolides or in *Plocamium cartilagineum.* Besides, further studies of cardenolides led to the formulation of therapy for human heart failure as well as their potential as agents for cancer, cystic fibrosis, and other polyglutamine-related diseases.[30]

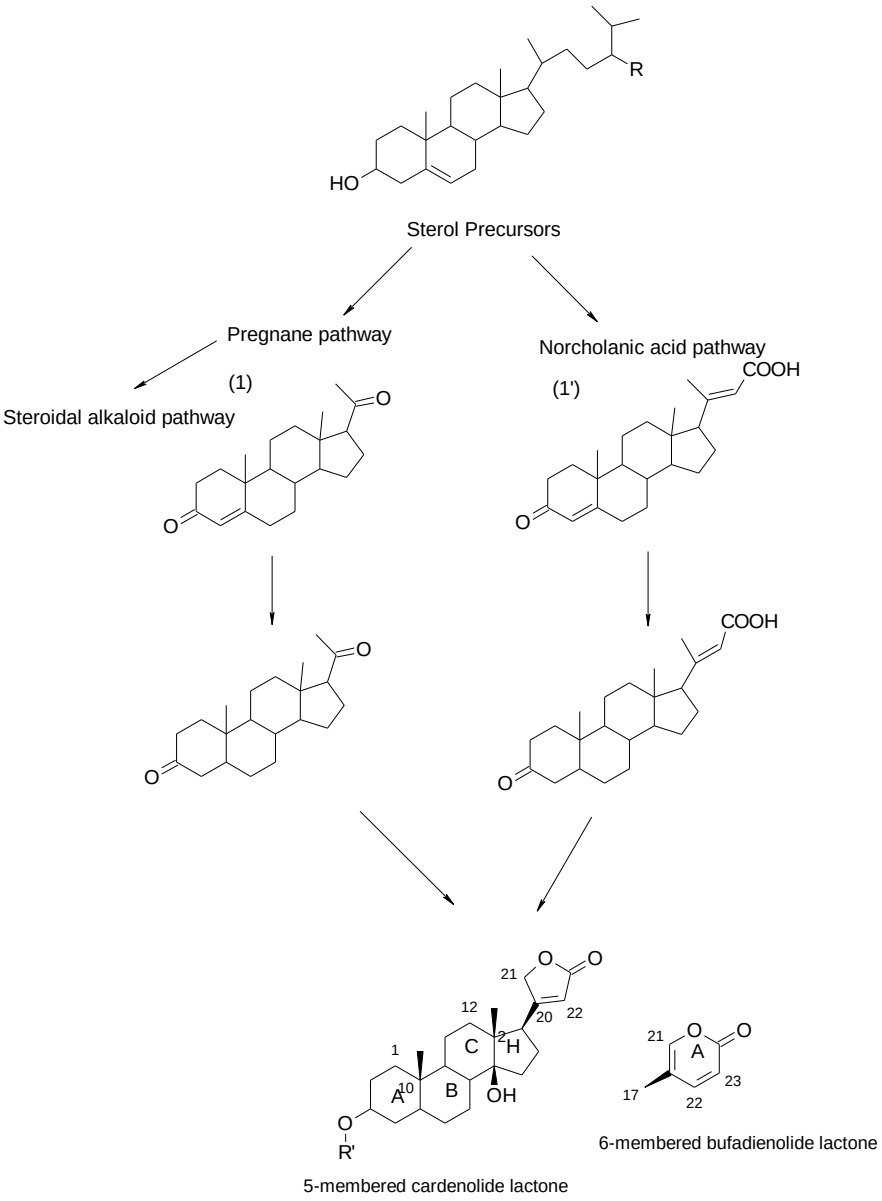

Figure 1.6 Schematic of cardenolide production[27]

*1.2 **Human health and threatening diseases***

1.2.1 Amoebic infections

The first report of free-living amoebic infections in animals was in the 1950s by Culbertson, et al.[31], followed by the first human fatalities a few years thereafter in four

victims.[32] Free-living amoebae threaten the central nervous system, causing primary amoebic meningoencephalitis (PAM) and granulomatous amoebic encephalitis (GAE).[33] PAM occurs in healthy individuals and, therefore, the infection is classed as pathogenic. The symptoms are relatively rapid and have a high fatality rate. *N. fowleri* usually causes PAM and can lead to death within a week. The opportunistic parasite *Acanthamoeba* sp. causes GAE and affects the host's metabolic, immune, and psychological systems. Unlike *N. fowleri,* this disease occurs typically in patients that are immunocompromised, primarily chronically ill patients.

Acanthamoeba. There are more than 24 species and 15 genotypes of Acanthamoeba identified based on morphological characteristics. Acanthamoeba can exist in two stages throughout its life cycle: trophozoite and cyst stage. This amoeba uses its trophozoite stage to feed and reproduce, and its dormant cyst state when there is a lack of food or hydration. A transition between stages is dependent on environmental conditions and can quickly return from its dormant cyst stage by releasing the operculum (Figure 1.7). *Acanthamoeba* spp. are ubiquitous and have been isolated from soil, fresh and brackish waters, and contact lenses, as well as animals and humans.[34] Incubation periods of *Acanthamoeba* can range from several weeks to months. Infection occurs through the olfactory epithelium, respiratory tract, skin, and sinuses with the onset of the symptoms being gradual. Treatment of GAE usually combines therapies; however, an effective treatment against both life cycles of *Acanthamoeba* does not exist.[35]

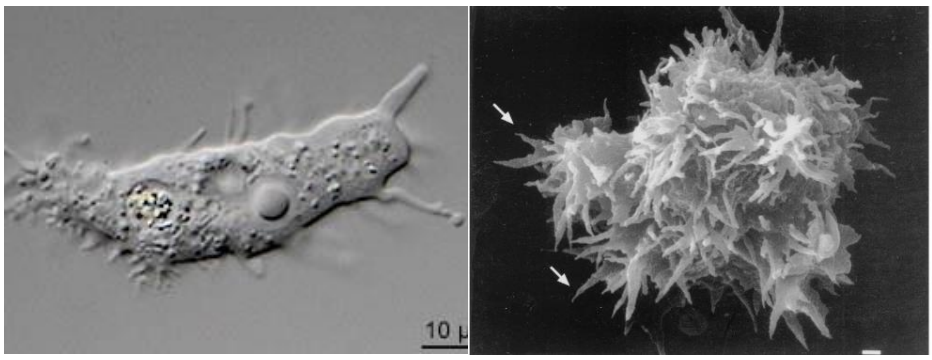

Figure 1.7 Scanning electron micrographs of *Acanthamoeba* sp., (Left to right) trophozoite[36] and cyst stage[35]

Naegleria fowleri. Figure 1.8 depicts three phases in which the free-living amoeba *Naegleria fowleri* can exist. First, encystment allows the transformation between the cyst and trophozoite stages, and the second phase called transformation involves the trophozoite and flagellate stage. The cyst is not affected by environmental factors. However, the trophozoite stage is the only phase in which it feeds and reproduces. In the flagellate stage, *N. fowleri* cannot encyst, feed or divide until it transforms into the amoeba.[37] The flagellate form is usually short-lived and lasts about an hour before it transforms back to the trophozoite.

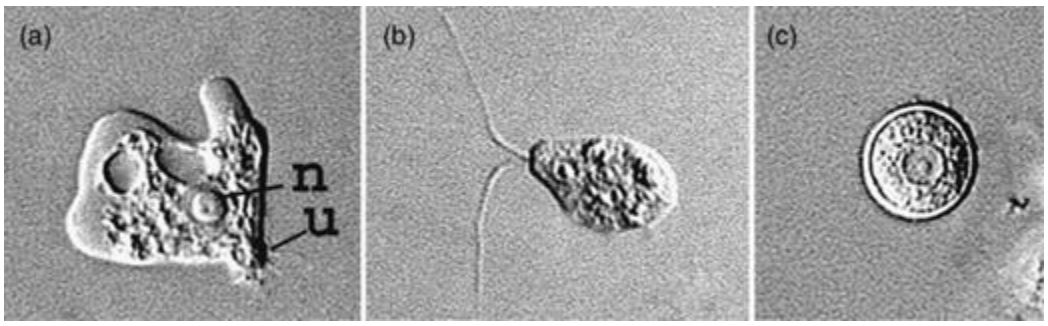

Figure 1.8 Micrographs of *N. fowleri* trophozoite, flagellate, and cyst stages[38]

N. fowleri is affiliated with warmer temperatures and flourish during the warmer months. With its ability to infect healthy individuals, more cases are reported during these months when human interaction with water is more frequent. Currently, there is no effective treatment for *N. fowleri* infections with only eight cases successfully treated, with the rest of the reported victims dying within the first week of symptoms onset.[38]

1.2.2 Malaria

A human becomes infected with *Plasmodium falciparum* when an infected mosquito bites and releases sporozoites that subsequently infect liver cells.[39] Once in the liver, the sporozoites develop into the merozoites which enter the bloodstream and invade red blood cells to develop into a trophozoite (Figure 1.9).[39] The current standard of care for malarial infections is artemisinin which acts by alkylating proteins within the parasite.[39] However, resistance to this drug occurs by 'delayed clearance' of the ring parasite, which the stage before it enters the blood.[39] Treatment of this disease is now focused on the liver stage of the parasite.

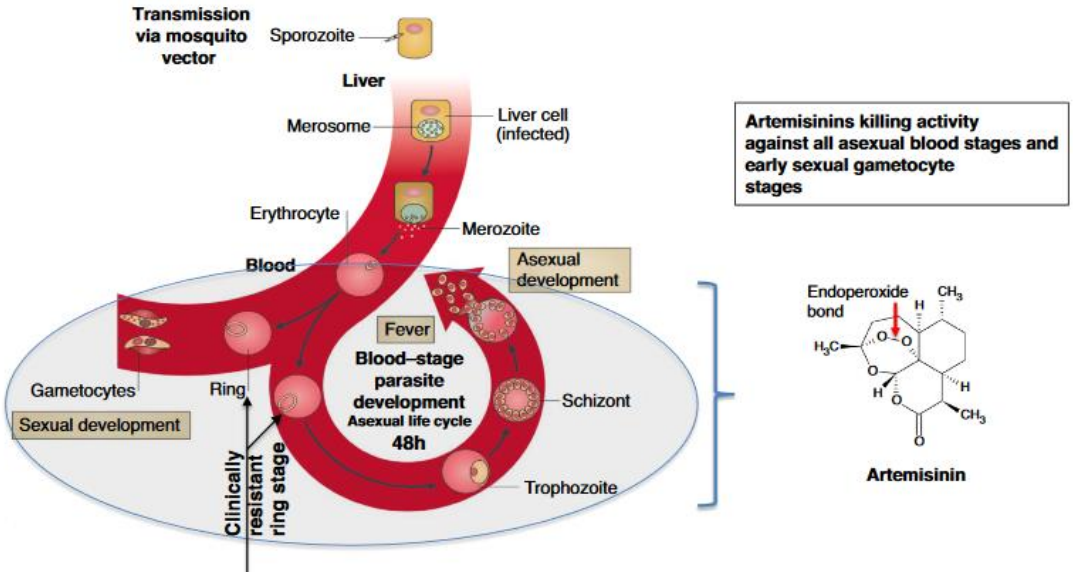

Figure 1.9 Stages of human malarial infection[39]

1.2.3 Leishmaniasis

Dengue, mycetoma, malaria, and leishmaniasis are a few of neglected communicable diseases that thrive in subtropical and tropical environments.[40] These

diseases affect over one billion people encompassing the poorest of the earth's population. Leishmaniasis is inoculated into the skin by sandflies with promastigotes that are immediately inducted by host cells. This communicable disease affects more than 2 million people with most of its cases in poverty-stricken communities. Prevention and management of leishmaniasis lies in vector control, vaccination, and access to affordable new drugs despite progress in diagnosis and treatment.[41] Visceral leishmaniasis is a fatal form of this leishmaniasis especially when left untreated.[42] New effective remedies that are accessible for poverty-stricken areas (highlighted in red in Figure 1.10) are needed in the effort against these tropical diseases.

Figure 1.10 The distribution of visceral leishmaniasis worldwide. The majority of VL cases occur in just six countries- Bangladesh, Brazil, Ethiopia, India, Nepal, and Sudan.[43]

Organisms from cold waters have contributed many biologically active compounds to the field of natural product chemistry. Therefore, seeking deep-sea corals as a new source of bioactive metabolites would be plausible. For example, the rarely reported

scaffolds of shagene A and B (**1.3** & **1.4**) from an undescribed Antarctic octocoral showed selective activity against *L. donovani.*[44]

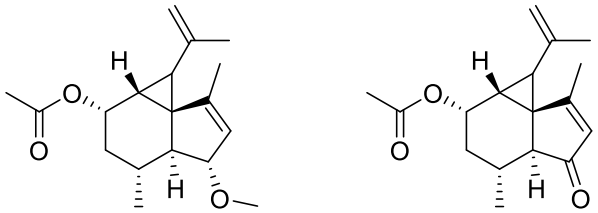

1.3 **1.4**

1.2.4 Bacterial infections

ESKAPE. *Enterococcus faecium, Staphylococcus aureus, Klebsiella pneumoniae, Acinetobacter baumannii, Pseudomonas aeruginosa,* and *Enterobacter* species are the leading causes of nosocomial infections worldwide.[45] This panel of bacteria, referred to as the ESKAPE pathogens, is responsible for over 75,000 deaths acquired in U.S. hospitals in 2011.[45] Antimicrobial resistance to drugs correlates with the increase in the numbers of nosocomial infections and deaths. Two gram-positive (*E. faecium* and *S. aureus*) and four gram-negative bacteria (*K. pneumoniae, A. baumannii, P. aeruginosa,* and *Enterobacter* sp.) compose this group of 'bad bugs'.[46] These bacterial pathogens can resist drugs through several mechanisms: drug inactivation or alteration; modification of drug binding sites; reduced intracellular drug accumulation; and biofilm formation.[45] These mechanisms have led to antibiotic resistance against potent antibiotics.

Mycobacterium tuberculosis. Tuberculosis (TB) is a bacterial infection caused by the *M. tuberculosis* complex.[47] In 2011, the World Health Organization (WHO) reported over 1.4 million deaths from TB.[48] The treatment of this bacterial infection requires early detection; drug resistance screening and effective treatment regimens for a minimum of

six months. Repurposed drugs remain the primary care of treatment for a TB infection including, rifamycins, clofazimine, and β-lactams.[47,48] TB can exist in an asymptomatic form increasing the need for a shorter and less toxic treatment.[47]

1.2.5 Neurotoxicity

According to the Center for Disease Control, approximately 3 million births in 2017 were reported in the United States, which is the lowest reported over the past three decades. Inversely, the neurobehavioral development disorders such as autism and attention deficit hyperactive disorder,[49] increased by 17 percent within one decade.[50] Relative to other diseases, there are consequences associated,[51] such as reduced quality of life, lessened academic achievement, and disruptive behavior. The majority of these neurodevelopmental disorders do not have a reasonable explanation as to the cause which leads to the influence of non-genetic, environmental factors such as industrial chemicals.[50,52]

Ntera-2 (NT-2) is a teratocarcinoma cell line derived from human testicular cancer. It has the potential to be induced into postmitotic neurons with similar phenotypes of neurotransmitters.[53,54] Ntera-2 expresses tetanus toxin receptors and the neurofilament protein, NF 195. Retinoic acid induces the carcinomic cells into neurons displayed in Figure 1.11.[55,56] Incubation of these cells with retinoic acid showed increasing levels of choline acetyltransferases (ChAT) and were only detected in the cells that showed neuronal morphology.[56] NT-2 has been extensively studied for its potential as a neuronal cell model. Transplantation of these retinoic acid-induced cells was successful in a mouse brain for more than one year. About 89% of the cells survived for 14 months in this animal model deeming it successful for further *in vivo* testing of neurogenesis.[57]

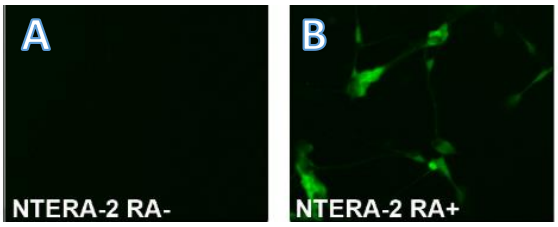

Figure 1.11 Micrographs of Ntera-2 cells (a) before addition of retinoic acid (b) after addition of retinoic acid. [58]

1.3 Pharmacognosy: The Role of Natural Products in Drug Discovery and Development

Natural products presented their value to humanity as far back as 2800 BC.[59] The search for therapeutic remedies in plants, herbs, fungi, and other botanical sources predates recorded history and lays the foundation for modern medicine.[14] Chinese, Egyptian, Greek, Indian, Roman, and Syrian civilizations utilized the therapeutic abilities of natural products. The Egyptian and Greeks utilized opium, derived from *Papaver somniferum,* to relieve headaches and joint pains.[59] Also, the Indians treated Alzheimer's disease with the rhizomes of the *Curcuma longa*.[59] Another example of the benefits of plants in ancient therapies is the *Ginkgo biloba* utilized as a Chinese tradition to treat circulatory and dementia disorders.[59] As modern medicine developed, plants remained an inspiration for drug leads.

1.3.1 Cancer Therapeutics

Commiphora myrrha is the tree utilized in the formation of myrrh from its resin (Figure 1.12). Its anti-inflammatory and disinfectant properties led to its use in stomach ailments, circulatory discomforts, and certain skin diseases. Also, myrrh display potential in anti-cancer drug discovery by inhibition of a protein overexpressed within cancerous

cells. Its potency does not match other anti-cancer plant drugs, but it is selective because it targets those cells and not healthy cells.[61–64]

Figure 1.12 Resin on *Commiphora myrrha.* [61]

Sirolimus (**1.5**), commonly referred to as rapamycin, was first isolated in 1972 from *Streptomyces hygroscopicus.* The bacterium was isolated from the soil of an island named Rapa Nui, and the term was used in the name of the compound discovered.[65] This macrocyclic polyketide has several clinical uses; it was initially developed as an antifungal drug and later to inhibit mTOR (mammalian target of rapamycin). This mechanism accounts for its immunosuppressive and antiproliferative properties, which makes it an excellent anti-cancer drug as a mediator of tumor growth and cell division.[66] Rapamycin is also used during transplant surgery to prevent organ rejection by the body.[66]

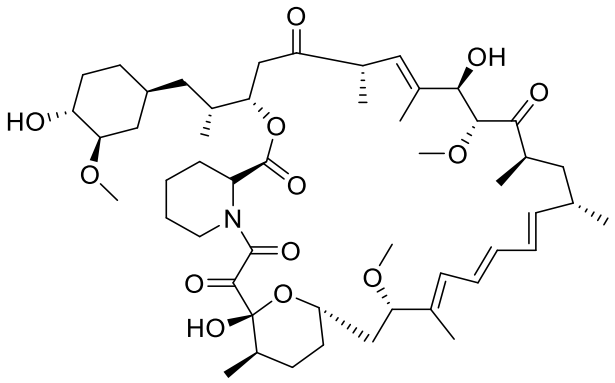

1.5

Geldanamycin (**1.6**) belongs to the benzoquinone class. It is a natural product derived from the polyketide metabolic pathway and was also isolated from a *Streptomyces* bacterium.[67] This compound elicits moderate activity against protozoa, bacteria, and fungi. Furthermore, it facilitates the degradation of proteins usually mutated in tumor cells. The Hsp90 (Heat Shock Protein 90) protein is a biological target investigated in cancer research for anti-cancer agents. Geldanamycin was found to bind to the receptor of Hsp90, leading to a nonfunctional protein and its anti-cancer properties.[68–70]

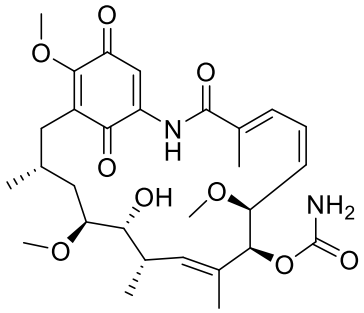

1.6

1.3.2 Anti-infectives

Bacteria, fungi, viruses, and a host of protists and other parasites are the cause of infectious diseases threatening public health. Natural products are one of the major

pioneers of innovative therapeutic agents for infectious diseases. Despite natural products' successes in the pharmaceutical industry, 90% of the earth's biological diversity 'remains untapped'.[71] With increasing drug resistance, the search for novelty is a continuous effort for structural diversity.[72] One of nature's under-represented sources is microorganisms with less than one percent of fungi and bacteria culturable. [73]

Microbial metabolites are significant in human health and demonstrated by the award of the 2015 Nobel Prize of Physiology of Medicine.[74] This award acknowledges three recipients for the formulation of anti-infective drugs derived from natural products. The impact of the 16-membered lactone named avermectin (**1.7**) and the sesquiterpene artemisinin (**1.8**) allowed William Campbell, Satoshi Omura, and Tutu Youyou to share this prestigious award.[74] Avermectins were considered 'splendid gifts' from a microbial source as anthelmintics discovered by collaborative efforts of Campbell and Omura.[74] This Nobel Prize recognized the enormous impact the polyketide had on decreasing the instances of river blindness and elephantiasis.

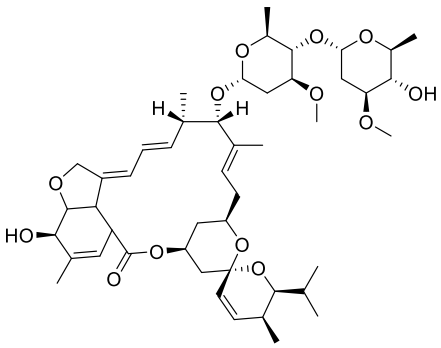

1.7

Artemisinin (**1.8**) also referred to as ginghasaou was discovered in 1971 from a low-temperature ethyl ether extract. Artemisinin was the active ingredient in a traditional Chinese herbal medicine used to treat malaria.[75] This sesquiterpene contains a peroxide

moiety which increased interest in its stability and therefore further synthetic research efforts led to derivatization of artemisinin into a more potent compound named dihydroartemisinin (DHA) (**1.9**).[75] Further biological studies of this compound concluded that the endoperoxide is necessary for its antimalarial properties as seen in DHA. This discovery alleviated the cost of the previous antimalarial treatment using the alkaloid quinine (**1.10**), produced by the Cinchona *(Cinchona ledgerianna)* bark. This traditional Chinese medicine was significant in the 1600s for treatment of malaria, and centuries later. However, the isolation of quinine encouraged the analysis of *Artemesia annua* leading to the discovery of artemisinin, an efficient and affordable malaria treatment.[74,75]

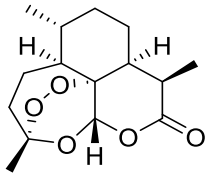

1.8

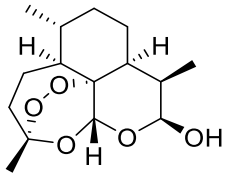

1.9

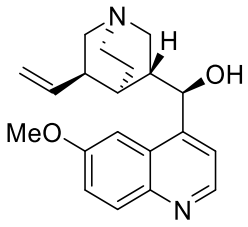

1.10

Plants have demonstrated the significance of natural products for treating human disease. Terrestrial organisms are extensively studied as natural product resources. The demand for new drugs promoted the search for new sources of biologically active compounds in underexplored environments and unique ecological niches. The ocean is earth's biggest environment, yet one of the understudied environments.

1.4 ***Marine Natural Products: Successes in Drug discovery***

The turning point of marine natural products as potential bioactive agents came in the 1980s when the first marine metabolite was entered into preclinical and clinical

studies. With this spark of interest in marine communities, associated technology to access the underexplored deep-sea environment influenced the ROV and submersibles.[76] Marine organisms >1000 meters were accessible and increased in bioactivity from marine secondary metabolites was evident.[77] For a relatively young division of deep-sea natural products, 40 years led to the discovery of over 500 compounds.[78]

1.4.1 The 1960s -1970s: The rise of marine natural product chemistry

Plants serve as the basis of traditional medicine systems and the oldest recorded form of treatment for human illnesses.[79] Terrestrial organisms are reliable sources of bioactive natural products with over 80% of earth's human population dependent on plants as traditional medicine.[71] It is proposed that the chemodiversity in the marine environment surpasses that of terrestrial habitats.[80] Therefore, interest is directed to the marine environment for chemical novelty in the era of drug resistance and new inspirations for incurable human diseases.

Marine natural product chemistry started with the collection of shallow water and intertidal organisms and expanded to deeper depths in the 1960s when SCUBA equipment was accessible for scientific use.[81] ROVs and manned-submersibles gave access to depths greater than 1000m, which vastly increased the scope of marine natural products.[77] With 70% of the earth belonging to the marine environment, great potential lies within for novelty in chemical structure as well as biologically active compounds.

The marine environment demonstrated its potential within the first decade. Cytarabine (**1.11**) was the first marine-derived approved drug. This nucleoside was

initially isolated from a sponge but later identified as a *Streptomyces griseus* metabolite.[82,83] Ara- C, the trademarked name of cytarabine, was approved in the 1960s for the treatment of myeloid leukemia, non-Hodgkin's lymphoma, and meningeal leukemia and is still considered the best form of treatment for these cancerous diseases.[83] Ara- C disrupts DNA replication by replacing the sugar moiety of the normal nucleoside with a β-D-arabinofuranose leading to cellular toxicity.[83]

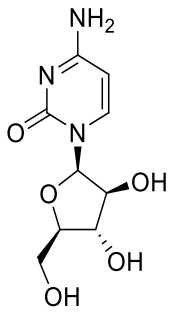

1.11

1.4.2 1970s-1990s

The decades following the first marine approved drug led to an increase in compounds reported from marine sources. An example is bryozoans, which are sessile animals that received much less interest than other marine fauna;[84] nevertheless, they exhibited potential in drug discovery as a reliable source for bioactive agents. *Bugula neritina* is the bryozoan that produces protein kinase C activators called bryostatins. Bryostatins have a macrocyclic lactone with polyoxygenation throughout the compound. This type II polyketide was initially isolated in the 1980s and characterized by x-ray crystallography.[85] Bryostatins are activators of protein kinase C (PKC) through upregulation of the protein kinase; this activation causes the breakdown of PKC that renders bryostatin as drugs.[82] Bryostatins have created intense research activities for derivatives to enhance the therapeutic potential.[82] Success in synthesizing these

polyketides was only possible for the derivatives, but synthetic methods were unsuccessful for bryostatin-1 (**1.12**). The derivatives and analogs lack the potency of bryostatin 1, so further efforts to acquire more of this potent PKC inhibitor led to the aquaculture of the *B. neritina.*[80]

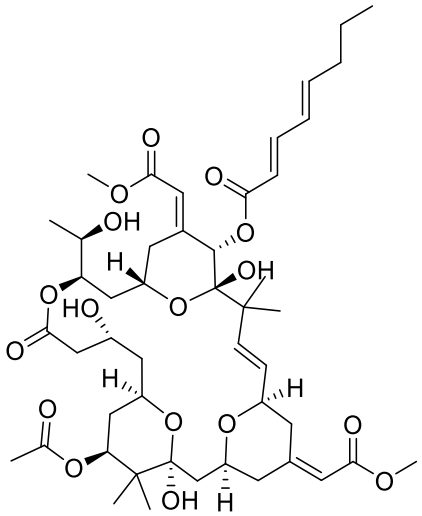

1.12

1.4.3 The 2000s to present

At the turn of the century, the focus shifted to microbial sources for marine natural products. With the increase in reported metabolites of microbial origin and the ease of increasing biomass, microbes addressed well-known limitations of marine invertebrate sources. Nevertheless, studies of marine invertebrates continued because previous successes displayed the potential for producing bioactive compounds. Trabectedin (**1.13**) trademarked Yondelis® is an alkaloid isolated from the Caribbean tunicate, *Ecteinascidia turbinata.*[86] This compound is structurally complex, containing two fused quinoline rings, a 10-membered lactone bridge, a sulfide, and a spiro moiety. This complex alkaloid

exhibits potent activity against cancer due to its ability to intercalate the DNA minor groove. [47–50]

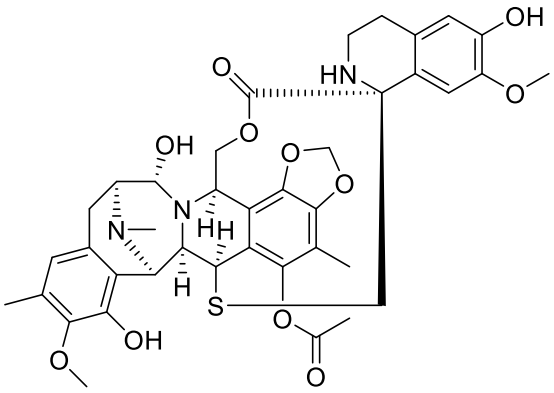

1.13

Marine algae have been used therapeutically for thousands of years, first documented in the Chinese *Materia Medica* in 200 BC. [77] Marine algae continue to be a source for bioactive metabolites, and considerable research focuses on the ecological interactions of predator-prey relationships. Kahalalide F (**1.14**) was initially isolated from the sea slug, *Elysia rufescens,* but assumed that it is a green alga metabolite, attained by feeding.[82,89] Kahalalide F is responsible for inducing lysosomal and cell membrane permeability in cancerous cells. This cyclic depsipeptide is the most bioactive compound derived from a marine green alga. It is another anticancer drug candidate derived from the marine environment.[82]

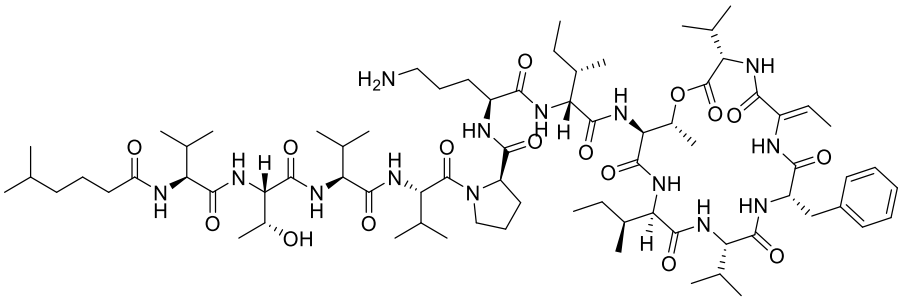

1.14

1.5 ***Research objectives***

Marine environments are understudied compared to their terrestrial counterparts. Terrestrial plants, animals, and fungi have shown their potential for chemical novelty and diversity. This dissertation will discuss the same applications for the marine community and its inhabitants. The search for novel bioactive structures encourages the quest of ecological niches. Natural products remain the most chemically diverse in comparison to combinatorial or synthetic approaches. Within this dissertation, understudied environments from both tropical and polar environments will be investigated. The microbes, flora, and fauna of two diverse communities were investigated for new compounds with biological activity.

The first section focuses on microorganisms specifically endophytic fungi. Chapter two of this dissertation focuses on endophytic fungi isolated from mangrove communities. Chemical analysis of the fungal isolates followed infusion of epigenetic modulators into the cultures. This project aims to isolate new, bioactive compounds. In pursuit of the goal, we isolated bioactive compounds previously reported. In the literature, hundreds of secondary metabolites reported per annum. Therefore, dereplication strategies were introduced for early identification of these compounds to reduce the chance of known mycotoxin re-isolation.

The second part of this dissertation reports chemistry isolated from the marine environments of Antarctica. In specific, chapter three focuses on an Antarctic red alga, *Delisea pulchra,* and the suite of known metabolites isolated from the specimen and their biological activities. Chapter four explores the deep-sea of Antarctica by describing the chemical investigation of several octocorals. An array of new and known terpenoids were

successfully isolated and fully characterized. Moreover, they were all tested against a variety of biological targets displaying selectivity among the assays.

1.6 *References*

(1) Theis, N.; Lerdau, M. The evolution of function in plant secondary metabolites. *Int. J. Plant Sci.* **2003**, *164*, S93–S102.

(2) Paul, V. J.; Puglisi, M. P.; Ritson-Williams, R. Marine chemical ecology. *Nat. Prod. Rep.* **2006**, *23*, 153–180.

(3) Raguso R. A.., Agrawal A. A., Douglas A. E., Jander G. ., Kessler A., P. K. and T. J. S. The raison d'etre of chemical ecology. *Ecology* **2015**, *96*, 617–630.

(4) Hanson, J. R. The biosynthesis of secondary metabolites. In *Natural Products: The Secondary Metabolites*; Abel, E. W., Ed.; Royal Society of Chemistry: Cambridge, 2003; Vol. 17, pp 105–130.

(5) Maschek, J. .; Baker, B. J. The chemistry of algal secondary metabolism. In *Algal Chemical Ecology*; Amsler, C. D., Ed.; Springer Berlin Heidelberg: Berlin, Heidelberg, 2008; pp 1–24.

(6) Staunton, J.; Weissman, K. J. Polyketide biosynthesis: a millennium review. *Nat. Prod. Rep.* **2001**, *18*, 380–416.

(7) Cox, R. J. Polyketides, proteins and genes in fungi: programmed nano-machines begin to reveal their secrets. *Org. Biomol. Chem.* **2007**, *5*, 2010.

(8) Lorente, A.; Makowski, K.; Albericio, F.; Alvarez, M. Bioactive marine polyketides as potential and promising drugs. *Ann. Mar. Biol. Res.* **2014**, *1*, 1003–1012.

(9) Diyabalanage, T.; Amsler, C. D.; McClintock, J. B.; Baker, B. J. Palmerolide A, a cytotoxic macrolide from the Antarctic tunicate *Synoicum adareanum*. *J. Am. Chem. Soc.* **2006**, *128*, 5630–5631.

(10) Gershenzon, J.; Dudareva, N. The function of terpene natural products in the natural world. *Nat. Chem. Biol.* **2007**, *3*, 408–414.

(11) Mann, J. Metabolites derived from mevalonate: isoprenoids. In *Secondary Metabolism*; Clarendon Press: Oxford, 1978; pp 79–151.

(12) Buchanan, B. B. Secondary metabolites. In *Biochemistry and molecular biology of plants*; Gruissen, W., Jones, R. L., Eds.; American Society of Plant Phytologists: Rockville, MD, 2000; pp 1250–1318.

(13) Roberts, M. M. F.; Wink, M. Introduction. In *Alkaloids:biochemistry, ecology, and medicinal applications*; Springer US: Boston, MA, 1998; pp 1–7.

(14) Wink, M. A short history of alkaloids. In *Alkaloids*; Springer US: Boston, MA, 1998; pp 11–44.

(15) Wink, M. Chemical ecology of alkaloids. In *Alkaloids*; Springer US: Boston, MA, 1998; pp 265–300.

(16) Schmeller, T.; Wink, M. Utilization of alkaloids in modern medicine. In *Alkaloids*; Springer US: Boston, MA, 1998; pp 435–459.

(17) K. Marasco, E.; Schmidt-Dannert, C. Exploring and accessing plant natural product biosynthesis in engineered microbial hosts. In *Medicinal Plant Biotechnology*; Wiley-VCH Verlag GmbH: Weinheim, Germany, 2008; pp 287–

317.

(18) Yamada, Y.; Yoshimoto, T.; Yoshida, S. T.; Sato, F. Characterization of the promoter region of biosynthetic enzyme genes involved in berberine biosynthesis in *Coptis japonica*. *Front. Plant Sci.* **2016**, *7*, 1352–1362.

(19) Iwabe, N.; Kuma, K.; Hasegawa, M.; Osawa, S.; Miyata, T. Evolutionary relationship of archaebacteria, eubacteria, and eukaryotes inferred from phylogenetic trees of duplicated genes. *Proc. Natl. Acad Sci.* **1989**, *86*, 9355–9359.

(20) https://www.rom.on.ca/en/blog/the-rules-of-taxonomy-how-species-are-named (accessed Oct 16, 2018).

(21) Stone, M. J.; Williams, D. H. On the evolution of functional secondary metabolites (natural products). *Mol. Microbiol.* **1992**, *6*, 29–34.

(22) Levine, J. F. Vancomycin: a review. *Med. Clin. North Am.* **1987**, *71*, 1135–1145.

(23) Williams, D. H.; Maplestone, R. A. Why are secondary metabolites biosynthesized? Sophistication in the inhibition of cell wall biosynthesis by vancomycin group antibiotics. In *Ciba Foundation Symposium 171- Secondary Metabolites: their function and Evolution*; Chadwick, D. J., Whelan, J., Eds.; Wiley-Blackwell: Wiley, 2007; pp 45–63.

(24) Bergström, G. Chemical ecology = chemistry + ecology! *Pure Appl. Chem.* **2007**, *79*, 2305–2323.

(25) Ferrari, M. C. O.; Wisenden, B. D.; Chivers, D. P. Chemical ecology of predator–

prey interactions in aquatic ecosystems: a review and prospectus. *Can. J. Zool.* **2010**, *88*, 698–724.

(26) Malcolm, S. B. Milkweeds, monarch butterflies and the ecological significance of cardenolides. *Chemoecology* **1994**, *5–6*, 101–117.

(27) Agrawal, A. A.; Petschenka, G.; Bingham, R. A.; Weber, M. G.; Rasmann, S. Toxic cardenolides: chemical ecology and coevolution of specialized plant-herbivore interactions. *New Phytol.* **2012**, *194*, 28–45.

(28) Núñez-Pons, L.; Avila, C. Natural products mediating ecological interactions in antarctic benthic communities: a mini-review of the known molecules. *Nat. Prod. Rep.* **2015**, *32*, 1114–1130.

(29) Amsler, M.; Amsler, C.; von Salm, J.; Aumack, C.; McClintock, J.; Young, R.; Baker, B. Tolerance and sequestration of macroalgal chemical defenses by an antarctic amphipod: a 'cheater' among mutualists. *Mar. Ecol. Prog. Ser.* **2013**, *490*, 79–90.

(30) Krishna, A. B.; Manikyam, H. K.; Sharma, V. K.; Sharma, N. Plant cardenolides in therapeutics. *Int. J. Indig. Med. Plants* **2015**, *48*, 1871–1896.

(31) Culbertson, C. G.; Smith, J. W.; Cohen, H. K.; Minner, J. R. Experimental infection of mice and monkeys by *Acanthamoeba*. *Am. J. Pathol.* **1959**, *35*, 185–197.

(32) Fowler, M.; Carter, R. Acute pyogenic meningitis probably due to *Acanthamoeba* sp.: a preliminary report. *Brit. Med. J.* **1965**, *2*, 740–742.

(33) Schumacher, D. J.; Tien, R. D.; Lane, K. Neuroimaging findings in rare amebic

infections of the central nervous system. *AJNR. Am. J. Neuroradiol.* **1995**, *16*, 930–935.

(34) Khan, N. A. *Acanthamoeba* : biology and increasing importance in human health. *FEMS Microbiol. Rev.* **2006**, *30*, 564–595.

(35) Marciano-Cabral, F.; Cabral, G. *Acanthamoeba* spp. as agents of disease in humans. *Clin. Microbiol. Rev.* **2003**, *16*, 273–307.

(36) https://www.arcella.nl/acanthamoeba (accessed Nov 26, 2018).

(37) John, D. T. Primary amebic meningoencephalitis and the biology of *Naegleria fowleri*. *Annu. Rev. Microbiol.* **1982**, *36*, 101–123.

(38) Visvesvara, G. S.; Moura, H.; Schuster, F. L. Pathogenic and opportunistic free-living amoebae: A*canthamoeba* spp., B*alamuthia mandrillaris* , N*aegleria fowleri* , and S*appinia diploidea*. *FEMS Immunol. Med. Microbiol.* **2007**, *50*, 1–26.

(39) Suresh, N.; Haldar, K. Mechanisms of artemisinin resistance in *Plasmodium falciparum* malaria. *Curr. Opin. in Pharmacol.* **2018**, *42*, 46–54.

(40) Hotez, P. J.; Woc-Colburn, L.; Bottazzi, M. E. Neglected tropical diseases in central america and panama: review of their prevalence, populations at risk and impact on regional development. *Int. J. Parasitol.* **2014**, *44*, 597–603.

(41) Murray, H. W.; Berman, J. D.; Davies, C. R.; Saravia, N. G. Advances in leishmaniasis. *Lancet* **2005**, *366*, 1561–1577.

(42) Alves, F.; Bilbe, G.; Blesson, S.; Goyal, V.; Monnerat, S.; Mowbray, C.; Muthoni Ouattara, G.; Pécoul, B.; Rijal, S.; Rode, J.; Solomos, A.; Strub-Wourgaft, N.;

Wasunna, M.; Wells, S.; Zijlstra, E. E.; Arana, B.; Alvar, J. Recent development of visceral leishmaniasis treatments: successes, pitfalls, and perspectives. *Clin. Microbiol. Rev.* **2018**, *31*, 1–30.

(43) Chappuis, F.; Sundar, S.; Hailu, A.; Ghalib, H.; Rijal, S.; Peeling, R. W.; Alvar, J.; Boelaert, M. Visceral leishmaniasis: what are the needs for diagnosis, treatment and control? *Nat. Rev. Microbiol.* **2007**, *5*, 873–882.

(44) von Salm, J. L.; Wilson, N. G.; Vesely, B. A.; Kyle, D. E.; Cuce, J.; Baker, B. J. Shagenes A and B, new tricyclic sesquiterpenes produced by an undescribed Antarctic octocoral. *Org. Lett.* **2014**, *16*, 2630–2633.

(45) Santajit, S.; Indrawattana, N. Mechanisms of antimicrobial resistance in eskape pathogens. *BioMed Res. Internati.* **2016**, *2016*, 1–8.

(46) Boucher, H. W.; Talbot, G. H.; Bradley, J. S.; Edwards, J. E.; Gilbert, D.; Rice, L. B.; Scheld, M.; Spellberg, B.; Bartlett, J. Bad bugs, no drugs: no eskape! an update from the infectious diseases society of america. *Clin. Infect. Dis.* **2009**, *48*, 1–12.

(47) Zumla, A.; Nahid, P.; Cole, S. T. Advances in the development of new tuberculosis drugs and treatment regimens. *Nat. Rev. Drug Discov.* **2013**, *12*, 388–404.

(48) Ma, Z.; Lienhardt, C.; McIlleron, H.; Nunn, A. J.; Wang, X. Global tuberculosis drug development pipeline: the need and the reality. *Lancet (London, England)* **2010**, *375*, 2100–2109.

(49) Landrigan, P. J.; Lambertini, L.; Birnbaum, L. S. A research strategy to discover the environmental causes of autism and neurodevelopmental disabilities. *Environ. Health Perspect.* **2012**, *120*, a258–a260.

(50) Grandjean, P.; Landrigan, P. Developmental neurotoxicity of industrial chemicals. *Lancet* **2006**, *368*, 2167–2178.

(51) Bellinger, D. C. Interpreting epidemiologic studies of developmental neurotoxicity: conceptual and analytic issues. *Neurotoxicol. Teratol.* **2009**, *31*, 267–274.

(52) Grandjean, P.; Landrigan, P. J. Neurobehavioural effects of developmental toxicity. *Lancet Neurol.* **2014**, *13*, 330–338.

(53) Stern, M.; Gierse, A.; Tan, S.; Bicker, G. Human ntera2 cells as a predictive *in vitro* test system for developmental neurotoxicity. *Arch. Toxicol.* **2014**, *88*, 127–136.

(54) Pleasure, S. J.; Lee, V. M.-Y. NTera 2 cells: a human cell line which displays characteristics expected of a human committed neuronal progenitor cell. *J. Neurosci. Res.* **1993**, *35*, 585–602.

(55) Przyborski, S. A.; Morton, I. E.; Wood, A.; Andrews, P. W. Developmental regulation of neurogenesis in the pluripotent human embryonal carcinoma cell line ntera-2. *Eur. J. Neurosci.* **2000**, *12*, 3521–3528.

(56) Zeller, M.; Strauss, W. L. Retinoic acid induces cholinergic differentiation of ntera 2 human embryonal carcinoma cells. *Int. J. Dev. Neurosci.* **1995**, *13*, 437–445.

(57) Kleppner, S. R.; Robinson, K. A.; Trojanowski, J. Q.; Lee, V. M.-Y. Transplanted

human neurons derived from a teratocarcinoma cell line (ntera-2) mature, integrate, and survive for over 1 year in the nude mouse brain. *J. Comp. Neurol.* **1995**, *357*, 618–632.

(58) Couillard-Despres, S.; Quehl, E.; Altendorfer, K.; Karl, C.; Ploetz, S.; Bogdahn, U.; Winkler, J.; Aigner, L. Human *in vitro* reporter model of neuronal development and early differentiation processes. *BMC Neurosci.* **2008**, *9*, 31–39.

(59) Mukeshwar, P.; Debnath, M.; Gupta, S.; Chikara, S. K. Phytomedicine: an ancient approach turning into future potential source of therapeutics. *J. Pharmacogn. Phyther.* **2011**, *3*, 27–37.

(60) Bertrand, R.; Saliou, C.; Bottin, M. C.; Keith, G.; Packer, L. From ancient remedies to modern therapeutics: pine bark uses in skin disorders revisited. *Phyther. Res.* **2000**, *15*, 76–78.

(61) Mohamed, A. A.; Ali, S. I.; EL-Baz, F. K.; Hegazy, A. K.; Kord, M. A. Chemical composition of essential oil and in vitro antioxidant and antimicrobial activities of crude extracts of *Commiphora myrrha* resin. *Ind. Crops Prod.* **2014**, *57*, 10–16.

(62) Maradufu, A.; Warthen, J. D. Furanosesquiterpenoids from *Commiphora myrrh* oil. *Plant Sci.* **1988**, *57*, 181–184.

(63) Hanuš, L. O.; Rosenthal, D.; Řezanka, T.; Dembitsky, V. M.; Moussaief, A. Fast and easy GC/MS identification of myrrh resins. *Pharm. Chem. J.* **2008**, *42*, 719–720.

(64) Zou, Y.-H.; Zhao, L.; Xu, Y.-K.; Bao, J.-M.; Liu, X.; Zhang, J.-S.; Li, W.; Ahmed,

A.; Yin, S.; Tang, G.-H. Anti-inflammatory sesquiterpenoids from the traditional chinese medicine *Salvia plebeia*: regulates pro-inflammatory mediators through inhibition of nf-κb and erk1/2 signaling pathways in lps-induced raw264.7 cells. *J. Ethnopharmacol.* **2018**, *210*, 95–106.

(65) Vezina, C.; Kudelski, A.; Sehgal, S. N. Rapamycin (ay-22, 989), a new antifungal antibiotic. *J. Antibiot.* **1975**, *28*, 721–726.

(66) Butler, M. S.; Robertson, A. A. B.; Cooper, M. A. Natural product and natural product derived drugs in clinical trials. *Nat. Prod. Rep.* **2014**, *31*, 1612–1661.

(67) DeBoer, C.; Meulman, P. A.; Wnuk, R.; Peterson, D. H. Geldanamycin, a new antibiotic. *J. Antibiot.* **1970**, *23*, 442–447.

(68) Stebbins, C.; Russo, A.; Schneider, C.; Rosen, N.; Hartl, F. U.; Pavletich, N. Crystal structure of an hsp90–geldanamycin complex: targeting of a protein chaperone by an antitumor agent. *Cell* **1997**, *89*, 239–250.

(69) Supko, J. G.; Hickman, R. L.; Grever, M. R.; Malspeis, L. Preclinical pharmacologic evaluation of geldanamycin as an antitumor agent. *Cancer Chemother. Pharmacol.* **1995**, *36*, 305–315.

(70) Roe, S. M.; Prodromou, C.; O'Brien, R.; Ladbury, J. E.; Piper, P. W.; Pearl, L. H. Structural basis for inhibition of the hsp90 molecular chaperone by the antitumor antibiotics radicicol and geldanamycin. *J. Med. Chem.* **1999**, *42*, 260–266.

(71) Dias, D. A.; Urban, S.; Roessner, U. A historical overview of natural products in drug discovery. *Metabolites* **2012**, *2*, 303–336.

(72) Okeke, I. N.; Laxminarayan, R.; Bhutta, Z. A.; Duse, A. G.; Jenkins, P.; O'Brien, T. F.; Pablos-Mendez, A.; Klugman, K. P. Antimicrobial resistance in developing countries. Part i: recent trends and current status. *Lancet Infect. Dis.* **2005**, *5*, 481–493.

(73) Cos, P.; Vlietinck, A. J.; Berghe, D. Vanden; Maes, L. Anti-infective potential of natural products: how to develop a stronger *in vitro* 'proof-of-concept.' *J. Ethnopharmacol.* **2006**, *106*, 290–302.

(74) Shen, B. A new golden age of natural products drug discovery. *Cell* **2015**, *163*, 1297–1300.

(75) White, N. J. Qinghaosu (artemisinin): the price of success. *Science.* **2008**, *320*, 330–334.

(76) Soldatou, S.; Baker, B. J. Cold-water marine natural products, 2006 to 2016. *Nat. Prod. Rep.* **2017**, *34*, 585–626.

(77) Carte, B. K. Biomedical potential of marine natural products. *BioSci.* **1996**, *46*, 271–286.

(78) Skropeta, D.; Wei, L. Recent advances in deep-sea natural products. *Nat. Prod. Rep.* **2014**, *31*, 999–1025.

(79) Newman, D. J.; Cragg, G. M.; Snader, K. M. The influence of natural products upon drug discovery (antiquity to late 1999). *Nat. Prod. Rep.* **2000**, *17*, 215–234.

(80) Hu, G.-P.; Yuan, J.; Sun, L.; She, Z.-G.; Wu, J.-H.; Lan, X.-J.; Zhu, X.; Lin, Y.-C.; Chen, S.-P. Statistical research on marine natural products based on data

obtained between 1985 and 2008. *Mar. Drugs* **2011**, *9*, 514–525.

(81) David, B.; Wolfender, J.-L.; Dias, D. A. The pharmaceutical industry and natural products: historical status and new trends. *Phytochem. Rev.* **2015**, *14*, 299–315.

(82) Haefner, B. Drugs from the deep: marine natural products as drug candidates. *Drug Discov. Today* **2003**, *8*, 536–544.

(83) Gerwick, W. H.; Moore, B. S. Lessons from the past and charting the future of marine natural products drug discovery and chemical biology. *Chem. Biol.* **2012**, *19*, 85–98.

(84) Blunt, J. W.; Copp, B. R.; Keyzers, R. A.; Munro, M. H. G.; Prinsep, M. R. Marine natural products. *Nat. Prod. Rep.* **2017**, *34*, 235.

(85) Faulkner, D. J. Marine natural products: metabolites of marine invertebrates. *Nat. Prod. Rep.* **1984**, *1*, 551.

(86) D'Incalci, M.; Galmarini, C. M. A review of trabectedin (et-743): a unique mechanism of action. *Mol. Cancer Ther.* **2010**, *9*, 1–7.

(87) Blunt, J. W.; Copp, B. R.; Keyzers, R. A.; Munro, M. H. G.; Prinsep, M. R. Marine natural products. *Nat. Prod. Rep.* **2016**, *33*, 382–431.

(88) Newman, D. J.; Cragg, G. M. Natural products as sources of new drugs from 1981 to 2014. *J. Nat. Prod.* **2016**, *79*, 629–661.

(89) Folmer, F.; Jaspars, M.; Dicato, M.; Diederich, M. Photosynthetic marine organisms as a source of anticancer compounds. *Phytochem. Rev.* **2010**, *9*, 557–579.

SECTION A:

MICROORGANISMS CONTRIBUTION TO DRUG DISCOVERY

Natural products, produced for ecological purposes, often possess biological activity relevant for treating human ailments.[1] The discovery of the antibiotic, penicillin G (**A.1**), from the fungus *Penicillium* sp. directed attention to microorganisms for potential drug leads.[1] Cephalosporin C (**A.2**), chloramphenicol (**A.3**), and erythromycin (**A.4**) are antibacterial agents isolated from microbial sources after the discovery of penicillin.[1,2] Despite these prestigious findings a significant decline of natural products screening by pharmaceutical companies has occurred. One of the significant contributions that lead to the decline was the lack of technological advancement in fermentation, purification, and dereplication.[2] With new developments for a streamlined screening process, microorganisms provide renewable and reproducible material for faster access to natural products.[2]

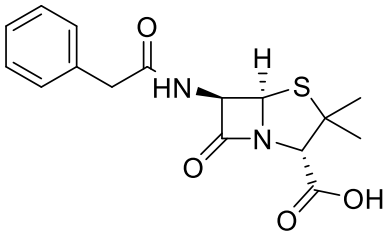

A.1

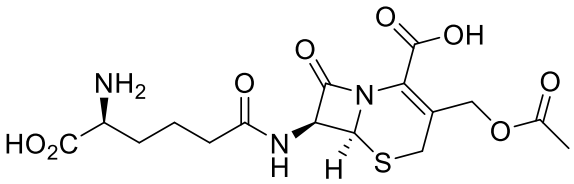

A.2

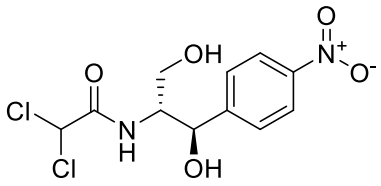

A.3

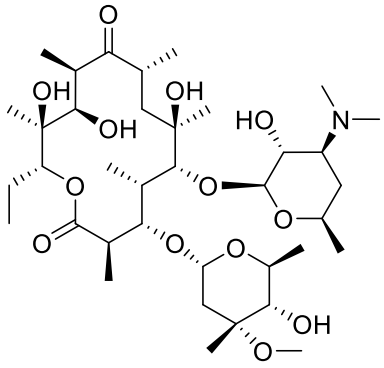

A.4

Combinatorial chemistry was another reason drug discovery efforts deviated from natural product screening.[3] This interest sparked from the ability of combinatorial libraries satisfying the high throughput screening timelines.[1] However, natural product chemists debate that combinatorial libraries failed to supplant the chemical diversity in natural products which may explain the decrease in new chemical entities reported in the past 30 years.[1] Studies show that natural products chemical diversity is more similar to approved drugs than synthetic libraries (Figure A.1).[4] These compounds are structurally complex with stereochemistry, concatenated polycyclic rings and reactive functional groups.[1] If new advances such as combinatorial biosynthesis and genomics is applied to microbial natural products then the benefits of high throughput and chemical diversity can be achieved.

Fungi remain one of the most studied microbial sources of natural products. The scope of fungal sources increased from saprophytic terrestrial strains to marine habitats and endophytes.[5] These fungal isolates are pursued for new biological activities as well as new compounds. For example, researchers analyzed slime fluxes in Japan for their fungal constituents. *Fusarium aquaeductuum* was isolated from slime fluxes in Japan and its extract found to be an inhibitor of mammalian adenosine triphosphatases.[6]

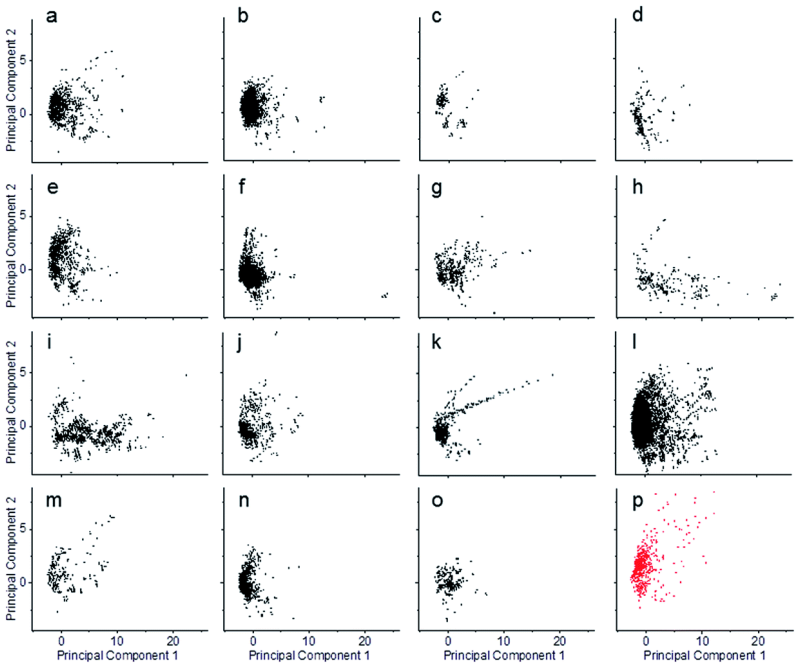

Figure A.1 Principal component analysis of 11 physico-chemical properties calculated for compounds reported from the top 15 MNP-producing phyla and approved drugs. (a) Actinobacteria, (b) Ascomycota, (c) Bryozoa, (d) Chlorophyta, (e) Chordata, (f) Cnidaria, (g) Cyanobacteria, (h) Dinophyta, (i) Echinodermata, (j) Mollusca, (k) Ochrophyta, (l) Porifera, (m) Proteobacteria, (n) Rhodophyta, (o) Tracheophyta, (p) approved drugs (red). Extracted from Natural Products Reports[4]

Aquastatin A (**A.5**) is responsible for the inhibition of Na+/K (+)-ATPase and H+/K(+)-ATPase with an IC_{50} of 7.1 μM and 6.2 μM, respectively.[6] Additional bioactivity studies determined several targets: treatment of gastric ulcers; moderate activity against an enzyme crucial for the spread of HIV(HIV-1 integrase); and it targeted type 2 diabetes and obesity.[7]

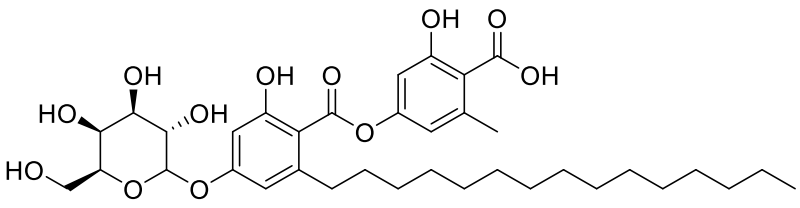

A.5

Fungi produce species specific metabolites, providing increased chemical diversity for biodiscovery.[1,2] Alkaloids, quinones, terpenoids, peptide, phenols and xanthones represents the chemical diversity from fungal origin.[8] An estimation of 10,000 fungal species are known with over a million classified as unidentified fungi, representing a prolific source for natural products.[5] The biological activity of these fungal metabolites entice pharmaceutical companies especially with recent developments. For example, within the last decade the FDA approved fingolimod (**A.6**) for the treatment of multiple sclerosis derived from its fungal metabolic precursor myrocin (**A.7**). **A.6** binds to most of the sphingosine-1-phosphate receptors.

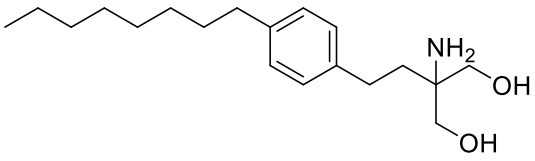

A.6

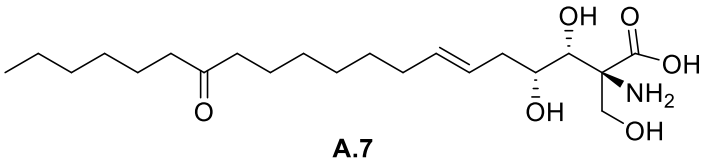

A.7

Microbial natural products have supplied therapeutic agents during the last century with over 130 commercial drugs and an additional 67 in various stages of clinical trials including antibacterial, antifungal, antiparasitic and other immunological diseases.[2] These numbers are result of natural products optimized as drug-like small molecules.[9] Natural product chemistry relevance in drug discovery relies heavily on the efficiency of selection, screening, dereplication, isolation, and structure elucidation.[1] Multiple method

development advances in these areas has increased the number of compounds reported from marine microorganisms. Fewer than 50 metabolites were reported from the 1980s – 90s to over 100 metabolites per annum in the last 20 years.[10] The latest marine natural product report reported over 600 microbial metabolites.

In this section, microorganisms isolated from ecological niches are exploited for their ability to rapidly respond to change and environmental stress. Several fungal cultures were analyzed from the internal tissues of a mangrove plant. With the drastic increase in reported compounds, dereplication strategies were implemented to reduce wasted time and effort. In chapter two, endophytic fungi are manipulated to increase the potential of synthesizing new, bioactive metabolites.

A.1 References

(1) Larsen, T. O.; Smedsgaard, J.; Nielsen, K. F.; Hansen, M. E.; Frisvad, J. C. Phenotypic taxonomy and metabolite profiling in microbial drug discovery. *Nat. Prod. Rep.* **2005**, *22*, 672–695.

(2) Lam, K. S. New aspects of natural products in drug discovery. *Trends Microbiol.* **2007**, *15*, 279–289.

(3) David, B.; Wolfender, J.-L.; Dias, D. A. The pharmaceutical industry and natural products: historical status and new trends. *Phytochem. Rev.* **2015**, *14*, 299–315.

(4) Blunt, J. W.; Carroll, A. R.; Copp, B. R.; Davis, R. A.; Keyzers, R. A.; Prinsep, M. R. Marine natural products. *Nat. Prod. Rep.* **2018**, *35*, 8–53.

(5) Schueffler, A.; Anke, T. Fungal natural products in research and development.

Nat. Prod. Rep. **2014**, *31*, 1425–1448.

(6) Hamano, K.; Kinoshita-Okami, M.; Minagawa, K.; Haruyama, H.; Kinoshita, T.; Hosoya, T.; Furuya, K.; Kinoshita, K.; Tabata, K.; Hemmi, A. Aquastatin a, an inhibitor of mammalian adenosine triphosphatases from *Fusarium aquaeductuum*. taxonomy, fermentation, isolation, structure determination and biological properties. *J. Antibiot.* **1993**, *46*, 1648–1657.

(7) Seo, C.; Sohn, J. H.; Oh, H.; Kim, B. Y.; Ahn, J. S. Isolation of the protein tyrosine phosphatase 1b inhibitory metabolite from the marine-derived fungus *Cosmospora* sp. sf-5060. *Bioorg. Med. Chem. Lett.* **2009**, *19*, 6095–6097.

(8) Higginbotham, S. J.; Arnold, A. E.; Ibañez, A.; Spadafora, C.; Coley, P. D.; Kursar, T. A. Bioactivity of fungal endophytes as a function of endophyte taxonomy and the taxonomy and distribution of their host plants. *PLoS One* **2013**, *8*, e73192–e73203.

(9) Shen, B. A new golden age of natural products drug discovery. *Cell* **2015**, *163*, 1297–1300.

(10) Hu, G.-P.; Yuan, J.; Sun, L.; She, Z.-G.; Wu, J.-H.; Lan, X.-J.; Zhu, X.; Lin, Y.-C.; Chen, S.-P. Statistical research on marine natural products based on data obtained between 1985 and 2008. *Mar. Drugs* **2011**, *9*, 514–525.

CHAPTER TWO:

USING EPIGENETICS TO UNRAVEL THE ANTI-PROTOZOAN POTENTIAL OF MANGROVE FUNGAL ENDOPHYTES

2.1 Mangrove Fungal Endophytes

Mangroves are complex ecosystems composed of halophytic tree and shrub species; these intertidal forests serve as coastal protection against storm surges and erosions in tropical and subtropical climates.[1,2] Approximately 70 species belonging to 40 genera, cover over 137,000 km^2 globally.[2] Mangroves persist in physiologically stressful conditions with repetitive disturbances and constant change.[2] These plants create forests of chemical, biological and microbial diversity.[3] Aside from ecological benefits, humans also harvest the leaves, stems, barks, roots, and fruits of mangrove plants for medicinal use.[4] Moreover, mangrove microbial studies show that these plants are rich in biologically active metabolites produced by associated endophytic fungi.[4]

The term endophyte originates from the combination of two Greek words; *endon* and *phyton,* meaning 'within plant'. The term defines any organism that dwells within a plant without infective symptoms.[5] Endophytes maintain a symbiotic relationship with host including parasitism, commensalism, and mutualism among other interactions.[5] Mainly, these microorganisms gain habitation and nutrition from their host plant and, in return, they, protect by producing bioactive metabolites that encourage growth and

competitiveness.[5] Thus, endophytes could be a dependable source of natural products for pharmaceutical and agricultural applications.

Xanalteric acid I and II (**2.1** & **2.2**) are two metabolites isolated from mangrove fungal endophytes.[6] Kjer, et al. isolated the fungus *Alternaria* sp. from the leaves of the Chinese mangrove (*Sonneratia alba*).[6] The use of this plant in traditional medicine to treat skin and intestinal parasites encouraged the pursuit of biologically active metabolites.[6] Compounds **2.1** and **2.2** exhibited weak antibiotic activity against multidrug-resistant *Staphylococcus aureus*.[6]

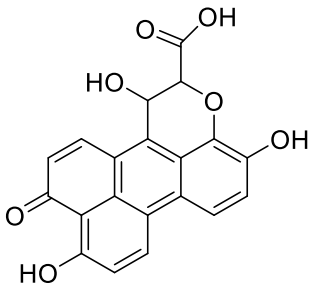

2.1

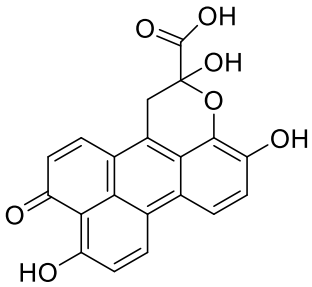

2.2

Endophytic microorganisms from terrestrial sources have demonstrated their biomedical importance since the discovery of the anticancer drug taxol (**2.3**).[7–9] Taxol was initially isolated from the Pacific Yew tree (*Taxus brevifolia*) but later it was discovered that an endophytic fungus (*Taxomyces adreanae*) produced this potent terpene.[10,11] The discovery of taxol and other natural product therapeutics directed attention to endophytic microbial secondary metabolites from marine and terrestrial sources.[12]

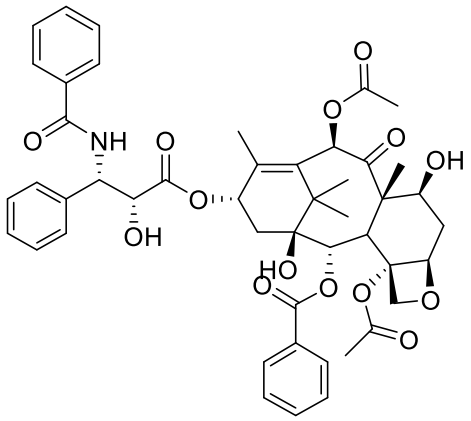

2.3

Approximately one million species of endophytic fungi exist. Considered hyper-diverse, there is considerable potential for chemical diversity.[13–15] There are only a few strains of endophytic fungi described demonstrating how underrepresented they are. New strains of microorganisms that colonize plants in different ecological niches and ecosystems may be a source of novel secondary metabolites.[5]

2.2 Targeting Epigenetic Pathways of Endophytic Fungi for Drug Discovery

Fungi and bacteria can generate a complex chemical profile.[16] For instance, a *Streptomyces* bacterium produced four compounds originating from three biogenetic pools. The gabosines D (**2.4**) and E (**2.5**) are products of the sugar pathway, hexayclinic acid (**2.6**) biosynthetically originates from type I polyketide pathway and **2.7** is a derivative of the nucleoside angustmycin A. Manipulation of cultivation conditions can influence biosynthesis at transcriptional, translational and enzyme levels to yield variations of new natural products.[16]

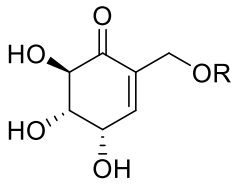

2.4 R = Ac
2.5 R = H

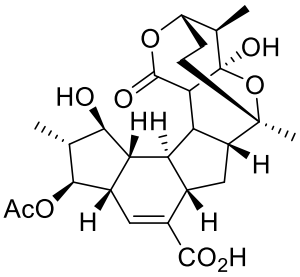

2.6

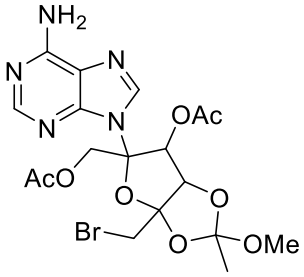

2.7

While 99% of microorganisms that exist in nature remain unculturable, it is easier to access the metabolomes of those that will culture by varying culture conditions.[17,18] Manipulation of growth conditions emulating environmental stressors such as antibiotics,[19] antifungals,[20] salinity[21,22] or simply adding unsterilized portions of microbial-associated hosts[20] has proven successful. The one strain-many compounds (OSMAC) approach aims to maximize secondary metabolism of microorganisms by changing the fermentation conditions such as culture vessel, enzyme inhibitors, or aeration rate to 'wake up' silent gene clusters.[23] Enzyme inhibitors that can combat the suppression of metabolic pathways in laboratory conditions and the low success rate of cultivation by phenotypic change to the DNA without alteration to the genetic code defines epigenetics.[24] DNA methylation, non-coding RNAs, histone covalent modification, methylation, and other modifications of cytosines on the DNA are molecular mechanisms involved in altering gene expression.[25,26] Histone acetylation is one of the well-studied mechanisms for chromatin remodeling. Histone acetylation has shown great potential in uncovering new fungal secondary metabolites.[27]

2.2.1 Histone-acetylation

Histone acetylation, first described in 1964, is regulated by two families of enzymes: histone acetyltransferases (HAT) and histone deacetylase (HDAC).[28] HATs catalyze the transfer of an acetyl group to the ε-amino group of lysine side chains to neutralize the positive charge using acetyl-CoA. This transfer results in a relaxed conformation of the chromatin, allowing transcription. HDACs oppose the mechanism of HATs to restore the lysine residues to its initial positive charge by reversing the acetylation of the lysine residue (Figure 2.1). HAT and HDAC are useful for targeting genes and sequence-specific transcription factors.[29] The euchromatin conformation is the most favorable for gene expression, compared to its tightly coiled heterochromatin conformation, which disfavors gene expression.

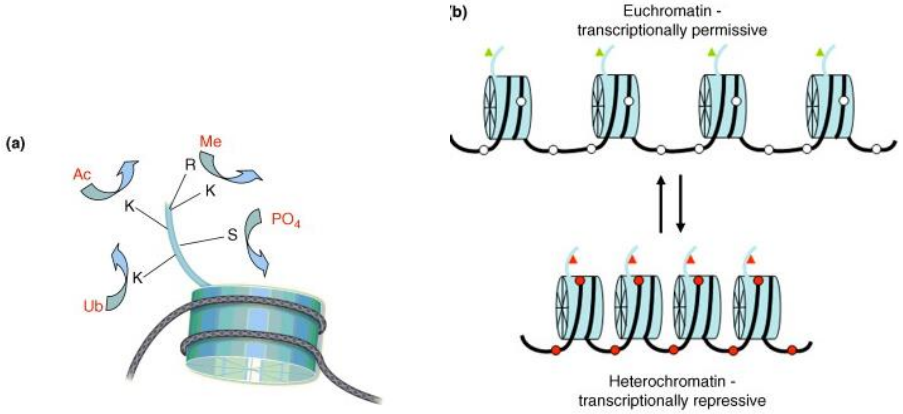

Figure 2.1. Illustration of **(a)** posttranslational modifications that occur on histone proteins that participate in chromatin remodeling. **(b)** The conformational changes that occur in chromatin, induced by posttranslational modification of histones and DNA that impact gene transcription.[30]

In the search for new chemodiversity, inhibition of HDACs may upregulate secondary metabolism. Beau et al. described the effects of the varying concentrations of an HDAC inhibitor on *Aspergillus niger.*[31] LC/MS analysis determined that sodium

butyrate (**2.8**) as an HDAC inhibitor was active at 100 μM, displaying distinctive peaks not present in the untreated fungal extract and later identified as a new natural product. Using epigenetic modulators increase the potential of expressing cryptic gene clusters to potentially synthesize new metabolites.

2.2.2 DNA methylation

DNA methylation is another popular mechanism of gene expression under epigenetic regulation. DNA methyltransferases (DNMTs) execute the transfer of a methyl group to the C-5 position of a cytosine residue from *S*-adenosyl-methionine (SAM).[24] Studies by Beau et al. determined the optimal DNMT inhibitor for fungal epigenetics and selected the widely used 5-azacitidine (**2.9**) at an optimal concentration of 50 μM and an incubation period of 21 days.[31] Although there were no results of a modified culture using a DNMT inhibitor, increased activity against methicillin-resistant *Staphylococcus aureus* was seen in the small-scale DNMT treated culture when compared to the untreated. In addition to new secondary metabolites, biological activity increased within the chemically modified cultures.

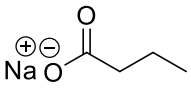

2.8

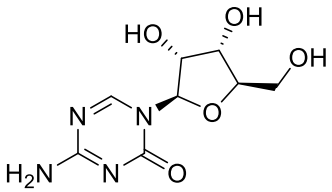

2.9

Endophytic fungi usually spend most of their lifetime dormant in the host until signaled to be a facultative pathogen.[5] Therefore, most of the potential biochemical activity when biotic stressors are detected. In laboratory conditions, microorganisms do

not express the full complement of genetically-encoded secondary metabolites.[14] It is difficult to fully imitate environments with extreme and harsh stressors. Many microorganisms depend on several factors to thrive; the number of uncultivable microbes illustrates our lack of knowledge. The successfully cultured microbes grown in laboratory conditions may suppress their defensive mechanisms, prompting the silence of biosynthetic pathways responsible for generating secondary metabolites.[32] Recent advances in epigenetics revealed an approach for expressing silent gene clusters in microorganisms to discover novel secondary metabolites.[23]

2.3 Dereplication Strategies

Bioassay-guided fractionation methodologies are usually a part of high throughput natural products screening. Even though validation of this method is evident by successful isolation of bioactive compounds, it is a rather costly method with high risks of isolating known compounds.[33] Thus, dereplication techniques are necessary for early identification of known versus new compounds. Moreover, they are a useful tool to reduce wasted efforts and financial resources.[33] As described, the OSMAC approach yields permutations of metabolites from the same metabolic pathways. With the increasing number of microbial natural products reported every year reiterative isolation is inevitable. However, recent developments have established multiple avenues for early identification of known compounds using hyphenated techniques. LC-UV, LC-MS, LC-MS/MS, and LC-NMR are used individually or in combination based on their advantages.[34] Dereplication strategies can become complicated especially when taxonomy is not available. Fungal natural product chemistry is rich in bioactive metabolites called mycotoxins, but rapid identification of these compounds through taxonomy can be tedious.

Several techniques can harness the metabolome of an extract. Liquid chromatography paired with a detector of some sort is the basis of the workflow in de-replication. However, the data obtained is useless if it is not compared to known compounds. Several sources of natural products compose databases such as Metlin and Agilent Mycotoxin libraries of MS/MS spectral data. MS/MS or Tandem MS refers to a multistep experiment within mass spectrometry, including ionization of compounds from a primary source, followed by fragmentation of precursor ions. The second quadrupole generates the MS2 providing a fingerprint for that compound (Figure 2.2).

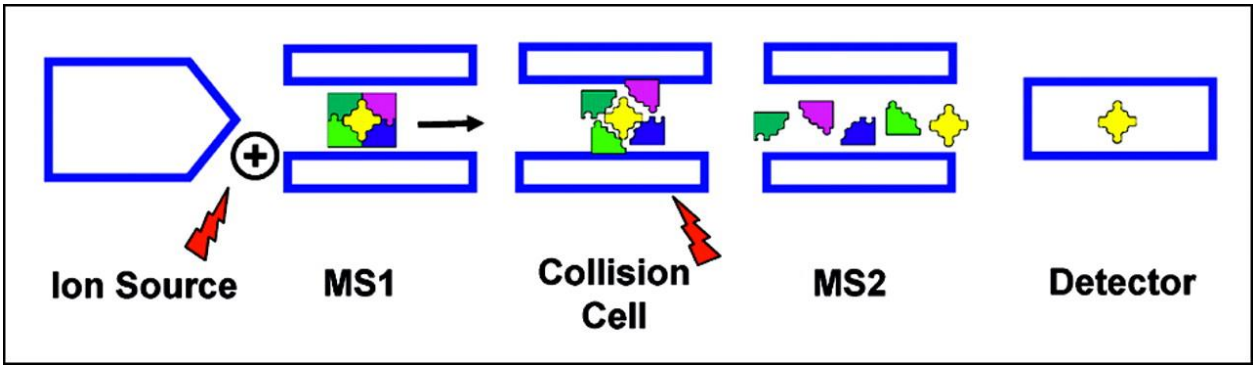

Figure 2.2 Overview of tandem MS[35]

With dereplication methodologies applied to natural product screening for new and bioactive metabolites, the limitations of natural product studies are reduced. The rate-determining step in this dereplication process is the amount of data available in the databases. Accuracy in this strategy can result in the identification of similar compounds with similar chemical profiles. Therefore, an additional step for confirmation of the compound should be incorporated.

2.4 Research objectives

Fungal endophytes are underrepresented among microbial sources for new compounds as a result of their hidden nature.[14] Chemical diversity is evident with reports of polyketides, alkaloids, peptides, proteins, shikimates, isoprenoids as well as hybrids of these metabolites. With only a few plants extensively studied for their endophytic fungal biodiversity and chemodiversity, a plethora of plants and ecological niches remain untouched as targets for biologically active natural products.

Within this chapter, the screening of mangrove fungal endophytes from Western Florida and Tapachula, Mexico against amoebic pathogens is a continuation of an established high throughput screening program. Extracts from fungal endophytes collected from the mangrove plants were screened against pathogenic parasites. Subsequently, small-scale hits in these biological assays were grown in large scale cultivation to pursuit the biologically active component of the extracts. Further developments into the identification of these active components incorporated tandem mass spectrometry. The addition of mass spectrometry allowed incorporation of dereplication databases for early identification of known fungal metabolites and prioritizing fractions with unidentified compounds.

The three fungal endophytes previously described were grown in two different treatments, the addition of DNA methyltransferase inhibitors (DNMTi), also in the absence of an epigenetic modulator (Control). However, bioassay-guided isolation of active fungal extracts led to the isolation of previously described mycotoxins. This method of fractionation does not distinguish known and new compounds and should be coupled with chemical analysis to be effective. With over 246,000 natural products reported[36] and

approximately 4000 added per annum, the risk of re-isolating known compounds increases. Dereplication strategies are considered an essential tool to detect known compounds in early stages of the isolation process.[33]

Tandem MS is an analytical tool for developing dereplication strategies in the pharmaceutical industry for identification of proteins,[37] lipids[38], and small molecules providing simplified sample prep and a low limit of detection.[39] Coupling tandem MS with HPLC provides an effective route of fast detection of known compounds. In the following section, a protocol established by Knestrick,[40] using MS/MS spectrometry facilitated the fractionation of an active fungal extract displaying anti-amoebic activity. At each stage of separation, the samples were prioritized based on identification of compounds from an Agilent Mycotoxin database. Samples that contained mycotoxins were de-prioritized, and the remaining samples were further separated.

2.5 High Throughput Screening Against Amoebic Infections

2.5.1 Naegleria fowleri

In this project, a high throughput screen against a panel of infectious disease utilized miniaturized culture conditions to examine the effects of epigenetic regulators on secondary metabolite expression.[3] Of the 9048 samples screened against *N. fowleri,* 57 extracts displayed a 33-67% inhibition at the lower concentration of 5 µg/mL. There was a higher number of actives at the higher concentration of 50 µg/mL with a total of 271 actives with inhibition more significant than 33% (Figure 2.3).

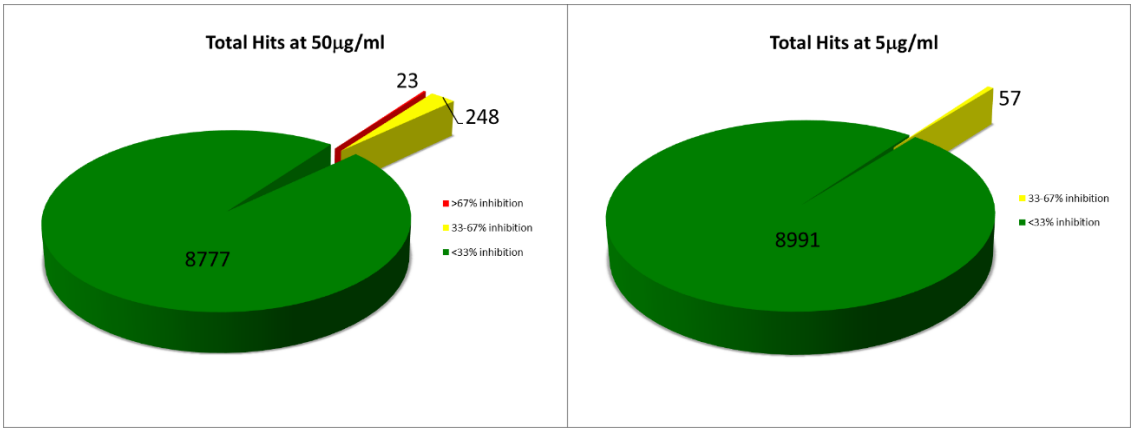

Figure 2.3 Numbers of active hits at 5 µg/mL and 50 µg/mL against *N. fowleri* at three concentrations.[3]

After identification of the extracts active against *N. fowleri*, efforts were then focused on identifying the active components. To refine the number of actives a scaling system was introduced to prioritize the active extracts. Cytotoxicity screening provided an activity index (AI) for each active extract. All cytotoxic extracts were eliminated leaving five fungal organisms. One of the five was grown with an epigenetic regulator (DNMTi) (Table 2.1).

Table 2.1 Extracts with activity index > 9 against *N. fowleri.*

Sample ID	Parasite IC_{50} (µg/mL)	Cytotox IC_{50} (µg/mL)	Index
TAP14-58A-4-Control(A)	0.19	> 50	>270
TAP14-151C-1-Control(B)	0.21	> 50	>236
TAP14-151C-1Control(A)	0.27	> 50	>183
TAP14-58A-4-DNMT(A)	0.35	> 50	>141
TAP14-58A-5-Control(A)	0.54	> 50	>92
TAP14-58A-4-Control(C)	0.90	> 50	>56
TAP14-58A-5-Control(B)	0.85	39	46
TAP14-58A-4-DNMT(B)	1.2	> 50	>41
TAP14-151C-1-Control(C)	1.3	> 50	>37
CC10-31A-2- Control(C)	1.6	25	16
TAP14-58A-4-Control(B)	3.7	> 50	>13
CC10-31A-2-Control(A)	2.1	21	9.7
CC10-31A-2-Control(B)	2.8	26	9.3

2.5.2 Acanthamoeba sp.

To further investigate the potential of the fungal library, a second amoeba was incorporated into the screen. Following protocols from the previous amoeba screen, the samples were tested at two concentrations – 50 µg/mL (high) and 5 µg/mL (low). In this assay against *Acanthamoeba* sp. 142 extracts were deemed active at the high concentration, and 36 extracts were active at 5 µg/mL (Figure 2.4).

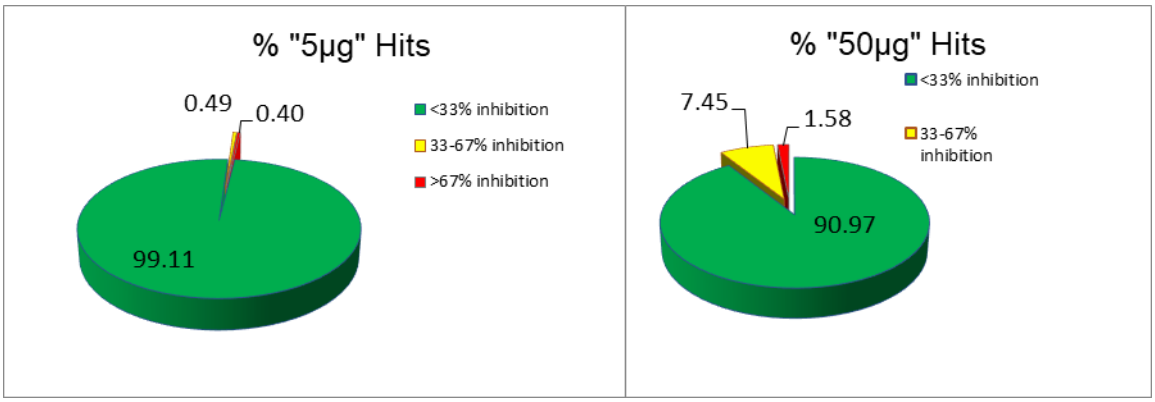

Figure 2.4 Percentage of active hits at 5 µg/mL and 50 µg/mL with inhibition >67%against *Acanthamoeba* sp. (Figure created by Christopher Rice, University of Georgia)

The prioritization protocol determined cytotoxicity using J774 cell line of the 36 potent fractions. The activity index requirement for this was reduced to 1 because the initial criteria would eliminate all but one organism. As with the previous representation, only control and DNMT conditions appeared in the prioritized extracts. (Table 2.2)

Table 2.2 Extracts that have SI greater than 1 against *Acanthamoeba* sp.

Sample ID	Parasite IC50 (µg/ml)	Cytotoxicty IC50 (µg/ml)	Selecti vity Index
TAP14-55A-2-CONTROL(B)	3.0	> 50	>17
TAP14-55A-2-CONTROL(A)	3.3	> 50	>15
TAP14-55A-2-CONTROL(C)	3.4	47	14
TAP14-55A-2-DNMT(C)	2.9	25	8.7
TAP14-55A-2-DNMT(A)	3.7	28	7.5
TAP14-55A-2-DNMT(B)	11	> 50	>4.6
HM13-18C-2(B)	12	50	4.2

2.6 Bioassay-directed fractionation of a Penicillium sp. (TAP14-55A-2-DNMT)

The root tissue of a white mangrove plant was collected in Tapachula, Mexico for isolation of endophytic fungi. The tissue culture was surface sterilized and placed on an agar plate made with actino solid media. After isolation of this *Penicillium* fungus from the 'field' agar plate the fungus was grown on Sabouraud dextrose agar (SDA) and subsequently stored in 20% glycerol stock solution. For large scale growth a swab of the glycerol stock containing this fungus was inoculated onto SDA plate. After 50% of the gar was covered with fungal lawn, cubes of agar inoculated with the fungus were transferred into broth and then onto the rice medium.

The sample TAP14-55A-2 grown under DNMTi conditions possessed an average selectivity index of 7 (Table 2.2). Large scale cultivation increased the biomass for chemical analysis to 25.0 g of crude material. This sample was subjected to separation via liquid-liquid extraction using a 70% aqueous MeOH mixture to dissolve the sample and distilled *n*-hexane for partition. The partition separated into two layers, a lipophilic and a hydrophilic layer, which was collected separately using a separatory funnel. The lipophilic layer was expected to extract the lipids and fatty acids that dominated the

extracts. The hydrophilic layer, therefore, was pursued, which displayed an IC_{50} of 4.83 µg/mL and was subjected to further liquid-liquid extraction using EtOAc and H_2O.

The organic layer retained an IC_{50} of 5.03 µg/mL against *Acanthamoeba* sp. A total mass of 1.8 g remained and was dried onto silica gel in preparation for normal phase MPLC. A gradient using *n*-hexane and EtOAc resulted in 11 MPLC fractions. Bioassay-guided fractionation coupled with NMR analysis determined the prioritization of fractions. The relatively nonpolar fractions D and F had an IC_{50} of 21.1 and 22.6 µg/mL, respectively, and analysis of their ^1H NMR spectrum led to further fractionation. Semi-preparative normal phase HPLC of fraction D led to eight fractions. The sixth peak displayed ^1H NMR with terpene-like signals and was subsequently purified using reverse phase HPLC yielding SALT-12. SALT-13 was the major component of fraction F and was isolated using normal phase HPLC (Scheme 2.1).

2.6.1 Elucidation of SALT-12

Analysis of the ^1H NMR spectrum indicated that SALT-12 had eight methyl groups; three vinyl methyl groups, one oxygen bearing methyl and the remaining were aliphatic methyl groups. HRESIMS (*m/z* 487.273) $[M+H]^+$ revealed the molecular formula as $C_{28}H_{38}O_7$ (calcd for $C_{28}H_{39}O_7$)matching literature values of andrastin A (**2.10**). This meroterpenoid is a fungal metabolite originally isolated from a *Penicillium* sp. identified as an inhibitor of the protein farnesyltransferase at 24.7 µM. The biosynthetic pathway was determined to be a hybrid of a sesquiterpene and a tetraketide relating them to another compound named citreohybridonol with a C-6/C-23 lactone bridge.

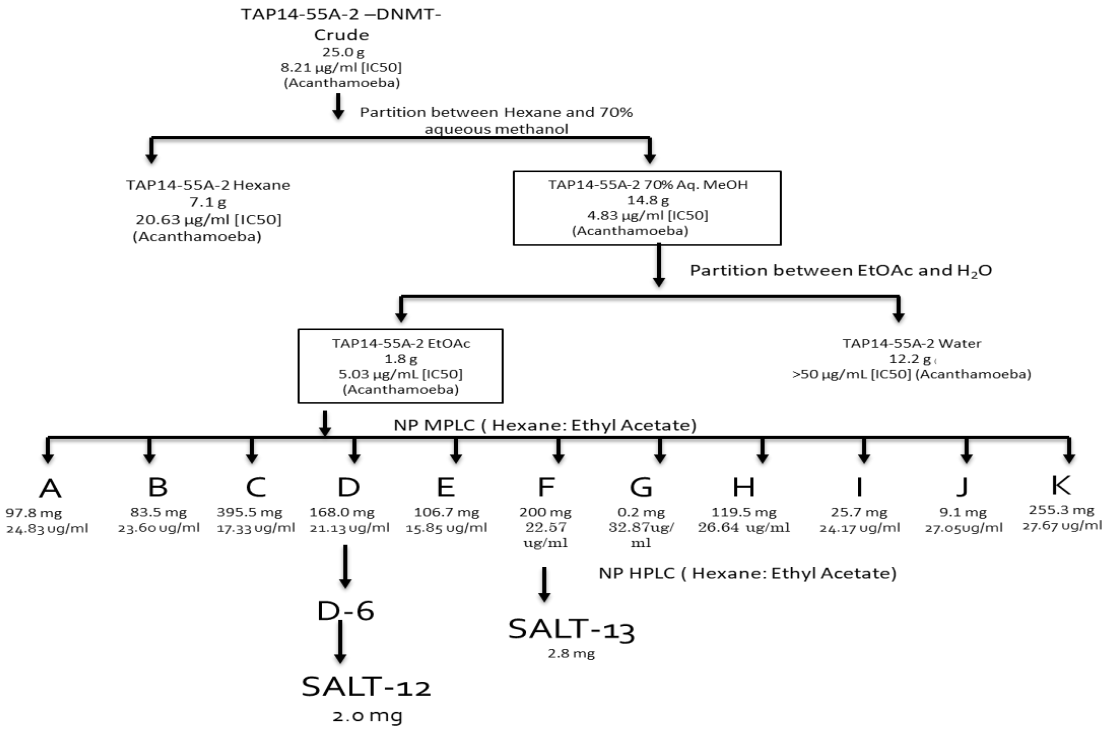

Scheme 2.1 Bioactivity-guided fractionation of TAP14-55A-2-DNMT

Analysis of the ^{1}H and ^{13}C NMR spectra (Table 2.3) identified four carbonyls (an aldehyde, a ketone, and two esters) and two pairs of olefinic carbons, accounting for six of ten degrees of unsaturation, indicating a four-membered ring scaffold. Two-dimensional NMR data confirmed the identification of SALT-12. The HSQC NMR spectrum facilitated the identification of eight methyl groups, four methylene groups, five methine carbons, and eleven quaternary carbons. The COSY spectrum established the spin systems which were utilized to form the scaffold of the structure when coupled with the HMBC experiment. The HMBC was key component to assigning carbons especially in the proton deficient portion of the scaffold. Assignment of the keto-enol ring relied heavily on the HMBC and ^{1}H NMR shifts.

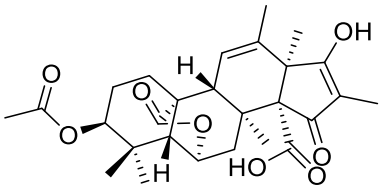

2.10

Table 2.3 ^{1}H NMR (400 MHz) and ^{13}C NMR (125 MHz) Data of SALT-12 and Andrastin A in MeOH-d_4

Position	SALT-12		Andrastin A
	δ_C, mult.	δ_H (J in Hz)	δ_C, mult.
1	29.2, CH_2	0.98, ddd (5.0, 12.4, 13.0) 2.30, ddd (3.3, 3.3, 12.4)	29.0, CH_2
2	24.5, CH_2	1.59, m 2.05, m	24.3, CH_2
3	79.2, CH	4.62, dd (2.4, 2.4)	79.0, CH
4	38.2, C		38.0, C
5	49.8, CH	1.84, dd (2.4, 15.7)	49.6, CH
6	18.1, CH_2	1.70, m 2.08, m	17.9, CH_2
7	33.7, CH_2	2.25, ddd (3.1, 3.1, 12.9) 3.00, ddd (4.0, 12.9, 13.0)	33.5, CH_2
8	43.0, C		42.8, C
9	55.0, CH	2.13, br s	54.8, CH
10	53.6, C		53.4, C
11	123.8, CH	5.39, br s	123.6, CH
12	137.2, C		137.0, C
13	58.0, C		57.8, C
14	69.0, C		68.8, C
15	187.8, C		187.4, C
16	114.7, C		114.5, C
17	200.1, C		200.4, C
18	172.4, C		172.2, C
19	21.4, CH_3	2.05, s	21.2, CH_3
20	27.3, CH_3	0.95, s	27.1, CH_3
21	21.7, CH_3	0.88, s	21.5, CH_3
22	20.0, CH_3	1.24, s	19.8, CH_3
23	206.8, CH	10.18, s	206.8, CH
24	20.0, CH_3	1.75, br s	19.8, CH_3
25	16.4, CH_3	1.16, s	16.0, CH_3
26	171.8, C		171.8, C
27	52.3, CH_3	3.58, s	52.2, CH_3
28	6.4, CH_3	1.59, s	6.4, CH_3

2.6.2 Elucidation of SALT-13

SALT-13 resulted after two rounds of chromatographic separation of MPLC fraction F (Scheme 2.1). The molecular formula of SALT-13 deduced as $C_{17}H_{24}O_6$ (calcd for $C_{17}H_{25}O_6$) from HRESIMS (*m/z* 307.1572 $[M+H]^+$) and one-dimensional NMR data (Table 2.4). SALT-13 matched mass and chemical formula for eremofortin D, but spectroscopic data was not found for this compound in the literature. Therefore, two-dimensional NMR data facilitated the elucidation of this compound for confirmation.

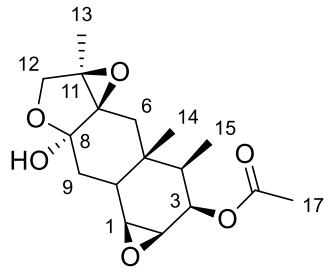

2.11

The degree of saturation was calculated as six with only one designated to the ester carbonyl at δ_C 171.0 (C-16), and the remaining indicated a five-ring skeleton. Moreover, 23 protons (five methines, three methylenes, and four methyls) were assigned using HSQC NMR data with DEPT filter, and the remaining proton was allocated to a hydroxy group. The COSY NMR spectrum revealed a six-membered spin system containing three oxymethines H-1, H-2, H-3, H-4 (δ_H 3.17, 3.47, 5.25, 1.66, respectively), and the methylene signals at δ_H 2.31 and 1.92 (H_2-9) with the shielded methine at δ_H 2.26 (H-10). Correlations of H-10 to the quaternary carbon at δ_C 38.4 (C-5) and the methine δ_C 43.9 (C-4) established a six-membered ring. HMBC was utilized heavily to assign the adjacent six-membered ring. H_2-9 correlated to the deshielded C-8 (δ_C 102.1) and C-7 (δ_C 68.3). Moreover, the sp^3 methylene signals at δ_H 1.81, 1.39 (H_2-6) correlated to C-8 and C-5.

Table 2.4 ^{1}H NMR (400 MHz) and ^{13}C NMR (100 MHz) Data for SALT-13 in $CDCl_3$

Position	δ_C , Mult.	δ_H (J in Hz)
16	171.0, C	
8	102.0, C	
3	71.3, CH	5.25, t (5.39 x2)
12	69.8, CH_2	3.84, d (1.17)
7	68.3, C	
11	61.1, C	
1	57.5, CH	3.17, d (3.86)
2	50.2, CH	3.47, t (4.47 x2)
4	43.9, CH	1.66, q
10	41.7, CH	2.26, brs
5	38.4, C	
6	35.6, CH_2	1.81, d
		1.39, d
9	34.3, CH_2	2.31, d
		1.92, dd
17	20.9, CH_3	2.14, s
14	15.5, CH_3	1.17, s
13	11.3, CH_3	1.46, s
15	9.7, CH_3	0.92, d (7.08)

The deshielded oxygen-bearing methylene at δ_H 3.84 (H-12) was placed in the furan ring because of its HMBC correlations to C-7 and C-8 and C-11 (δ_C 61.1). The remainder of the furan included two deshielded carbons, C-7 and C-11 established by their ^{13}C NMR shifts. The scaffold of the compound was established as a 6,6,5-fused ring system. Three methyl groups, one ester, one hydroxy and two oxygens were remaining after the scaffold of the compound was formed. The ester was placed as an acetyl substituent on C-3 (δ_C 71.3) because of the deshielded shift of methine (H-3) assigned to this carbon by HSQC. The doublet methyl signal at δ_H 0.92 (H_3-15,) was assigned as a substituent on C-4 because it was the only shielded methine remaining with an incomplete valence and confirmed by the COSY correlation of H_3-15 and H-4. The shielded methyl singlet at δ_H 1.17 (H_3-14) indicated its assignment to quaternary center, C-5 along with the supporting

HMBC correlation. The final methyl group H_3-13 (δ_H 1.46) was assigned by HMBC to the oxygen-bearing carbon, C-1. The hydroxyl group was verified as a substituent on C-8 because of its ^{13}C NMR shift indicating a hemiketal as it is adjacent to the oxygen of the furan ring. The valence of four oxygen-bearing carbons was incomplete, yet only two oxygens remained. Therefore, the remaining oxygens were assigned as epoxides satisfying the unsaturation of this compound.

Stereochemical analysis of SALT-13 required a NOESY experiment for the assignment of the achiral centers. The methyl H_3-14 displayed a correlation to the methyl group on the acetate unit (H_3-17). These bonds were placed on the same face in axial positions. The deshielded shift of H-6a indicated the anisotropic effect of the adjacent epoxide and was placed on the same face. H-6a also shared an NOE correlation with H-14, therefore the were all placed on the same face of the molecule. H_3-17 also displayed a weak NOE correlation to H-15. The multiplicity of the protons on H_2-9 facilitated their configuration relative to the H-10 methine; H-9a displayed a doublet and H-9b a doublet of doublets which indicated that H-9a formed a 90° angle to the methine H-10. Comparison of this configuration matched the crystal structure reported in the literature.

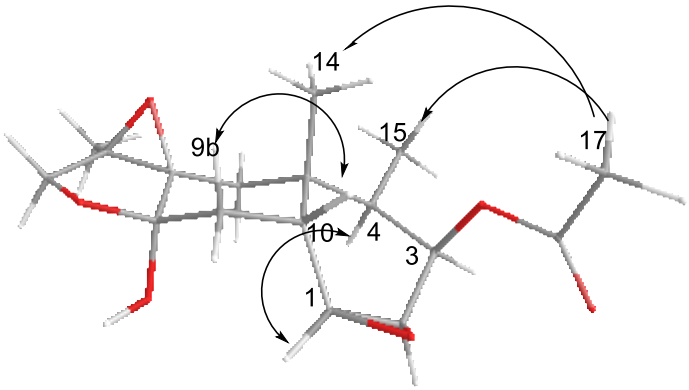

Figure 2.5 Structure of SALT-13 showing relative stereochemical configuration.

The compound was tested in its pure form against *Acanthamoeba* sp., but it did not display significant activity. Cytotoxicity was also tested using the J774 cell line and it was inactive.

2.7 Bioassay-directed fractionation of TAP14-55A-2-Control extract

Following the previous section, this fungus was prioritized because of its selectivity index of 15. The same *Penicillium* sp. was grown in a different condition than the previous section. This fungus was grown in the absence of the epigenetic regulator. Large-scale cultivation increased the biomass of this extract to 36.1 g. The extract was subjected to separation via liquid-liquid extraction. A 70% aqueous MeOH mixture was used to dissolve the sample followed by de-fatting with distilled hexane to partition the extract into lipophilic and hydrophilic layers. The lipophilic layer was expected to extract the lipids and fatty acids that dominated the extracts. The lipophilic layer had an IC_{50} of 20.63 µg/mL and the hydrophilic layer displayed an IC_{50} of 4.83 µg/mL. The hydrophilic layer was further separated using EtOAc/H_2O for liquid-liquid extraction.

The EtOAc layer retained an IC_{50} of 5.03 µg/mL against *Acanthamoeba*. The organic layer yield 3.0 g and was dried onto silica gel in preparation for normal phase MPLC. The gradient of hexane and EtOAc resulted in 11 fractions. Bioassay-guided isolation coupled with NMR analysis determined the priority of fractions. Fraction F had characteristic peaks of alkaloid and terpene peaks in ^1H NMR spectrum; combined with an IC_{50} of 33.9 µg/mL, it was prioritized for further separation using NP HPLC. Eighteen fractions resulted from this chromatograph with activities ranging from 19-26 µg/mL (Scheme 2.2).

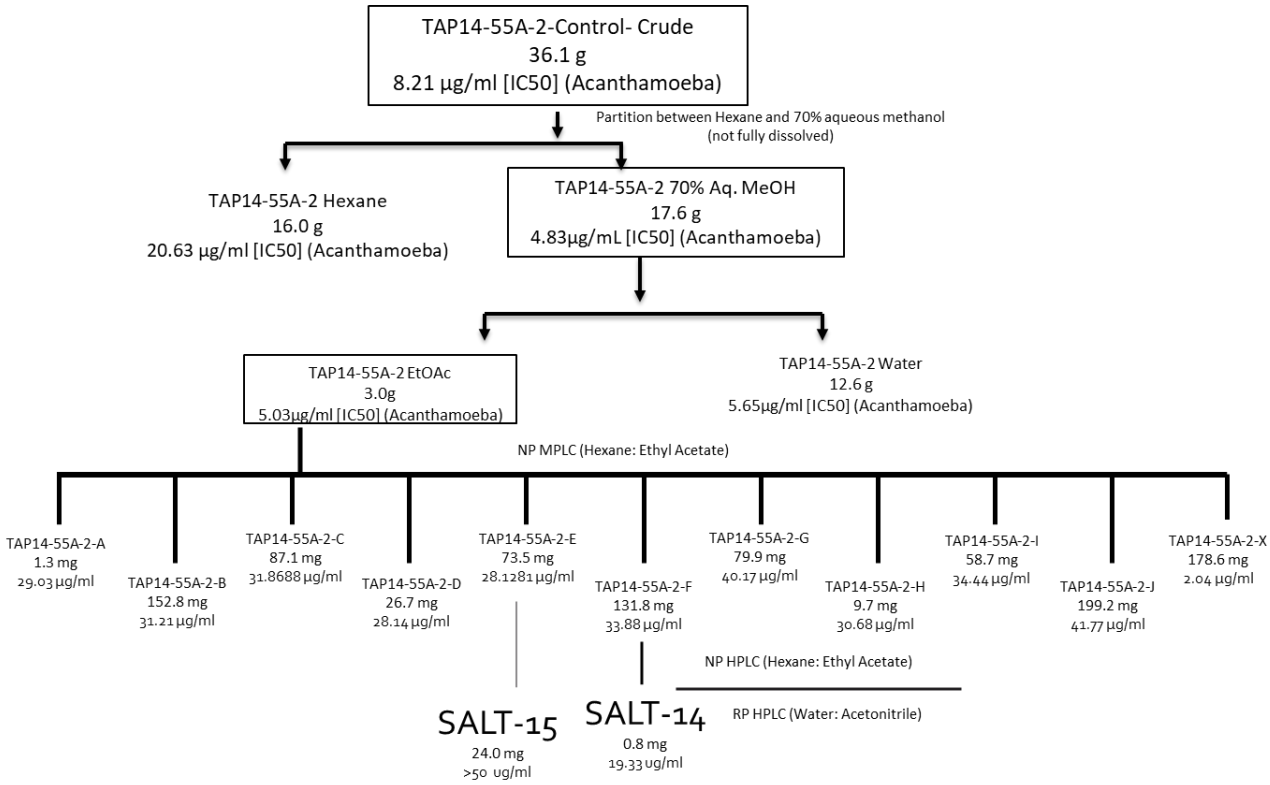

Scheme 2.2 Bioassay-guided fractionation of TAP14-55A-2-Control

2.7.1 Identification of SALT-15

MPLC fraction E, Scheme 2.2, was subjected to LCMS analysis, which determined a single principal component. The HRESIMS indicated that the molecular formula of that compound was $C_{28}H_{44}O_3$ (calcd $C_{28}H_{42}O_2$), indicating the degree of unsaturation as seven. The ^{13}C NMR spectrum displayed 28 carbons, including two pairs of olefinic carbons (Table 2.5). The HSQC NMR experiment accounted for 43 protons, including one hydroxy group. The ^{13}C NMR spectrum suggested the presence of three oxygen-bearing carbons, in agreement with the total number of oxygens. A peroxide moiety was then formed with the remaining two oxygens on C-5 and C-8. Comparison of the NMR data to the reported values of ergosterol peroxide indicated that SALT-15 NMR shifts were similar

(Table 2.5). SALT-15 was tested against *Acanthamoeba* sp. but did not display any activity against this free-living amoeba.

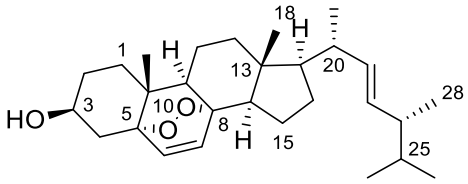

2.13

Table 2.5 Comparison of NMR data for SALT-15 (400 MHz and 125MHz, $CDCl_3$) and ergosterol peroxide (25.2 MHZ, $CDCl_3$)

Position	SALT-15		Ergosterol peroxide
	δ_C Mult.	δ_H (J in Hz)	δ_C (Literature)
1	34.6, CH_2		34.7, CH_2
2	30.0, CH_2		30.0, CH_2
3	66.3, CH	3.97, m	66.2, CH
4	36.9, CH_2		36.8, CH_2
5	82.1, C		82.1, C
6	135.4, CH	6.51, d (8.7)	135.0, CH
7	130.7, CH	6.24, d (8.7)	130.5, CH
8	79.4, C		79.3, C
9	51.0, CH		51.0, CH
10	36.9, C		36.9, C
11	23.3, CH_2		23.4, CH_2
12	39.7, CH_2		39.7, CH_2
13	44.5, C		44.5, C
14	51.6, CH		51.6, CH
15	20.6, CH_2		20.6, CH_2
16	28.6, CH_2		28.6, CH_2
17	56.1, CH		56.1, CH
18	12.8, CH_3	0.82, s	12.8, CH_3
19	18.1, CH_3	0.88, s	18.1, CH_3
20	39.7, CH		39.6, CH
21	20.8, CH_3	0.91, d (6.6)	20.8, CH_3
22	135.2, CH	5.22, dd (15.2, 7.6)	135.3, CH
23	132.2, CH	5.14, dd (15.3, 8.2)	132.1, CH
24	42.7, CH		42.7, CH
25	33.0, CH		33.0, CH
26	19.6, CH_3	0.82, d (12.6)	19.6, CH_3
27	19.9, CH_3	0.83, d (17.1)	19.9, CH_3
28	17.5, CH_3	1.00, d (6.6)	17.5, CH_3

2.8 Bioassay-directed fractionation of CC10-31A-2-Control

The stem tissue was collected from mangrove plant along the Courtney Campbell bridge in Tampa, Florida. This sample was surface sterilized and inoculated onto a field plate. Gradual isolation of fungal cultures resulted after weeks of growth on the field agar plate. This unidentified fungus was then grown on Sabouraud dextrose agar (SDA) for further analysis.

Selected from the top 5 organisms with activity index greater than 9 against *N. fowleri,* this fungus was grown in the absence of the epigenetic modulators. After extraction, the dried sample with a mass of 23.0 g was subjected to separation via liquid-liquid partition using 70% aqueous MeOH and *n*-hexane followed by the partition of the aqueous methanol partition fraction with EtOAc/H_2O. As previously mentioned, the lipophilic layer was expected to extract the lipids and fatty acids that dominated the extracts in the first partition and the second partition aimed to remove hydrophilic substances. The EtOAc layer yielded 3.0 g of sample and was subsequently dried onto silica gel and further purified by normal phase MPLC using a gradient of hexane to EtOAc. This separation resulted in 21 fractions with potent activity as low as 0.06 µg/mL. Bioassay-guided fraction coupled with NMR analysis determined the priority of fractions. Fractions P and Q were prioritized and subjected to NP HPLC followed by RP HPLC (Scheme 2.3).

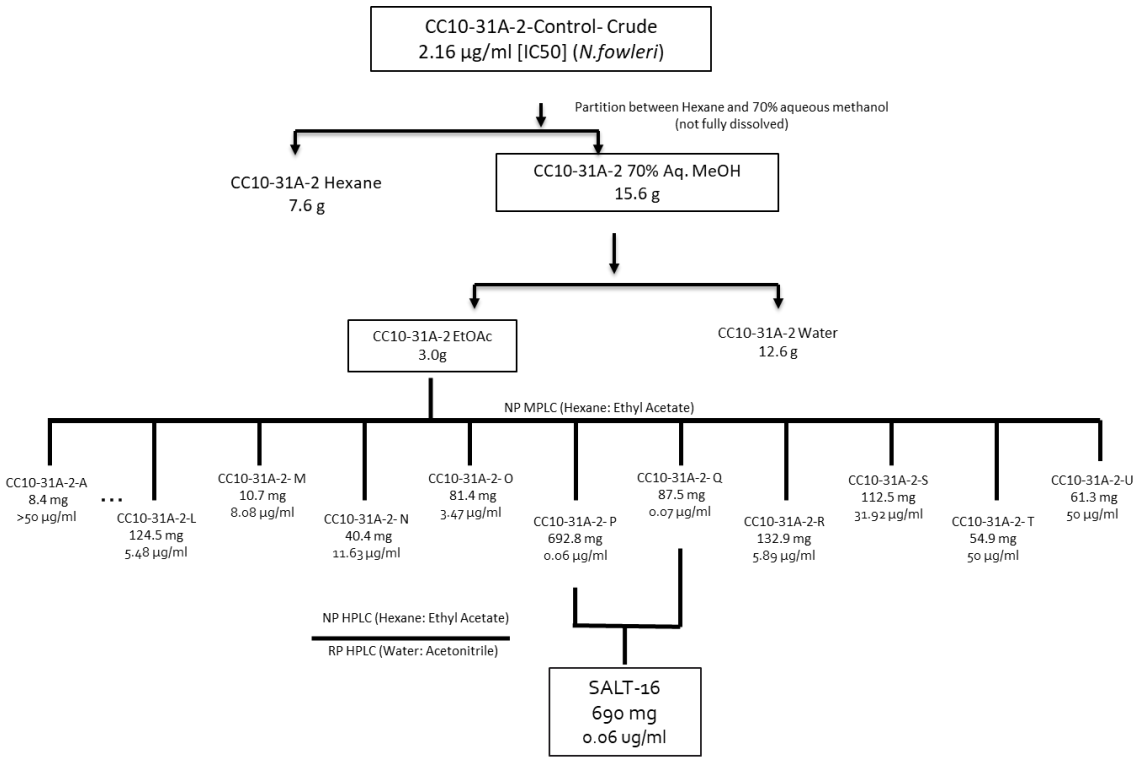

Scheme 2.3 Bioactivity-directed purification of CC10-31A-2 Control

2.8.1 Structure elucidation of SALT-16

Fraction P exhibited activity against *Naegleria fowleri* at a concentration of 0.06 µg/mL, placing it as a high priority for identification of the active component. HRESIMS showed a molecular formula of $C_{28}H_{33}NO_7$ (calcd $C_{22}H_{28}NO_7$), which indicated 12 degrees of unsaturation. The ^{13}C NMR spectrum displayed ten olefinic carbons and three carbonyls, suggesting a four-ring skeleton. gHSQCAD NMR accounted for 31 of the 33 protons within the compound. The ^{1}H NMR displayed signals within the aromatic region, which were assigned to an aromatic ring with partial structures formed and utilizing online databases assisted in identifying similar scaffolds. The search led to the assignment of SALT-16 as cytochalasin E (**2.17**). The stereochemical configuration was confirmed by x-ray crystallography. Cytochalasins are known for their potency and toxicity against

numerous disease targets as well as their cytotoxicity in mammalian cells. Cytochalasin E was initially isolated from a *Mycotypha* sp. and inhibits actin polymerization angiogenesis and tumor growth.

Table 2.6 ^{1}H-NMR (500 MHz) and ^{13}C-NMR (125 MHz) Data for SALT-16 in $CDCl_3$ and cytochalasin E (100 MHz, $CDCl_3$)

Position	SALT-16		Cytochalasin E
	δ_C, mult.	δ_H (*J* in Hz)	δ_C
1	170.1, C		170.5, C
3	53.7, CH	3.78, br s	53.9, CH
4	47.9, CH	3.03, dd (4.4, 2.4)	47.8, CH
5	35.8, CH_2	2.27, m	36.0, CH
6	57.2, C		57.5, C
7	60.5, CH	2.64, m	60.8, CH
8	45.8, CH	2.64, m	45.9, CH
9	87.0, C		87.4, C
10	44.9, CH_2	2.90, dd (13.5, 5.0)	44.7, CH_2
		2.72, dd (15.5, 7.0)	13.3, CH_3
11	13.2, CH_3	1.07, d (8.0)	19.9, CH_3
12	19.7, CH_3	1.26, s	128.7, CH
13	128.9, CH	5.89, dd (15.0, 8.0)	131.6, CH
14	131.5, CH	5.22, m	39.3, CH_2
15	39.0, CH_2	2.64, m	41.0, CH
		2.15, br d	212.0, C
16	40.8, CH	2.90, m	77.6, C
17	211.7, C		120.5, CH
18	76.7, C		142.3, CH
19	120.3, CH	5.59, d (12.0)	149.5, C
20	142.1, C	6.43, d (12.0)	20.3, CH_3
22	150.9,		24.5, CH_3
23	20.0, CH_3	1.14, d (7.0)	136.1, C
24	24.3, CH_3	1.46, s	129.9, CH
1’	135.9, C		128.7, CH
2’, 6’	129.5, CH	7.16, d (7.2)	127.5, CH
3’, 5’	128.3, CH	7.32, t (7.2)	128.3, CH
4’	127.3, CH	7.27, t (7.2)	127.3, CH

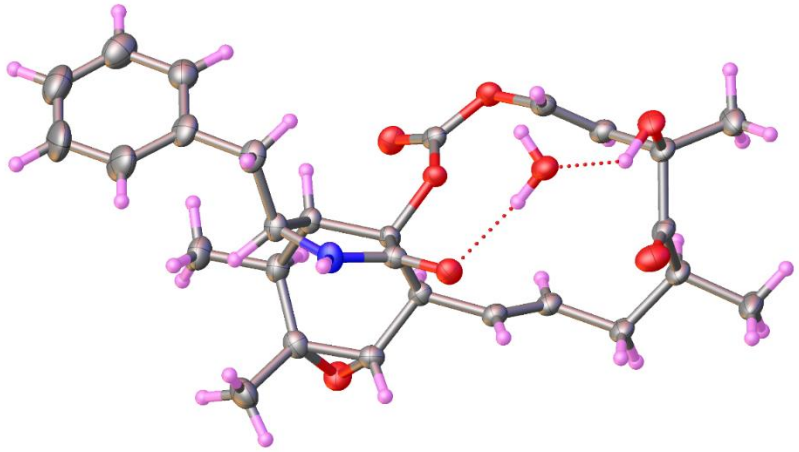

Figure 2.6 Crystal structure of SALT-16 (**2.17**)

2.9 Mass-directed Fractionation of HF14-27C-6b-DNMT

The *Penicillium* sp. was also isolated from a plant of the Floridian mangrove forests. The sample followed protocols previously described for collection of the fungal isolate. Collection of the plant was near the Howard Frankland bridge area on the western area of Tampa, Florida. This sample was part of the screening program and was assigned as a high priority sample after initial screen. With the isolation of several known compounds from bioassay-guided fractionation, a new approach was adapted for the fractionation of this extract.

The methanol extract of HF14-27C-6b-DNMT was active against the brain-eating amoeba, *N. fowleri.* Initially, it exhibited activity in the lower tested concentration (5 ug/mL) with moderate inhibition. However, it was selected for chemical analysis using Tandem-tandem MS methodology and library dereplication. After extraction and liquid-liquid partition (Scheme 2.4), the EtOAc layer was subjected to filtration using three different filter sizes. Unlike the other fungal cultures, preparatory RP HPLC was utilized for initial fractionation to align fractions with the LC/MS experiment. In the case of the crude extract

obtained from fungus HF14-27C-6b-DNMT, a 60-minute gradient yielded 12 fractions. After collection, all fractions were submitted for tandem MS experiment for dereplication purposes.

Fractions F, G, and H were the only samples that did not give substantial hits as mycotoxins. Further separation was performed on these three fractions using NP semi-preparative HPLC yielding three, five and ten subfractions for fractions F, G, and H, respectively. Fractions H-5 and H-9 were the only fractions that did not contain a mycotoxin using the tandem MS dereplication tool. After determining the purity of the samples, fraction H-5 was determined to be a newly isolated fungal metabolite. One- and two-dimensional NMR data were obtained for structure elucidation of SALT-17 and was identified as a new meroterpenoid.

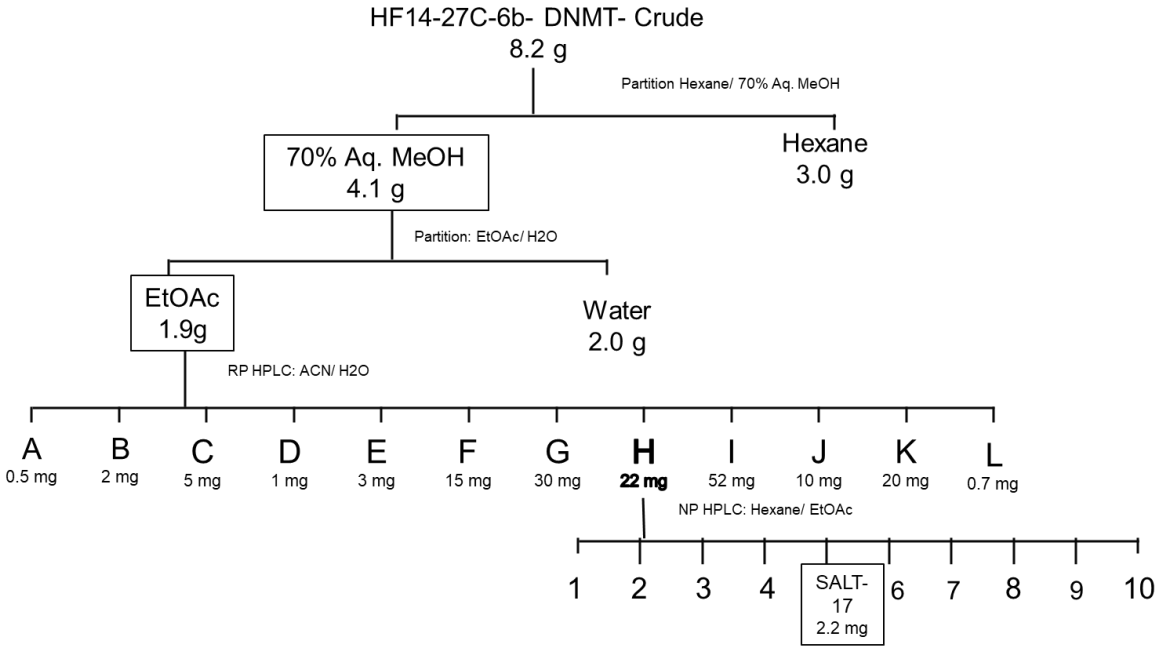

Scheme 2.4 Tandem ms-guided fractionation of HF14-27C-6b-DNMT

2.9.1 Structure elucidation of SALT- 17

The HRESIMS (*m/z* 475.2351) $[M+H]^+$ analysis of SALT-17 was consistent with a molecular formula of $C_{26}H_{34}O_7$ (calcd $C_{26}H_{35}O_7$), calculating 10 degrees of unsaturation in this compound. The ^{13}C NMR data (Table 2.7) confirmed the presence of two ketone (δ_C 202.8 and 202.6), two ester (δ_C 167.6 and 175.7), and two olefinic carbon (δ_C 127.9 and 143.2) resonances; this accounted for five of the calculated degrees of unsaturation, indicating that the remaining unsaturation resulted from five rings. The ^1H NMR data (Table 2.7) displayed seven signals representing methyl singlets at δ_H 1.07, 1.11, 1.29, 1.30, 1.40, 1.59, and 3.62 (H-20, H-19, H-23, H-22, H-24, H-21, and H-26, respectively) , a vinylic methine δ_H 5.59 (H-11), an oxymethine δ_H 4.16 (H-3), and several overlapping multiplets. The HSQC experiment facilitated the assignments of the overlapping proton signals to their respective carbons revealing four methylenes and a methine (H-5) in the region of δ_H 1.5-2.25. Two protons remained unassigned by the HSQC experiment, indicating their attachment to heteroatoms.

A bicyclic ring was assigned using HMBC and COSY experiments. H_3-19 and H_3-20 shared $^{2\text{-}3}J_{HC}$ correlations as well as similar proton shifts suggesting their assignment as a geminal dimethyl group on a quaternary carbon (C-4, δ_C 37.5). The downfield shift of H-3 suggested attachment to an ester group (C-18, δ_C 175.7) and confirmed by HMBC correlation. $^3J_{HC}$ correlation of H-3 to C-1(δ_C 31.2) and C-2 were confirmed by the $^3J_{HH}$ COSY spin system of H-1a (δ_H 1.72) to H-2a (δ_H 2.01) to H-3. HMBC correlations of H_2-1 to C-5 (δ_C 49.8) and C-10 (δ_C 46.5) completed a six-membered ring.

A vinylic proton at δ_H 5.59 (H-11) was essential for establishing the formation of two more ring systems. $^{2\text{-}3}J_{HC}$ HMBC correlations from H-11 to C-10 provided attachment

Table 2.7 ^{1}H NMR (500 MHz) and ^{13}C NMR (125 MHz) data of HF14-27C-6b-DNMT-H-5 ($CDCl_3$)

Position	δ_C, mult.	δ_H (*J* in Hz)
1	31.0, CH_2	1.72, m 2.25, td
2	21.4, CH_2	2.01, m 2.10, m
3	84.4, CH	4.16, br d
4	37.5, C	
5	49.8, CH	1.58, m
6	31.4, CH_2	2.00, m 2.53, m
7	20.8, CH_2	1.56, m 1.65, m
8	39.6, C	
9	143.2, C	
10	46.5, C	
11	127.9, CH	5.59, s
12	76.1, C	
13	53.2, C	
14	75.5, C	
15	202.8, C	
16	72.3, C	
17	202.6, C	
18	175.7, C	
19	27.4, CH_3	1.11, s
20	22.4, CH_3	1.07, s
21	24.7, CH_3	1.59, s
22	24.1, CH_3	1.30, s
23	7.6, CH_3	1.29, s
24	10.6, CH_3	1.40, s
25	167.6, C	
26	52.2, CH_3	3.62, s

to the first ring system. A tri-substituted double bond containing the other olefinic carbon C-9 (δ_C 143.2) correlated to the quaternary carbons C-8, 12, 13 (δ_C 39.6, 76.1, 53.2) and the methyl C-22 (δ_C 24.1). The second ring closure was facilitated by the second spin system assigned in the COSY spectrum of H-6 and H-7 and corroborated by HMBC correlations of H_2-7 to C-8 and C-9. The cyclopentadione assignment relied heavily on the methyl groups for placement of the quaternary carbons C-13 and C-14. H_3-23

correlated to the deshielded carbons C-13, C-14, and the ketone C-15 in the HMBC experiment. This methyl was assigned as a substituent on the quaternary center, C-13. Another methyl group (H_3-24) correlated to C-12, 13, 16 and 17, which placed the ketone adjacent to C-14 and C-16 forming a cyclopenta-diketone ring and completing the planar structure of SALT-17.

After establishing the planar structure of **2.14**, relative stereochemical assignment for each chiral center was considered using a NOESY experiment. The methyl groups (H_3-21, 22, 26) displayed correlations with each other. The *cis* attachment of the five-membered ring to the cyclohexenol was established through NOE correlation of the methoxy (H_3-26) to the methyl group (H_3-23). This compound is very similar to the published structure of atlantinone B (2.15). These NOE correlations were compared with the literature values atlantinone B (2.15)[41] and secured the relative stereochemical configuration of SALT-17.

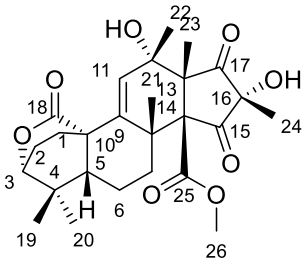

2.14

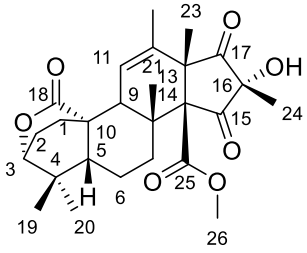

2.15

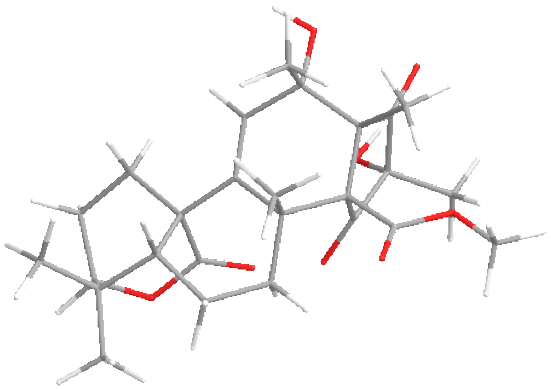

Figure 2.7 Three-dimensional structure of SALT-17 (**2.14**) displaying relative stereochemical configuration

SALT-17 was tested for its anti-amoebic activity against *Naegleria fowleri* and *Acanthamoeba* sp. They did not display any activity against the free-living amoebas. Further cytotoxic testing was performed using the A549 cell line and was determined that this compound was not cytotoxic. Additional screening was done against *Enterococcus faecium, Staphylococcus aureus, Klebsiella pneumoniae, Acinetobacter baumannii, Pseudomonas aeruginosa,* and *Enterobacter* species (ESKAPE); *Mycobacterium tuberculosis; Clostridium difficile;* and the respiratory syncytial virus (RSV). Results are pending for these assays.

2.10 Discussion and Conclusion

Within this chapter, four fungal strains were subjected to large-scale fermentation for chemical evaluation and isolation of bioactive compounds with anti-amoebic activity. Three of the endophytic fungal extracts were analyzed using bioassay-guided fractionation, which resulted in the isolation of known toxins and nuisance compounds. To eliminate the re-isolation of these mycotoxins, we established a dereplication protocol utilizing tandem MS and an in-house library of mycotoxins.

The tandem mass dereplication was incorporated into the fractionation of an extract that was moderately active against *N. fowleri.* This mass-directed fractionation led to the isolation of a new meroterpene. This class of compound was also isolated from a *Penicillium* sp. extract within our lab; Demers isolated citreohybriddione D from an HDAC treated culture.[42] Moreover, atlantinone B is also a meroterpene isolated from a DNMT treated culture of *Penicillium citreonigrum.* [41] Epigenetics prove its benefits of accessing silent gene clusters with the suite of similar compounds derived from the *Penicillium* genera.

2.11 References

(1) Calcul, L.; Waterman, C.; Ma, W.; Lebar, M.; Harter, C.; Mutka, T.; Morton, L.; Maignan, P.; Olphen, A.; Kyle, D.; Vrijmoed, L. ; Pang, K.-L.; Pearce, C.; Baker, B. J. Screening mangrove endophytic fungi for antimalarial natural products. *Mar. Drugs* **2013**, *11*, 5036–5050.

(2) Friess, D. A. Mangrove forests. *Curr. Biol.* **2016**, *26*, R746–R748.

(3) Demers, D.; Knestrick, M.; Fleeman, R.; Tawfik, R.; Azhari, A.; Souza, A.; Vesely, B.; Netherton, M.; Gupta, R.; Colon, B.; Rice, C.; Rodríguez-Pérez, M.; Rohde, K.; Kyle, D.; Shaw, L.; Baker, B. Exploitation of mangrove endophytic fungi for infectious disease drug discovery. *Mar. Drugs* **2018**, *16*, 376–386.

(4) Ananda, K.; Sridhar, K. R. Diversity of endophytic fungi in the roots of mangrove species on the west coast of India. *Can. J. Microbiol.* **2002**, *48*, 871–878.

(5) Nisa, H.; Kamili, A. N.; Nawchoo, I. A.; Shafi, S.; Shameem, N.; Bandh, S. A. Fungal endophytes as prolific source of phytochemicals and other bioactive

natural products: a review. *Microb. Pathog.* **2015**, *82*, 50–59.

(6) Kjer, J.; Wray, V.; Edrada-Ebel, R.; Ebel, R.; Pretsch, A.; Lin, W.; Proksch, P. Xanalteric acids i and ii and related phenolic compounds from an endophytic *Alternaria* sp. isolated from the mangrove plant *Sonneratia alba*. *J. Nat. Prod.* **2009**, *72*, 2053–2057.

(7) Alvin, A.; Miller, K. I.; Neilan, B. A. Exploring the potential of endophytes from medicinal plants as sources of antimycobacterial compounds. *Microbiol. Res.* **2014**, *169*, 483–495.

(8) Newman, D. J.; Cragg, G. M. Natural products as sources of new drugs from 1981 to 2014. *J. Nat. Prod.* **2016**, *79*, 629–661.

(9) Newman, D. J.; Cragg, G. M. Natural products as sources of new drugs over the last 25 years. *J. Nat. Prod.* **2007**, *70*, 461–477.

(10) Stierle, A.; Strobel, G.; Stierle, D. Taxol and taxane production by *Taxomyces andreanae*, an endophytic fungus of pacific yew. *Science.* **1993**, *260*, 214–216.

(11) Wani, M. C.; Taylor, H. L.; Wall, M. E.; Coggon, P.; McPhail, A. T. Plant antitumor agents. vi. Isolation and structure of taxol, a novel antileukemic and antitumor agent from *Taxus brevifolia*. *J. Am. Chem. Soc.* **1971**, *93*, 2325–2327.

(12) Schueffler, A.; Anke, T. Fungal natural products in research and development. *Nat. Prod. Rep.* **2014**, *31*, 1425–1448.

(13) Shao, C.-L.; Wang, C.-Y.; Gu, Y.-C.; Wei, M.-Y.; Pan, J.-H.; Deng, D.-S.; She, Z.-G.; Lin, Y.-C. Penicinoline, a new pyrrolyl 4-quinolinone alkaloid with an

unprecedented ring system from an endophytic fungus *Penicillium* sp. *Bioorg. Med. Chem. Lett.* **2010**, *20*, 3284–3286.

(14) Elsebai, M. F.; Tejesvi, M. V.; Pirttilä, A. M. Endophytes as a novel source of bioactive new structures. In *Advances in Endophytic Research*; Springer India: New Delhi, 2014; pp 191–202.

(15) Buatong, J.; Phongpaichit, S.; Rukachaisirikul, V.; Sakayaroj, J. Antimicrobial activity of crude extracts from mangrove fungal endophytes. *World J. Microbiol. Biotechnol.* **2011**, *27*, 3005–3008.

(16) Bode, H. B.; Bethe, B.; Höfs, R.; Zeeck, A. Big effects from small changes: possible ways to explore nature's chemical diversity. *ChemBioChem* **2002**, *3*, 619.

(17) Su, C.; Lei, L.; Duan, Y.; Zhang, K.-Q.; Yang, J. Culture-independent methods for studying environmental microorganisms: methods, application, and perspective. *Appl. Microbiol. Biotechnol.* **2012**, *93*, 993–1003.

(18) Amann, R. I.; Ludwig, W.; Schleifer, K. H. Phylogenetic identification and *in situ* detection of individual microbial cells without cultivation . Phylogenetic identification and *in situ* detection of individual microbial cells without cultivation. *Microbiol. Rev.* **1995**, *59*, 143–169.

(19) Davari, B.; Khodavaisy, S.; Ala, F. Isolation of fungi from housefly (*Musca domestica*) at slaughter house and hospital in Sanandaj, Iran. *J. Prev. Med. Hyg.* **2012**, *53*, 172–174.

(20) Kjer, J.; Debbab, A.; Aly, A. H.; Proksch, P. Methods for isolation of marine-derived endophytic fungi and their bioactive secondary products. *Nat. Protoc.* **2010**, *5*, 479–490.

(21) Mbata, T. I. Isolation of fungi in hyper saline dead sea water. *Sudan. J. public Heal.* **2008**, *3*, 170–172.

(22) Wen, L.; Cai, X.; Xu, F.; She, Z.; Chan, W. L.; Vrijmoed, L. L. P.; Jones, E. B. G.; Lin, Y. Three metabolites from the mangrove endophytic fungus *Sporothrix* sp. (#4335) from the South China sea. *J. Org. Chem.* **2009**, *74*, 1093–1098.

(23) Chiang, Y.-M.; Chang, S.-L.; Oakley, B. R.; Wang, C. C. Recent advances in awakening silent biosynthetic gene clusters and linking orphan clusters to natural products in microorganisms. *Curr. Opin. Chem. Biol.* **2011**, *15*, 137–143.

(24) Foulks, J. M.; Parnell, K. M.; Nix, R. N.; Chau, S.; Swierczek, K.; Saunders, M.; Wright, K.; Hendrickson, T. F.; Ho, K.-K.; McCullar, M. V.; Kanner, S. B. Epigenetic drug discovery: targeting dna methyltransferases. *J. Biomol. Screen.* **2012**, *17*, 2–17.

(25) Arrowsmith, C. H.; Bountra, C.; Fish, P. V.; Lee, K.; Schapira, M. Epigenetic protein families: a new frontier for drug discovery. *Nature* **2012**, *11*, 384–400.

(26) DeWoskin, V. A.; Million, R. P. The epigenetics pipeline. *Nat. Rev. Drug Discov.* **2013**, *12*, 661–662.

(27) Beau, J.; Mahid, N.; Burda, W. N.; Harrington, L.; Shaw, L. N.; Mutka, T.; Kyle, D. E.; Barisic, B.; van Olphen, A.; Baker, B. J.Epigenetic tailoring for the production

of anti-infective cytosporones from the marine fungus *Leucostoma persoonii*. *Mar. Drugs* **2012**, *10*, 762–774.

(28) Allfrey, V. G.; Faulkner, R.; Mirsky, A. E. Acetylation and methylation of histones and their possible role in the regulation of RNA synthesis. *Proc. Natl. Acad. Sci. U. S. A.* **1964**, *51*, 786–794.

(29) Göttlicher, M.; Minucci, S.; Zhu, P.; Krämer, O. H.; Schimpf, A.; Giavara, S.; Sleeman, J. P.; Coco, F. Lo; Nervi, C.; Pelicci, P. G.; Heinzel, T. Valproic acid defines a novel class of HDAC inhibitors inducing differentiation of transformed cells. *EMBO J.* **2001**, *20*, 6969–6978.

(30) Copeland, R. A.; Olhava, E. J.; Scott, M. P. Targeting epigenetic enzymes for drug discovery. *Curr. Opin. Chem. Biol.* **2010**, *14*, 505–510.

(31) Beau, J. Drug discovery from floridian mangrove endophytes. Ph.D. Dissertation, University of South Florida, Tampa, FL, 2012.

(32) Williams, R. B.; Henrikson, J. C.; Hoover, A. R.; Lee, A. E.; Cichewicz, R. H. Epigenetic remodeling of the fungal secondary metabolome. *Org. Biomol. Chem.* **2008**, *6*, 1895–1897.

(33) El-Elimat, T.; Figueroa, M.; Ehrmann, B. M.; Cech, N. B.; Pearce, C. J.; Oberlies, N. H. High-resolution MS, MS/MS, and UV database of fungal secondary metabolites as a dereplication protocol for bioactive natural products. *J. Nat. Prod.* **2013**, *76*, 1709–1716.

(34) Lang, G.; Mayhudin, N. A.; Mitova, M. I.; Sun, L.; van der Sar, S.; Blunt, J. W.;

Cole, A. L. J.; Ellis, G.; Laatsch, H.; Munro, M. H. G. Evolving trends in the dereplication of natural product extracts: new methodology for rapid, small-scale investigation of natural product extracts. *J. Nat. Prod.* **2008**, *71*, 1595–1599.

(35) Cowan, T. M. Neonatal screening by tandem mass spectrometry. *Neoreviews* **2005**, *6*, e539–e548.

(36) http://dnp.chemnetbase.com/faces/chemical/ChemicalSearch.xhtml (accessed Sep 24, 2018).

(37) Craig, R.; Beavis, R. C. Tandem: matching proteins with tandem mass spectra. *Bioinformatics* **2004**, *20*, 1466–1467.

(38) Brügger, B.; Erben, G.; Sandhoff, R.; Weiland, F. T.; Lehman, W. H. Quantitative analysis of biological membrane lipids at the low picomole level by nano-electrospray ionization tandem mass spectrometry. *Proc. Natl. Acad Sci.* **1997**, *94*, 2339–2344.

(39) Petrović, M.; Hernando, M. D.; Díaz-Cruz, M. S.; Barceló, D. Liquid chromatography–tandem mass spectrometry for the analysis of pharmaceutical residues in environmental samples: a review. *J. Chromatogr. A* **2005**, *1067*, 1–14.

(40) Knestrick, M. A. From florida to antarctica: dereplication strategies and chemical investigations of marine organisms. Ph. D. Dissertation, University of South Florida, Tampa, FL, 2018.

(41) Dalsgaard, P. W.; Petersen, B. O.; Duus, J. Ø.; Zidorn, C.; Frisvad, J. C.; Christophersen, C.; Larsen, T. O. Atlantinone a, a meroterpenoid produced by

Penicillium ribeum and several cheese associated *Penicillium* species. *Metabolites* **2012**, *2*, 214–220.

(42) Demers, D. H. Chemical investigations of fungal natural products for drug discovery. Ph.D. Dissertation, University of South Florida, Tampa, FL, 2017.

SECTION B:

ANTARCTIC BIODIVERSITY

B.1 Antarctica

The Antarctic extends from roughly latitude 60° S to the South Pole at 90°S including the continent, nearby islands and the Southern Ocean. Antarctica separated from Gondwana over 150 million years ago into its isolated ecosystem created by the Antarctic Circumpolar Current (ACC).[1] The lack of continents within the Drake passage create unique dynamics with zonal and meridional circulation; thus, distinguishing the ACC from other latitudinal currents (Figure B.1).[2] The ACC continuously circulates the continent providing nutrients and heat to the continent. Besides its attractive terrestrial faunal inhabitants, most of the biodiversity of the Antarctic is below the ice in its waters. Sessile organisms dominate the benthos and heavily rely on physical and chemical biotic interactions.[3] Predation, spatial and nutrition competition, and fouling are few of the roles for which chemical mediation is necessary.[4] The ecological studies of these compounds have benefitted mankind because of their associated pharmacological properties.[4]

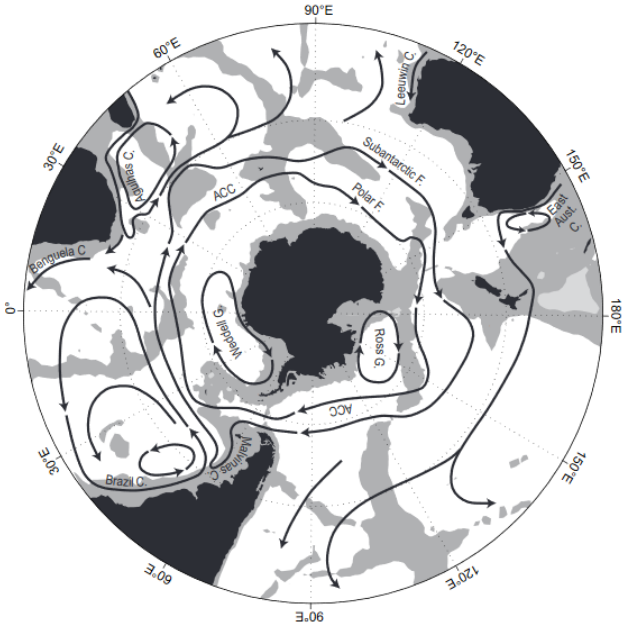

Figure B.1 Schematic map displaying the major currents in the southern hemisphere oceans. The two significant cores of the Antarctic Circumpolar Current (ACC) are Subantarctic Front and Polar Front.[1]

B.2 Antarctic benthic environment

Macroalgal forests dominate Antarctic shallow waters (Figure B.2) and are investigated for their chemical defenses.[5] Marine chemical ecology has progressed in the past 30 years because of technological improvement for collection and studies.[6] Polar climates are less diverse than tropical counterparts, but the biomass available in the polar communities is significant.[7] The Western Antarctic Peninsula displays considerable diversity within the macroalgae community with interesting ecological properties.[8] For example, the red alga *Plocamium cartilagineum* produces polyhalogenated monoterpenes with predation toxicity against *Odontaster Validus* and feeding deterrence against *Gondogeneia antarctica.*[9]

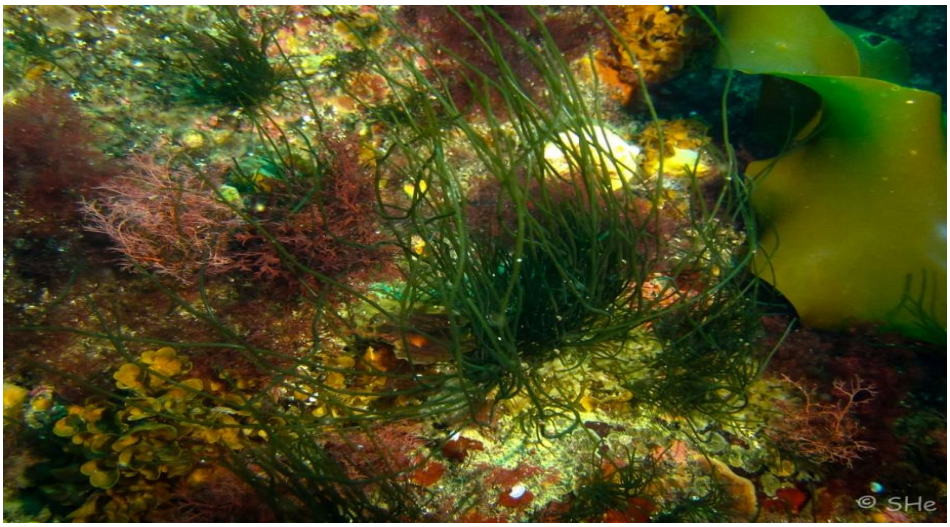

Figure B.2 An image of the underwater forest in Antarctica displaying green, brown and red algae. (Picture credit: Sabrina Heiser)

Soft corals belonging to the phylum Cnidaria are also significant organisms of Antarctica benthos as they are abundant in these polar communities. These sessile filter feeders have contributed significantly to the body of marine natural products literature. In the latest review by Blunt *et al.* approximately 20% of the reported marine metabolites were Cnidarian metabolites.[10] However, most of these compounds are isolated from temperate and tropical communities as these numbers are drastically low in the decadal review of cold water coral compounds.[11] Despite low numbers, the novelty among these compounds is evident along with significant biological activity.

Because it is underexplored and replete with biodiversity, Antarctica suits the criteria for a productive environment with diverse compounds. Within the past decade, less than 3% of marine metabolites were derived from Antarctica due to the complexity to access.[11] Despite the minor representation, the novelty is still prominent from cold environments. Chapters three and four of this section describes the chemical analysis of

Antarctic marine organisms from both shallow and deep waters. Their potential is demonstrated with the novelty and biomedical properties that the chemical components of the organisms contain. Chapter three will describe a class of polyketides isolated from an Antarctic red alga and chapter four will illustrate the potential of the deep sea with chemical analyses of octocorals.

B.3 References

(1) Meadows, J.; Mills, W. J.; King, H. G. R. *The Antarctic*; World Bibliographical Series; ABC-CLIO: Oxford, England, 1994.

(2) R. Rintoul, S.; W. Hughes, C.; Olbers, D. Chapter 4.6 the Antarctic circumpolar current system. In *Elsevier*; 2001; pp 271–302.

(3) Núñez-Pons, L.; Avila, C. Natural products mediating ecological interactions in Antarctic benthic communities: a mini-review of the known molecules. *Nat. Prod. Rep.* **2015**, *32*, 1114–1130.

(4) Figuerola, B.; Núñez-Pons, L.; Vazquez, J.; Taboada, S.; Cristobo, J.; Ballesteros, M.; Avila, C. Chemical interactions in Antarctic marine benthic ecosystems. In *Marine Ecosystems*; Cruzado, A., Ed.; Intech open access publisher: Rijeka, Croatia, 2012; pp 105–126.

(5) Knox, G. Biology of the Southern ocean, second edition; Marine Biology; CRC Press, 2006.

(6) McClintock, J.; Baker, B. Marine chemical ecology; McClintock, J., Baker, B., Eds.; Marine Science; CRC Press, 2001; pp 1–68.

(7) Amsler, C. D. Algal sensory chemical ecology. In *Algal Chemical Ecology*; Springer Berlin Heidelberg: Berlin, Heidelberg, 2008; pp 297–309.

(8) Maschel, J. .; Baker, B. J. The chemistry of algal secondary metabolism. In *Algal Chemical Ecology*; Amsler, C. D., Ed.; Springer Berlin Heidelberg: Berlin, Heidelberg, 2008; pp 1–24.

(9) Ankisetty, S.; Nandiraju, S.; Win, H.; Park, Y. C.; Amsler, C. D.; McClintock, J. B.; Baker, J. A.; Diyabalanage, T. K.; Pasaribu, A.; Singh, M. P.; et al. Chemical investigation of predator-deterred macroalgae from the Antarctic peninsula *J. Nat. Prod.* **2004**, *67*, 1295–1302.

(10) Blunt, J. W.; Carroll, A. R.; Copp, B. R.; Davis, R. A.; Keyzers, R. A.; Prinsep, M. R. Marine natural products. *Nat. Prod. Rep.* **2018**, *35*, 8–53.

(11) Soldatou, S.; Baker, B. J. Cold-water marine natural products, 2006 to 2016. *Nat. Prod. Rep.* **2017**, *34*, 585–626.

CHAPTER THREE:

CHEMISTRY OF AN ANTARCTIC RED ALGA

3.1 Rhodophyta chemistry

The richness of Rhodophyta secondary metabolites is evident in the abundance and diversity of natural products when compared to other macroalgae.[1] All major classes of secondary metabolites are represented within Rhodophyta excluding phlorotannins.[2] Red algae distinctively produce halogenated compounds accounting for 90% of reported metabolites.[3] In 2008, reports of new natural products from red algae reached 700 (figure 3.1).[4] The biological activity associated with these compounds encouraged pharmaceutical companies to investigate algal metabolites further.[4]

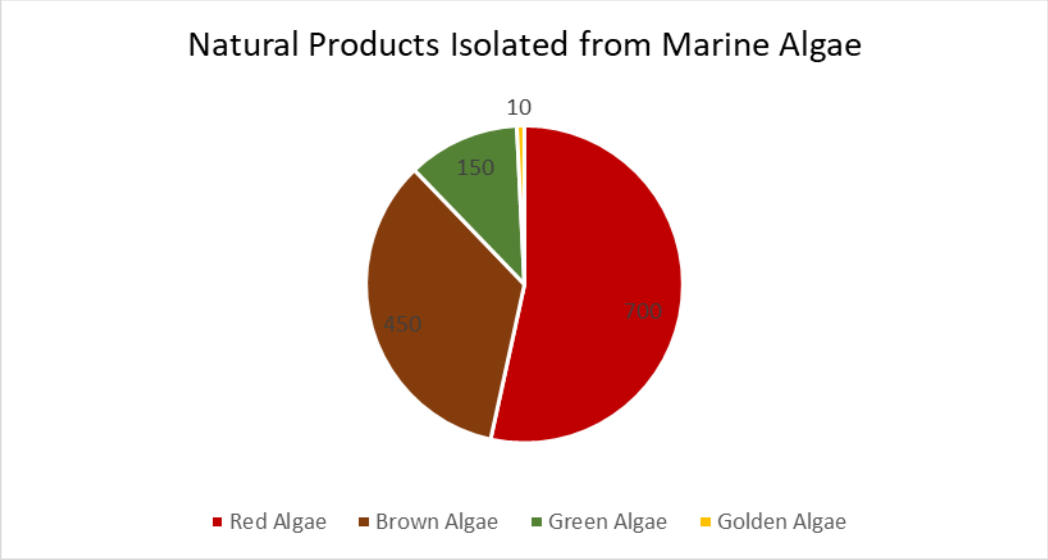

Figure 3.1 The number of novel compounds isolated from marine algae between 1985 and 2008.[4]

Halogens are commonly found in red algal metabolites, especially in terpenes, which are the largest reported class of red algal natural products. [5–8] Red seaweed is the only class of macroalgae that incorporates iodine, chlorine, and bromine into their metabolism. Genera such as *Laurencia*, *Plocamium, Chrondrophycus,* and *Osmundea* are prolific sources of halogenated terpenes.[9] *Laurencia* spp. elaborates the largest group of metabolites of Rhodophyta; abundant in halogenated sesquiterpenes and acetogenins. Structural diversity is evident within this genus, including spiro-ring fusions and genus-specific acetogenins, that contain enyenes and allenes like in laurepinnacin (**3.1**) and laurellene (**3.2**), respectively.[1] Despite the structural diversity within Rhodophyta, interest has declined as these compounds lack nonecological bioactivity.[1] For example, polyhalogenated monoterpenes are abundant within *Plocamium cartilagineum* and exhibit potent activity against its sympatric amphipods. Specifically, anverene (**3.3**) and epi-plocamene (**3.4**) have shown feeding deterrence against amphipods like *Gondogeneia antarctica.*[10–12]

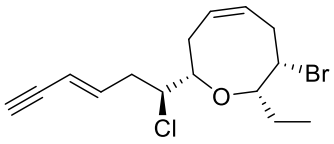

3.1

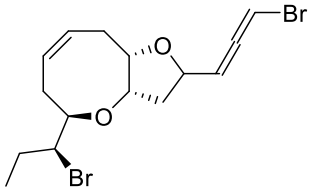

3.2

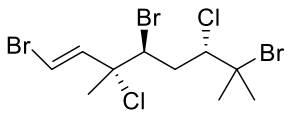

3.3

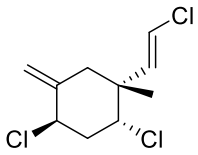

3.4

3.2 Polyketides and Drug discovery

While terpenes are dominant in Rhodophyta chemistry there are other classes of metabolites that also contribute. Polyketides are common among genera in Bonnemaisoniaccae and are usually linear halogenated ketones or branched lactones.[1] Polyketides belong to a major class of secondary metabolites. They are a diverse group

of compounds and are found mainly in plants, fungi, and bacteria. These metabolites are biosynthetically related to fatty acids because polyketides are derivatives of acetate, propionate, and other small carboxylic acids.[13,14] A complex class of enzymes, named polyketide synthase (PKS), synthesizes polyketides which facilitate the elongation of the carbon chain. Polyketide synthases are responsible for synthesizing these natural products that divide into three groups. Type I, II and III PKS are distributed among organisms and produce different classes of polyketides. Bacteria possess all three types, whereas both types I and III are found within fungi and type III PKS is the only one observed in plants.[13]

Polyketides have displayed a variety of biological properties because of their versatile biosynthetic production. These highly oxygenated and stereochemically-enriched scaffolds have enticing biological activities that led to successful drugs. Aflatoxin (**3.5**), a known mycotoxin isolated from the fungus *Aspergillus flavus*, is very toxic and can be mutagenic and teratogenic, and can cause immunosuppression in animals.[13] Aromaticity is present within the scaffold and derives from type III PKS. Another example of the biological significance derived from the polyketide biosynthetic pathway is lovastatin (**3.6**), a drug used in the treatment of elevated blood cholesterol levels.[13]

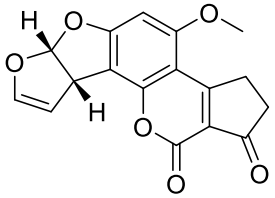

3.5

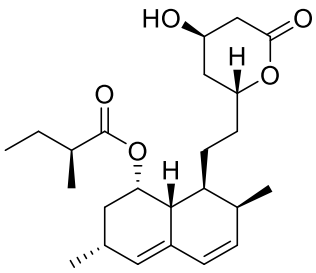

3.6

One of the main challenges that sessile animals and organisms must overcome is the colonization of microbes, which can have a detrimental effect on the survival of the organism.[12] Microbe colonization can lead to biofilm formation on the outer body surface of animals including macroalgae and seagrass, and non-living substrates that dwell on the ocean floor.[15] Bottom dwellers use mechanisms like surface sloughing to prevent heavy fouling to complement their chemical defense. Sponges, soft corals, ascidians, and algae utilize these defense mechanisms to reduce biofouling, especially against diatoms.[12] *Delisea pulchra*, a benthic red alga presents another example of chemical-mediated antifouling, a benthic red alga. A suite of polyketides isolated from this Antarctic red alga that displays antibiotic activity.

3.3 Delisea pulchra *and its chemistry*

Algal biodiversity is minimal in polar regions and non-existent in the deep-sea, but the majority of the reported compounds are isolated from *Delisea pulchra* (Figure 3.2).[17] A series of compounds called fimbrolides were initially isolated from the Antarctic red alga, *D. pulchra.* These secondary metabolites were determined to be antimicrobial and ecologically functional as antifouling agents.[11] Specialized cells store these halogenated furanones on both the interior and exterior of the alga thallus. The antimicrobial property that most of these compounds possess is due to the similarity in structure of the acylated homoserine lactone (AHL) and allows the compounds to fit in same specific receptor (Figure 3.3).[18]

Figure 3.2 Voucher photo of *Delisea pulchra.* Photo credit: Charles D. Amsler

AHL is a class of intercellular communication signals among many bacteria use to facilitate quorum sensing. Bacteria use quorum sensing to create colonies on the surfaces of its host, form biofilms and infect its host.[19] AHL regulates the enzyme that is responsible for host interactions that eventually lead to settling.[20–22] For example, *Pseudomonas aeruginosa* produces elastase to assist with its biofilm formation; a mechanism used to infect the lungs of cystic fibrosis patients.[18] Several metabolites from *D. pulchra* defend this red alga from this bacterial activity as antagonists.[18]

3.4 Research objectives

An Antarctic red alga previously studied was investigated for its chemical constituents. This seaweed is known to produce halogenated lactones derived from a polyketide synthase. The halogenated furanones are known to obstruct bacterial fouling of the red algae. This chapter details the isolation of these halogenated furanones and the screening of these compounds against the ESKAPE panel.

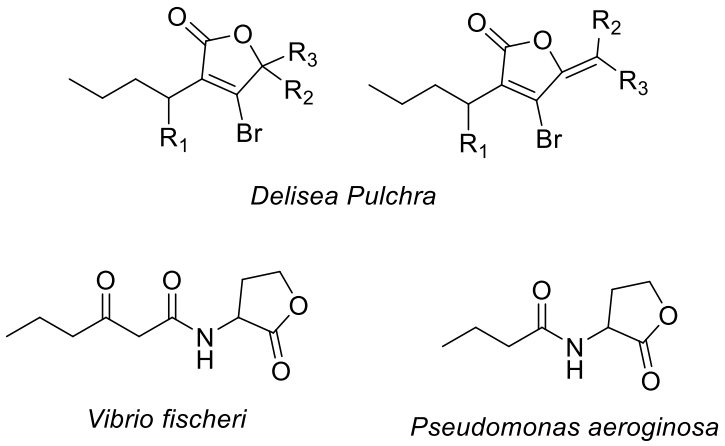

Figure 3.3 Scaffold of polyketides isolated from *Delisea* sp. and AHL from gram-negative bacteria. [18]

3.5 Isolation of Polyketides from Delisea Pulchra

The seaweed *D. pulchra* was collected in 2017 from the western peninsula of Antarctica during the late austral summer. Using SCUBA, accumulation of the red seaweed spanned over three months from the perimeter surrounding Palmer Station, Antarctica. Immediately after collection, the red alga was frozen for subsequent chemical analysis in our Floridian laboratory. The wet sample was immersed in 3:1/Dichloromethane (DCM): Methanol (MeOH) for an overnight extraction, which was repeated for three consecutive days followed by filtration (Scheme 3.1). The filtrate contained a mixture of two immiscible phases and therefore allowed to settle and separate into two layers. The organic layer was collected and concentrated resulting in 25.8g of dried extract. After evaporation, further separation of the organic layer was achieved by normal phase MPLC. A 50-minute gradient using *n*-hexanes and EtOAc as the mobile phase produced 27 fractions. After evaluation of the ^{1}H NMR spectrum of each fraction, the relatively non-polar fractions showed peaks indicative of the halogenated furanones previously isolated from the *Delisea* sp. The fractions of interest were then

subjected to normal phase HPLC that led to the purification of six known and two new compounds: E-fimbrolide, hydroxyfimbrolide, acetoxyfimbrolide, pulchralide A, pulchralide B, pulchralide C, tribromolactone, and dihydroxybromolactone.[23,24]

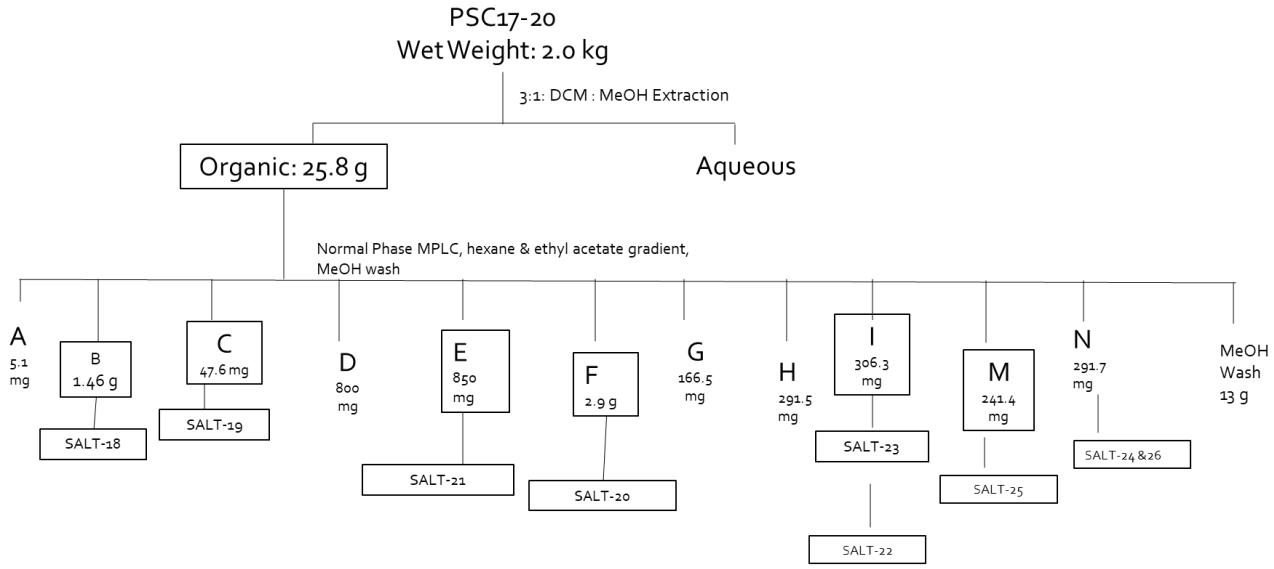

Scheme 3.1 Isolation of halogenated furanones from *Delisea* sp.

3.5.1 Structure elucidation of SALT-18 and 19

The first four lipophilic MPLC fractions yielded two similar compounds labeled SALT-18 (**3.7**) and SALT-19 (**3.8**). Comparison of the ^{1}H NMR resonances to the literature resulted in the identification of *E* and *Z* isomers of the previously reported polyketide scaffold, fimbrolide. Fimbrolides are abundant in this genus of red alga collected from Southern waters. The ^{1}H and ^{13}C NMR spectra (Table 3.1) were identical to the reported values of the brominated *E* and *Z* isomers of fimbrolide. The olefinic protons at δ_H 6.27, as well as signals for the commonly attached aliphatic chain, were observed both in the ^{1}H NMR spectrum at δ_H 2.41, 1.35 and 0.93 and in the ^{13}C NMR spectrum as δ_C 29.2,

Table 3.1 ^{13}C NMR comparisons of experimental and literature values of **3.7** and **3.8**

Position	**3.7**		**3.8**	
	δ_C Literature	δ_C Experimental	δ_C Literature	δ_C Experimental
1				
2	166.3	166.1	166.3	166.1
4	150.2	150.0	150.2	150.0
3	134.1	133.9	134.1	133.9
5	130.0	130.1	130.0	130.1
6	91.1	90.9	91.1	90.9
1’	29.2	29.0	29.2	29.0
2’	25.2	25.1	25.2	25.1
3’	22.6	22.4	22.6	22.4
4’	13.9	13.7	13.9	13.7

25.2, 22.6, 13.9. The lactone carbonyl at δ_C 166.3, along with the fully substituted double bond signals at δ_C 150.2 and 134.1. HRESIMS data confirmed the molecular formula as $C_9H_{10}O_2Br_2$ for the colorless oil. The distinction of the *E* and *Z* isomers is evident in the difference in shifts of the olefinic signals in the ^1H NMR. The *E*- isomer resonated at δ_H 6.56 and the *Z* at δ_H 6.24.

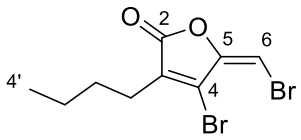

3.7

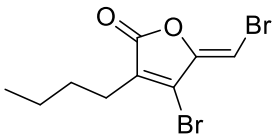

3.8

3.5.2 Structure elucidation of SALT-20

SALT- 20 (**3.9**) eluted from a less lipophilic MPLC fraction and was subjected to normal phase HPLC. Spectral data collected on the sixth fraction, eluted from the NP HPLC, revealed its identity as acetoxyfimbrolide. High-resolution ESI-MS data indicated a molecular formula of $C_{11}H_{12}Br_2O_4$ (calcd $C_{11}H_{13}Br_2O_4$). The mass difference indicated the difference of an acetyl group from the previously isolated fimbrolide, which was also

supported by the characteristic signals in the 1D NMR data. The methyl singlet resonating at δ_H 2.09 as well as the downfield methine shift at δ_H 5.52 indicated the acetyl substitution on the aliphatic chain. The ^{13}C NMR spectrum facilitated the identification of this compound with the resonances at δ_C 170.0 and δ_C 20.4 indicating the acetyl group. The furanone constituted by the ester carbonyl, and the olefinic unsaturation (δ_C 163.6, 149.6, 131.2).

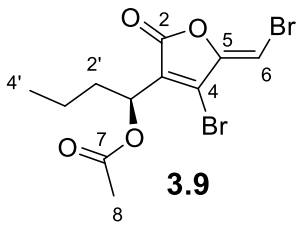

3.9

Table 3.2 ^{13}C NMR comparisons of experimental and literature values of **3.9**

Position	δ_C Literature	δ_C Experimental
7	170.0	170.1
2	163.6	163.7
4	149.6	149.6
3	131.2	131.3
5	130.0	130.4
6	93.3	93.3
1’	68.0	68.1
2’	33.5	33.6
8	20.4	20.5
3’	18.3	18.4
4’	13.5	13.5

The comparison of the oxymethine value to the previously assigned *R*-configuration reported in the literature facilitated the assignment of the acetyl group. The exocyclic double bond assigned as *Z* because of the downfield shift of the bromomethine at δ_H 6.38.

3.5.3 Structure elucidation of SALT-21

SALT-21 (**3.10**) obtained when MPLC fraction F was subjected to an NP semi-prep HPLC column using a gradient of *n*-hexanes and EtOAc. The molecular formula of the yellow oil was determined as $C_9H_{10}O_3Br_2$ (calcd $C_9H_{11}O_3Br_2$) using HRESIMS. NMR data suggested that this compound was hydroxyfimbrolide. This compound was also previously isolated from an Antarctic *Delisea* sp. As observed in the other compounds, hydroxyfimbrolide contained the same scaffold comprising of the α,β-unsaturated γ-lactone and the acyl chain. However, the lack of the acetyl group was evident in the ^{1}H and ^{13}C NMR spectra, but the de-shielded shift of an oxygen-bearing carbon was again found at δ_C 67.3. The signals were identical to the shifts reported in the literature. Further analysis of the mass spectroscopy data displayed the loss of water indicative of the loss of a hydroxyl group.

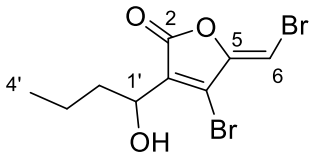

3.10

The chemical shift of the bromomethine also determined the assignment of the exocyclic olefin configuration as Z.

3.5.4 Structure elucidation of SALT-22, 23 & 24

The fifth purified compound was an amorphous powder collected from the NP HPLC. SALT-22 (**3.11**) molecular formula was determined to be $C_{22}H_{24}Br_4O_8$ (calcd $C_{22}H_{25}Br_4O_8$) using high-resolution ESIMS. The molecular formula was twice of SALT-20

Table 3.3 ^{13}C NMR comparisons of experimental and literature values of **3.10**

Position	δ_C Hydroxyfimbrolide	δ_C SALT-21
1		
2	165.5	165.2
3	133.6	133.4
4	129.7	129.6
5	149.9	149.7
6	67.7	67.3
2’	38.1	37.7
3’	18.8	18.6
4’	13.9	13.6
1’	93.7	93.4

(**3.9**) and identified it as a dimer. The resonances of 12 protons within the ^1H NMR spectrum aligned with those of **3.9**. However, the olefinic proton had an upfield shift of δ_H 5.16 compared to acetoxyfimbrolide at δ_H 6.38. Further analysis of this compound led to the confirmation that this compound was pulchralide A,[23] previously isolated in the Baker lab.[25] The aliphatic chain, acetyl substituent, and the bromomethine that are characteristic of this compound were all present in the ^1H NMR spectrum. However, the distinction of this compound from its monomeric counterpart, acetoxyfimbrolide, was also observed in the ^{13}C NMR spectrum with the lack of the trisubstituted enolic double bond carbons. Pulchralide A stereochemical evaluation was conducted by comparison of SALT-22 with the literature evaluation. Although previously reported as crystalline, recrystallization was unsuccessful.

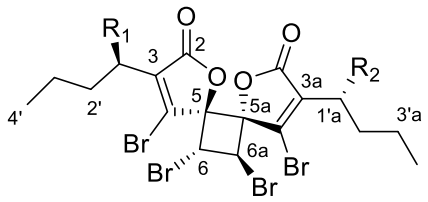

3.11 R_1: OAc; R_2: OAc
3.12 R_1: H; R_2: H
3.13 R_1: OAc; R_2: H

Table 3.4 ^{13}C NMR comparisons of experimental and literature values of **3.11**

Position	δ_C pulchralide A	δ_C SALT-22
1		
2/2a	164.9	164.9
3/3a	134.5	134.5
4/4a	139.7	139.7
5/5a	90.4	90.4
6/6a	43.9	43.9
1'/1'a	68.5	68.5
2'/2'a	33.8	33.8
3'/3'a	18.6	18.6
4'/4'a	13.8	13.8

The same fraction from the NP MPLC afforded an additional dimer which was annotated as SALT- 23 (**3.12**). The functionality of this compound was similar to pulchralide A as it was also a dimer based on its high-resolution mass spectral analysis. The chemical formula was determined to be $C_{18}H_{20}O_4Br_4$ (calcd $C_{18}H_{21}O_4Br_4$), indicating that the compound lacks two acetyl groups when compared to pulchralide A. The 1D NMR spectrum assisted with identifying the compound. An allylic methylene was observed rather than an oxymethine. The ^{13}C NMR spectrum displayed the characteristic peaks of the lactone and butyl chain; however, it lacked the acetoxy signals, which is indicative of the dimerized fimbrolide, pulchralide B.[23] Pulchralide B was also determined to be a C_2 dimer as reported in the literature rather than the meso dimer. Optical rotation values of $[\alpha]^{25}_D$ +4.26° (*c* 0.06, $CHCl_3$) match those of the literature, which ruled out the meso configuration.

A white solid eluted as the primary compound of MPLC fraction N. The SALT-24 (**3.13**) molecular formula was found to be $C_{20}H_{22}O_6Br_4$ (calcd $C_{20}H_{23}O_6Br_4$) using HRESIMS, which suggested that this compound was the third dimeric compound, pulchralide C.[23]

Table 3.5 ^{13}C NMR comparisons of experimental and literature values of **3.12**

Position	δ_C pulchralide B	δ_C SALT-23
1		
2/2a	167.4	167.4
3/3a	137.1	137.1
4/4a	138.2	138.2
5/5a	90.5	90.5
6/6a	44.1	44.1
1'/1'a	29.0	29.0
2'/2'a	25.5	25.5
3'/3'a	22.4	22.4
4'/4'a	13.9	13.9

Analysis of the proton NMR spectrum showed signals representative of acetoxyfimbrolide as well as fimbrolide. The acetyl methyl at δ_H 2.09 with its substitution represented with the methine at δ_H 5.49 confirmed its acetoxyfimbrolide resemblance. The additional signals also resembled fimbrolide at δ_H 2.38. Comparison of the literature data confirmed that fraction N was pulchralide C with the dimerization of acetoxyfimbrolide and fimbrolide.

Table 3.6 ^{13}C NMR comparisons of experimental and literature values of **3.13**

Position	δ_C pulchralide C	δ_C ESALT-24
1		
2	167.0	167.0
2a	165.3	165.3
3	135.5	135.5
3a	134.5	134.5
4	140.9	140.9
4a	139.7	139.7
5	93.3	93.3
5a	88.1	88.1
6	47.7	47.7
6a	44.4	44.4
1'	68.8	68.8
1'a	33.4	33.4
2'	28.5	28.5
2'a	25.4	25.4
3'	22.5	22.5
3'a	18.7	18.7
4'	13.9	13.9
4'a	13.8	13.8

Stereochemistry for **3.13** was determined using through bond correlation and its associated coupling constants. The bromomethine protons were coupled with *J*=10 Hz therefore, they were assigned as *trans*.

3.5.5 Structure elucidation of SALT-25 & 26

MPLC fraction M was subjected to NP HPLC, and further purification was performed using analytical RP HPLC. SALT- 25 (**3.14**) was isolated as a white solid and its molecular formula determined to be $C_{11}H_{13}O_4Br_3$ (calcd $C_{11}H_{14}O_4Br_3$) from evaluation of the high-resolution mass spectrometry. The degree of unsaturation calculated as four accounted for two ester-type carbonyl, one olefin and one ring. The HSQC spectrum identified two methyl, three methylene, and one methine groups. The overlapping methylene signals around δ_H 3.70 (H_2-6) indicated that it bears an electron withdrawing group which was assigned a bromine. Analysis of the HMBC spectrum showed correlation of H_2-6 to δ_C 103.5 (C-5). The deshielding of C-5 and HMBC correlation to the ester carbonyl at δ_C 165.5. The HMBC experiment assisted with assigning the furanone with H-1' (δ_H 69.5) correlating to δ_H 142.6 (C-3) and δ_H 133.5 (C-4). H-1' also correlated with the carbonyl of the acetyl group. The COSY spectrum revealed a spin system with H_2-2', H_2-3', H_3-4'. All the atoms were assigned except two bromines that would satisfy the valence of C-5 and the olefin carbon C-4.

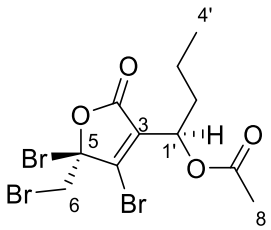

3.14

This compound has been reported as a precursor to synthesizing acetoxyfimbrolide.[24] The compound, referred to as tribromolactone in the paper, was obtained using Br_2 and CH_2Cl_2 for bromination of the exocyclic olefin on the terminal position as well as in the γ position. However, this is the first report of this compound from a natural source.

Table 3.7 NMR data for compound **3.14** ($CDCl_3$)

Position	δ_C[b], Multiplicity	δ_H[a] (*J* in Hz)
1	-	
2	165.5, C	
3	142.6, C	
4	133.5, C	
5	103.5, C	
1’	69.5, CH	5.42, m
2’	34.1, CH_2	1.93, m 1.88, m
3’	18.5, CH_2	1.44, m
4’	13.6, CH_3	0.96, t
6	32.8, CH_2	3.78, *ol* 3.65, *ol*
7	171.4, C	

[a] 400 MHz [b] 100 MHz

An additional compound was isolated as a crystalline solid from MPLC fraction N using NP semi-preparative HPLC. The molecular formula of SALT-26 (**3.15**) was assigned using high-resolution ESIMS and determined to be $C_{11}H_{14}0_5Br_2$. Evaluation of the ^1H NMR signals showed similarities to tri-bromolactone; however, the bromo-methylene protons were more shielded than found in SALT-25. The pair of doublets resonating at δ_H 3.60 and δ_H 3.86 was assigned to C-6 (δ_C 40.6) using HSQC. The one-dimensional ^{13}C NMR spectrum displayed a downfield shift of C-5 (δ_C 121.3), which confirmed the change in substituents when comparing to the tri-bromolactone. The de-

shielding of C-5 is supported by the additional hydroxyl group observed in the molecular formula, making this a hemiketal.

Table 3.7 NMR data for compound **3.15**

Position	δ_C[b], Multiplicity	δ_H[a] (*J* in Hz)
1	-	
2	165.5, C	
3	142.6, C	
4	133.5, C	
5	121.3, C	
1’	69.5, CH	5.42, m
2’	34.1, CH_2	1.93, m 1.88, m
3’	18.5, CH_2	1.44, m
4’	13.6, CH_3	0.96, t
6	32.8, CH_2	3.60, *ol* 3.86, *ol*
7	171.4, C	
8	20.1, CH_3	

[a] 400 MHz [b] 100 MHz

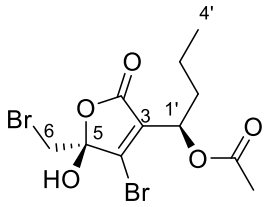

3.15

An NOE experiment assisted with the stereochemical assignment of C-5 and C-1’. The acetyl methyl did not have correlation to the methylene protons on C-6. However, H_2-6 protons displayed an NOE correlation to H-1’. Single crystal x-ray analysis established the stereochemical configuration

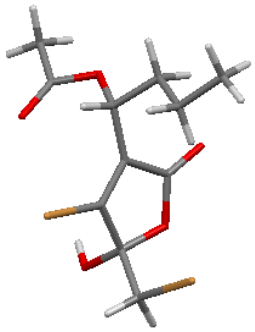

Figure 3.4 Crystal structure of SALT-26

3.6 Biological activity of Delisea pulchra *metabolites*

The halogenated polyketide metabolites isolated from *D. pulchra* were tested against a panel of six bacterial pathogens referred to as the ESKAPE panel (*Enterococcus faecium*, *Staphylococcus aureus*, *Klebsiella pneumoniae*, *Acinetobacter baumannii*, *Pseudomonas aeruginosa*, *Enterobacter* species). Compounds **3.7**, **3.8** and **3.9** gave minimum inhibitory concentration as low as 3 µg/mL against the gram-positive bacteria, *E. faecium,* and *S. aureus* (Table 3.8). Further studies of these compounds will include testing on the biofilms of these bacterial pathogens.

Table 3.8 Biological activity against ESKAPE panel

Sample ID	E	S	K	A	P	E
Acetoxyfimbrolide	**<3**	**<3**	**>50**	**>50**	**>50**	**>50**
Hydroxyfimbrolide	**6.25**	**12.5**	**>50**	**>50**	**>50**	**>50**
E-fimbrolide	**<3**	**<3**	**>50**	**>50**	**>50**	**>50**
Z-fimbrolide	**50**	**<3**	**>50**	**>50**	**>50**	**>50**
Pulchralide A	**>50**	**>50**	**>50**	**>50**	**>50**	**>50**
Pulchralide B	**12.5**	**>50**	**>50**	**>50**	**>50**	**>50**
Pulchralide C	**50**	**>50**	**>50**	**>50**	**>50**	**>50**
PSC17-20-M-3-b	**>50**	**>50**	**>50**	**>50**	**>50**	**>50**

- MIC recorded in µg/mL

3.7 Discussion and Conclusion

In this chapter, we have observed the potential of understanding the ecological interactions within these susceptible communities as it provides insight into microbial interactions. Interspecies and intraspecies communication is important for medicinal applications, particularly in this time of increasing drug resistance. Several well-known compounds were isolated called fimbrolides. This class of compounds has known antibiotic activity, which increased interest in the synthetic studies of this scaffold for further tests in drug development. However, only three of the compounds isolated were active against two Gram-positive bacteria from the ESKAPE panel. It is noteworthy that the compounds isolated were inactive against all four gram-negative bacteria.

3.8 References

(1) Maschek, J.; Baker, B. J. The chemistry of algal secondary metabolism. In *Algal Chemical Ecology*; Amsler, C. D., Ed.; Springer Berlin Heidelberg: Berlin, Heidelberg, 2008; pp 1–24.

(2) Blunt, J. W.; Carroll, A. R.; Copp, B. R.; Davis, R. A.; Keyzers, R. A.; Prinsep, M. R. Marine natural products. *Nat. Prod. Rep.* **2018**, *35*, 8–53.

(3) Paul, V. J.; Cruz-Rivera, Edwin; Thacker, R. W. Chemical Mediation of Macroalgal–Herbivore Interactions: Ecological and Evolutionary Perspectives. In *Marine Chemical Ecology*; McClintock, J., Baker, B., Eds.; Marine Science; CRC Press, 2001; pp 227 – 250.

(4) Hu, G.-P.; Yuan, J.; Sun, L.; She, Z.-G.; Wu, J.-H.; Lan, X.-J.; Zhu, X.; Lin, Y.-C.; Chen, S.-P. Statistical research on marine natural products based on data

obtained between 1985 and 2008. *Mar. Drugs* **2011**, *9*, 514–525.

(5) Hay, Mark E.; Fenical, W. Marine plant- herbivore interactions: the ecology of chemical defense. *Annu. Rev. Ecol. Syst.* **1988**, *19*, 111–145.

(6) Bergström, G. Chemical ecology = chemistry + ecology! *Pure Appl. Chem.* **2007**, *79*, 2305–2323.

(7) Fenical, W. Halogenation in the Rhodphyta: a review. *J. Phycol.* **1975**, *11*, 245–259.

(8) Van Alstyne, K. L.; Dethier, M. N.; Duggins, D. O. Spatial patterns in macroalgal chemical defenses. In *Marine Chemical Ecology*; McClintock, J., Baker, B., Eds.; CRC Press: Boca Raton, 2001.

(9) Kladi, M.; Vagias, C.; Roussis, V. Volatile halogenated metabolites from marine red algae. *Phytochem. Rev.* **2004**, *3*, 337–366.

(10) Figuerola, B.; Núñez-Pons, L.; Vazquez, J.; Taboada, S.; Cristobo, J.; Ballesteros, M.; Avila, C. Chemical interactions in Antarctic marine benthic ecosystems. In *Marine Ecosystems*; Cruzado, A., Ed.; Intech open access publisher: Rijeka, Croatia, 2012; pp 105–126.

(11) Paul, V. J.; Puglisi, M. P.; Ritson-Williams, R. Marine chemical ecology. *Nat. Prod. Rep.* **2006**, *23*, 153–180.

(12) Núñez-Pons, L.; Avila, C. Natural products mediating ecological interactions in Antarctic benthic communities: a mini-review of the known molecules. *Nat. Prod. Rep.* **2015**, *32*, 1114–1130.

(13) Cox, R. J. Polyketides, proteins and genes in fungi: programmed nano-machines begin to reveal their secrets. *Org. Biomol. Chem.* **2007**, *5*, 2010.

(14) Hanson, J. R. The classes of natural product and their isolation. In *Natural Products*; Royal Society of Chemistry: Cambridge, 2003; Vol. 17, pp 1–34.

(15) Puglisi, M. P.; Sneed, J. M.; Sharp, K. H.; Ritson-Williams, R.; Paul, V. J. Marine chemical ecology in benthic environments. *Nat. Prod. Rep.* **2014**, *31*, 1510–1553.

(16) Shin, J.; Seo, Y.; Rho, J.-R.; Baek, E.; Kwon, B.-M.; Jeong, T.-S.; Bok, S.-H. Suberitenones A and B: sesterterpenoids of an unprecedented skeletal class from the Antarctic sponge *Suberites* sp. *J. Org. Chem.* **1995**, *60*, 7582–7588.

(17) Lebar, M. D.; Heimbegner, J. L.; Baker, B. J. Cold-water marine natural products. *Nat. Prod. Rep.* **2007**, *24*, 774–797.

(18) Manefield, M.; de Nys, R.; Kumar, N.; Read, R.; Givskov, M.; Steinberg, P.; Kjelleberg, S. Evidence that halogenated furanones from *Delisea pulchra* inhibit acylated homoserine lactone (ahl)-mediated gene expression by displacing the ahl signal from its. *Microbiology* **1999**, *145*, 283–291.

(19) Harder, T.; Campbell, A. H.; Egan, S.; Steinberg, P. D. Chemical mediation of ternary interactions between marine holobionts and their environment as exemplified by the red alga *Delisea pulchra*. *J. Chem. Ecol.* **2012**, *38*, 442–450.

(20) Dworjanyn, S. A.; De Nys, R.; Steinberg, P. D. Localisation and surface quantification of secondary metabolites in the red alga *Delisea pulchra*. *Mar. Biol.* **1999**, *133*, 727–736.

(21) Andersen, J. B.; Eberl, L.; Anthoni, U.; Christophersen, C.; Givskov, M.; Rasmussen, T. B.; Steinberg, P.; Manefield, M.; Kjelleberg, S. How *Delisea pulchra* furanones affect quorum sensing and swarming motility in *Serratia liquefaciens*. *Microbiology* **2000**, *146*, 3237–3244.

(22) De Nys, R.; Steinberg, P. D.; Willemsen, P.; Dworjanyn, S. A.; Gabelish, C. L.; King, R. J. Broad spectrum effects of secondary metabolites from the red alga *Delisea pulchra* in antifouling assays. *Biofouling* **1995**, *8*, 259–271.

(23) Ankisetty, S.; Nandiraju, S.; Win, H.; Park, Y. C.; Amsler, C. D.; McClintock, J. B.; Baker, J. A.; Diyabalanage, T. K.; Pasaribu, A.; Singh, M. P.; Maiese, W. M.; Walsh, R. D.; Zaworotko, M. J.; Baker, B. J. Chemical investigation of predator-deterred macroalgae from the Antarctic peninsula. *J. Nat. Prod.* **2004**, *67*, 1295–1302.

(24) de March, P.; Font, J.; Gracia, A.; Qingying, Z. Easy access to 5-alkyl-4-bromo-2(5H)-furanones: synthesis of a fimbrolide, an acetoxyfimbrolide, and bromobeckerelide. *J. Org. Chem.* **1995**, *60*, 1814–1822.

(25) Nandiraju, S. Chemical and biological investigation of the Antarctic red alga delisea pulchra. M.S. Thesis, University of South Florids, Tampa, FL, 2004.

CHAPTER FOUR:

CHEMICAL DIVERSITY OF ANTARCTIC DEEP-SEA CORALS

NOTE TO READER: Portions of this chapter contain reproduced information and data from an article published in the Journal of Natural Products with permission from the American Chemical Society(ACS).[1] Further permissions related to the material excerpted should be directed to the ACS. (See appendix C)

4.1 Octocorallia: a terpene 'gold-mine.'

Soft corals and gorgonians within Octocorallia are reliable sources to search for novel bioactive compounds as drug leads.[2] These organisms are sessile invertebrates with soft, fleshy and fragile outer tissues lacking physical defense; thus they survive competitive environments because of chemical defense.[2] The secondary metabolites have biochemical defensive roles such as antifeeding, cytotoxicity, reproduction, antifouling, allelopathy, and other ecological benefits.[2] An Antarctic gorgonian, *Dasystenella acanthine,* yielded three sesquiterpene metabolites; *trans*-β-farnesene (**4.1**), furanoeudesmane (**4.2**), and isofuranodiene (**4.3**).[3] Compounds **4.2** and **4.3** displayed ichthyotoxicity activity at 10 ppm against *Gambusia affinis* suggesting that these compounds may be involved in this organism's defense.[3]

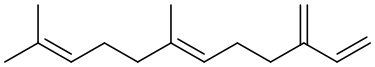

4.1

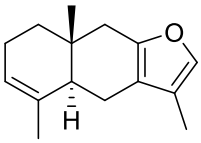

4.2

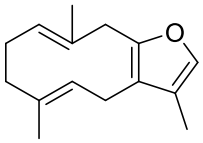

4.3

Gorgonians corals display the largest chemodiversity of secondary metabolites including diterpenes and sesquiterpenes.[4] Moreover, these corals provide a wealth of new metabolites that exhibit a range of biological activities.[4–6] In a review of diterpenoids isolated from gorgonians, 17 different scaffolds were reported from 13 genera of gorgonian corals.[4] Gorgonian corals yield 178 briarane-type diterpenes.[4] This number constituted more than half of the diterpene compounds reported in that review. From the initial isolation of briarein, there have been hundreds of derivatives isolated from multiple species, genera, and orders of octocorals. Briarane diterpenoids represented the largest group of natural products isolated from this Order. Briarane-type scaffold have generated considerable biomedical interest because of their structural complexity and associated biological activities.[7,8] For example, a suite of briarane derivatives were isolated from a Taiwanese gorgonian coral.[7,8] The fragilides (**4.4**-**4.13**) are compounds with unusual structural features observed in fragilide E (**4.8**), with rare acetylation on carbon 20.[9] Moreover, fragilide F (**4.9**) is one of the rare occurrences of halogenation on a briarane scaffold.[10] Further, fragilide H (**4.11**) is the first briarane reported to contain a hemiacetal group and fragilide I (**4.12**) the first 9-isovaleroxy group.[10] The chemical diversity among this class of compounds complements the biological activity. Fragilides C (**4.6**), E (**4.8**) and J (**4.13**) displayed varying levels of anti-inflammatory activity.[4]

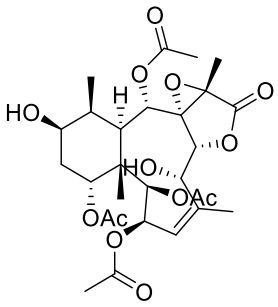

4.4

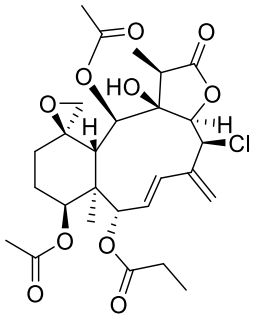

4.5

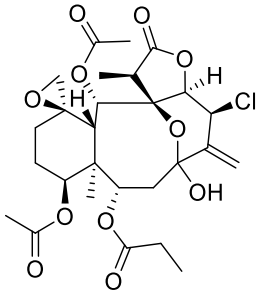

4.6

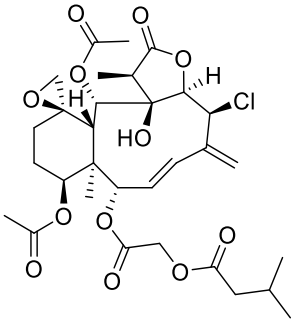

4.7

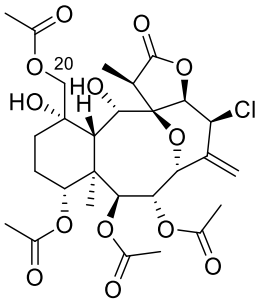

4.8

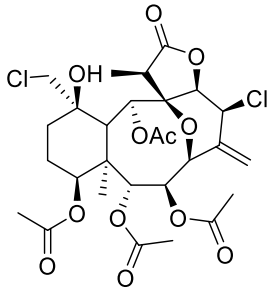

4.9

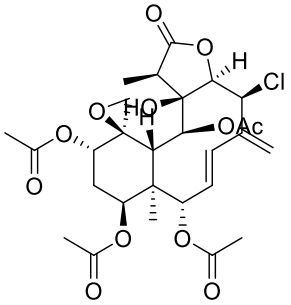

4.10

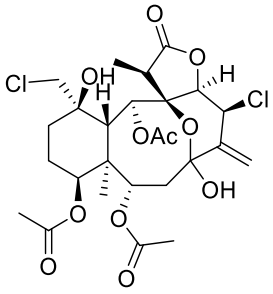

4.11

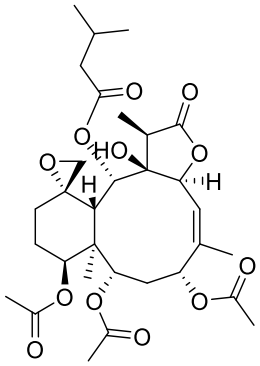

4.12

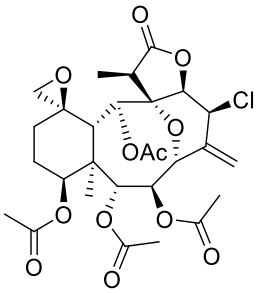

4.13

The briarane-type compounds are common to corals across multiple orders of Octocorallia. A series of compounds named anthoptilides (**4.14**-**4.18**) were isolated from a coral of the order Pennatulacea.[11] It is another order of Octocorallia chemically enriched with toxic metabolites.[8] It is worth mentioning that this group of compounds is the first to be isolated from the *Anthoptilum* sp.[12] The anthoptilides contains structural novelty within anthoptilide A and D; the former has a tiglate group and the latter a benzoate group as

substitutions on carbon 2. Both functionalities are uncommon to briarane. Thus, corals specifically octocorals present a source of new bioactive metabolites.

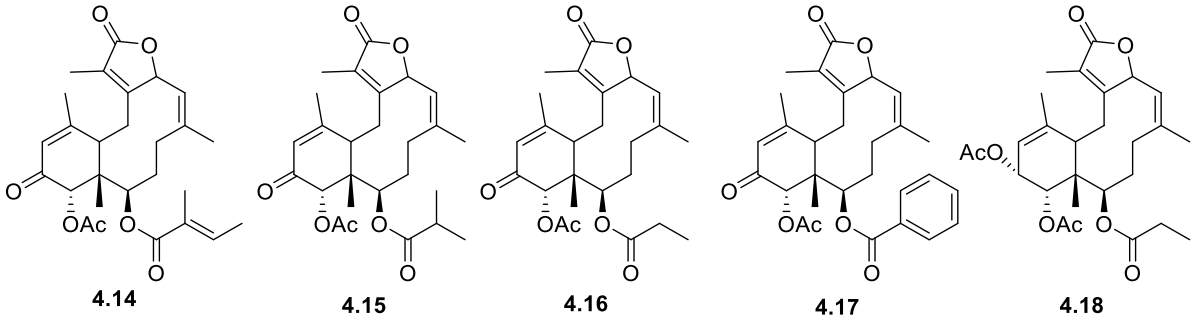

4.2 The Deep-sea

The deep sea harbors a myriad of marine species only encountered at considerable depths.[13] These inhabitants experience extreme conditions in the absence of light and high pressures, therefore they adapt biochemically and physiologically to survive these conditions.[13] For instance, every 10 m below sea level pressure increases by 1 atm; thus, deep-water organisms biochemically adjust to cope with pressures higher than 10 atm or even 1000 atm. These adaptations influence gene regulation and metabolic pathways increasing the diversity of natural products from their shallow water counterparts.[13]

Up to 2013, reports have appeared describing 578 marine natural products from depths ranging from 50 to over 5000 m.[12–14] This number represents less than 2% of the > 30,000 marine natural products described.[12] The oceans cover 70% of earth's surface, and 95% of this area has depths greater than 1000 m.[14] Difficulties of accessing these depths made deep-sea research tedious; but, improved technology and submersibles gave access to this underexplored environment.[15] With the ocean being home for over 10 million species, competition is high giving rise to high species diversity.[16] Besides coral

reefs and rainforests, deep-water communities comprise some of the most biodiverse and species-rich habits.[16] With such diversity and relatively low numbers of natural products, the deep sea is an excellent environment for finding novel compounds as drug leads.

4.3 Antarctic Deep-Sea Corals

The chemical accounts for Antarctic deep-sea corals are scarce; however, the few records illustrate that they are prolific in sesquiterpenes.[13,14,17,18] As mentioned above, *D. acanthine* is a gorgonian coral collected in Antarctic waters at a depth of 300 m.[3] This coral yield three sesquiterpenes which displayed activity in an ichthyotoxicity assay.[3] Another Deep-sea Antarctic soft coral, *Alcyonium paessleri,* produces two classes of sesquiterpenes; called alcyopterosins and paesslerins.[19] Both scaffolds are rare classes with unique functionalities the alcyopterosins contained compounds with nitrate ester substituents, and the paesslerins presented a new tricyclic scaffold with moderate cytotoxicity.[19] In 2003 a report of two sesquiterpenes isolated from the gorgonian coral, *Ainigmaptilon antarcticus.* Ainigmaptilone A inhibit predation by *Odontaster validus* also showed selective antibiotic activity against sympatric Antarctic bacteria.[20] Shagenes A and B are also sesquiterpenoid metabolites from an unidentified soft coral collected in the Southern Ocean surrounding Antarctica.[21] Shagene A elicits selective activity against visceral leishmaniasis with no cytotoxicity.[21]

4.4 Research objectives

As previously stated, the number of metabolites from Antarctic deep-sea corals are relatively low compared to other marine biotas. The compounds isolated from these corals are fruitful in novelty with reports of first occurrence functionalities or skeletons. Sesquiterpenes are the most reported terpene from Antarctic corals. With only a small

portion of Antarctic corals represented in the literature, a wealth of chemistry may be found from these benthic organisms.

Antarctic waters are rich in chemical and biological diversity, especially in the deep seas. With this assessment, this chapter describes the chemical investigation of three corals from the deep waters of Antarctica. We collected the corals from depths ranging between 600 m and 1000 m. The collection of these corals used trawling onboard R/V Nathaniel B. Palmer during the austral autumn. The first coral described is a gorgonian coral, *Plumarella delicatissima.* This sea fan is the first of this genus to be studied from Antarctic waters. Using chromatographic methods to purify secondary metabolites and study their pharmacological properties. Two other corals, a sea pen and an undescribed octocoral, from the deep Antarctic sea composed this chapter. Isolation of the secondary metabolites and biological testing were the primary objectives of this project.

4.5 Furanocembranoids and Leishmaniasis

4.5.1 Diterpenes isolated from Plumarella delicatissima

In the following section, the chemical investigation of an Antarctic deep-sea coral, *Plumarella delicatissima* (Figure 4.1), is described. Cembrene-derived diterpenes and a nor-diterpene were isolated, described, and tested against multiple biological assays including bacterial pathogens, cancer cell lines, and parasites. However, the only compound that displayed significant anti-parasitic activity is the known diterpene, pukalide aldehyde. In specific, the soft coral-derived diterpene exhibited activity against the infected macrophage form of *Leishmania donovani,* and no significant activity in the A549 mammalian cells illustrating its selectivity for the parasite relative to mammalian cells.

Figure 4.1 Photo of *Plumarella delicatissima* (Photo Credit: Bill Baker)

4.5.2 Collection and processing of Plumarella delicatissima

Plumarella delicatissima specimens were collected in April of 2013 from depths between 800-950m by trawling near the Falkland Islands in the Southern Ocean (Plateau of Fascination, S 50° 8.453' W 55° 28.106'). The samples were immediately frozen and stored for chemical analysis. The frozen coral was freeze-dried and extracted using a Soxhlet apparatus with refluxing CH_2Cl_2. Analysis of the ^1H NMR spectrum from the organic extract indicated the presence of terpenes. The extract was dried onto silica gel and subjected to normal-phase MPLC. Normal phase semi-preparative HPLC was used for the initial purification, though some metabolites required an additional purification step using reversed-phase analytical HPLC, yielding the seven compounds including the new keikipukalides A (12 mg), B (5 mg), C (3 mg), D (18 mg), E (48 mg) , and the known derivatives, pukalide aldehyde (4 mg) and ineleganolide (3 mg) [**4.19**- **4.25**] (Scheme 4.1).

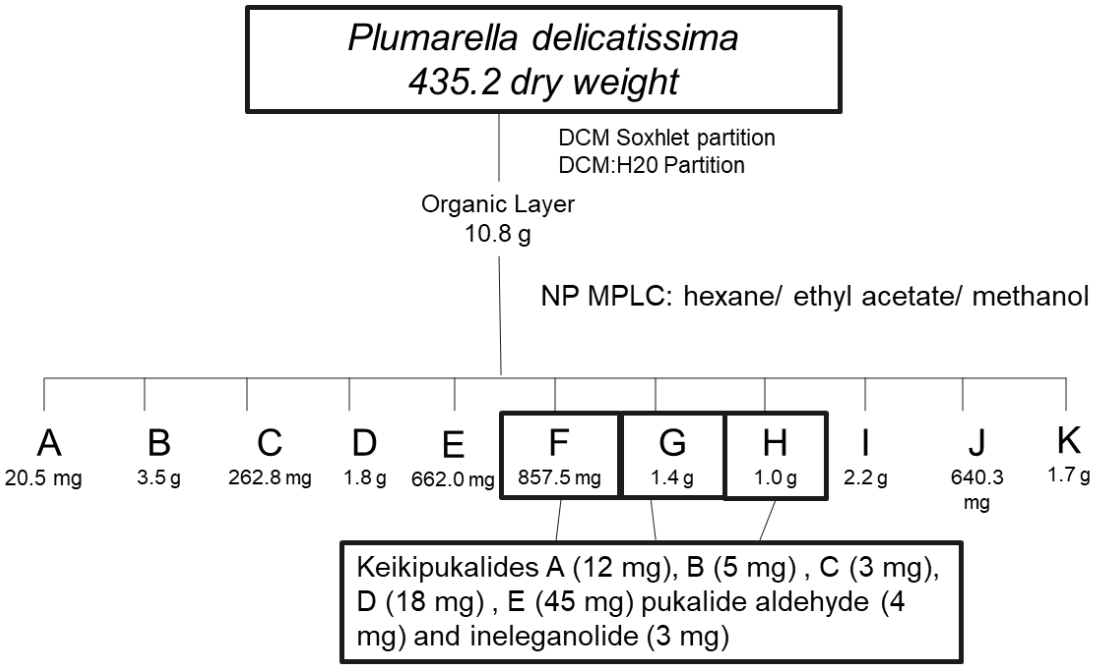

Scheme 4.1 Isolation of keikipukalide A-E, pukalide aldehyde and ineleganolide.

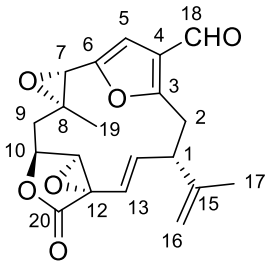

Keikipukalide A (**4.19**)

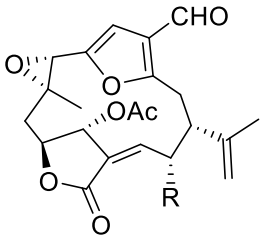

Keikipukalide B (4.**20**), R = OAc
Keikipukalide C (**4.21**), R = H

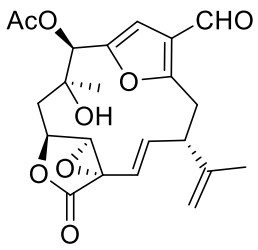

Keikipukalide D (**4.22**)

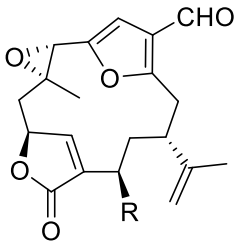

Keikipukalide E (**4.23**), R = OAc
Pukalide Aldehyde (**4.24**), R = H

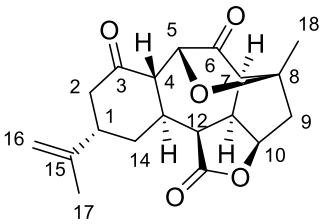

Ineleganolide (**4.26**)

4.5.3 Structure elucidation of keikipukalides

Keikipukalide A (**4.19**) is a crystalline solid with a chemical formula of $C_{20}H_{20}O_6$ (calcd for $C_{20}H_{20}O_6$, 356.1260) based on high-resolution ESIMS, ^1H and ^{13}C NMR data (Table 4.1). Eleven degrees of unsaturation were calculated for this molecule with six of those assigned to the aldehyde and ester-type carbonyls and four olefins, indicating a five-ringed structure. The HSQC spectrum depicted a terminal methylene based on δ_H 4.56 (H-16a) and δ_H 4.97 (H-16b) to δ_C 113.6 (C-16). H_2-16 was determined to be a part of the isopropylene substituent with HMBC correlations among C-15 (δ_C 143.5), C-17 (δ_C 23.2) and C-1 (δ_C 47.1). The COSY spectrum showed C-1 as a part of a spin system containing the olefinic methines at δ_H 5.14 (H-13) and δ_H 7.41 (H-14) along with the methylene signals at δ_H 3.31 (H-2a) and δ_H 3.42 (H-2b). Extension of this system through HMBC correlations placed a furan ring adjacent to C-2 (δ_C 31.0). The furan ring was established with the olefinic singlet at δ_H 6.47 (H-5) correlating to the fully substituted olefin δ_C 162.2 (C-3) and δ_C 124.3 (C-4) as well as its adjacent olefinic carbon at C-6 (δ_C 149.2). The deshielding of C-6 was affiliated with its attachment to oxygen as seen in C-3, but further deshielding effects suggested an electron withdrawing substituent on C-4. The HMBC spectrum was useful for the assignment of the aldehyde as the signal at δ_H 9.89 (H-18), which correlated to C-4 and C-5. Going back to the $^4J_{HH}$ spin system, H-13 correlated in the HMBC spectrum to the lactone ester at δ_C 169.0 (C-20). Further HMBC correlation of H-11 (δ_H 4.09) to C-10 (δ_C 75.3), C-12 (δ_C 58.0), and C-20 established the butenolide, which was adjacent to H_2-9 in a COSY spin system. HMBC helped to establish the C_{14} macrocyclic ring with correlations of H-9 among the remaining carbons C-7 (δ_C 54.6), C-8 (δ_C 56.9), and C-19 (δ_C 21.3). With three of the five rings established and two

Table 4.1. NMR Data for Keikipukalide A [1]

Position	$^{13}C^{bc}$, type	$^{1}H^{ab}$ (*J* in Hz)	HMBC[a]
1	47.1, CH	3.47, m	3,14
2a	31.0, CH_2	3.31, m	1,3,4,14,15
2b		3.42, m	1,15
3	162.2, C		
4	124.3, C		
5	105.6, CH	6.47, s	3,4,6
6	149.2, C		
7	54.6, CH	4.01, s	5,6,8
8	56.9, C		
9a	40.4, CH_2	2.09,dd (15.6, 1.8)	8,10,11,19
9b		2.58,dd (15.6, 4.2)	7,8
10	75.3, CH	4.78, dd (4.0, 2.7)	
11	64.1, CH	4.09, s	10,12,20
12	58.0, C		
13	115.6, CH	5.14,dd (16.3, 1.5)	1,14,20
14	145.8, CH	7.41,dd (16.3, 4.4)	15
15	143.5, C		
16a	113.6, CH_2	4.56, s	
16b		4.97, s	1,17
17	23.2, CH_3	1.70, s	1,15,16
18	184.3, CH	9.89, s	4,5
19	21.3, CH_3	1.23, s	7,8,9
20	169.0, C		

[a]$CDCl_3$, 400 MHz. [b] Reported in ppm
[c]$CDCl_3$, 100 MHz, multiplicity determined by HMQC.

oxygens unaccounted for, epoxides at C-7/8 and C-11/12 could complete the planar structure of keikipukalide A (Figure 4.2).

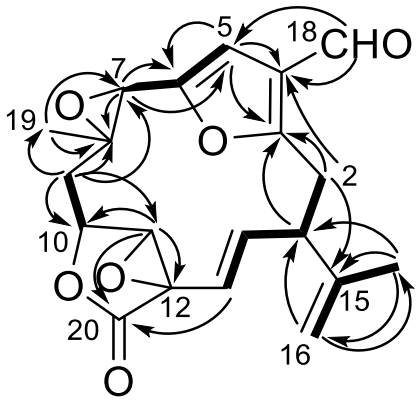

Figure 4.2. Key COSY (—) and HMBC (→) correlations establishing the planar structure of keikipukalide A.[1]

Stereochemical evaluation of keikipukalide A was informed by through-bond or through-space correlations. The lack of coupling between H-10 and H-11 indicated a *trans* relationship between them placing the epoxide oxygen and C-10 on opposite faces of the butenolide. The C-13/C-14 olefin was defined as *trans* is based on the large coupling constant (16.3 Hz). The NOESY experiment suggested the C7/C8 epoxide was *trans* based on H-9a and H-7 correlation. Further assignments were obtained through X-ray analysis. The crystallographic metadata (Appendix C) assigned the configuration depicted in Figure 4.3 as the absolute configuration of keikipukalide A.

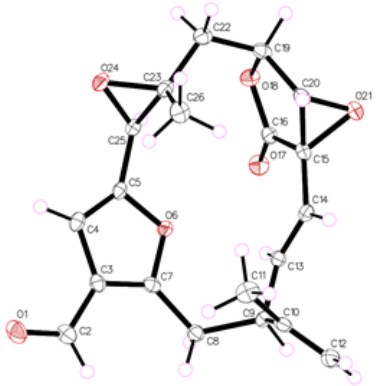

Figure 4.3. The asymmetric unit of keikipukalide A. Anisotropic displacement parameters is drawn at 50% probability.[1]

Keikipukalide B (**4.20**) was isolated as an oil with a formula of $C_{24}H_{26}O_9$ (calcd for $C_{20}H_{18}O_5$, 338.1154) based on mass spectrometric analysis and the ^{1}H and ^{13}C NMR data (Tables 4.2 and 4.3). An additional four carbons, six protons, and three oxygens were present in this compound compared to keikipukalide A. The one-dimensional NMR data displayed additional signals indicating the addition of two acetate groups. Analysis of the 2D data (Appendix C) found similar structural features to keikipukalide A between C-1 and C-10. HMBC correlations placed one of the acetate groups as a substituent on C-11 giving it a deshielded shift of δ_C 72.9. Also, C-12 could be assigned as an olefinic carbon

Table 4.2. ^{1}H NMR Data for Keikipukalides B-E [1]

Position	**2**[a]	**3**[a]	**4**[a]	**5**[b]
1	3.18, t (4.4)	3.01 m	3.19, m	4.07, dt (9.9, 5.9)
2 a	3.45, d (4.4)	3.49, dd (15.7, 4.4)	3.37, dd (14.2, 5.5)	3.00, d (4.7)
b		3.12, dd (15.7, 5.3)	2.99, dd (14.3, 10.4)	2.99 (s)
3				
4				
5	6.46, s	6.46, s	6.62, s	6.44, s
6				
7	4.03,s	4.02, s	5.71, s	4.12, s
8				
9 a	1.97, dd (15.3, 3.4)	1.94, dd (15.2, 3.1)	2.14, dd (8.9, 4.1)	2.22, dd (15.0, 3.3)
b	2.61, dd (15.3, 3.4)	2.60, dd (15.2, 3.6)		2.53,ddd (15.0, 6.4, 3.7)
10	4.70, t (3.3)	4.66,t (3.4)	4.62, t (4.7)	5.25, dt (3.6, 1.7)
11	5.65, s	5.62, s	3.77, br s	7.31, d (1.3)
12				
13	6.54, d (9.1)	6.69, dd (11.6, 2.8)	5.72, d (15.9)	5.85, d (6.2)
14 a	6.97, d (9.1)	4.23, dd (17.3, 11.7)	5.57, dd (15.9, 10.0)	1.26, br d (15.0)
b	-	2.75,ddd (17.9, 9.0, 2.2)	-	2.58,ddd (15.0, 6.4, 3.4)
15				
16 a	4.34, s	4.53, s	4.84, s	4.92, s
b	4.96, s	4.93, s	4.90, s	5.03, s
17	1.82, s	1.78, s	1.82, s	1.91, s
18	9.86, s	9.90, s	9.87, s	9.86, s
19	1.17, s	1.20, s	1.47, s	0.98, s
20				
21				
22	2.12, s	2.10, s	2.21, s	2.01, s
23				
24	2.11, s			

[a] Recorded in $CDCl_3$ (400 MHz) [b] Recorded in $CDCl_3$ (500 MHz).

instead of the oxygen-bearing carbon, establishing an exocyclic olefin with C-13 (δ_C 145.6). The oxymethine adjacent to C-13 correlated to the carbonyl of the acetate group, completing the C_{14} macrocyclic ring and the planar structure of keikipukalide B.

Table 4.3. ^{13}C NMR Data for Keikipukalides B-E [1]

Position	**2**[b]	**3**[a]	**4**[a]	**5**[b]
1	47.4, CH	40.8, CH	49.2, CH	36.7, CH
2	28.7, CH_2	30.7, CH_2	31.2, CH_2	33.1, CH_2
3	161.6, C	162.4, C	163.0, C	162.3, C
4	123.4, C	123.3, C	124.5, C	123.2, C
5	104.7, CH	105.1, CH	106.2, CH	104.5, CH
6	149.5, C	149.7, C	150.3, C	149.8, C
7	54.7, CH	54.4, CH	75.4, CH	54.8, CH
8	56.3, C	56.8, C	74.3, C	56.8, C
9	40.1, CH_2	40.4, CH_2	37.9, CH_2	39.9, CH_2
10	81.0, CH	80.8, CH	75.8, CH	77.7, CH
11	72.9, CH	73.9, CH	67.7, CH	151.1, CH
12	127.4, C	124.1, C	58.2, C	134.8, C
13	145.6, CH	151.6, CH	121.1, CH	68.6, CH
14	70.6, CH	30.4, CH_2	134.4, CH	35.7, CH_2
15	143.1, C	144.8, C	144.6, C	148.5, C
16	114.8, CH_2	113.0, CH_2	111.2, CH_2	111.3, CH_2
17	24.7, CH_3	23.7, CH_3	21.4, CH_3	20.7, CH_3
18	184.2, CH	184.4, CH	184.3, CH	184.4, CH
19	20.7, CH_3	20.99, CH_3[c]	31.3, CH_3	19.7, CH_3
20	166.6, C	168.2, C	171.6, C	170.3, C
21	170.6, C	170.6, C	169.0, C	170.5, C
22	21.2, CH_3[c]	21.03, CH_3[c]	20.9, CH_3	20.6, CH_3
23	169.4, C			
24	21.0, CH_3[c]			

[a] Recorded in $CDCl_3$ (100 MHz) [b] Recorded in $CDCl_3$ (125 MHz). Multiplicity determined by HSQC (**2** and **5**) or HMQC (**3** and **4**). [c] Interchangeable

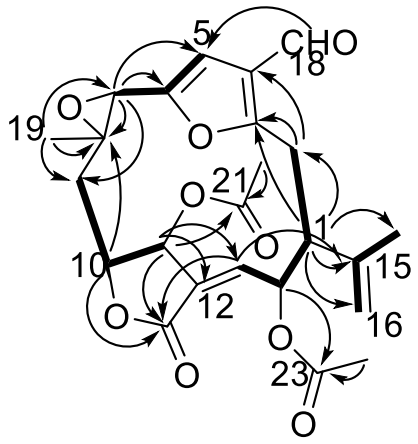

Figure 4.4. Key COSY (**—**) and HMBC (→) correlations establishing the planar structure of keikipukalide B.[1]

The stereochemical assignment of keikipukalide B was based on chemical shifts and coupling constants, compared to keikipukalide A. All the asymmetrical carbons match

those in keikipukalide A including the C-7/C-8 epoxide, H-10, and H-11. They also match the known derivative pukalide. The $\Delta^{12,13}$ olefin was assigned as *Z* based on observation of NOESY correlation between H-11 and H-13. The X-ray analysis of keikipukalide A facilitated in assigning the configuration between H-1 and H-14, indicating a 90° dihedral angle. The negligible $^{3}J_{1,14}$ coupling confirmed this configuration.

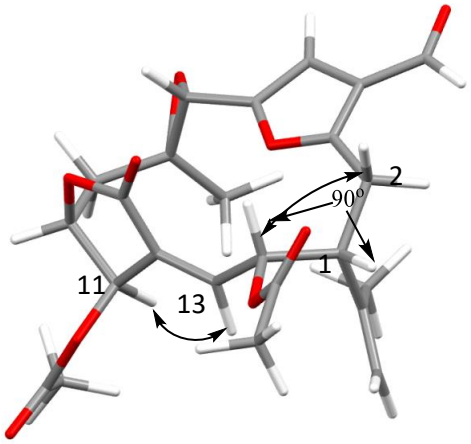

Figure 4.5 Relative configuration of keikipukalide B (4.19) C-1 and C-14 based on $^{3}J_{1,14}$ ~ 0 and NOESY (↔) correlations.[1]

Keikipukalide C (**4.21**) was isolated as a white semi-solid with a formula of $C_{22}H_{24}O_7$ (cald $C_{20}H_{20}O_5$, 340.1307) based on mass spectrometric, ^{1}H and ^{13}C NMR data (Tables 4.2 and 4.3). Eleven degrees of unsaturation were accounted for in this compound as with keikipukalide A. An acetate group was observed accounting for the difference in formula. Figure 4.6 shows the planar structure of keikipukalide C showing the same scaffold as the previous keikipukalides described. However, C-14 is assigned as methylene instead of the oxymethine in keikipukalide B. The configuration of keikipukalide C was the same as keikipukalide B including the *trans* C-7/C-8 epoxide as well as the H-10 and H-11 configurations based on the NOESY experiment.

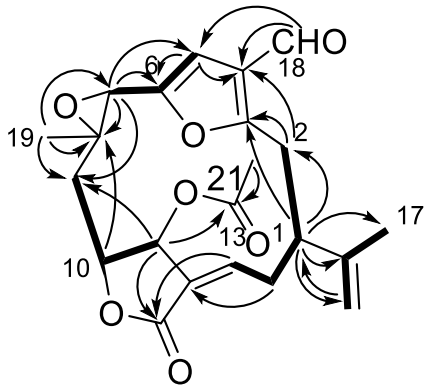

Figure 4.6 Key COSY (**—**) and HMBC (→) correlations establishing the planar structure of keikipukalide C.[1]

Keikipukalide D (**4.22**) was isolated as an amorphous solid and its chemical formula calculated as $C_{22}H_{24}O_8$ (calcd for $C_{20}H_{20}O_6$, 356.1260) from mass spectrometric and NMR data. After establishing the characteristic scaffold using 2D NMR data, a deshielded shift was observed in positions C-7 and C-8 (δ_C 75.4 and 74.3). C-7 correlated to an acetate carbonyl (δ_C 169.0), and the remaining oxygen was assigned as a hydroxyl substituent on C-8. The remaining structure was similar to keikipukalide A which assisted with assigning the stereochemical configuration of this compound. The NOESY correlations between H-7, H-11, and H-19 placed the hydrogens on the same face of the molecule.

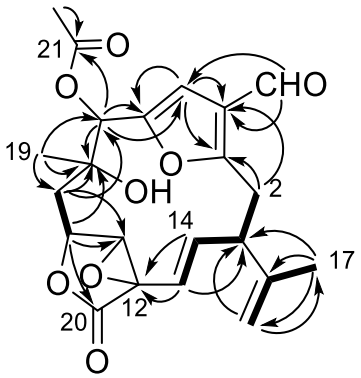

Figure 4.7 Key COSY (**—**) and HMBC (→) correlations establishing the planar structure of keikipukalide D.[1]

Keikipukalide E (**4.23**) was isolated as a crystalline solid with a chemical formula of $C_{22}H_{24}O_7$ (calcd for $C_{22}H_{25}O_7$, 401.1600) assigned by HRESIMS and 1D NMR data.

The formula of this compound matched its isomer keikipukalide C, but analysis of the COSY and HMBC NMR spectra matched pukalide aldehyde (**4.24**).[2] The HSQC spectrum indicated the methine doublet δ_H 5.85 (H-13) was on C-13 (δ_C 68.6). The deshielded shift indicated that an acetate group was adjacent to C-13 rather than C-11 in keikipukalide C (Figure 4.8). The stereochemical configuration of keikipukalide E (Figure 4.13) was assigned by the crystallographic metadata (Appendix C) of the X-ray analysis.

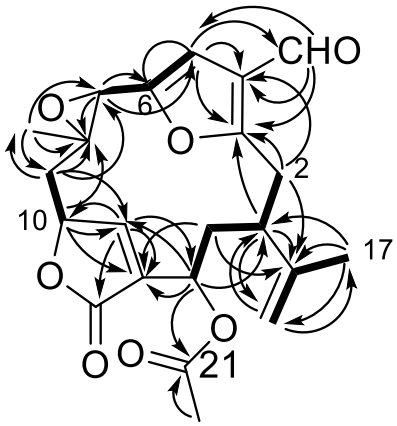

Figure 4.8 Key COSY (—) and HMBC (→) correlations establishing the planar structure of keikipukalide E.[1]

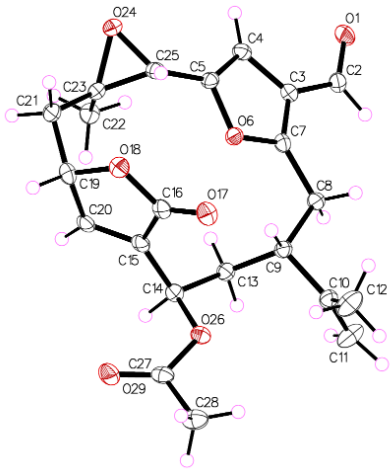

Figure 4.9 Asymmetric unit of keikipukalide E. Anisotropic displacement parameters are drawn at 50% probability.[1]

Compound **4.24**, another furan cembrenoid diterpene was also isolated from the organic extract of the Antarctic deep-sea gorgonian, *P. delicatissima.* This furan cembrane along with numerous related compounds was previously reported from

Lophogorgia sp.[2] Lophotoxin (**4.25**), one of the furanocembranoids isolated from this genus of soft coral, displayed potent, irreversible inhibition of nerve transmission when compared to its less potent counterparts.[2]

Ineleganolide (**4.26**), a known bioactive diterpenoid was also isolated from the DCM extract of *P. delicatissima*. Following the same isolation scheme as the keikipukalides, ineleganolide was purified from an MPLC fraction using gradient of *n*-hexanes and EtOAc, then subsequently separated on an HPLC NP silica column (*n*-hexane/EtOAc) followed by RP HPLC utilizing a C-18 column (MeOH/H_2O). This norditerpene was initially isolated from the Formosan soft coral, *Sinularia inelegans* and like the previously described compounds, it is related to cembrane diterpenes with the loss of a single carbon (C18) from the C_{20} skeleton.[22] These norcembranoids are common to *Sinularia* sp. and are proposed to undergo similar biogenetic pathways inclusive of converting of the C18 functional group for decarboxylation, leading to the norcembrane structure.[23] Supporting spectroscopic data for ineleganolide(**4.26**), and pukalide aldehyde (**4.24**) are located in Appendix C.

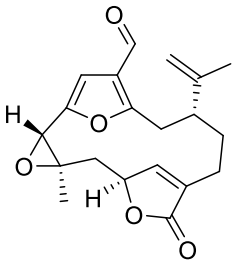

4.24

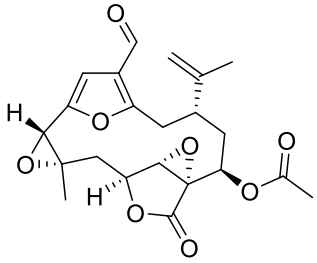

4.25

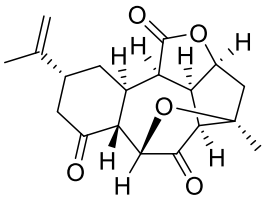

4.26

Table 4.4 Comparison of experimental and literature ^{13}C NMR shifts for **4.24** and **4.26**

Position	δ_C (literature); multiplet **4.24**	δ_C (experimental); multiplet **4.24**	δ_C (literature); multiplet **4.26**	δ_C (experimental); multiplet **4.26**
1	40.5, CH	41.0	40.2	40.1
2	31.2, CH_2	31.2	44.3	44.3
3	162.7, C	162.7	206.2	206.3
4	123.3, C	123.1	49.7	49.6
5	104.2, CH	104.2	77.4	77.3
6	149.9, C	149.8	211.9	212.0
7	54.8, CH	54.9	62.4	62.3
8	57.7, C	57.1	90.9	90.9
9	39.9, CH_2	40.5	45.4	45.3
10	77.8, CH	77.8	83.0	83.0
11	148.1, CH	148.1	43.7	43.6
12	136.7, C	137.5	46.9	46.9
13	22.7, CH_2	22.8	33.1	33.1
14	32.3, CH_2	32.3	32.6	32.5
15	145.2, C	145.3	145.8	145.9
16	113.5, CH_2	113.7	22.5	22.5
17	18.8, CH_3	18.8	113.6	113.7
18	184.5, CH	184.5	20.1	20.1
19	19.9, CH_3	19.9	175.8	175.9
20	170.0, C	174.0		

4.5.4 Biological activity of keikipukalides and their known derivatives

The seven terpenoids isolated from *P. delicatissima* were evaluated against infectious disease targets. *Leishmania donovani* was quite sensitive, displaying an IC_{50} of 1.9-12 μM for the diterpenes (Table 4.5) in the infected macrophage assay, compared to the IC_{50} of 6.2 for miltefosine, a drug currently used for the treatment of leishmaniasis. No mammalian cytotoxicity was detected in the compounds below 50 μM. However, testing against other infectious diseases, including, *Naegleria fowleri*, the *Enterococcus faecium*, *Staphylococcus aureus*, *Klebsiella pneumoniae*, *Acinetobacter baumanii*, *Pseudomonas aeruginosa*, and *Enterobacter* species, the ESKAPE panel of drug-resistant bacteria and *Clostridium difficile*, found none of these pathogens susceptible to

the compounds. Although this seeming specificity for *L. donovani* is promising for this scaffold, most of these compounds contain the neurotoxic pharmacophore of lophotoxin, which may prove to be a liability. It is noteworthy to mention that ineleganolide is known for its cytotoxicity against P-388 cell line,[23] however, it was not determined to be cytotoxic against the A549 cell line.

Table 4.5. Bioactivity of *Plumarella* Terpenes (IC_{50}, μM)[a1]

	Leishmania donovani	A549 Cytotoxicity
Keikipukalide A (**4.19**)	>28	>50
Keikipukalide B (**4.20**)	8.5	>50
Keikipukalide C (**4.21**)	8.8	>50
Keikipukalide D (**4.22**)	12	>50
Keikipukalide E (**4.23**)	8.8	>50
Pukalide Aldehyde (**4.24**)	1.9	>50
Ineleganolide (**4.26**)	4.4	>50
Miltefosine (control)	6.2	Not determined

[a] The > symbol indicates the sample was inactive at the highest concentration tested

4.6. Briarane- type diterpenes as an anti-parasitic and anti-cancer lead

The narrator states, "Upon the sands of this island of Sombrero we found a small twig growing up like a young tree, and on offering to pluck it up, it shrinks down to the ground, and sinks, unless held very hard. On being plucked up, a great worm is found to be its root, and as the tree growth in greatness, so doth the worm diminish; and as soon as the worm is entirely turned into tree, it rooteth in the earth, and so becomes great. This transformation is one of the strangest wonders that I saw in all my travels: For, if this tree is plucked up when young, and the leaves and bark stripped off, it becomes a hard stone when dry, much like white coral: thus is this worm twice transformed into different natures. Of these we gathered and brought home many."

Figure 4.10 An excerpt from an anonymous chronicler of Captain James Lancaster's voyage to the East Indies in the 1600s describing the collection of a sea pen.

Anthoptilum, the descriptive term given to identify this genus of octocoral, is derived from the combination of the Greek term ‘Anthos’ and ‘ptilum’ meaning flower and spear, respectively. ‘Anthos’ describes the flower appearance of the polyps that are branched out and ptilum is for its overall shape of a spear. Figure 4.11 shows the overall shape of the coral after collection.

Figure 4.11 Snapshots of *Anthoptilum* sp. Displaying the full length of the organism, pendulum, and polyps. Photo credit: Bill Baker

The coral *Anthoptilum* sp. was collected by trawl at a depth of 662-944 m during an austral autumn cruise aboard the R/V Nathaniel B. Palmer in the vicinity of the Scotia Arc. The sample was kept frozen after collection then freeze-dried in preparation for chemical analysis. This sea pen was exhaustively extracted using a Soxhlet extractor with refluxing DCM, then subsequently partitioned using DCM and brine for initial separation. Dereplication of the organic extract using ^{1}H NMR data gave insight that briarane-type compounds were present in the sample. The DCM fraction was dried onto silica and subjected to NP MPLC. Further evaluation of the fractions led to the purification of four new compounds using NP HPLC and RP HPLC for purification.

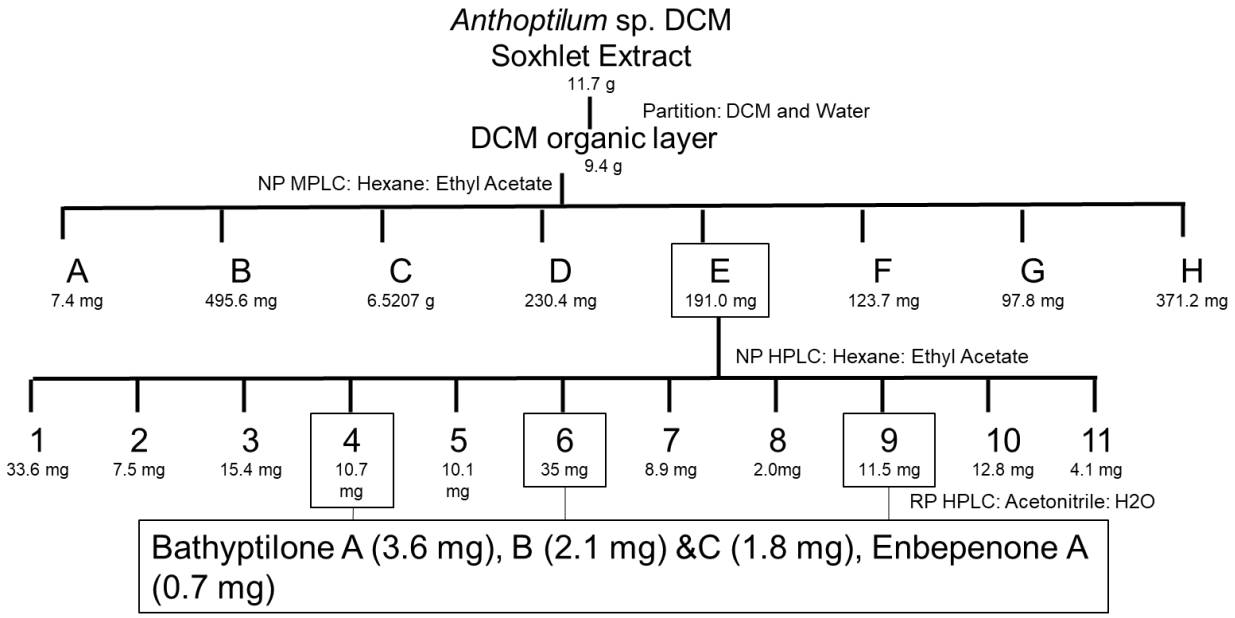

Scheme 4.2 Isolation scheme for *Anthoptilum* sp.

Bathyptilone A-C (**4.27**-**4.29**) and a new scaffold of a trinorditerpene, enbepenone A (**4.30**) likely derived from a briarane precursor were isolated from this Antarctic pennatulacean. The structures of these compounds were determined by one- and two-dimensional NMR analysis, the three-dimensional conformation was confirmed using X-ray crystallography.

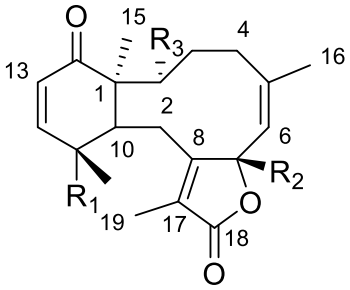

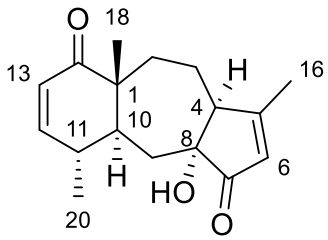

4.27 R_1: OH, R_2: OH, R_3:H
4.28 R_1: H, R_2: OH, R_3: OAc
4.29 R_1:OH, R_2: H, R_3:H

4.30

4.6.1 Structure elucidation of bathyptilones and enbepenone

Bathyptilone A (**4.27**) was isolated as crystalline solid with a molecular formula of $C_{20}H_{26}O_5$ (calcd $C20H_{27}O_5$) confirmed by HRESIMS with supporting ^{1}H and ^{13}C NMR data (Table 4.6). The ^{13}C NMR spectrum indicated the presence of a ketone, an ester, four quaternary, four methine, four methylene, and four methyl groups, and two oxygen-bearing carbons; accounting for all carbons and protons present in the molecule. A tricyclic scaffold was indicated by the degree of unsaturation, as five of these were identified by the ^{13}C resonances of the ketone at δ_C 204.3 (C-14), ester δ_C 171.4 (C-18) and the 6 olefinic peaks (δ_C 160.6, 124.0, 145.2, 125.7, 151.5, 127.3).

The first of the tricycle rings was identified using the spin system of the olefinic protons from the COSY spectrum. The protons at δ_H 6.63 (H-12) and δ_H 5.96 (H-13), had a correlation in the HMBC spectrum to δ_C 203.7 (C-14), a methine at δ_C 41.3 (C-10), a quaternary carbon δ_C 50.3 (C-1) and a carbon bearing an electron withdrawing group at δ_C 69.2 (C-11). These correlations resulted in a six-membered α,β-unsaturated ketone. A hydroxy group was assigned to C-11 as well as the methyl singlet δ_H 1.35 (H-20) based on HMBC correlation.

A ten-membered ring was assigned adjacent to the six-membered ring by the HMBC spectrum. The constituents of the ring were identified using both COSY and HMBC experiments. The COSY spectrum showed that H_2-2 connected to H-3b which was connected to H-4b, each of which correlated by HMBC to the two olefin carbons at δ_C 160.6 (C-5) and δ_C 124.0 (C-6). The carbon at position 5 was found to be a quaternary carbon by HSQC data and was substituted with a vinylic methyl δ_H 1.78 (H_3-16) based on the HMBC correlation. The olefinic singlet that resonated at δ_H 5.32 (H-6) showed an

Table 4.6. NMR Spectroscopic Data for bathyptilone A in $CDCl_3$

Position	$^{13}C^a$, type	$^{1}H^b$ (*J* in Hz)	HMBC[b]
1	50.2, C	-	
2α	21.8, CH_2	1.54, m	14
β		1.84, m	1, 3, 4
3α	31.6, CH_2	1.52, m	2, 4
β		1.98, m	1, 2, 4, 10, 15
4α	29.5, CH_2	1.26, m	
β		1.85, m	3, 5, 6
5	145.3, C	-	
6	124.1, CH	5.35, s	4, 5, 7, 16
7	106.2, C	-	
8	160.7, C	-	
9α	22.7, CH_2	2.47, d (15.8)	1, 8, 10, 11, 17
β		3.25, dd (9.5, 15.3)	7, 10, 11, 17
10	41.4, CH	3.14, d (9.5)	1, 8, 9, 11, 15
11	69.3, C	-	
12	151.7, CH	6.63, d (10.0)	10, 11, 14, 20
13	127.4, CH	5.96, d (10.0)	1, 11
14	203.7, C	-	
15	24.2, CH_3	1.16, s	1, 2, 3, 10, 14
16	23.5, CH_3	1.78, s	4, 6, 5
17	125.8, C	-	
18	171.7, C	-	
19	9.1, CH_3	1.95, s	8, 17, 18
20	30.4, CH_3	1.35, s	10, 11, 12

[a]125 MHz, multiplicity determined by HSQC. [b]500 MHz.

HMBC correlation to a deshielded carbon δ_C 106.1 (C-7). According to the HSQC experiment, this carbon was not assigned a proton which suggest it could be a ketal. The completion of this ten-membered ring was done with the assistance of the COSY spectrum by observation of correlation between the broad doublet δ_H 3.14 (H-10) and the doublet δ_H 1.54 (H-9a). The protons H_2-9 displayed HMBC correlation to the ester at δ_C 171.7 (C-18), and two olefinic quaternary carbons δ_C 145.16 (C-8) and δ_C 125.7 (C-17). These correlations were critical for the construction of the last ring of the tricyclic scaffold which was identified as a γ-lactone. The vinylic methyl at δ_H 1.95 (H-19) correlated to C-

8, C-17 and C-18 in the HMBC experiment. The olefin carbons C-17 and C-8 were assigned α,β to the ester, respectively. Despite the lack of protons in the proximity of the lactone moiety, the chemical shifts of the carbons allowed the connection of C-7 to the oxygen of the ester creating the hemiketal functionality. C-8 valance was completed with a bind connecting it to C-7 and C-9. The briarane skeleton was identified with this tricyclic ring system with oxidation of C-7, 11, 14 and 19.

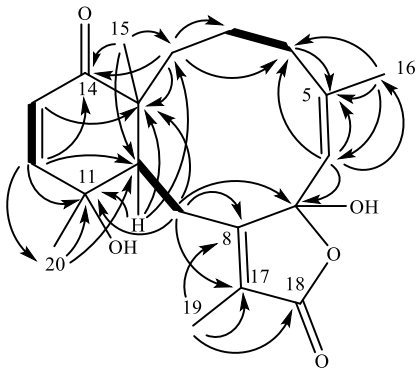

Figure 4.12. Key COSY (▬) and HMBC (→) correlations establishing the planar structure of bathyptilone A.

The relative configuration of **4.27** was assigned using a NOESY experiment. The proton at position 10 showed correlation to H-20 and H-2a correlated to H-15. The absence of correlation between H-15 and H-10 indicated that the two protons were on different faces of the molecule. Reports have shown that the C-15 methyl and H-10 in the briarane skeleton always have opposing stereochemical assignments.[8] Recrystallization of this compound yielded crystals suitable for X-ray crystallographic analysis confirming the data suggested by NOESY correlations and resulted in the absolute configuration of **4.27** (Figure 4.13)**.**

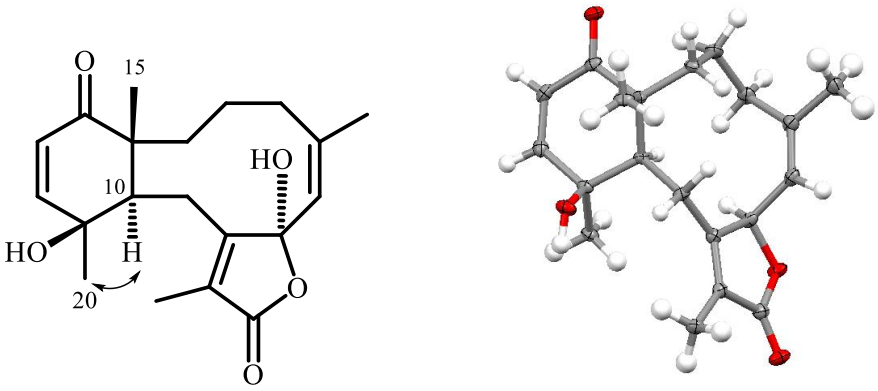

Figure 4.13. The asymmetric unit of bathyptilone A. Anisotropic displacement parameters were drawn at 50% probability.

Bathyptilone B (**4.28**) was isolated as crystalline solid with a molecular formula of $C_{22}H_{28}O_6$ (calcd for $C_{20}H_{24}O_4$) confirmed by HRESIMS with supporting ^{1}H and ^{13}C NMR data (Table 4.7). The degree of unsaturation for this compound is nine, which was one more unsaturation than compound **4.27**. Analysis of the 2D NMR data established the tricyclic briarane skeleton. The ^{13}C NMR spectrum displayed two additional carbons compatible with an ester carbonyl and a methyl group indicating an acetate functionality. The acetyl group could be placed on the oxygen-bearing carbon at δ_C 77.9 (C-2), which was found to be a methylene in bathyptilone A. The downfield shift of H-2 (δ_H 5.87) supports the assignment of the acetyl group on this carbon. The acetyl group accounted for two carbons and two oxygens which required that oxidation was not found at C-11. The HSQC correlation of the δ_H 2.46 (H-11) also confirmed the C-11 assignment.

Table 4.7. ^{1}H and ^{13}C NMR data for bathyptilone B & bathyptilone C

	bathyptilone B		bathyptilone C	
Position	C, type[a]	^{1}H (J in Hz)[b]	C, type	^{1}H (J in Hz)
1	52.5, C	-	50.4, C	-
2α B	77.9, CH	5.87*, m	31.9, CH_2	1.99*, m 1.51*, m
3α B	27.6, CH_2	3.91, m 1.88, m	22.1, CH_2	1.86*, m 1.57*, m
4α B	26.3, CH_2	1.96, m 2.33, m	29.7, CH_2	1.88*, m 1.28*, m
5	146.0, C	-	145.5, C	-
6	122.8, CH	5.24, s	124.4, CH	5.37, s
7	106.3, C	-	70.8, C	-
8	161.3, C	-	160.9, C	-
9α B	28.4, CH_2	3.64, d 2.40, m	22.9, CH_2	3.26, m 2.50, d
10	41.4, CH	3.32, br t	41.6, CH	3.16, d
11	38.0, CH	2.46, m	69.5, C	-
12	154.8, CH	6.63, br d (10.25)	151.9, CH	6.65, d
13	127.0, CH	5.94*, dd	127.6, CH	5.99, d
14	201.4, C	-	203.9, C	-
15	16.7, CH_3	1.10, s	24.5, CH_3	1.18, s
16	23.2, CH_3	1.75, s	23.7, CH_3	1.81, s
17	124.3, C	-	126.0, C	-
18	9.13, CH_3	1.90, s	9.3, CH_3	1.97, s
19	171.7, C	-	171.9, C	-
20	18.8, CH_3	1.13, d (1.12)	30.7, CH_3	1.37, s
21	169.5, C	-		
22	21.2, CH_3	2.03, s		

[a]125 MHz, multiplicity determined by HSQC. [b]500 MHz.

Comparison of bathyptilone A NOESY experiment to that of bathyptilone B assisted with the stereochemical configuration of bathyptilone B. The *cis* conformation of the C-1/C-10 remained the same. An NOE correlation of H_3-10 to the doublet H_3-20 establishing their relative conformation on the same face. The acetate methyl H_3-22 correlation to H3-15 place these methyl groups on the opposing side of the H_3-10/H_3-20. Recrystallization of this compound (Figure 4.14) confirmed the stereochemical assignments.

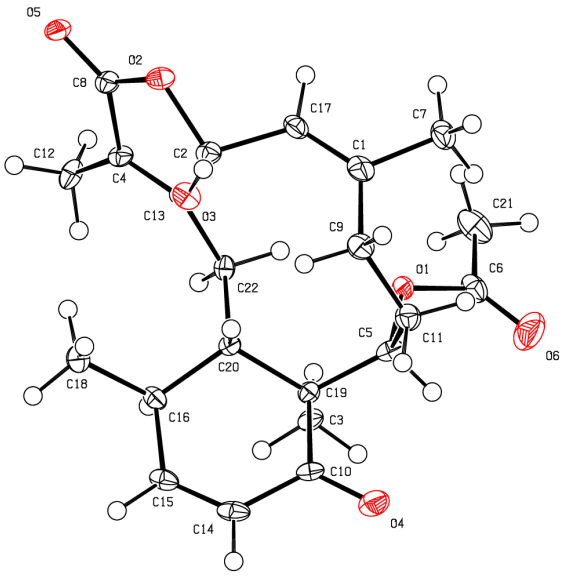

Figure 4.14 Asymmetric unit of bathyptilone B. Anisotropic displacement parameters were drawn at 50% probability.

The molecular formula of the crystalline bathyptilone C (**4.29**) was established as $C_{20}H_{26}O_4$ (calcd for $C_{20}H_{27}O_4$) by HRESIMS and supported by ^1H and ^{13}C NMR data (Table 4.7). The hemiacetal signal in the ^{13}C NMR spectrum was not observed in this compound as it did in bathyptilones A (**4.27**) and B (**4.28**). Relative to bathyptilone A, the HSQC spectrum established that H-7 was a methine which, in the HMBC spectrum, displayed correlation to C-8, 17 and 18, which established the lactone ring.These data suggested that bathyptilone C (**4.29**) is C-8 deoxo bathyptilone A

The three-dimensional analysis was done using an NOESY experiment utilizing through bond and space correlations. As with previously mentioned compounds, the singlet methyl (H-20) showed correlation to H-10, but both signals lacked correlation to, indicating that they are on the opposing face of H_3-15. Recrystallization of this compound allowed us to perform single crystal X-ray crystallography which confirmed the data suggested by NMR experiments and confirm the configuration of C-7. (Figure 4.15).

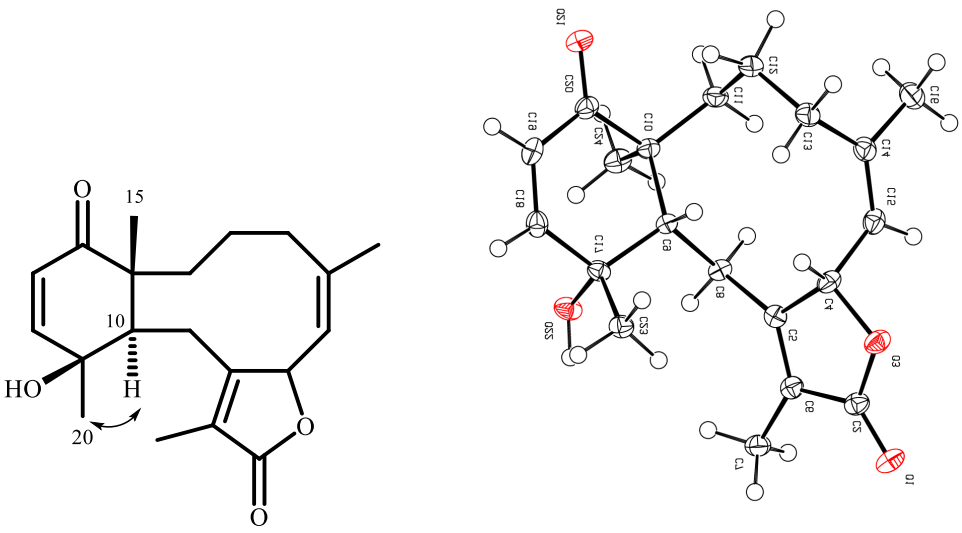

Figure 4.15 Asymmetric unit of bathyptilone C. Anisotropic displacement parameters were drawn at 50% probability.

The molecular formula for enbepenone A (**4.30**) was determined as $C_{17}H_{22}O_3$ (calcd for $C_{17}H_{23}O_3$) by HRESIMS, ^{1}H and ^{13}C NMR data. The decrease in carbon atoms relative to the bathyptilones initially characterized this compound as a sesquiterpene with a possible acetyl substitution. However, the degree of unsaturation and the 1D ^{13}C NMR data (Table 4.8) indicated otherwise. There are seven degrees of unsaturation out of which the two ketone carbonyls and two pairs of olefinic carbons represented four. A tricyclic scaffold designated the remaining three unsaturations. Similarly, to the bathyptilones a cyclohexenone was a part of the scaffold established by the COSY spectrum. The olefinic protons H-12 and H-13 formed a $^{3}J_{HH}$ with the methine H-11 which displayed correlation in the HMBC to C-10. The HMBC experiment correlated H-12 to the ketone (C-14) as well as H-13 to C-1. A seven-membered ring was established based on HMBC experiment rather than a ten-membered in the bathyptilones. The protons H_2-2, H_2-3 and H-4 shared reciprocated HMBC correlations among each other. H-4 also

correlated to a fully substituted olefin carbon C-5. The vinylic methyl (H_3-16) showed a long range COSY coupling to the vinylic proton (H-6). The ^{13}C NMR spectrum suggested that this pair of olefin carbons were conjugated to a ketone carbonyl which was confirmed by the HMBC experiment. The cyclopentenone was supported by the deshielded shift of C-8 suggesting a hemiketal functionality adjacent to C-7. HMBC correlations facilitated the connection between C-8 and C-4, also H_2-9 bridged connection between C-10 and C-8 establishing the 6,7,5-tricyclic scaffold.

Table 4.8. NMR data for enbepenone A (**4.30**)

Position	^{13}C, type	^{1}H (*J* in Hz)
1	52.8, C	-
2	31.9, CH_2	1.14, m 1.39, m
3	19.5, CH_2	1.20, m 1.30, m
4	46.3, CH	2.20, m
5	177.5, C	-
6	133.2, CH	5.85, s
7	205.4, C	-
8	99.5, C	-
9	28.3, CH_2	1.36, m 1.46, dd (12.4, 7.0)
10	32.2, CH	1.35, dq (7.0, 7.0)
11	36.1, CH	2.08, m
12	153.6, CH	6.57, dd (10.9, 6.2)
13	128.0, CH	6.07, d (10.9)
14	202.9, C	-
15	19.3, CH_3	1.24, s
16	25.7, CH_3	2.09, s
17	-	-
18	-	-
19	-	-
20	19.6, CH_3	1.09, d (6.8)

The stereochemistry was established using NOESY correlations for relative conformations. H-10 showed a strong correlation to the methyl doublet H_3-20 which indicated their proximity; however the methyl singlet of H-15 did not have a NOESY

correlation to H-10. The *cis* configuration of C-1/C-10 found in the bathyptilone still remained in this scaffold. Recrystallization produced crystals for crystal X-ray analysis. The crystallographic metadata (Flack parameter -0.03(13)), Bijvoet-Pair Analysis and Bayesian Statistics Method (Appendix C) facilitated assignment of the absolute configuration of enbepenone A as shown in figure 4.16.

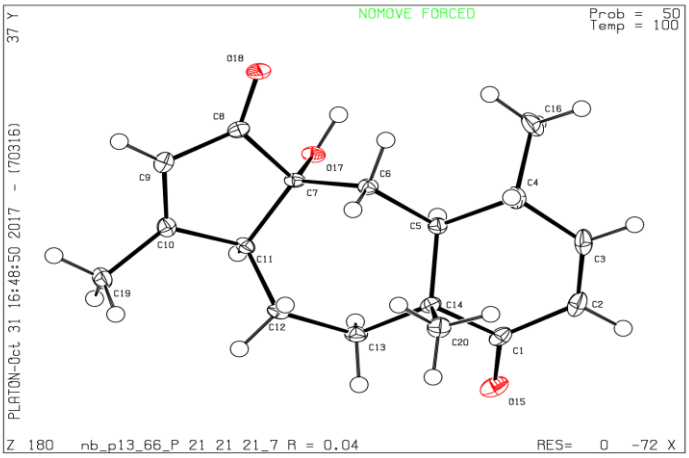

Figure 4.16. The asymmetric unit of enbepenone A. Anisotropic displacement parameters were drawn at 50% probability.

4.6.2 Biological Activity of Bathyptilone in Ntera2 assay

Several cell types were analyzed for sensitivity to these diterpenes. Of those tested, bathyptilone A was highly toxic to NT2 cells. Bathyptilone A effectively killed the NT2 cells at a concentration of 0.029 µM. A recent publication describes gedunin (**4.31**) as having activity against NT2 cells at 13.5 µM.[24] Based on this finding we speculated that bathyptilone A might prove to be an effective therapeutic strategy for specifically targeting neurotoxicity (Figure 4.17).

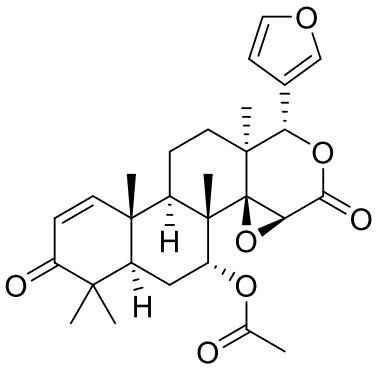

4.31

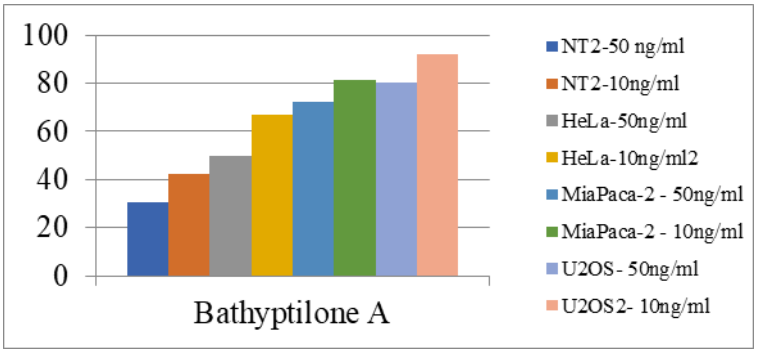

Figure 4.17. Bioactivity of bathyptilone A (**4.27**) against various cancer cell lines.

4.7 Halogenated Sesquiterpenes Potential as Anti-Tubercular Agents

Specimens of an unidentified coral (Figure 4.18) were collected during a late austral autumn cruise in 2013. These sessile organisms were collected near the Scotia Arc in the Southern Ocean via trawl. The coral was immediately frozen, subsequently freeze-dried (98.2 g) and exhaustively extracted using a Soxhlet extractor with refluxing DCM. The crude DCM extract was partitioned with brine. The organic layer was concentrated *in vacuo* resulting in 4.9 g of extract. After 1D ^{1}H NMR analysis, characteristic terpenoid peaks prompted further isolation. Normal phase MPLC was performed for the initial fractionation after drying the extract onto silica gel (Scheme 4.3). Further purification was carried out through a normal phase and reversed-phase HPLC.

This chromatogram resulted in the isolation of two new halogenated furan sesquiterpenes, scotianone A and B.

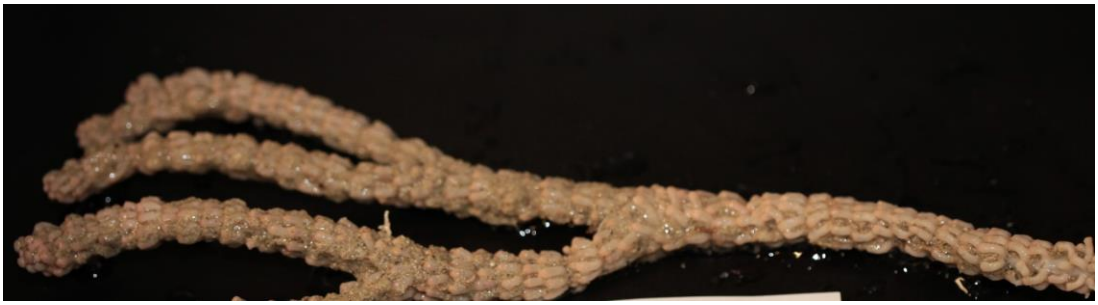

Figure 4.18 Unidentified octocoral collected in the Southern Ocean

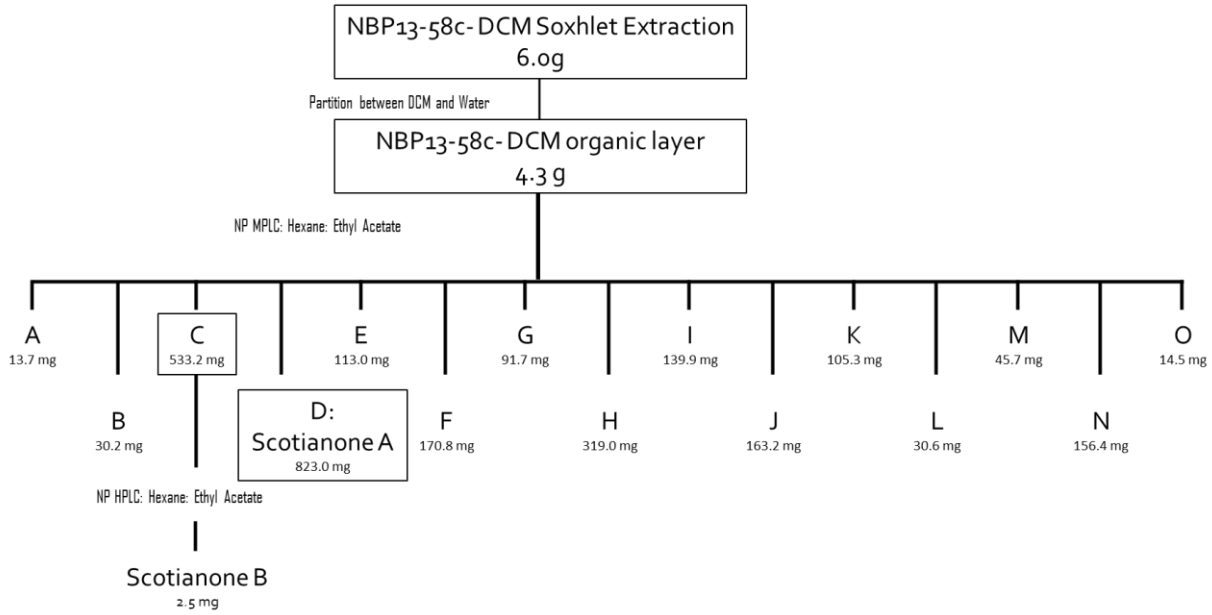

Scheme 4.3 Isolation Scheme of scotianones

4.7.1 Scotianones isolated from an Antarctic deep-sea octocoral

The molecular formula of $C_{15}H_{17}O_2Cl$ (calcd for $C_{15}H_{18}O_2Cl$) assigned to scotianone A (**4.32**) was deduced by HRESIMS and confirmed using 1D ^{1}H and ^{13}C NMR spectra (Table 4.9). This compound was very abundant in this coral extract yielding 823 mg. The multiplicity of the carbons was determined by the HSQC NMR experiment which

indicated a ketone carbonyl, five fully substituted olefinic carbons, a tri-substituted olefinic carbon, an sp^3 quaternary carbon, three methylene, one chloromethine, and three methyl groups. With four degrees of unsaturation accounted for, the remaining would propose a tricyclic structure. The first ring was assigned using COSY and HMBC experiments. A spin system was established in the COSY experiment with a $^3J_{HH}$ between the methylene at δ_H 2.32 (H_2-3), δ_H 2.04 (H-2a) and the deshielded methine at δ_H 4.13 (H-1). Extension of the spin system was achieved through HMBC correlations of H-3a to δ_C 142.7 (C-4) and H-2a to the quaternary carbon at δ_c 43.7 (C-10). The allylic methyl protons established the olefin within this ring with HMBC correlations to C-3, C-4, and δ_c 134.1 (C-5). The upfield methyl protons at δ_H 1.28 (H_3-15) suggested a six-membered ring based on the HMBC experiment displaying correlations to δ_C 67.2 (C-1,) C-5 and C-10. The protons H_2-9 shared HMBC correlations with C-15 and C-10, C-5 and the olefin carbon at δ_C 164.2 (C-8). A ketone, two pair of olefins, a methyl group, a chlorine and an oxygen atom remained to be assigned. The downfield shift of H-1 facilitated the placement of the chlorine atom on C-1. The aromatic proton at δ_H 7.06 (H-12) correlated to C-8 and C-11 in the HMBC experiment. The allylic methyl protons at δ_H 2.21 (H_3-13) also correlated to C-11 and C-12. The aromaticity within compound must result from a furan ring, placing H-12 near an electron withdrawing group. With no protons left to be assigned, ^{13}C NMR data was used to assign the remaining two carbons. The olefin carbon at δ_C 119.4 (C-7) formed a double bond with C-8 and completed the furan ring. The valance for C-8 and C-5 were not satisfied and through process of elimination the ketone was assigned between these olefin carbons. The ketone extended the conjugation of the furan which can justify the upfield shift of the carbonyl (Figure 4.19).

Table 4.9. NMR data of scotianone A ($CDCl_3$)

Position	$^{13}C^a$, type	$^{1}H^b$ (*J* in Hz)	HMBC[c]
1	67.2, CH	4.12, dd (9.1, 3.0)	2,3
2α	28.1, CH_2	2.04, mult.[d]	1,4,10
β		2.15, mult.[d]	
3	32.2, CH_2	2.32, q (6.7x 3)	1,5
4	142.5, C		
5	133.9, C		
6	187.6, C		
7	119.4, C		
8	164.1, C		
9 α	34.3, CH_2	2.72, d (17.1)	5,8,10,15
β		3.29, d (17.2)	8,10,15
10	43.5, C		
11	120.5, C		
12	139.6, CH	7.06, s	8,11
13	9.1, CH_3	2.21, s	11,12
14	21.5, CH_3	2.02, s	3,4,5
15	26.4, CH_3	1.28, s	1,5,9,10

[a]100 MHz, multiplicity determined by HSQC. [b]400 MHz. [c]600 MHz. [d]overlapped.

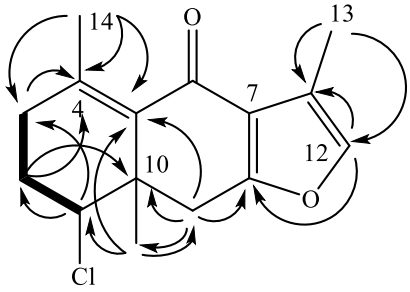

Figure 4.19. Key COSY (▬) and HMBC (→) correlations establishing the planar structure of scotianone A (**4.32**).

Stereochemical evaluation of scotianone A (**4.32**) was determined from through space or bond correlations. The NOESY experiment showed a correlation of H-1 to H-15 indicating that the chlorine attached to C-1 is on the opposite face of the molecule

supported by H-15 chemical shift. These absolute stereochemical configuration was confirmed by X-ray analysis (Figure 4.20) of the crystals as 1*S*,10*R*.

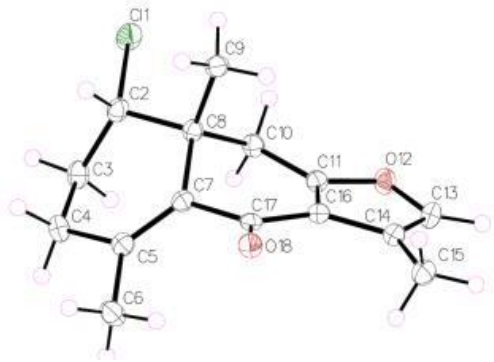

Figure 4.20 Asymmetric unit of scotianone A. Anisotropic displacement parameters were drawn at 50% probability.

Scotianone B (**4.33**) isolated as a white amorphous solid with a molecular formula of $C_{15}H_{17}O_2Cl$ (calcd for $C_{15}H_{18}O_2Cl$) determined by HRESIMS supported by one dimensional ^1H and ^{13}C NMR data (Table 4.10) establishing scotianone B as an isomer of scotianone A. Two distinct peaks (δ_H 5.23 and 5.54) in the olefinic region of the ^1H NMR spectrum correlated to the olefin carbon at δ_C 113.7 (C-14) in the HSQC experiment established the presence of an exocyclic olefin. A significant difference noted between scotianone B and scotianone A was the lack of a vinylic methyl group. With the low proton to carbon ration of this scaffold, the COSY was not so useful. Instead, the HMBC was relied on to elucidate the structure. Similar HMBC correlations were observed between scotianone A (**4.32**) and scotianone B (**4.33**) and confirmed that all the carbons matched with scotianone A, except C-5 and C-14 (Figure 4.21). The HSQC of scotianone B showed that the C-5 olefinic functionality was reduced to a methine singlet δ_H 3.58 with HMBC correlations to δ_C 31.9, 140.3, 192.1, 46.0, 21.2 (C-3, -4, -6, -10, -15). The methylene

singlets at δ_H 5.23(H-14a) and 5.54 (H-14b) were shown to be exocyclic protons based on the HSQC correlations. C-4 retention of its olefinic shift indicates that the exocyclic olefin C-14 was adjacent to it as opposed to the methyl in scotianone A.

Table 4.10. NMR data for scotianone B ($CDCl_3$, ppm)

Position	$^{13}C^a$, type	$^1H^b$ (*J* in Hz)
1	69.9, CH	4.24, s
2α	32.7, CH_2	2.64, dt (4.7, 13.0)
β		2.26, mult.[c]
3α	31.9, CH_2	2.18, dt (0.6, 3.9)
β		2.05, mult.
4	140.3, C	-
5	51.6, CH	3.58, s
6	192.1, C	-
7	119.8, C	-
8	164.1, C	-
9α	35.4, CH_2	3.69, d (17.1)
β		2.57, d (17.1)
10	46.0, C	-
11	119.1, C	-
12	139.5, CH	7.08, s
13	9.3, CH_3	2.22, s
14a	113.7, CH_3	5.54, s
b		5.23, s
15	21.2, CH_3	1.17, s

[a]150 MHz, multiplicity determined by HSQC. [b]400 MHz. [c]overlapped.

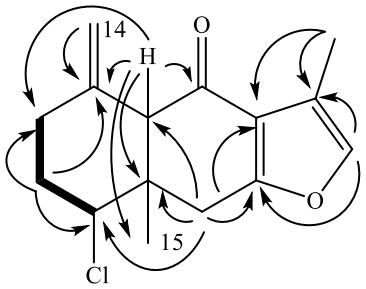

Figure 4.21 Key COSY (—) and HMBC (→) correlations establishing the planar structure of scotianone B.

The NOESY spectrum of scotianone B gave a correlation between H-1/H_3-15 which suggested that C-1 has similar orientation as depicted in scotianone A. The C-5/C-10 configuration is *trans* suggested by the absence of an NOE correlation (Figure 4.22).

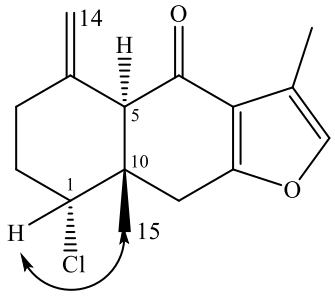

Figure 4.22 Key NOESY correlation of relative stereochemical assignments for scotianone B

4.7.2 Bioactivity of scotianones

Screening the two compounds in infectious disease bioassays, including the ESKAPE pathogens, *Clostridium difficile*, RSA virus, *Naegleria fowleri*, *Acanthamoeba* sp. and *Leishmania donovani* failed to identify significant bioactivity. Scotianone A displayed modest activity at 50 µg/ml in the *Mycobacterium tuberculosis* assay. Ongoing studies against other disease targets are in progress to identify the pharmaceutical significance of the isolated compounds.

4.8 Discussion and Conclusion

In this chapter, the details of the chemical investigation of three octocorals collected from depths of approximately 1000 m in the Southern Ocean are described. Encompassing one of the coldest environments, there are significantly less reported

natural products from the Southern Ocean than warmer seas, as cold-water organisms represent only 3% of natural products.

This chapter initially discussed the structure elucidation of cembrene-type diterpenes isolated from an Antarctic octocoral. Five new compounds were characterized and tested in a variety of biological assays to determine their antimicrobial, anti-amoebic and anti-inflammatory properties. The biological potential of these compounds was most significant against *Leishmania donovani.*

The second coral analyzed was another deep-sea dweller and was of the Pennatulacean Order. The chromatographic analysis of the CH_2Cl_2 extract yielded four new diterpenes derived from the briarane biosynthetic pathway. Three of these compounds were named bathyptilones meaning deep-sea spear, and the tri-norditerpenoid was called enbepenone representative of the research vessel's acronym (Nathaniel B. Palmer). The differences in the names were to distinguish the difference in scaffolds. Enbepenone presents an unreported scaffold in which it has a 6,7,5- tricyclic skeleton.

The third coral presented currently is not taxonomically identified but collected via trawling in the Southern Ocean near the Scotia Arc. The class of terpenes isolated from this octocoral belongs to furan sesquiterpenes. This class is present in the Myrrh resin which elicits analgesic properties. We were unable to establish a biomedical target for the two new halogenated sesquiterpenes isolated besides moderate activity against *M. tuberculosis.*

In summary, the three Antarctic corals presented four different classes of compounds from the isoprenyl biosynthetic pathway contributing 11 new natural products from the marine deep-sea environment. Structural diversity has elicited different bioactivity against different pathogenic targets for potential therapeutics. Keikipukalides, bathyptilones, enbepenone and the scotianones all displayed different bioactivity. Antiparasitic, antimicrobial and neurotoxicity are the biomedical properties observed in some capacity within these suites of compounds. Antarctic corals hold great potential for promising drug leads and further investigation of this fauna should continue.

4.9 References

(1) Thomas, S. A. L.; von Salm, J. L.; Clark, S.; Ferlita, S.; Nemani, P.; Azhari, A.; Rice, C. A.; Wilson, N. G.; Kyle, D. E.; Baker, B. J. Keikipukalides, furanocembrane diterpenes from the antarctic deep sea octocoral *Plumarella delicatissima*. *J. Nat. Prod.* **2018**, *81*, 117–123.

(2) Changyun, W.; Haiyan, L.; Changlun, S.; Yanan, W.; Liang, L.; Huashi, G. Chemical defensive substances of soft corals and gorgonians. *Acta Ecol. Sinica* **2008**, *28*, 2320–2328.

(3) Gavagnin, M.; Mollo, E.; Castelluccio, F.; Crispino, A.; Cimino, G. Sesquiterpene metabolites of the antarctic gorgonian *Dasystenella acanthina*. *J. Nat. Prod.* **2003**, *66*, 1517–1519.

(4) Lei, H. Diterpenoids of gorgonian corals: chemistry and bioactivity. *Chem. Biodivers.* **2016**, *13*, 345–365.

(5) Mariottini, G. L.; Grice, I. D. Antimicrobials from cnidarians. A new perspective for

anti-infective therapy? *Mar. Drugs* **2016**, *14*, 1–19.

(6) Aoki, S.; Okano, M.; Matsui, K.; Itoh, T.; Satari, R.; Akiyama, S. I.; Kobayashi, M. Brianthein A, a novel briarane-type diterpene reversing multidrug resistance in human carcinoma cell line, from the gorgonian *Briareum excavatum*. *Tetrahedron* **2001**, *57*, 8951–8957.

(7) Sheu, J.-H.; Chen, Y.-H.; Chen, Y.-H.; Su, Y.-D.; Chang, Y.-C.; Su, J.-H.; Weng, C.-F.; Lee, C.-H.; Fang, L.-S.; Wang, W.-H.; Wen, Z.-H., Wu, Y.-C., Sung, P.-J. Briarane diterpenoids isolated from gorgonian corals between 2011 and 2013. *Mar. Drugs* **2014**, *12*, 2164–2181.

(8) Su, Y.-D.; Su, J.-H.; Hwang, T.-L.; Wen, Z.-H.; Sheu, J.-H.; Wu, Y.-C.; Sung, P.-J. Briarane diterpenoids isolated from octocorals between 2014 and 2016. *Mar. Drugs* **2017**, *15*, 44–54.

(9) Sung, P.-J.; Li, G.-Y.; Chen, Y.-P.; Huang, I.-C.; Chen, B.-Y.; Wang, S.-H.; Huang, S.-K. Fragilide E, a novel chlorinated 20-acetoxybriarane from the gorgonian coral *Junceella fragilis*. *Chem. Lett.* **2009**, *38*, 454–455.

(10) W. Gribble, G. Recently discovered naturally occurring heterocyclic organohalogen compounds. *Heterocycles* **2012**, *84*, 157–207.

(11) Pham, N. B.; Butler, M. S.; Healy, P. C.; Quinn, R. J. Anthoptilides A−E, new briarane diterpenes from the australian sea pen *Anthoptilum cf. kukenthali*. *J. Nat. Prod.* **2000**, *63*, 318–321.

(12) http://pubs.rsc.org/marinlit.

(13) Skropeta, D.; Wei, L. Recent advances in deep-sea natural products. *Nat. Prod. Rep.* **2014**, *31*, 999–1025.

(14) Skropeta, D. Deep-sea natural products. *Nat. Prod. Rep.* **2008**, *25*, 1131–1166.

(15) Roberts, J. M. Reefs of the deep: the biology and geology of cold-water coral ecosystems. *Science.* **2006**, *312*, 543–547.

(16) Grassle, J. F.; Maciolek, N. J. Deep-sea species richness: regional and local diversity estimates from quantitative bottom samples. *Am. Nat.* **1992**, *139*, 313–341.

(17) Lebar, M. D.; Heimbegner, J. L.; Baker, B. J. Cold-water marine natural products. *Nat. Prod. Rep.* **2007**, *24*, 774–797.

(18) Soldatou, S.; Baker, B. J. Cold-water marine natural products, 2006 to 2016. *Nat. Prod. Rep.* **2017**, *34*, 585–626.

(19) Rodríguez Brasco, M. F.; Seldes, A. M.; Palermo, J. A. Paesslerins A and B: novel tricyclic sesquiterpenoids from the soft coral *Alcyonium paessleri*. *Org. Lett.* **2001**, *3*, 1415–1417.

(20) Iken, K. B.; Baker, B. J. Ainigmaptilones, sesquiterpenes from the Antarctic gorgonian coral A*inigmaptilon antarcticus*. *J. Nat. Prod.* **2003**, *66*, 888–890.

(21) von Salm, J. L.; Wilson, N. G.; Vesely, B. A.; Kyle, D. E.; Cuce, J.; Baker, B. J. Shagenes A and B, new tricyclic sesquiterpenes produced by an undescribed Antarctic octocoral. *Org. Lett.* **2014**, *16*, 2630–2633.

(22) Duh, C.-Y.; Wang, S.-K.; Chia, M.-C.; Chiang, M. Y. A novel cytotoxic

norditerpenoid from the formosan soft coral *Sinularia inelegans*. *Tetrahedron Lett.* **1999**, *40*, 6033–6035.

(23) https://www.oecd-ilibrary.org/environment/test-no-426-developmental-neurotoxicity-study_9789264067394-en (accessed Sep 2, 2018).

(24) Tharmarajah, L.; Samarakoon, S. R.; Ediriweera, M. K.; Piyathilaka, P.; Tennekoon, K. H.; Senathilake, K. S.; Rajagopalan, U.; Galhena, P. B.; Thabrew, I. *In vitro* anticancer effect of gedunin on human teratocarcinomal (ntera-2) cancer stem-like cells. *Biomed Res. Int.* **2017**, *2017*, 1–9.

APPENDICES

Appendix A: Experimental and Supplementary Information for Chapter Two

Microbial Isolation

Methods for Cultivating Fungal Cultures

LC-MS/MS Experimental Method

NMR Spectra

Microbial Isolation

SDB, PDB, TSA, Actinomycete Isolation Agar, Malt Extract Agar and Agar were used in various mixtures to compose solid media. These components produced by BD™ Difco™ were used in conjunction with nystatin, cycloheximide and chloramphenicol to facilitate the microbial isolation.

According to the manufacturer's instructions the media was mixed, heated and autoclaved to create agar plates using petri dishes produced by Fisherbrand™.

Mangrove tissue was collected from various parts of the tree including the bark, stem, roots and leaves. Subsequently, sterility was obtained using sterile water and IPA followed with sectioning of the tissue for inoculation onto agar plates with various media composition. The plates were incubated at room temperature up to 6 weeks allowing growth of fungi for isolation. During the incubation period, plates were monitored to transfer cubes of agar with the fungus attached to a plate of identical composition. Physical observation of the transfer determined isolation of the fungal culture. Transfer of the culture was repeated until isolation was confirmed.

Method for Cultivating Fungal Cultures

Fungal isolates were retrieved from storage in glycerol containing media and inoculated on SDA for growth. Three cubes of 1cm of the fungal culture were each transferred into sterile Eppendorf™ tubes containing 1.25 mL of three different conditions: SDB (control), 100 µM sodium butyrate in SDB (HDACi), and 100µM 5-aza-cytidine in SDB (DNMTi). After vigorous shaking of the inoculated broth it was transferred onto the solid rice media for 21 days of growth at room temperature.

LC-MS/MS Experimental Method

An Agilent™ LC-QToF equipped with an Electrospray Ionization (ESI) source was utilized to acquire LC-MS/MS experiments. At each stage of separation and/or fractionation MS-Tandem experiments were collected for analysis and prioritization. The samples were dissolved in MeOH and filtered using Phenomonex 0.2 µ syring filters. Crude samples were made to concentration of 1 mg/mL and purer samples were made at a concentration of 0.1 mg/mL. Chromatography was performed on the samples using a gradient of 2% H2O to 100% CAN on a Phemonenex® Kinetex® C-18 column (2.6 µm, 100 Å, 150x 3 mm). The instrument parameters are indicated below (Table A1)

Table A.1 Parameters used for LC-MS/MS acquisitions

Time Table			
Time [min]	A [%]	B [%]	Flow [mL/min]
0.00	90.00	10.00	0.40
0.01	98.00	2.00	0.40
2.00	98.00	2.00	0.40
10.00	2.00	98.00	0.40
12.00	2.00	98.00	0.40
12.01	98.00	2.00	0.40
14.00	98.00	2.00	0.40

HiP Sampler	
Injection Volume	10.0 µL

Pump	
Flow	0.40 mL/min

Injection with needle wash	Yes	Solvent A	H2O+0.1% Formic acid
Needle Wash Mode	Flush Port	Solvent B	ACN+0.1% Formic acid
Needle Wash Time	3.0 sec	Pressure Limit Min	0.00bar
Draw Speed	100.0 µL/min	Pressure Limit Max	600.00bar
Eject Speed	100.0 µL/min	Stop Time	14.00min
Draw Position	0.0 min	Posttime	1.00min
Equilibration Time	0.0 sec		
Sample Flush-out Factor	5.0x Inj. Volume		

QToF

Ion Source	Dual AJS ESI	Plot and Centroid Data Storage Threshold	
Ion Polarity	Positive	MS Abs Threshold	200
Data Storage	Both	Rel. Threshold (%)	0.01
LC Stream	MS	MS/MS Abs Threshold	5
Stop Time	As Pump	Rel. Threshold (%)	0.01
Cycle Time	1.7 s		
Gas Temp	300 °C	MS TOF Fragmentor	140 V
Drying Gas	8 l/min	MS TOF Skimmer	65 V
Nebulizer	30 psig	MS TOF OCT 1 RF Vpp	750 V
Sheath Gas Temp	300 °C	TOF Collision Energy	0 V
Sheath Gas Flow	11 l/min		
Dual AJS ESI Vcap	4000 V		
Caillary	0.00 uA		
Nozzle Voltage	500 V		
Chamber	0.00 UA		
MS		***MS/MS***	Auto
Mass Range Min	40 m/z	Mass Range Min	40 m/z
Mass Range Max	1300 m/z	Mass Range Max	1300 m/z
Acquisition Rate	1 spectra/s	Acquisition Rate	5 spectra/s
Acquisition Time	1000 ms/spectrum	Acquisition Time	200 ms/spectrum
Transients/spectrum	5971	Transients/spectrum	1118
		Isolation Width	Medium (~4 m/z)
		Collision Energy	0 mV, 10 mV 40 mV

Precursor Selection		***Chromatogram***	
Max Precursor Per Cycle	3	Label	TIC
Abs. Threshold	1000 counts	Expt Type	MS
Rel. Threshold (%)	0.01%	Polarity Effect	Both
Active Exclusion	Disabled	Offset	15

Excluded after	3 Spectra	Y-Range	10000000
Released after	0.5 min		

Reference Mass

		Ref.
Mass Correction	Enable	Masses
Detection Window	100ppm	121.0508
Min Height	1000 counts	922.0098
Min Height	1000 counts	922.0098

NMR Spectra

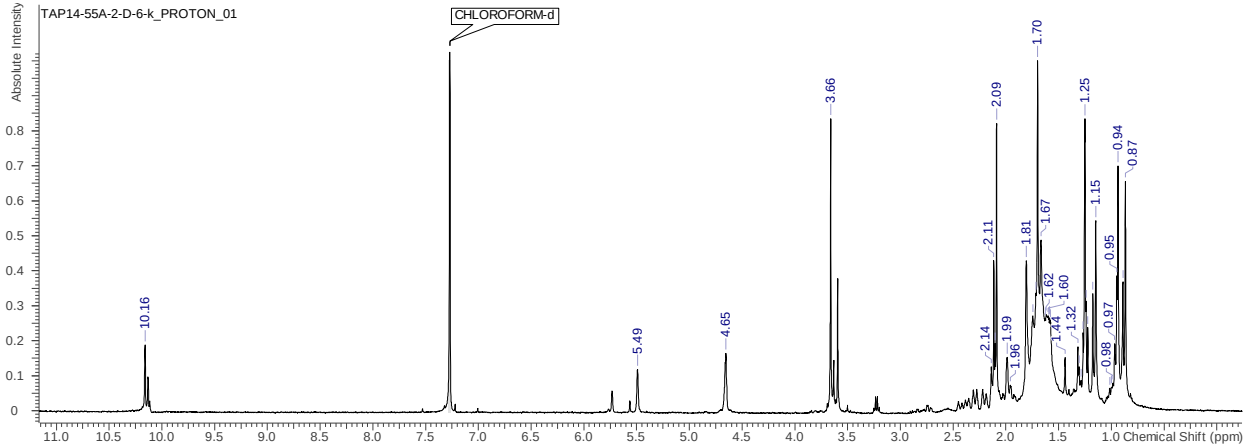

Figure Ai. ^{1}H NMR spectrum of SALT-12 (**2.21**) (400 MHz, $CDCl_3$)

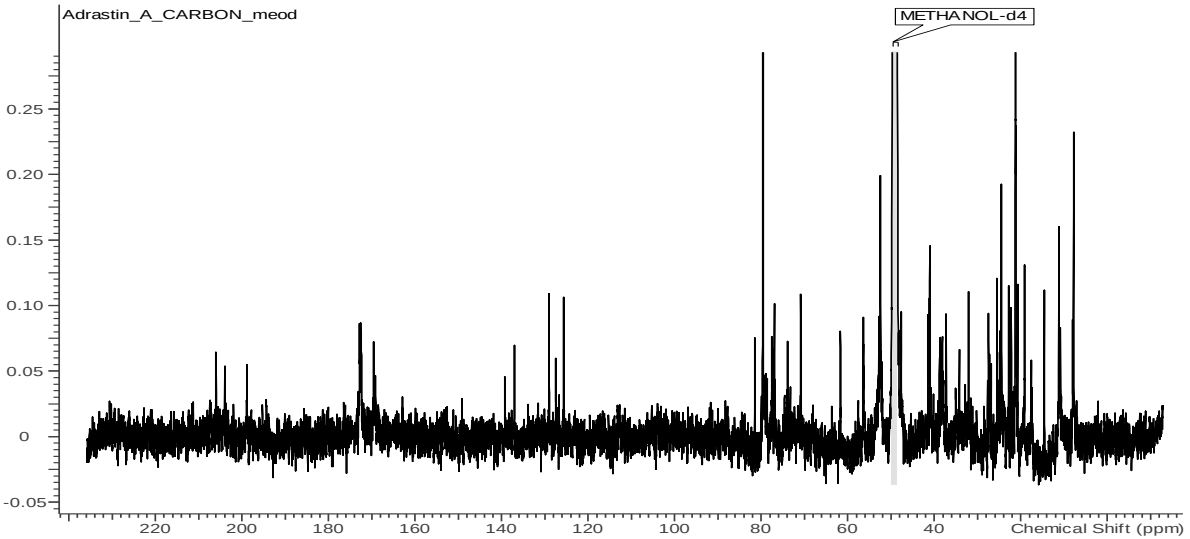

Figure Aii. ^{13}C NMR spectrum of SALT-12 (**2.21**) (125 MHz, $CDCl_3$)

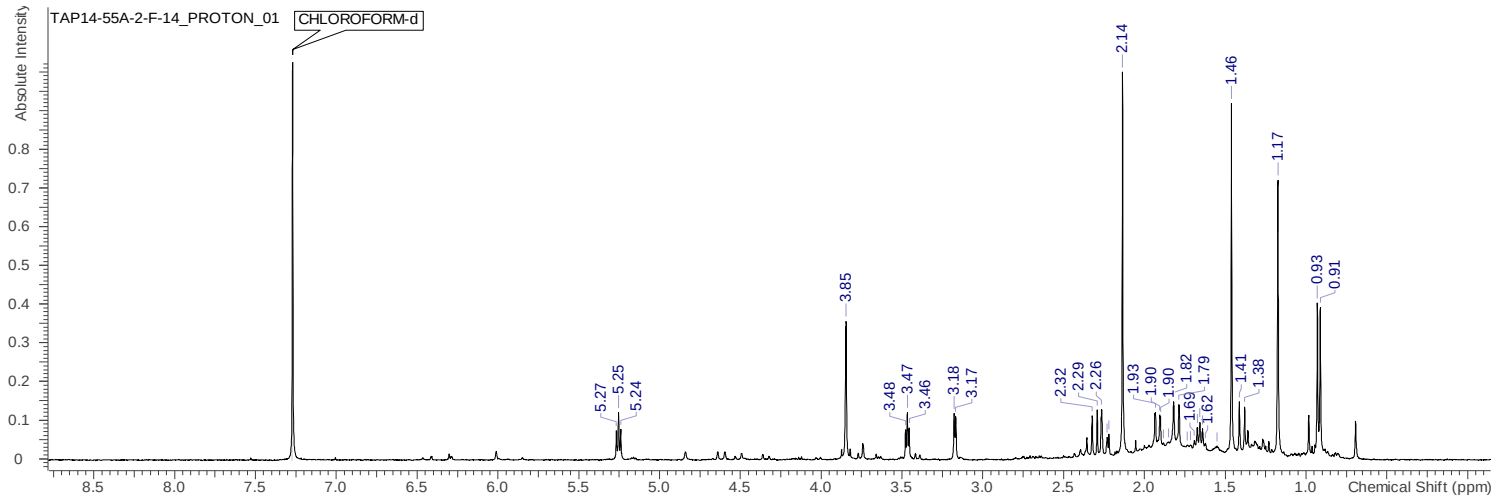

Figure Aiii. ^{1}H NMR spectrum (400 MHz, $CDCl_3$) of eremofortin D (**2.22**) (400 MHz, $CDCl_3$)

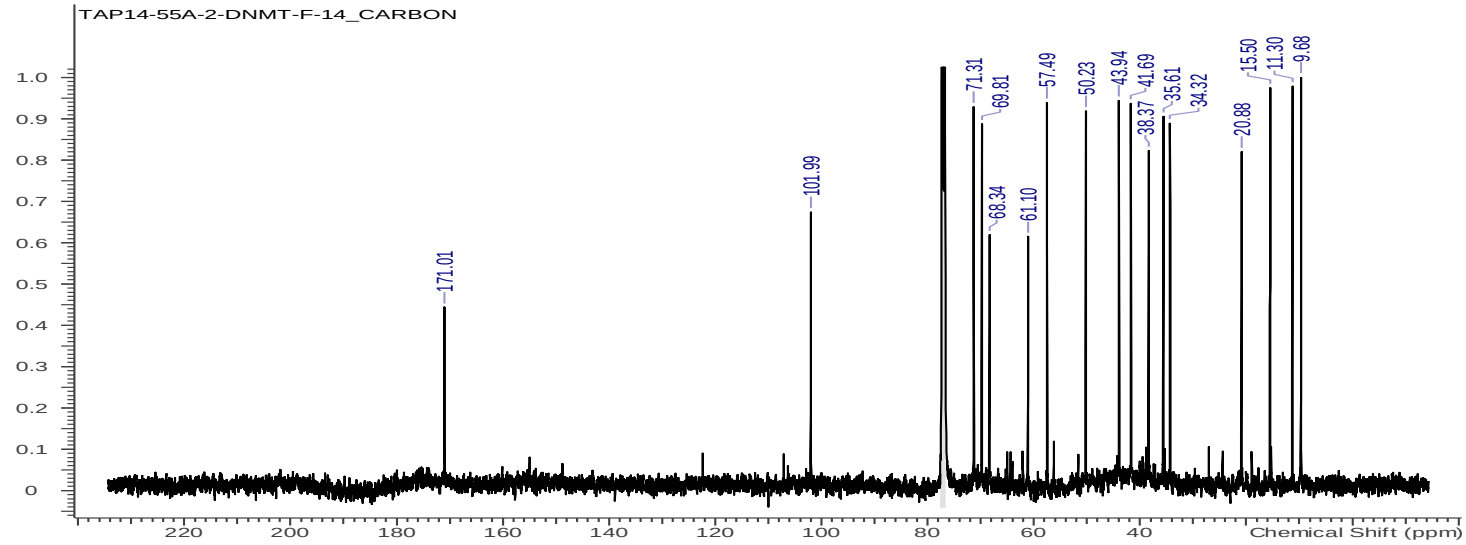

Figure Aiv. ^{13}C NMR spectrum (125 MHz, $CDCl_3$) of eremofortin D (**2.22**) (125 MHz, $CDCl_3$)

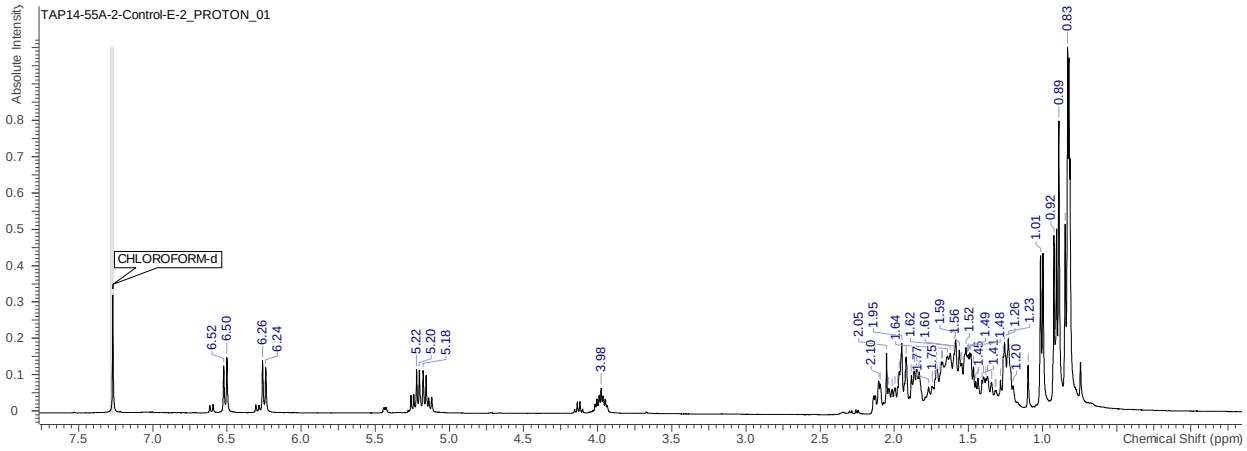

Figure Av. ^{1}H NMR spectrum (400 MHz, $CDCl_3$) of ergosterol peroxide (**2.24**)

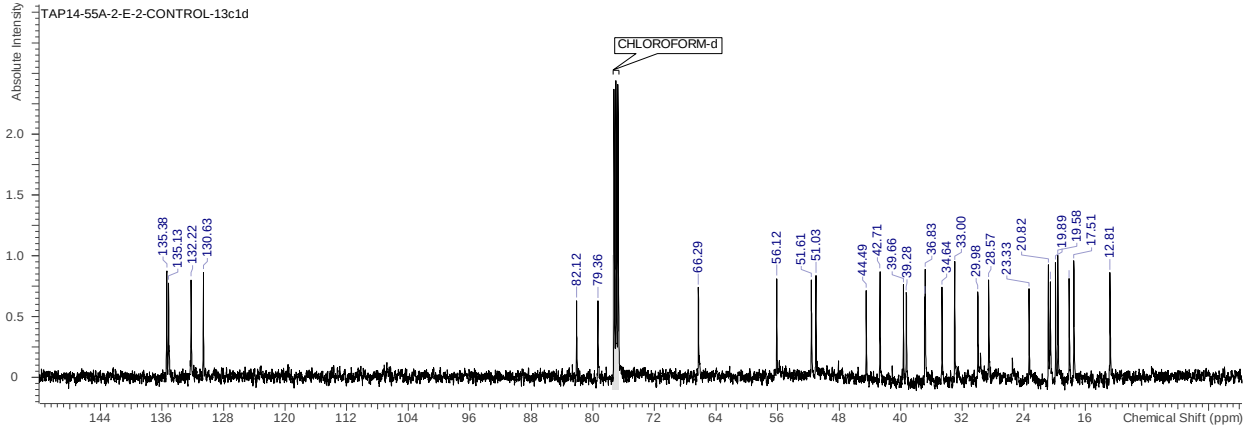

Figure Avi. ^{13}C NMR spectrum (125 MHz, $CDCl_3$) of ergosterol peroxide (**2.24**)

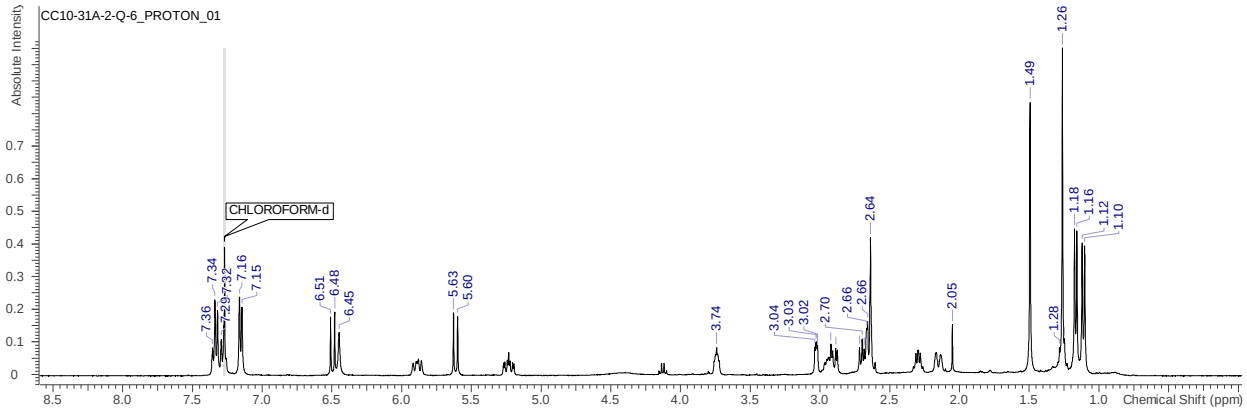

Figure Avii. ^{1}H NMR spectrum (400 MHz, $CDCl_3$) of cytochalasin E (**2.25**)

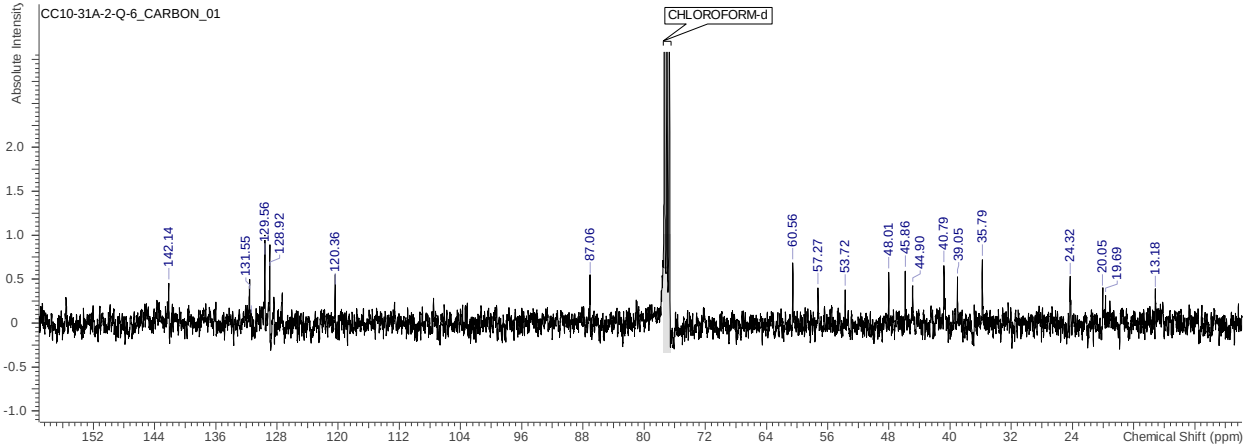

Figure Aviii. ^{13}C NMR spectrum (100 MHz, $CDCl_3$) of cytochalasin E (**2.25**)

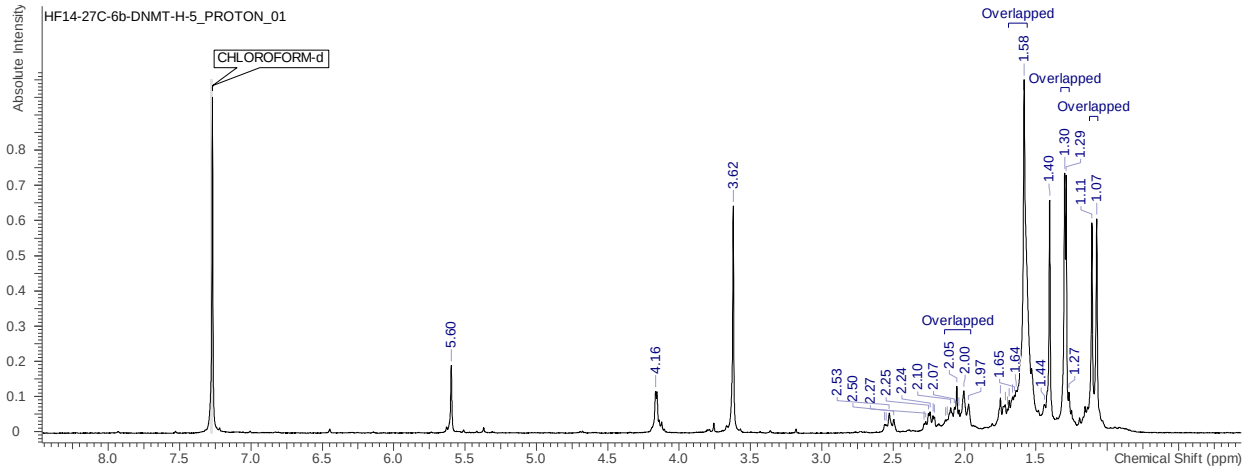

Figure Aix. ^{1}H NMR spectrum (400 MHz, $CDCl_3$) of SALT-17

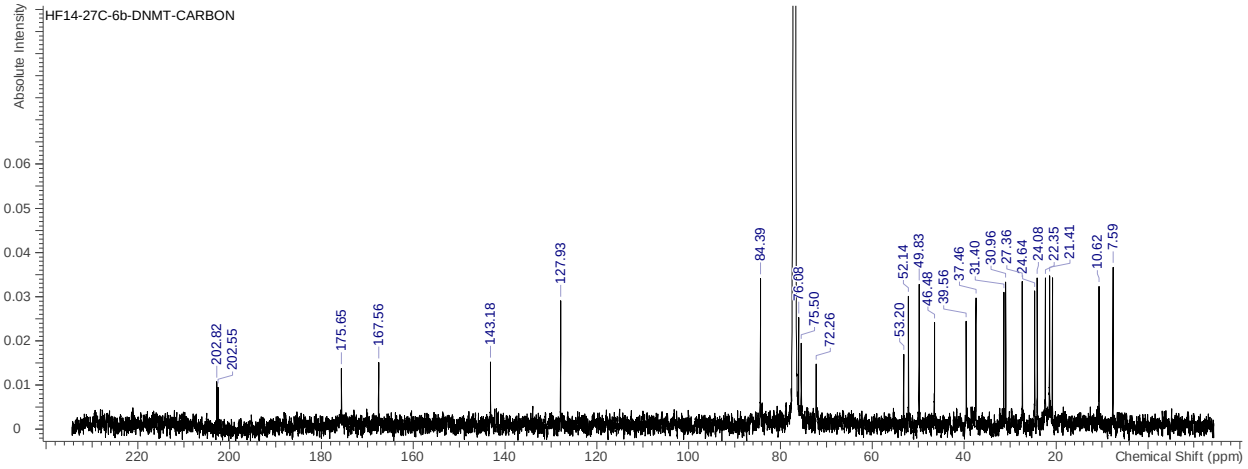

Figure Ax. ^{13}C NMR spectrum (125 MHz, $CDCl_3$) of SALT-17

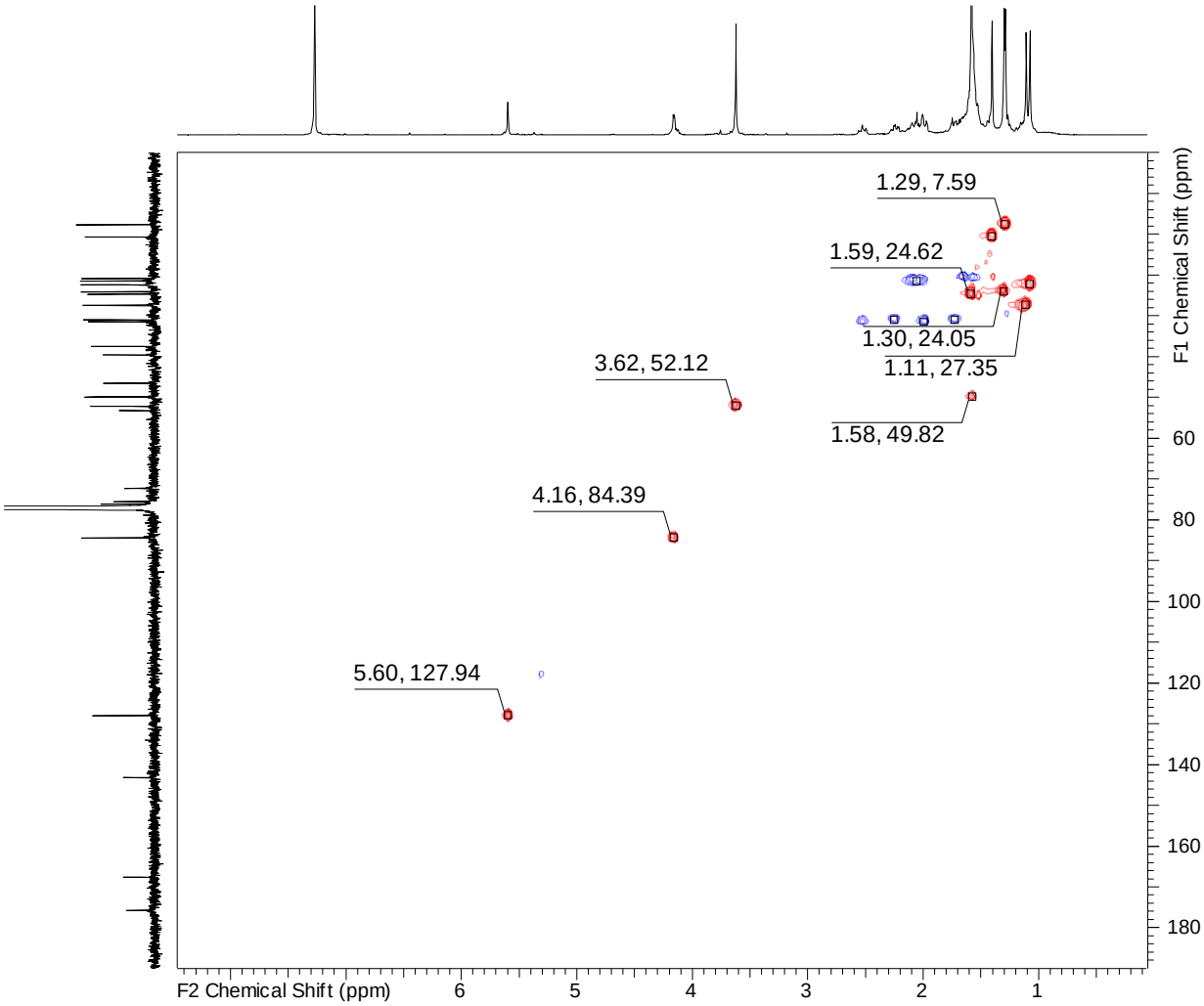

Figure Axi. ^{1}H-^{13}C gHSQCAD NMR spectrum (500 MHz, $CDCl_3$) of SALT-17

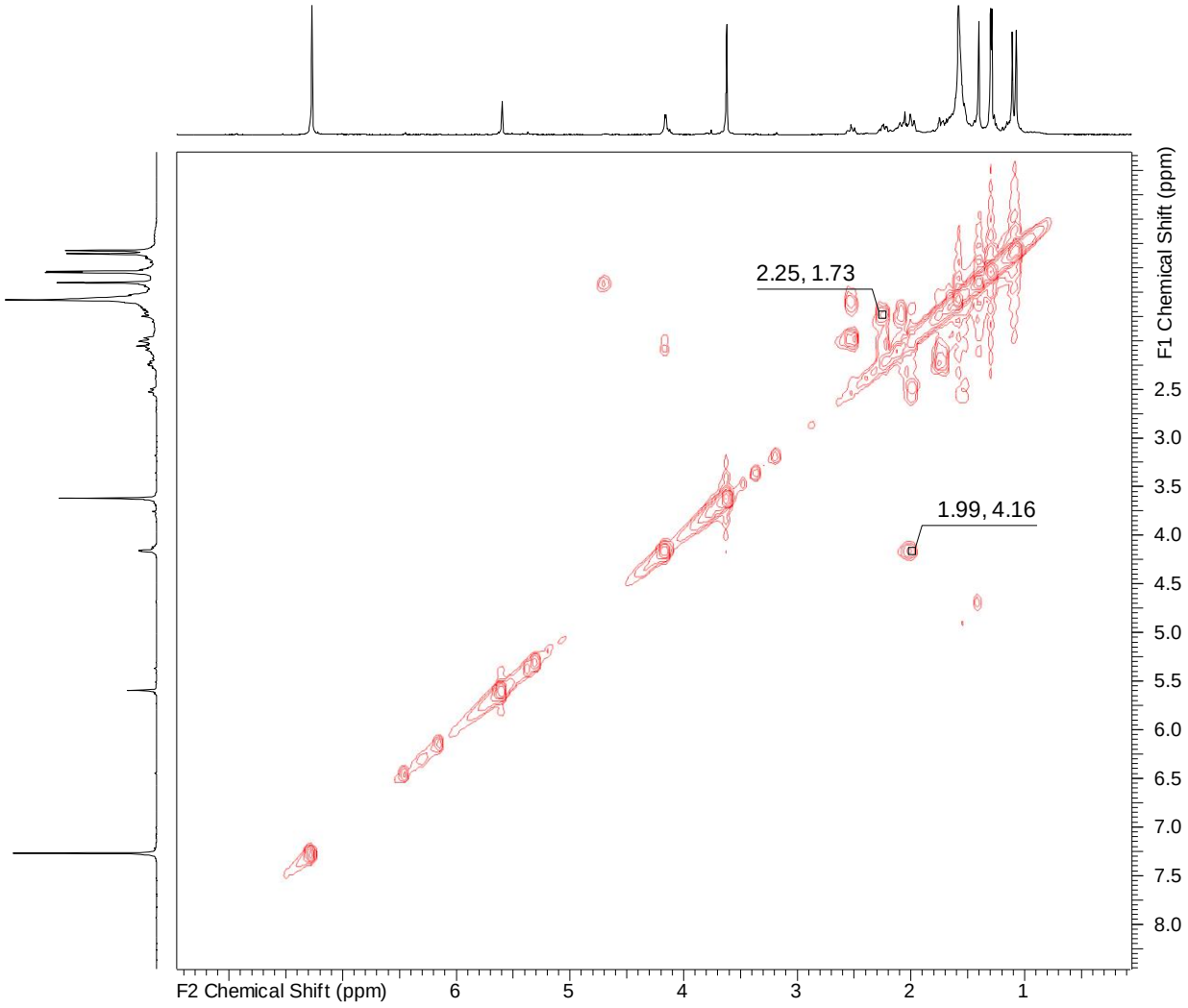

Figure Axii. ^{1}H-^{1}H gCOSY NMR spectrum (500 MHz, $CDCl_3$) of SALT-17

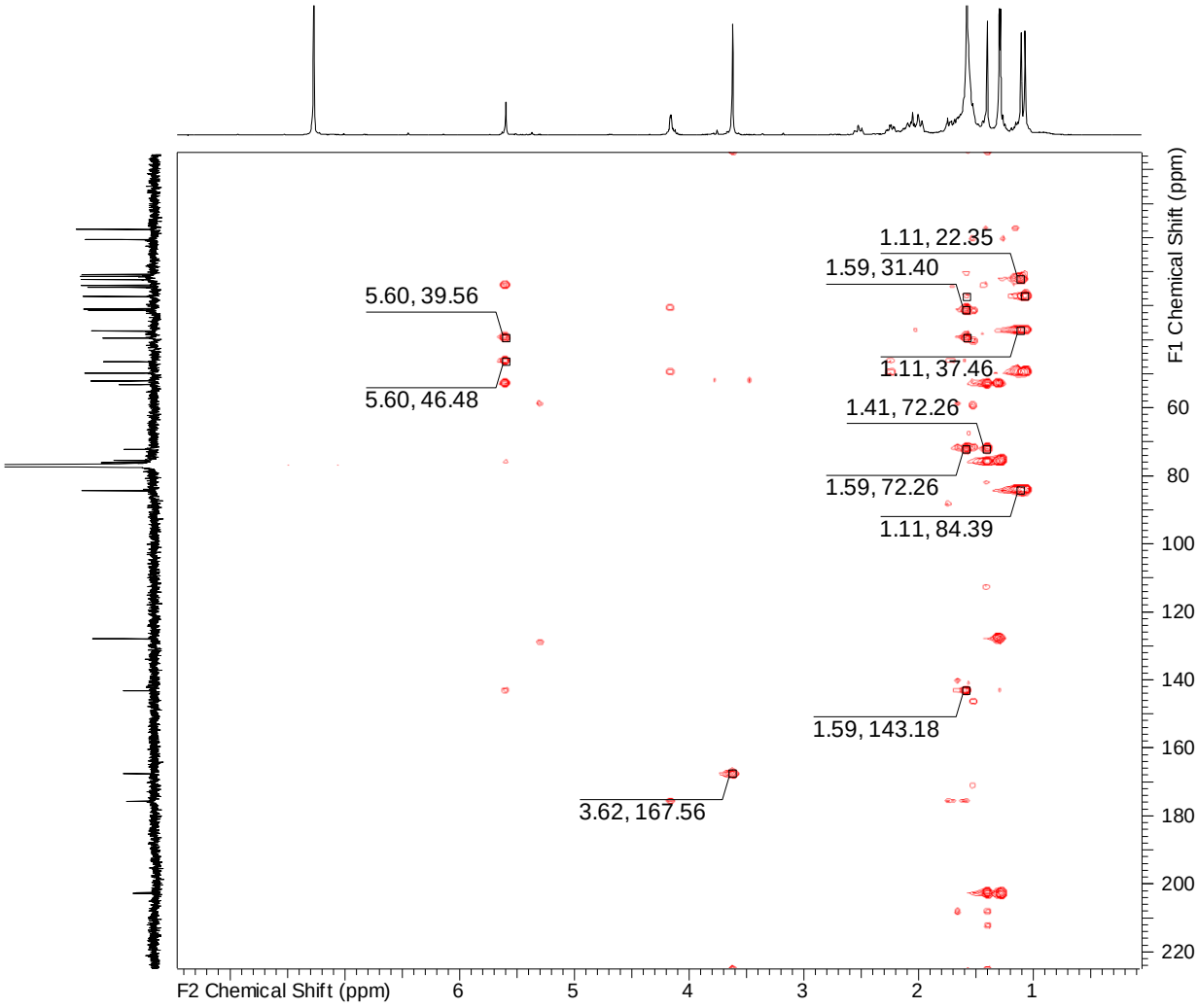

Figure Axiii. ^{1}H-^{13}C gHMBCAD NMR spectrum (500 MHz, $CDCl_3$) of SALT-17

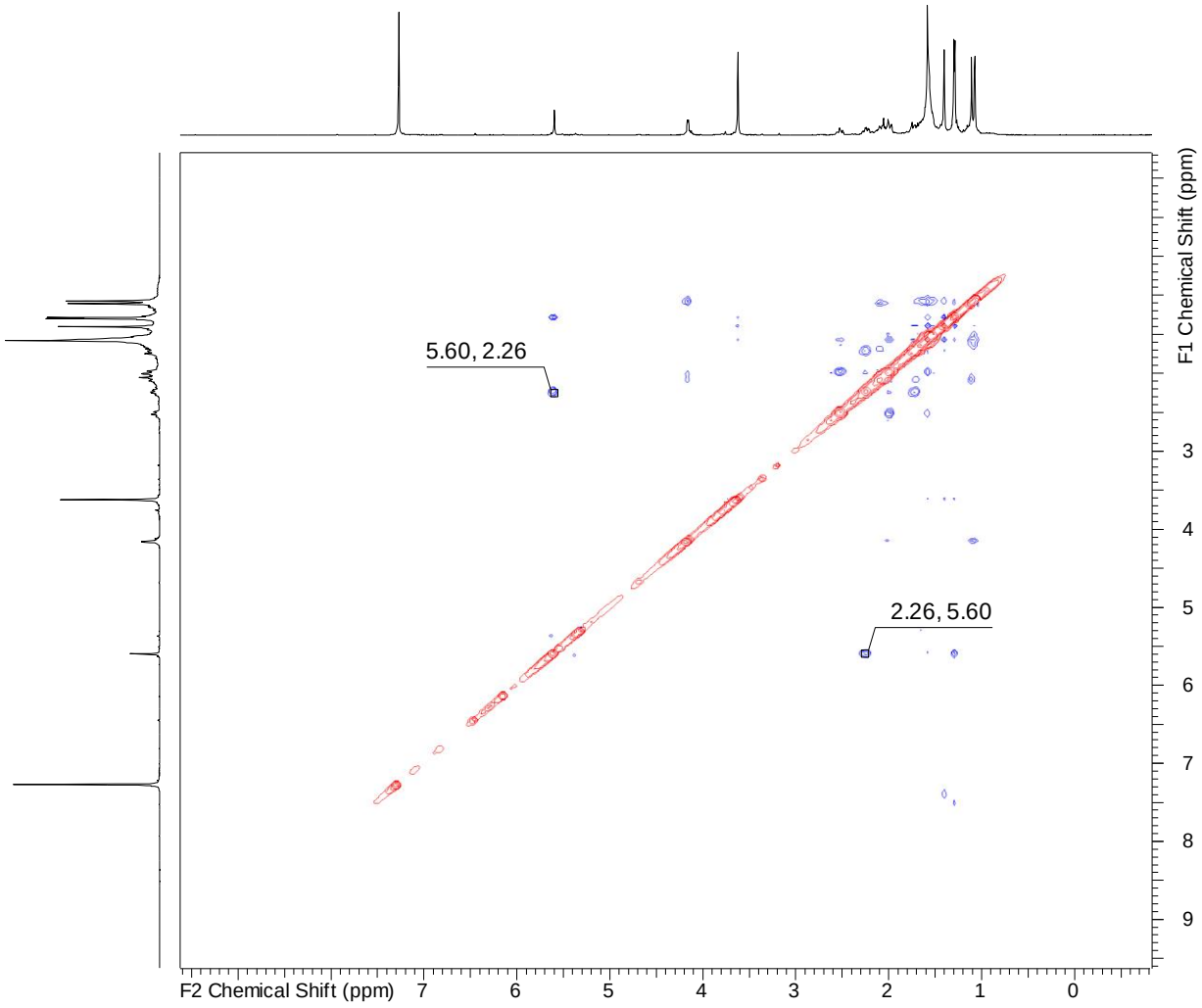

Figure Axiv NOESY NMR spectrum (500 MHz, $CDCl_3$) of SALT-17

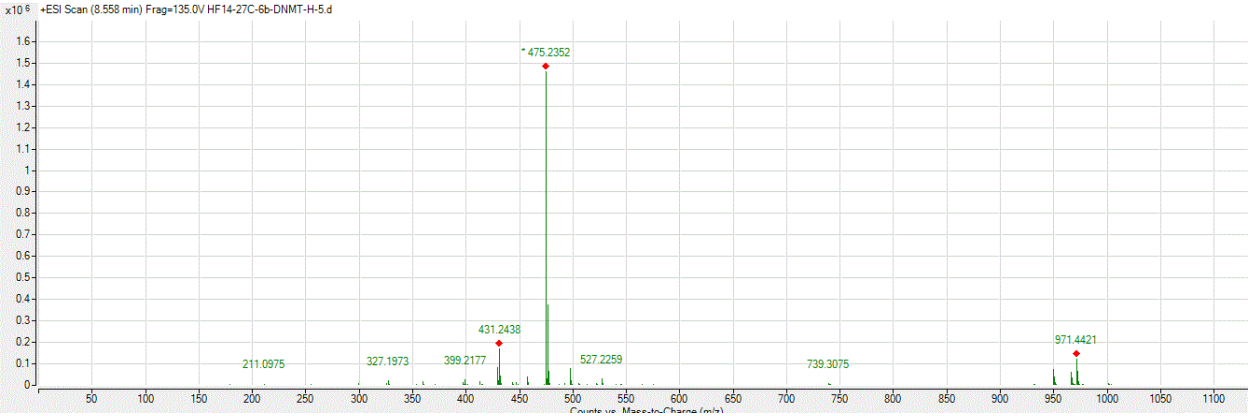

Figure Axv. Mass spectrum of SALT-17

Appendix B: Experimental and Supporting Data For Chapter Three

General Experimental Procedures

NMR data for compounds

General Experimental Procedures

Optical rotation was determined on a Rudolph Research Analytical AUTOPOL® IV with a sodium lamp (589 nm) and 0.1 dm cell at 25°C. 1D and 2D NMR spectra (^{1}H and ^{13}C NMR, HSQC, HMBC, COSY and NOESY spectra were obtained on either a Varian Inova 400, 500 or 600. High resolution mass spectra ESIMS were obtained on an Agilent LC-QToF or Agilent LC-ToF. HPLC was performed on a Shimadzu LC-20 equipped with an evaporative light scattering detector and a multiwavelength UV detector.

NMR data for compounds

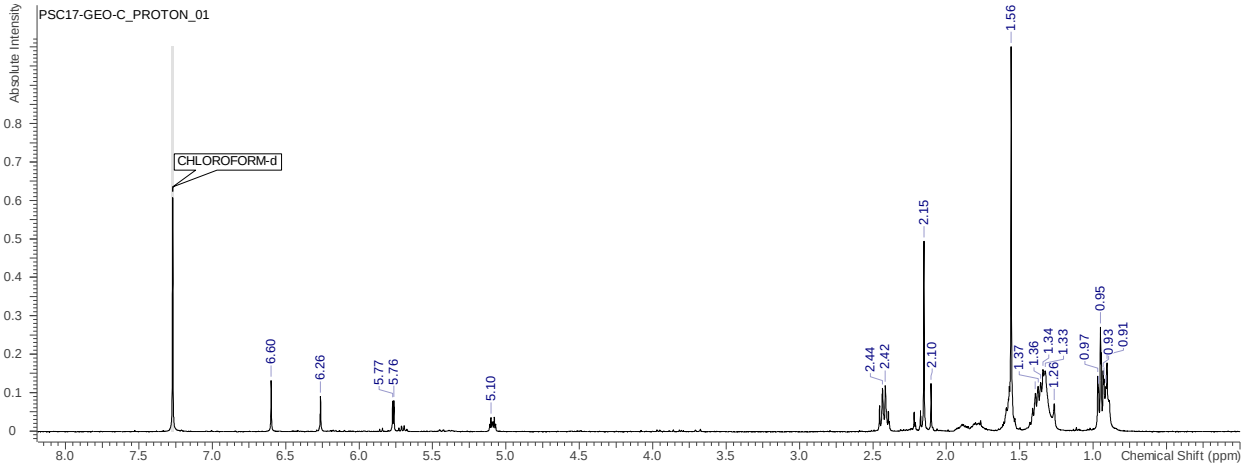

Figure Bi. ^{1}H NMR spectrum (400 MHz) of compound **3.7** in $CDCl_3$

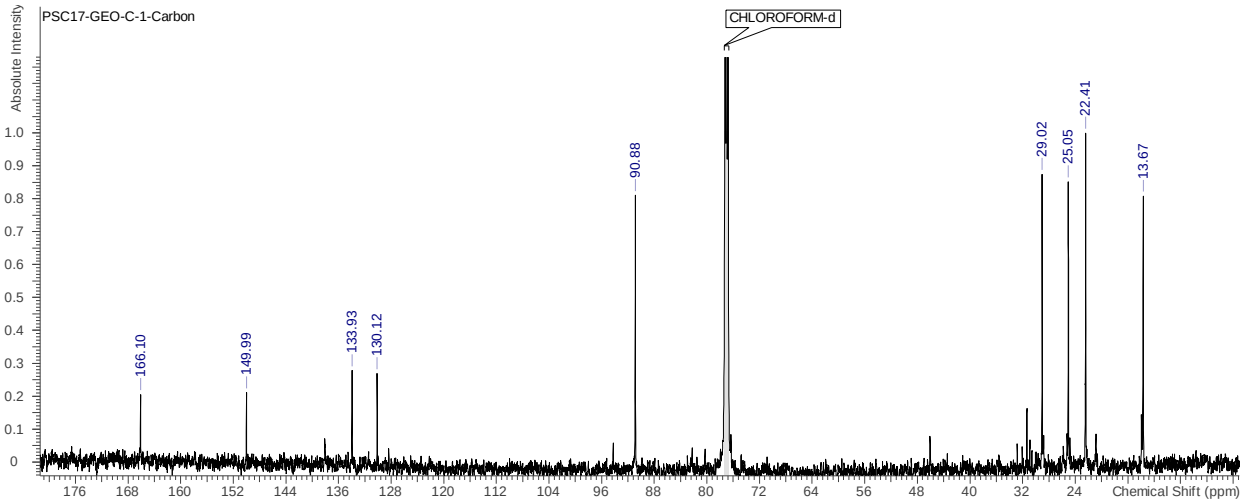

Figure Bii. ^{13}C NMR spectrum (100 MHz) of compound **3.7** in $CDCl_3$

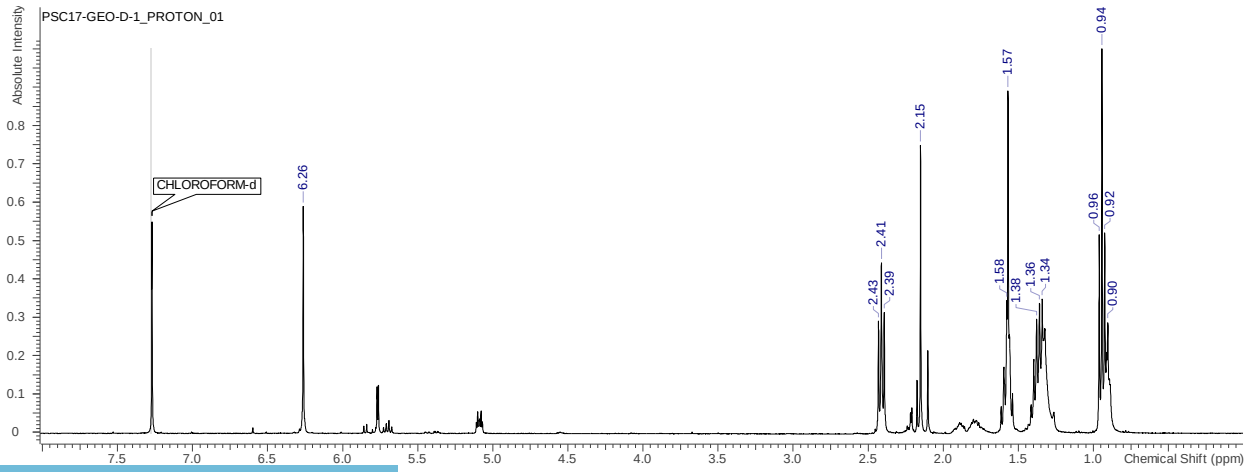

Figure Biii. ^{1}H NMR spectrum (400 MHz) of compound **3.8** in $CDCl_3$

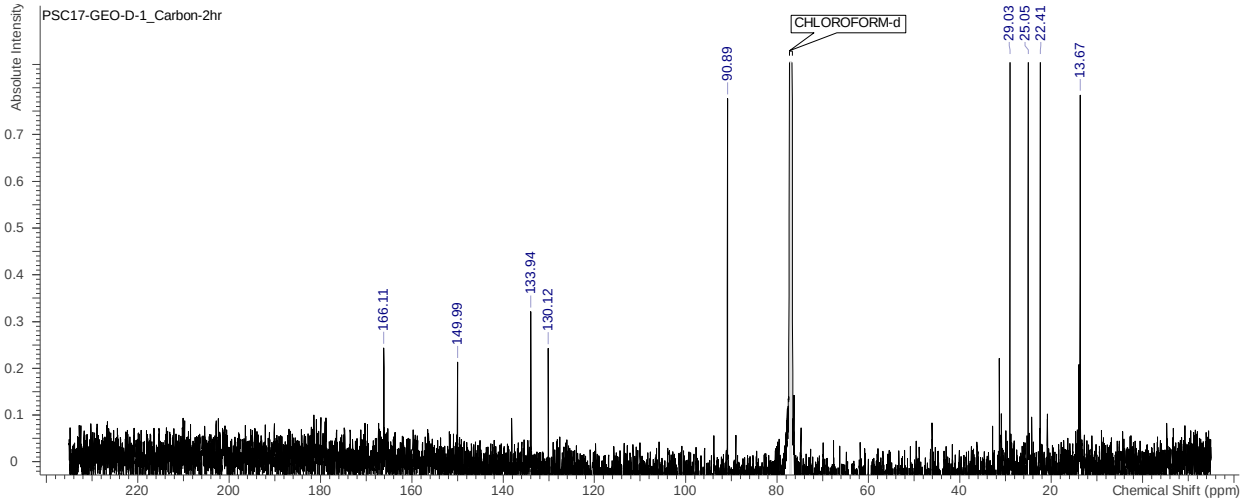

Figure Biv. ^{13}C NMR spectrum (100 MHz) of compound **3.8** in $CDCl_3$

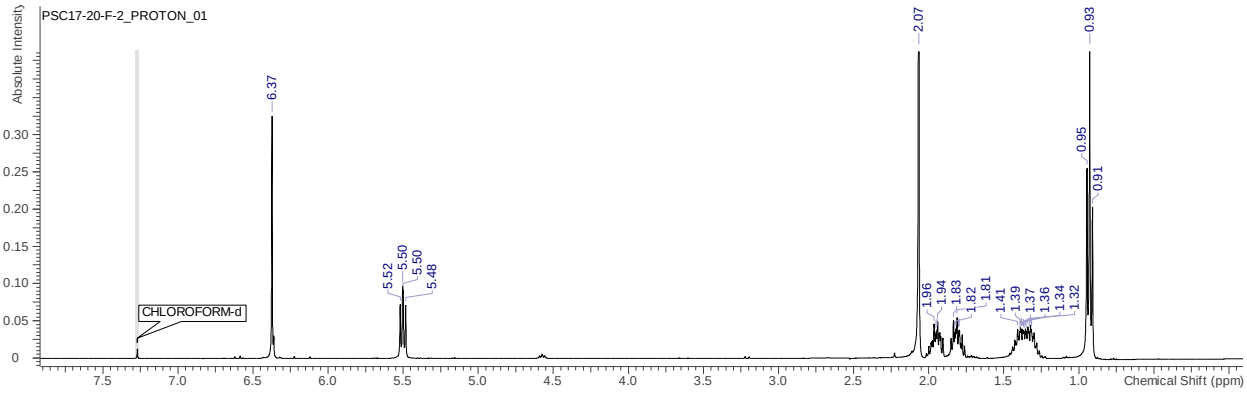

Figure Bv. ^{1}H NMR spectrum (400MHz) of compound **3.9** in $CDCl_3$

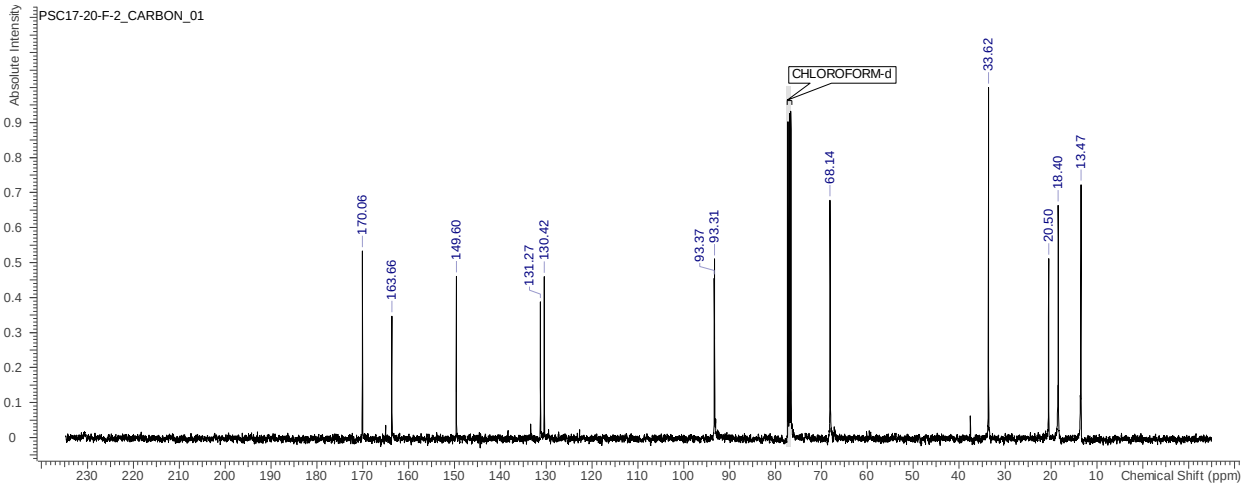

Figure Bvi. ^{13}C NMR spectrum (100MHz) of compound **3.9** in $CDCl_3$

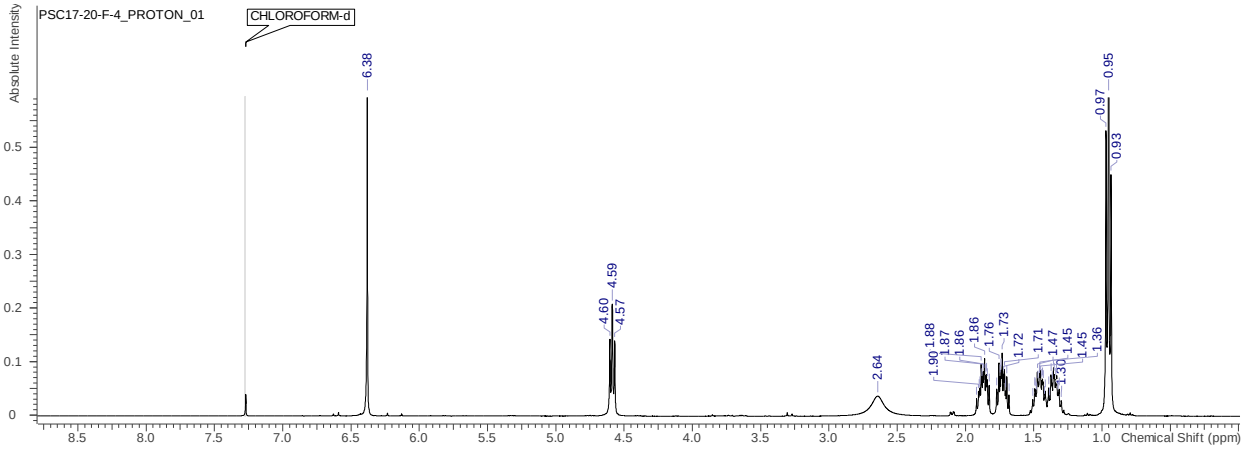

Figure Bvii. ^{1}H NMR spectrum (400MHz) of compound **3.10** in $CDCl_3$

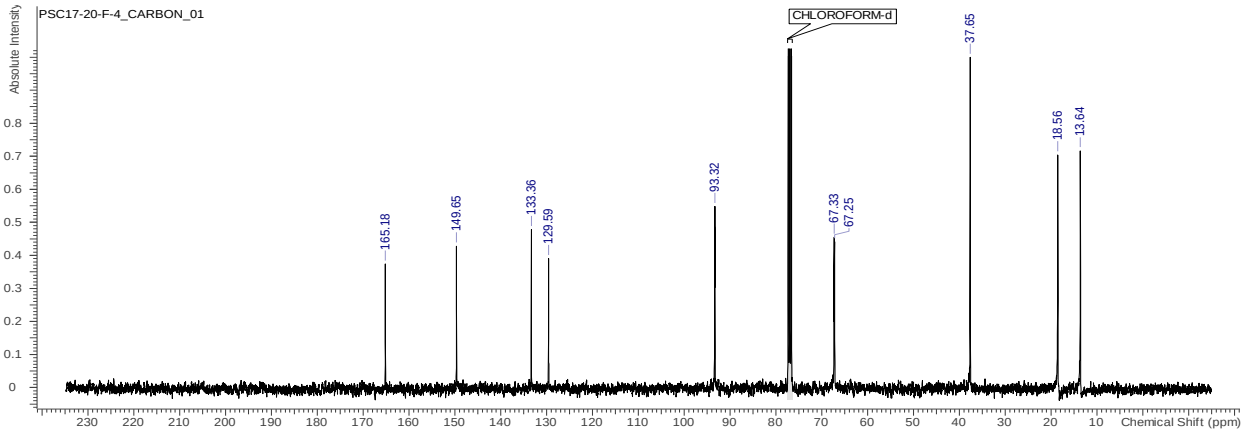

Figure Bviii. ^{13}C NMR spectrum (100 MHz) of compound **3.10** in $CDCl_3$

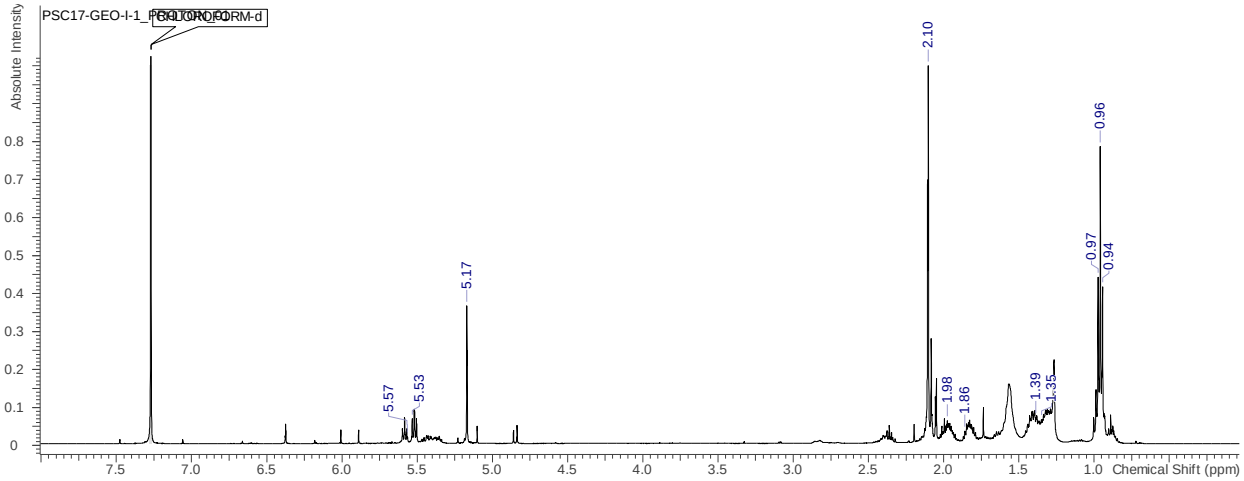

Figure Bix. ^{1}H NMR spectrum (400 MHz) of compound **3.11** in $CDCl_3$

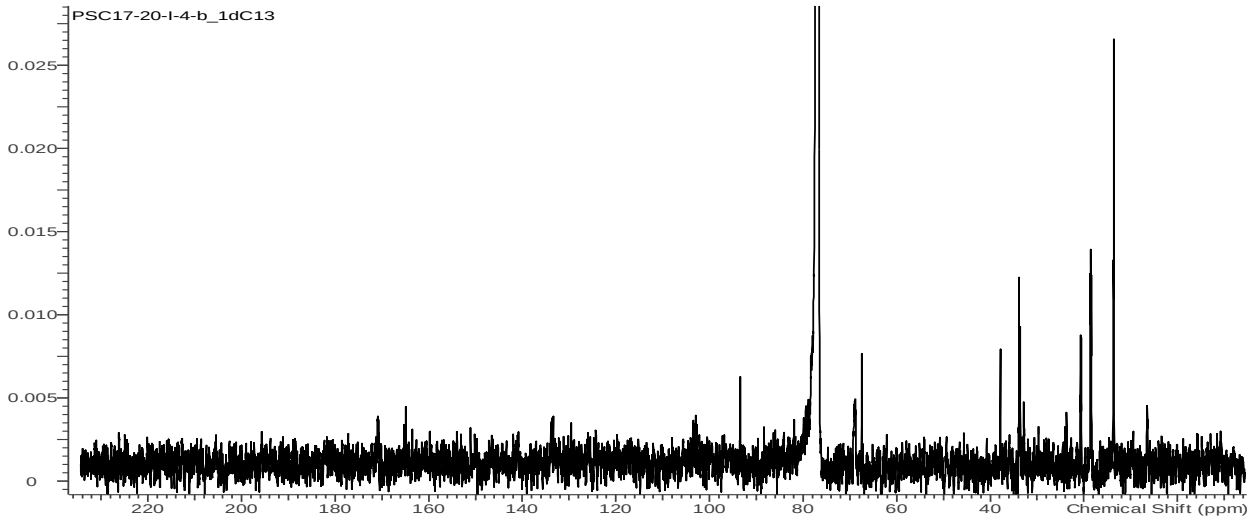

Figure Bx. ^{13}C NMR spectrum (125 MHz) of compound **3.11** in $CDCl_3$

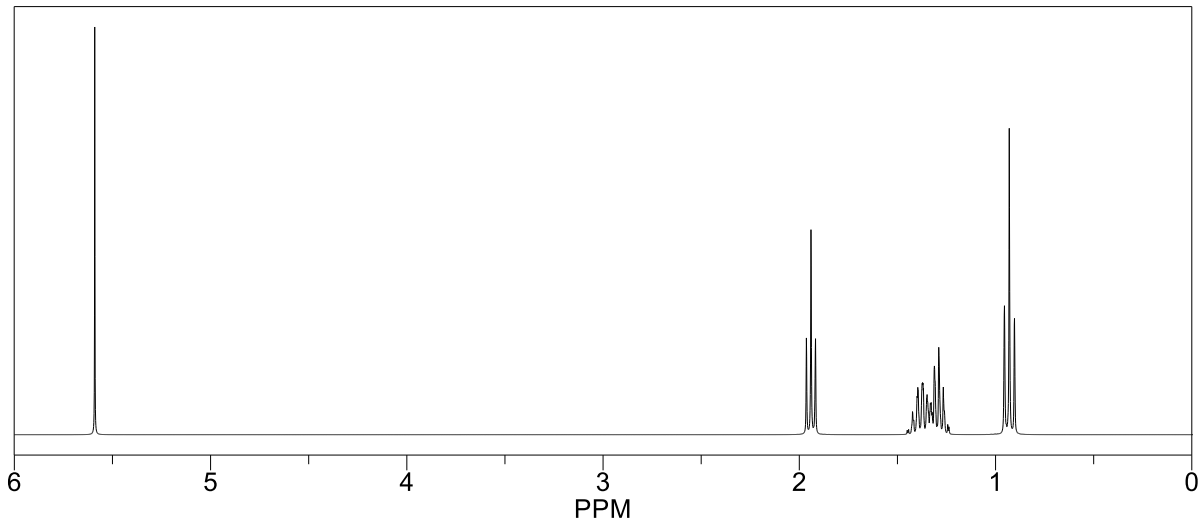

Figure Bxi. predicted ^{1}H NMR spectrum of compound **3.12** in $CDCl_3$

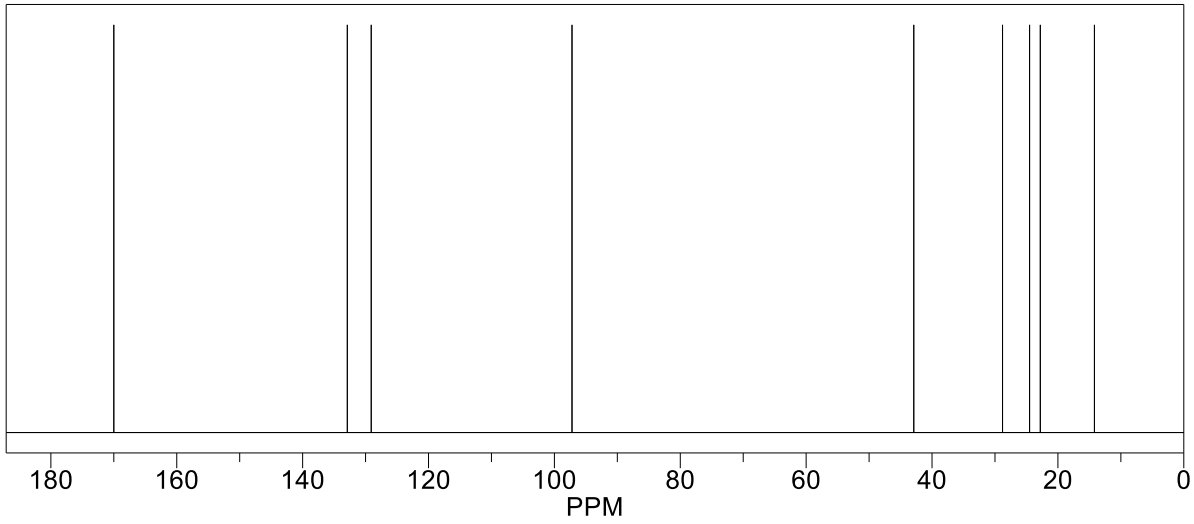

Figure Bxii. predicted ^{13}C NMR spectrum of compound **3.12** in $CDCl_3$

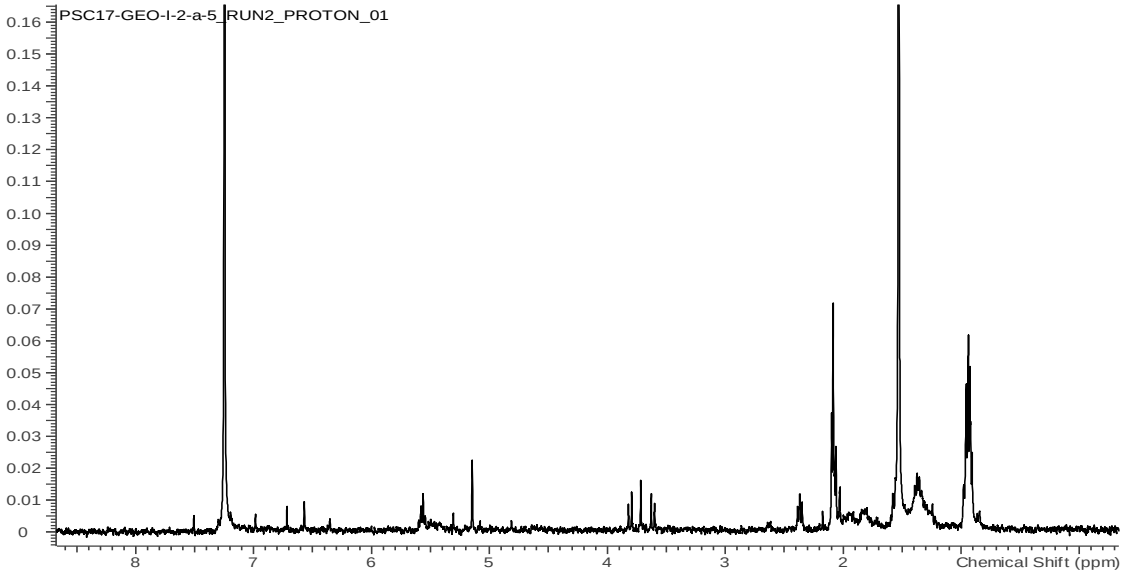

Figure Bxiii. ^{1}H NMR spectrum of compound **3.13** in $CDCl_3$

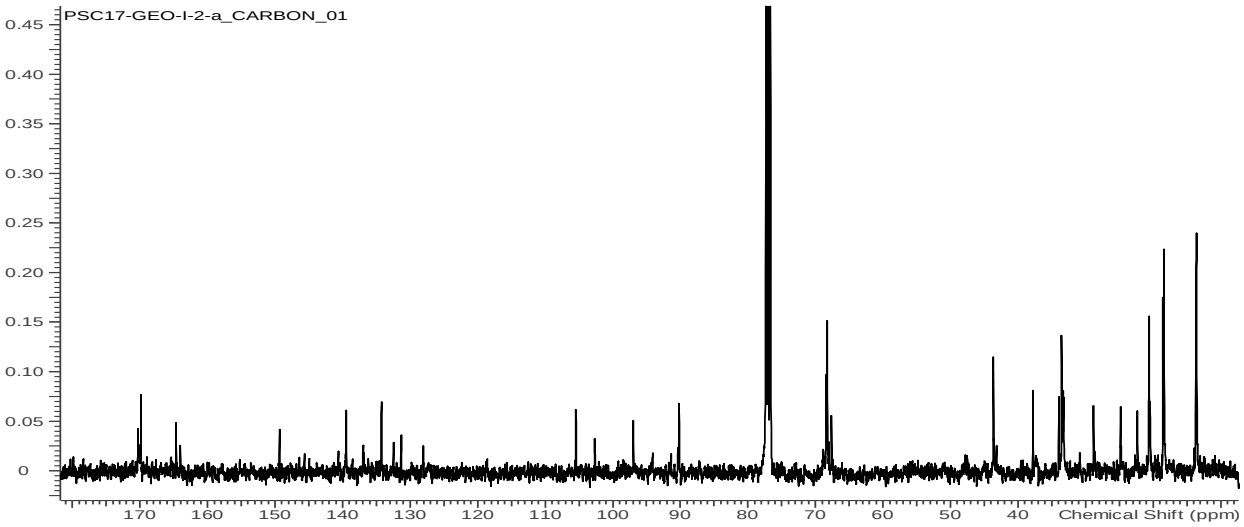

Figure Bxiv. ^{13}C NMR spectrum of compound **3.13** in $CDCl_3$

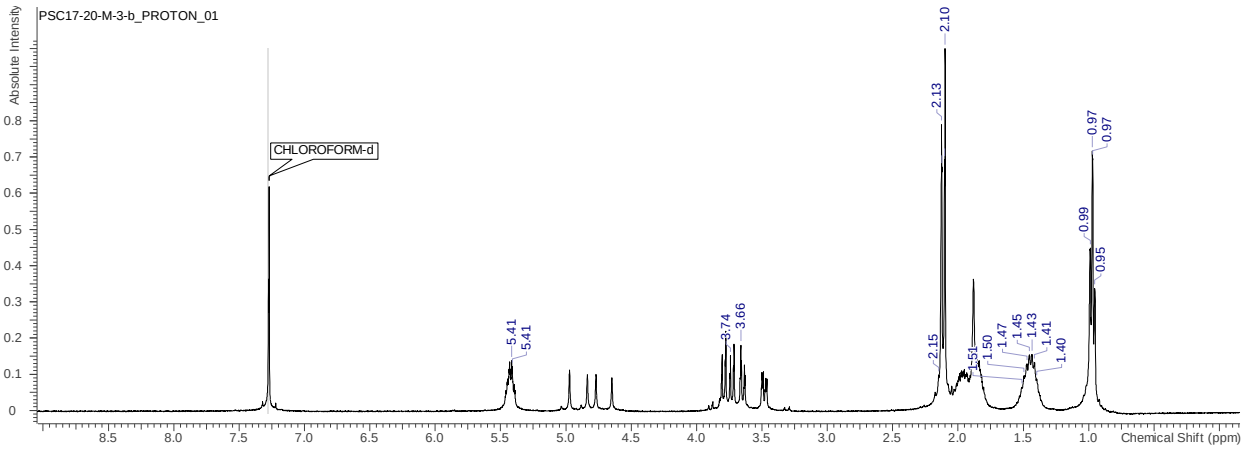

Figure Bxv. ^{1}H NMR spectrum (400MHz) of compound **3.14** in $CDCl_3$

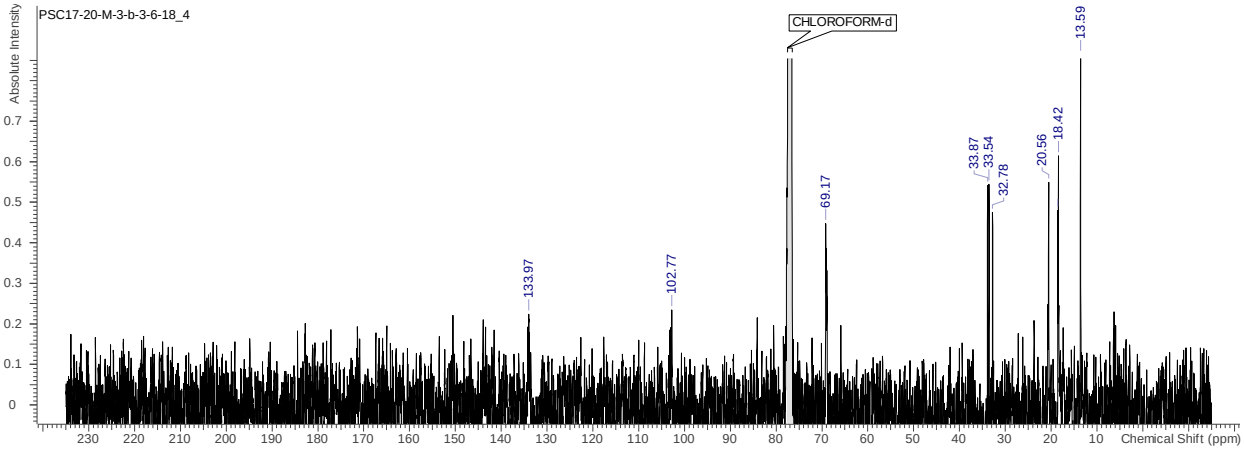

Figure Bxvi. ^{13}C NMR spectrum (100MHz) of compound **3.14** in $CDCl_3$

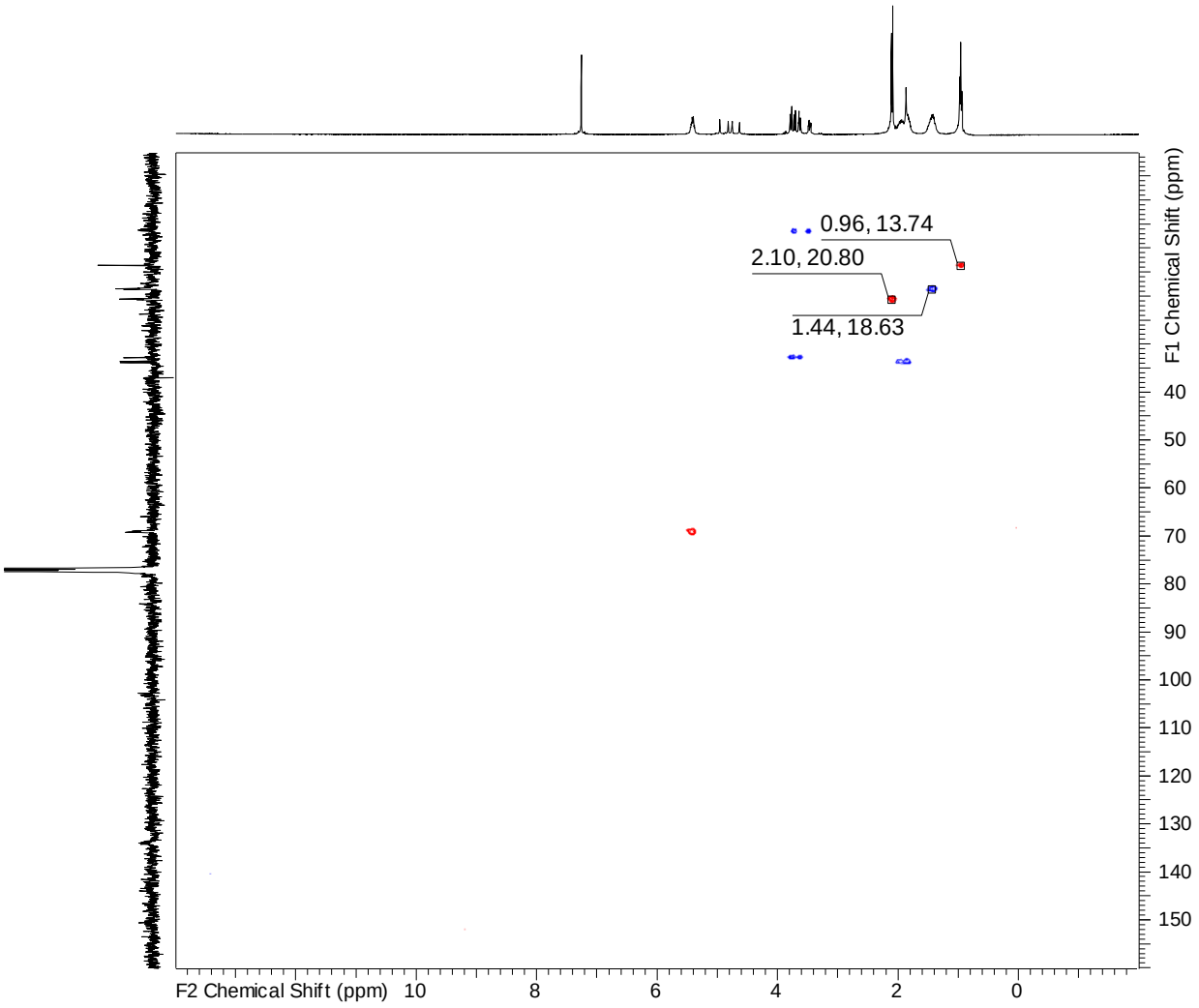

Figure Bxvii. gHSQCAD NMR spectrum (400MHz) of compound **3.14** in $CDCl_3$

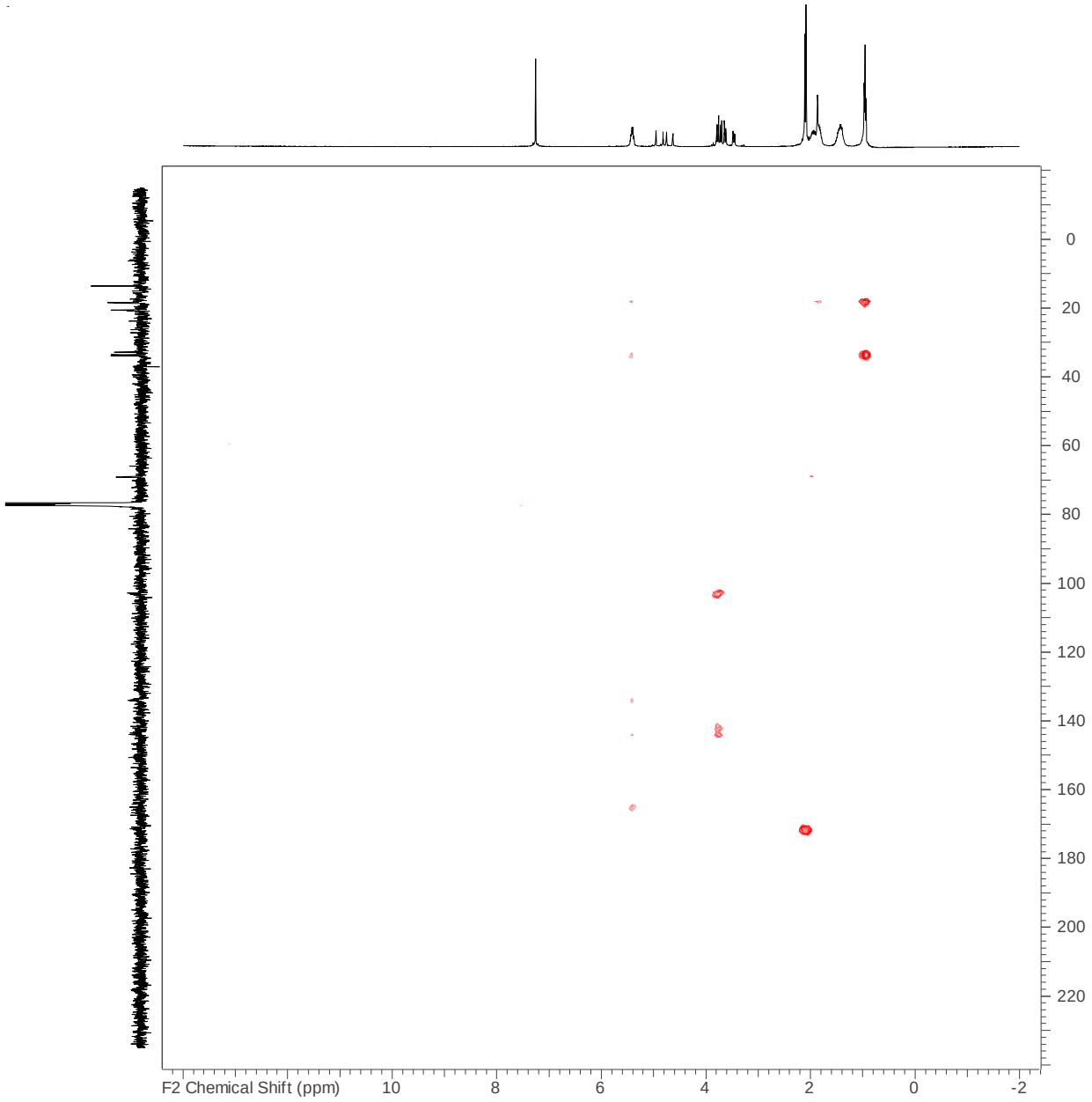

Figure Bxviii. gHMBCAD NMR spectrum of compound **3.14** in $CDCl_3$

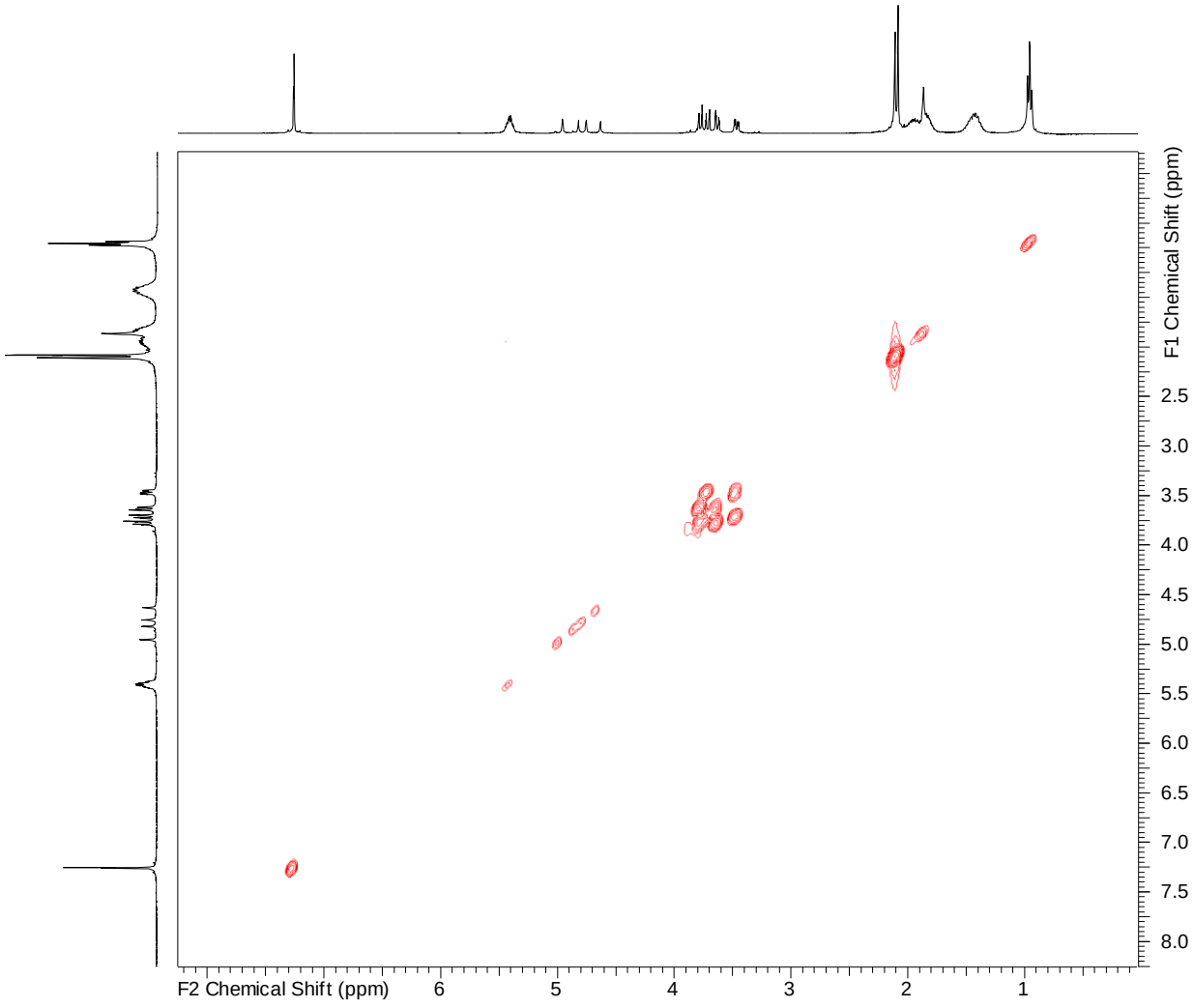

Figure Bxix. COSY NMR spectrum (400 MHz) of compound **3.14** in $CDCl_3$

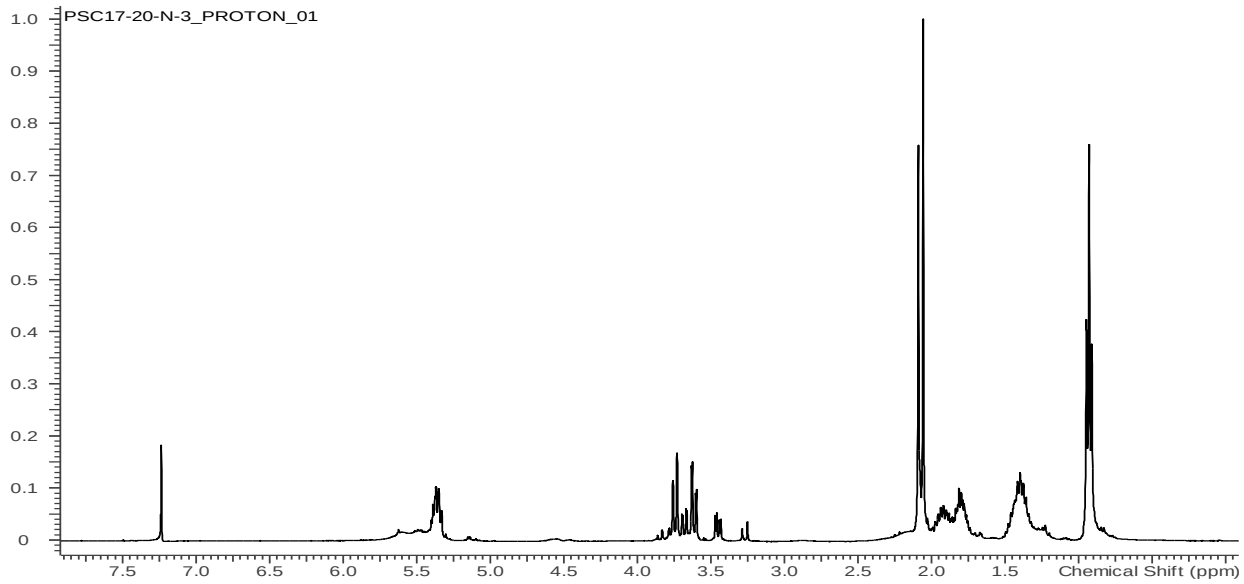

Figure Bxx. ^{1}H NMR spectrum (400 MHz) of compound **3.15** in $CDCl_3$

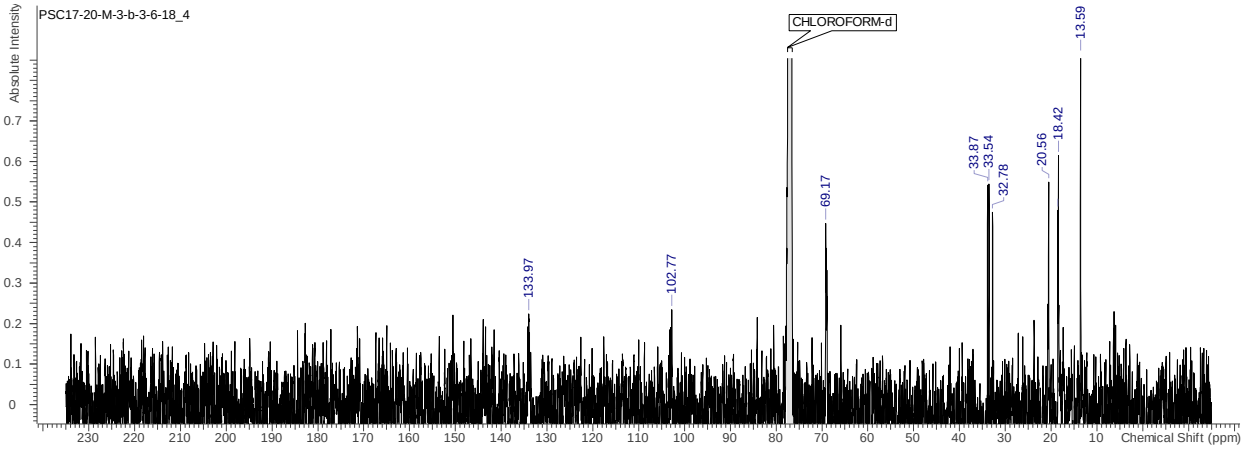

Figure Bxxi. ^{13}C NMR spectrum (125 MHz) of compound **3.15** in $CDCl_3$

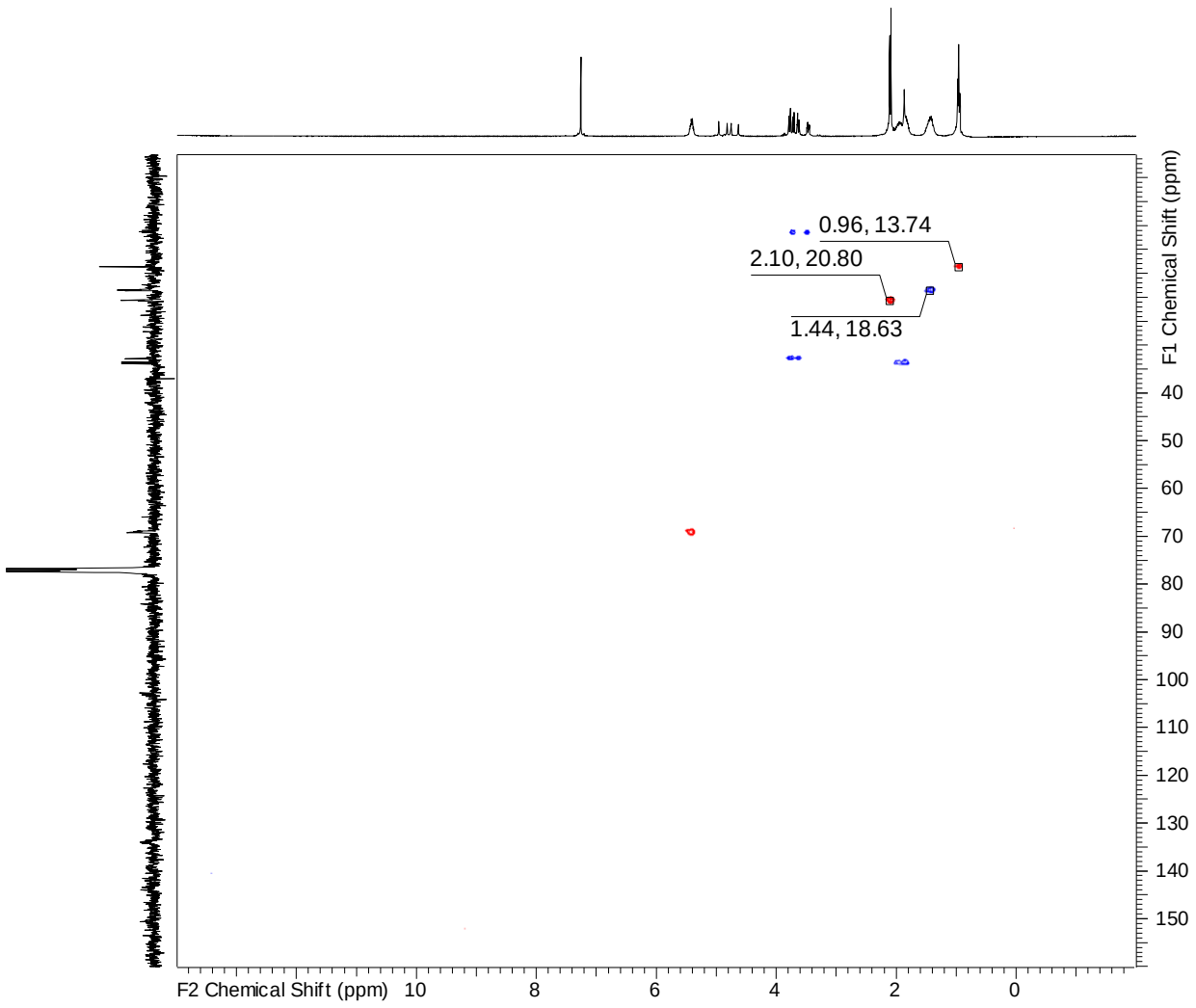

Figure Bxxii. gHSQCAD NMR spectrum (500 MHz) of compound **3.15** in $CDCl_3$

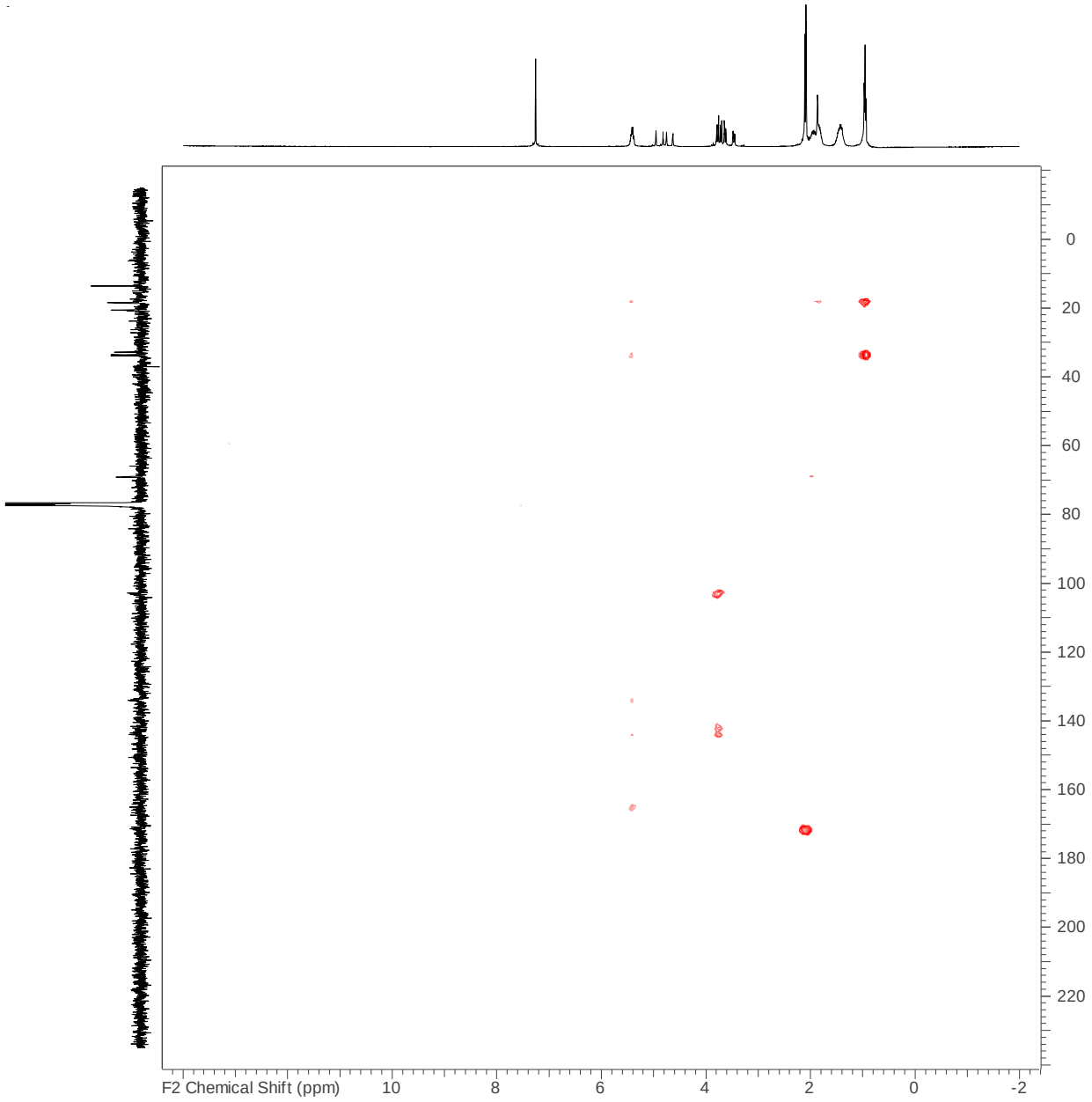

Figure Bxxiii. gHMBCAD NMR spectrum (500 MHz) of compound **3.15** in $CDCl_3$

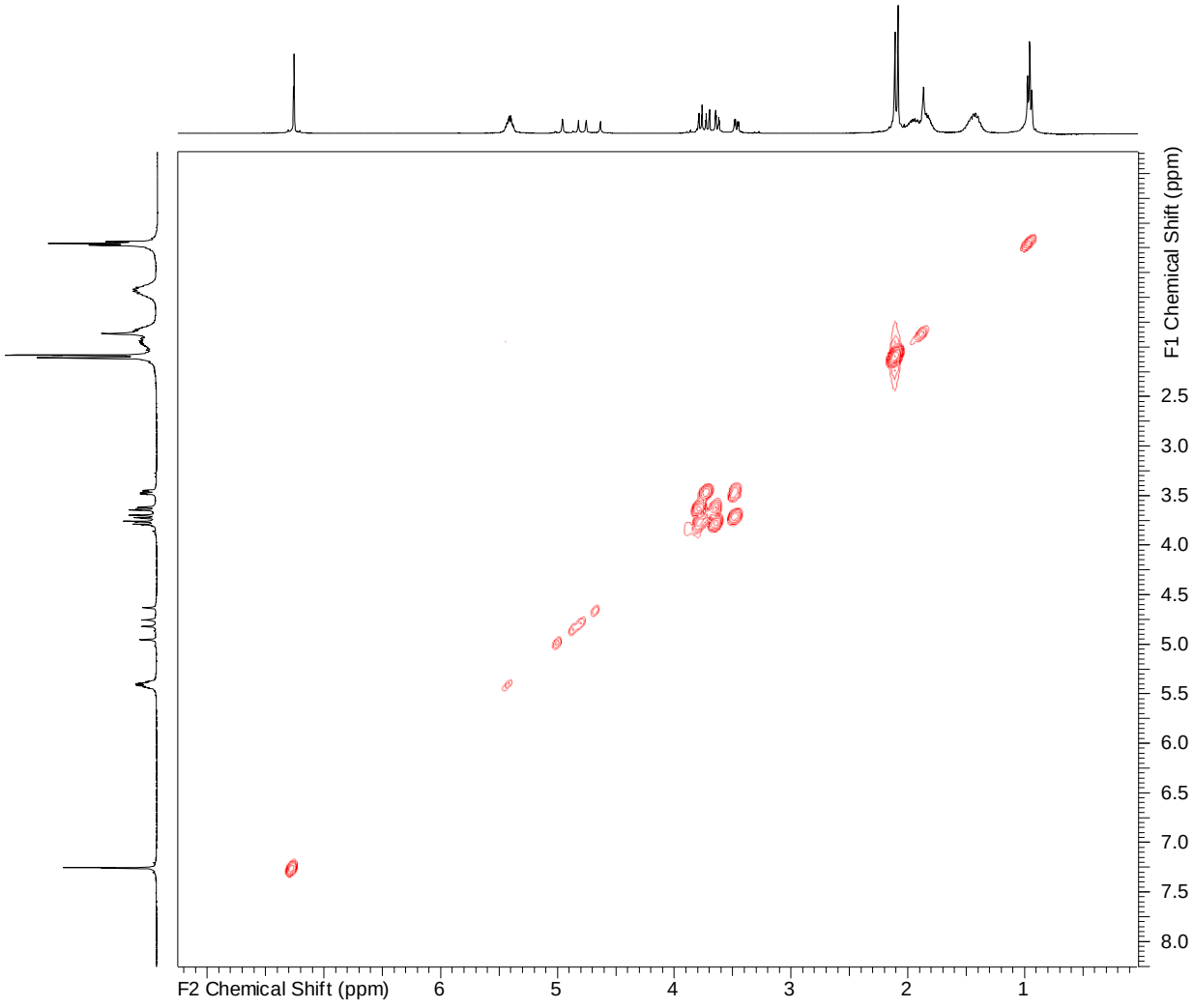

Figure Bxxiv. COSY NMR spectrum (500 MHz) of compound **3.15** in $CDCl_3$

Appendix C: Experimental and Supplemental Data for Chapter Four

General Experimental Data

Biological Material

Compounds NMR data

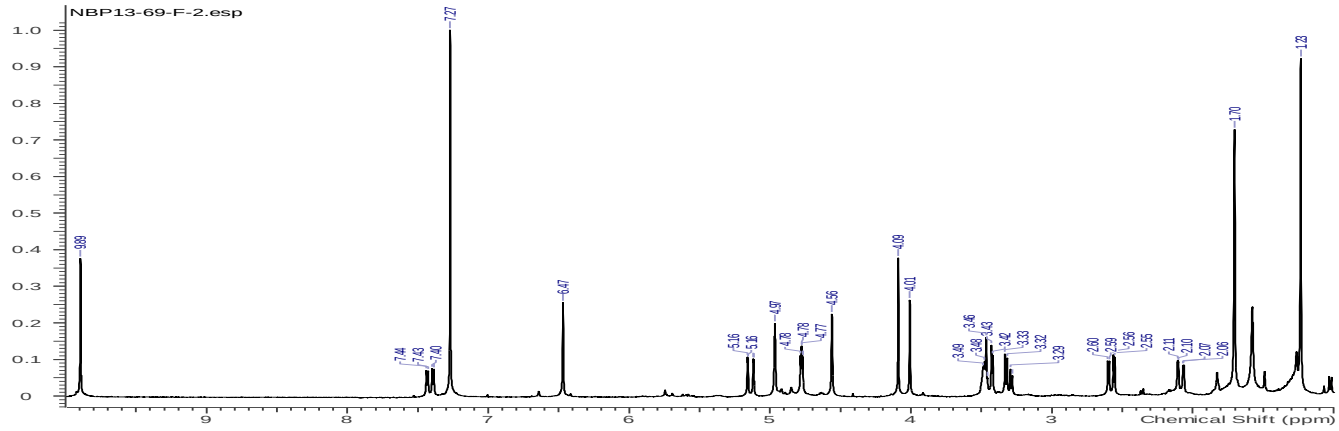

Figure Ci. ^{1}H NMR spectrum of keikipukalide A (**4.19**) in $CDCl_3$, 400 MHz

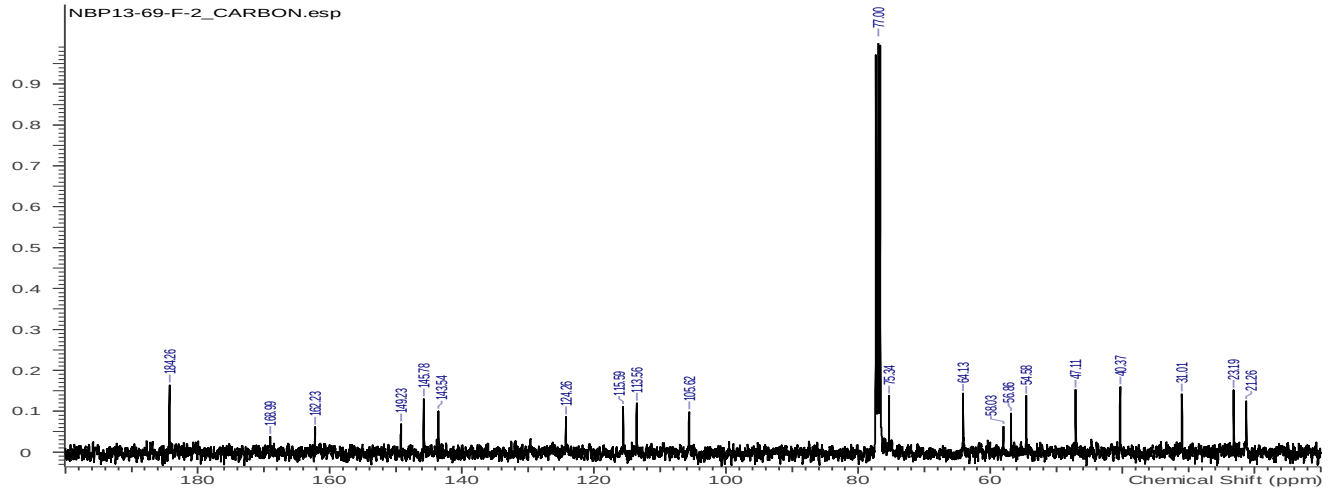

Figure Cii. ^{13}C NMR spectrum of keikipukalide A (**4.19**) in $CDCl_3$, 100 MHz

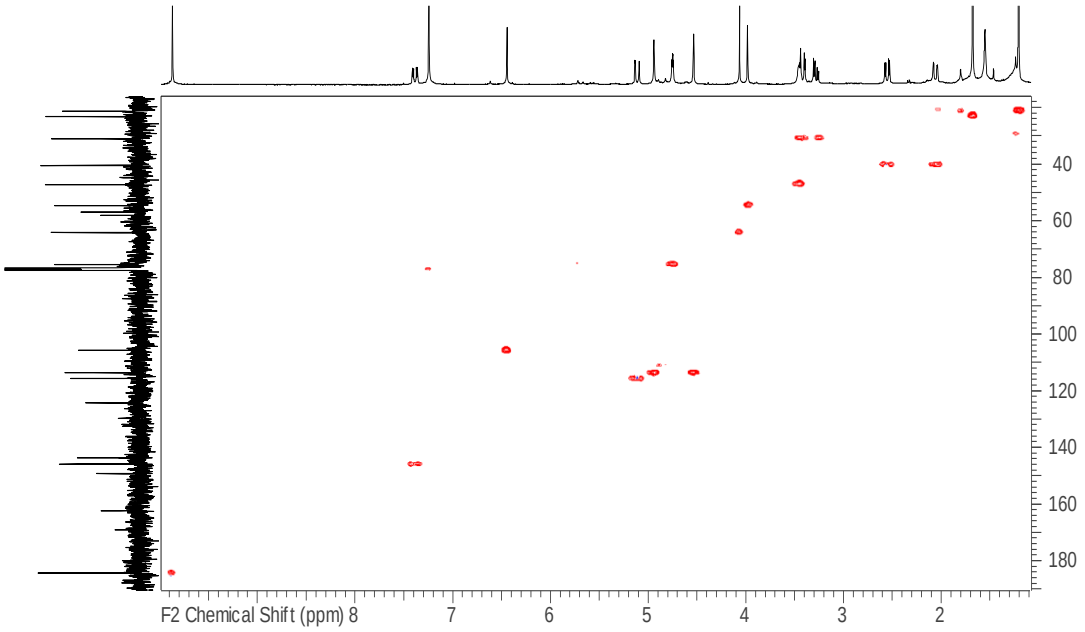

Figure Ciii. gHMQC of keikipukalide A (**4.19**) in $CDCl_3$, 400 MHz

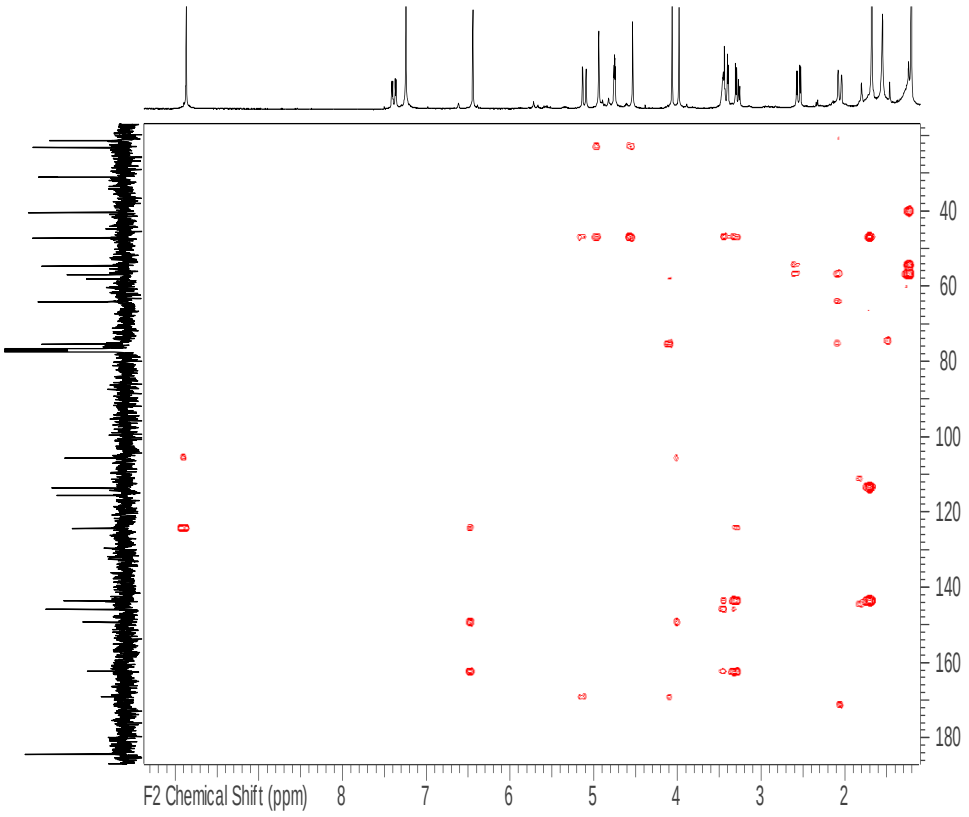

Figure Civ. gHMBC of keikipukalide A (**4.19**) in $CDCl_3$, 400 MHz

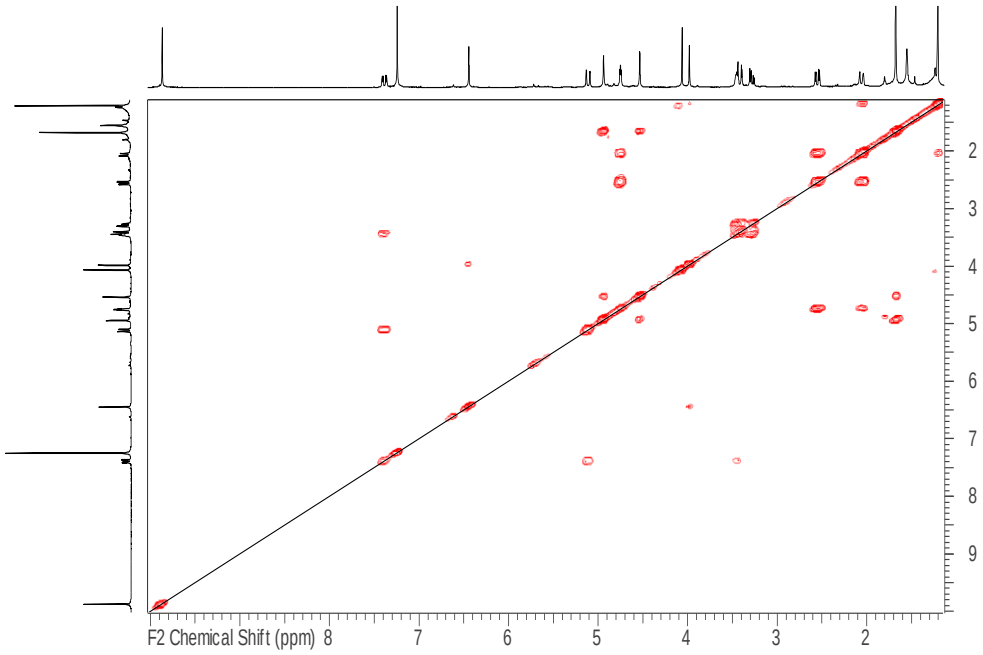

Figure Cv. gCOSY of keikipukalide A (**4.19**) in $CDCl_3$, 400 MHz

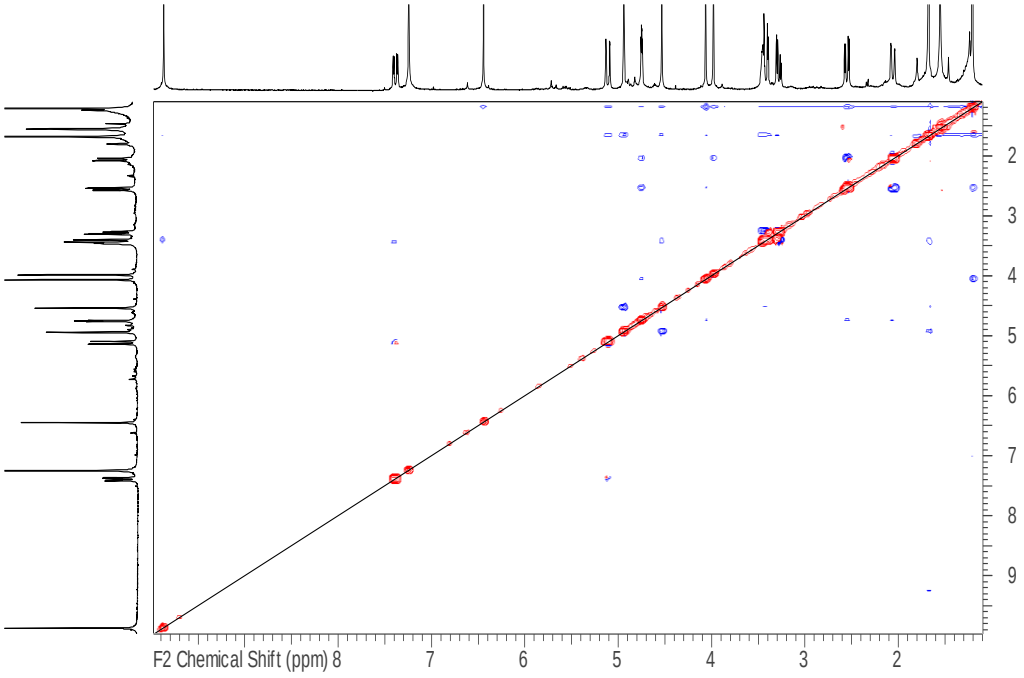

Figure Cvi. NOESY of keikipukalide A (**4.19**) in $CDCl_3$, 500 MHz

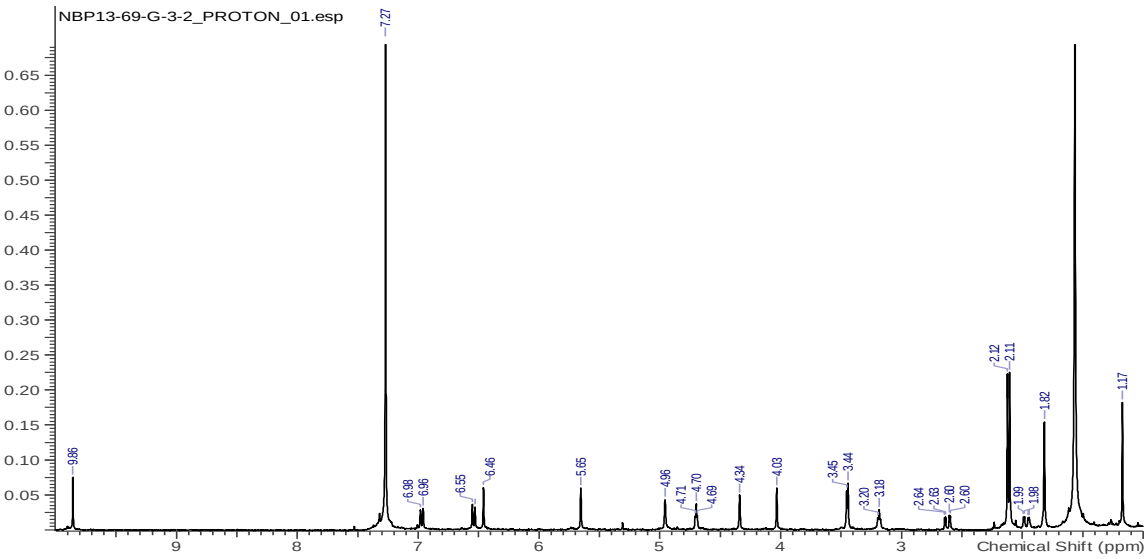

Figure Cvii. ^{1}H NMR spectrum of keikipukalide B (**4.20**) in $CDCl_3$, 400 MHz

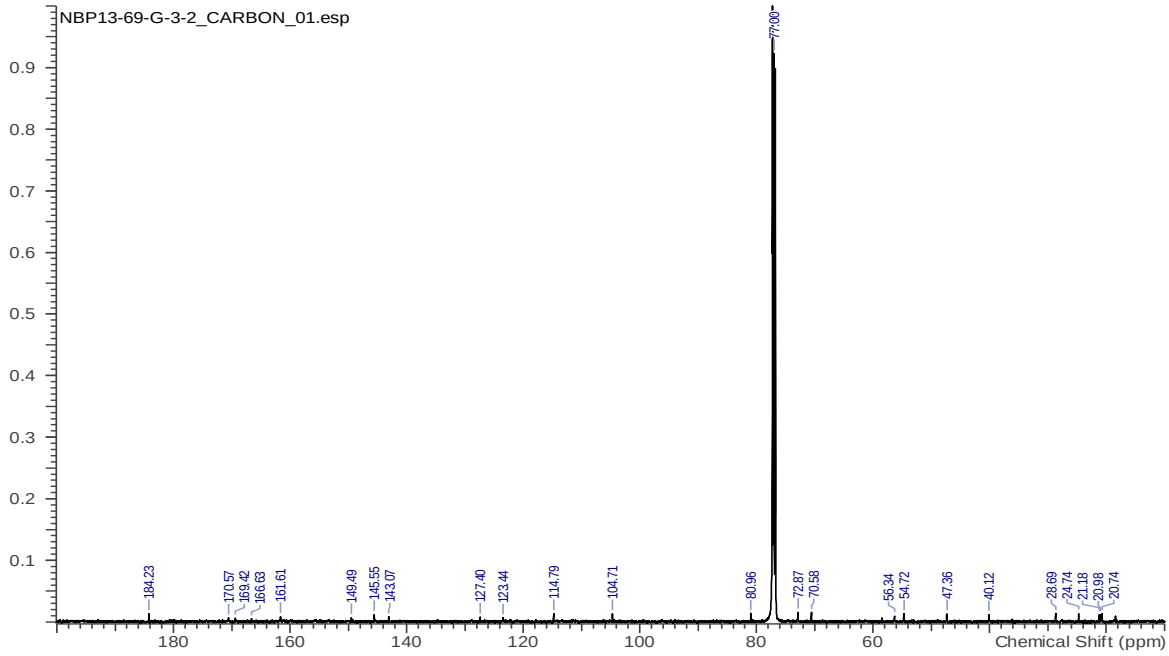

Figure Cviii. ^{13}C NMR spectrum of keikipukalide B (**4.20**) in $CDCl_3$, 125 MHz

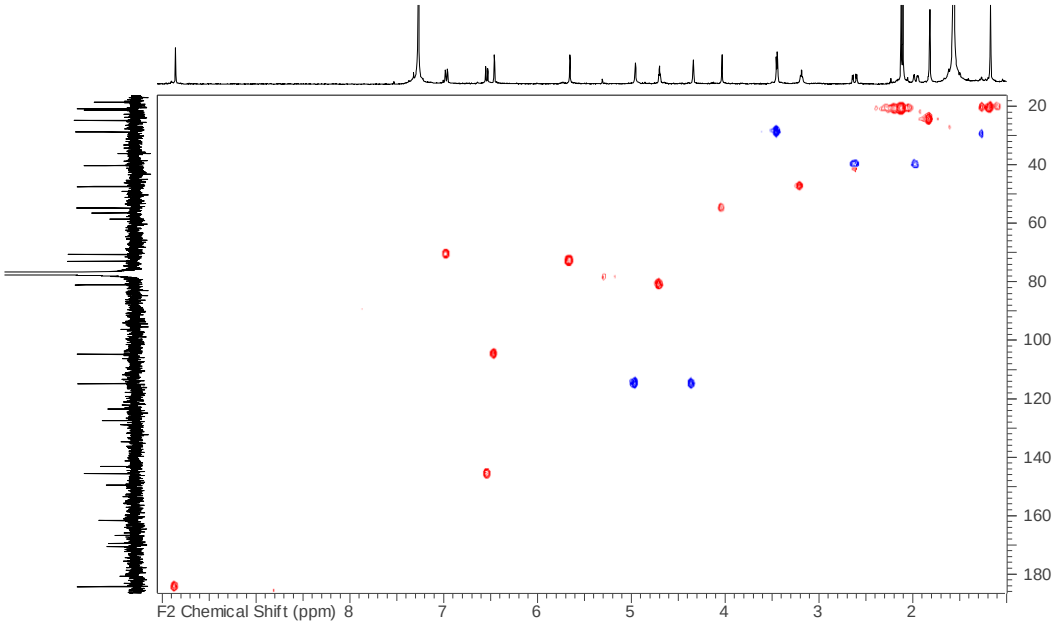

Figure Cix. gHSQC of keikipukalide B (**4.20**) in $CDCl_3$, 600 MHz

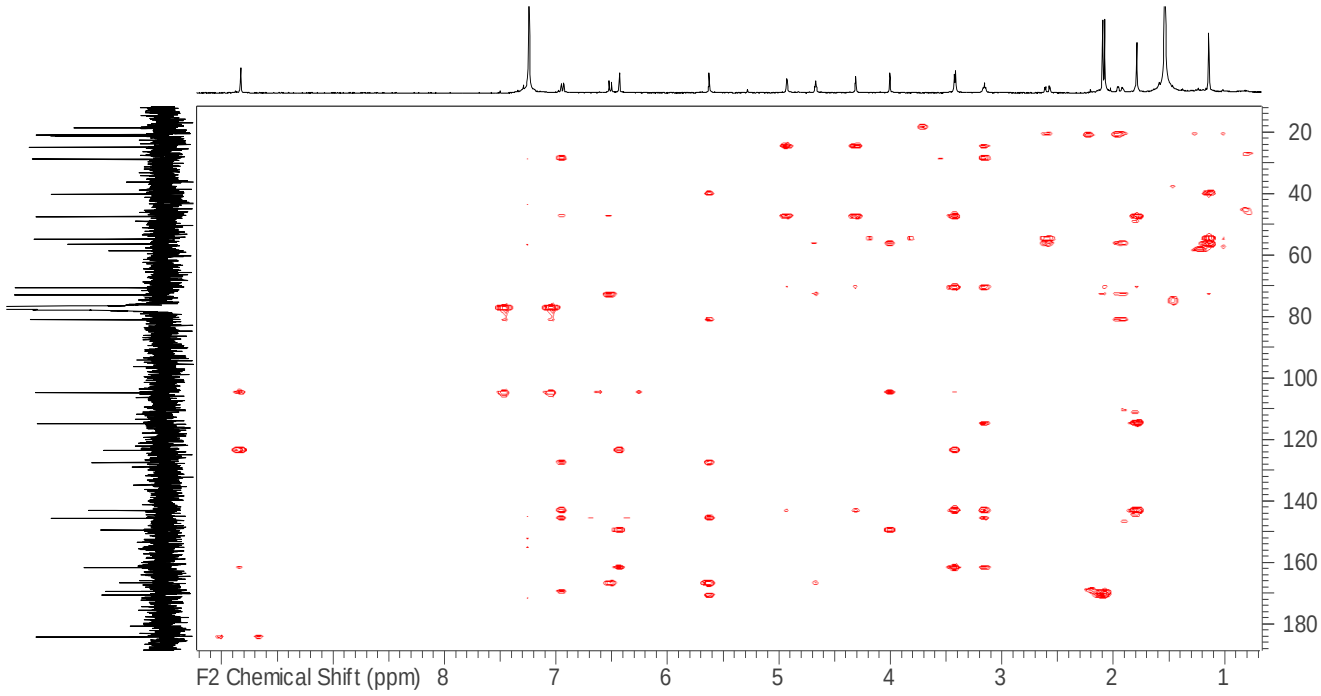

Figure Cx. gHMBC of keikipukalide B (**4.20**) in $CDCl_3$, 500 MHz

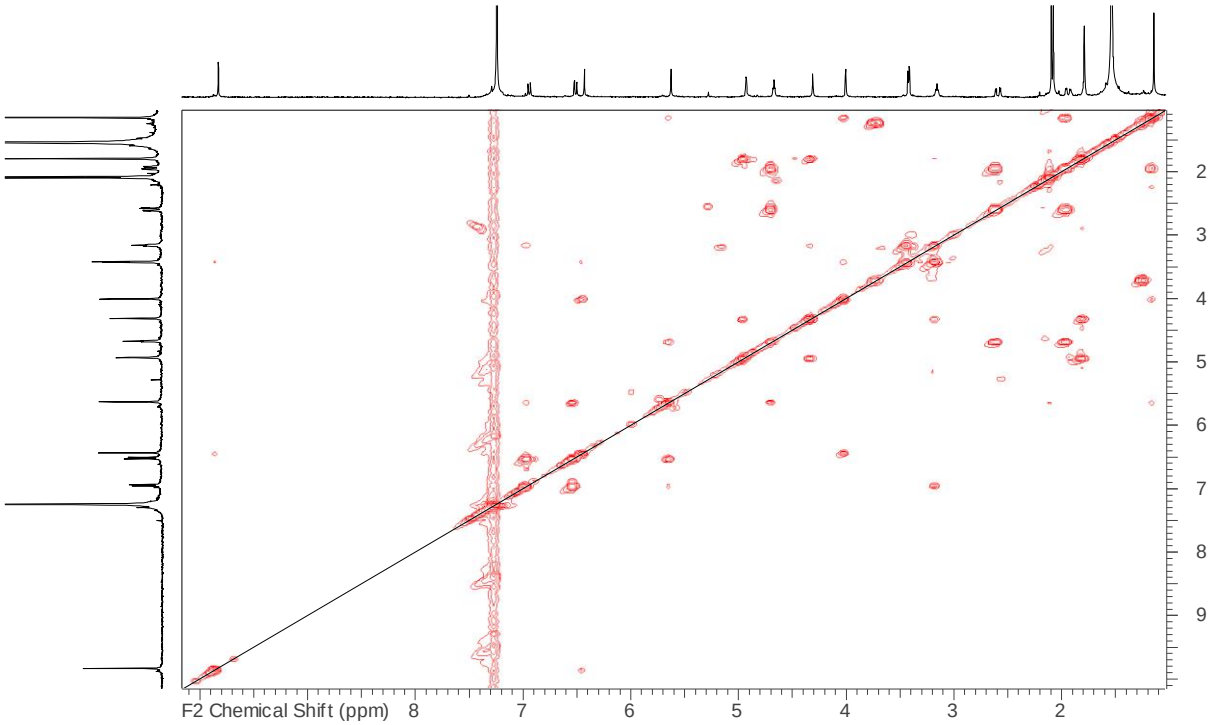

Figure Cxi. gCOSY of keikipukalide B (**4.20**) in $CDCl_3$, 500 MHz

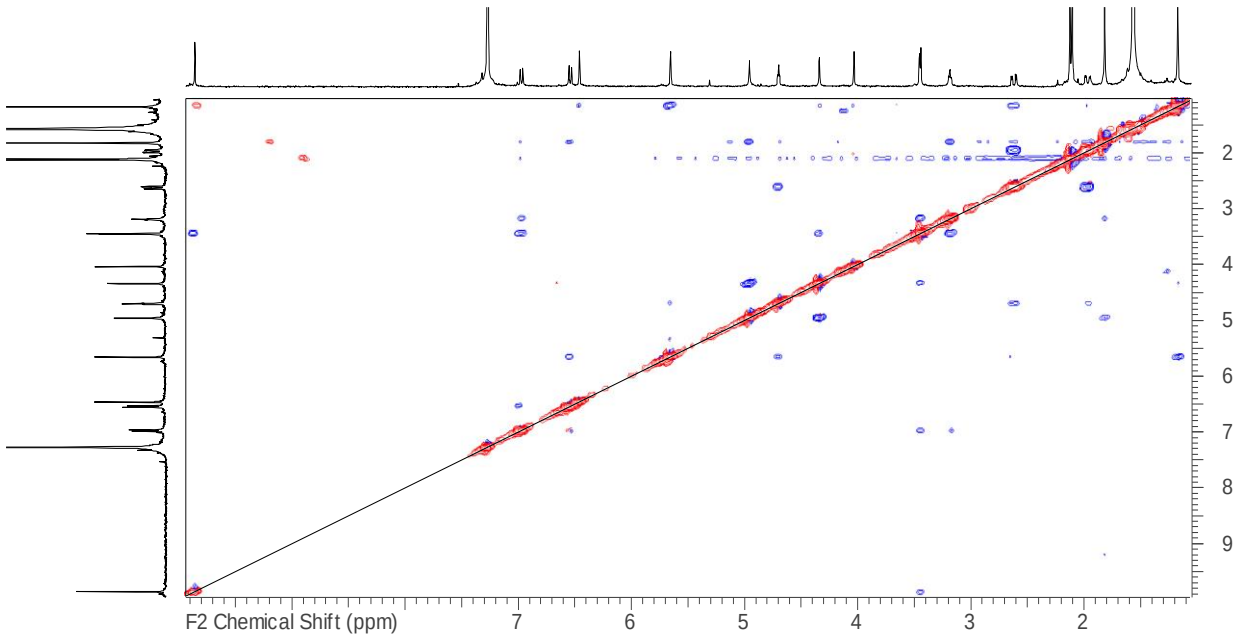

Figure Cxii. NOESY of keikipukalide B (**4.20**) in $CDCl_3$, 400 MHz

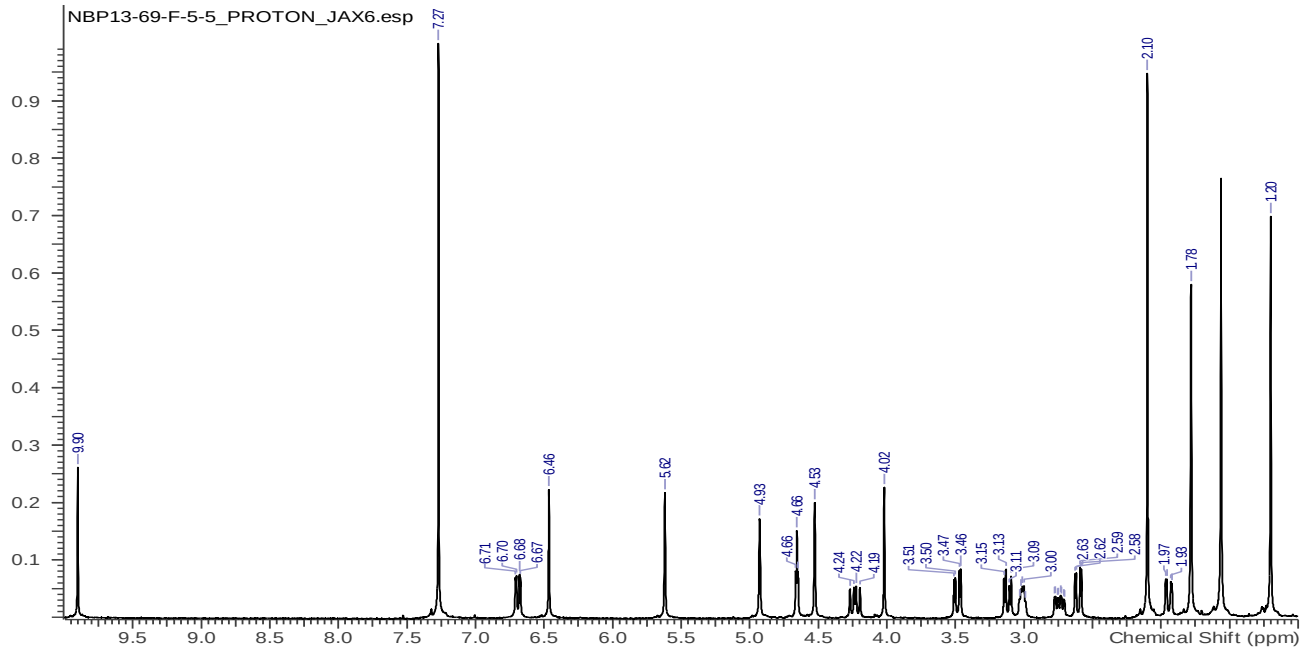

Figure Cxiii. ^{1}H NMR spectrum of keikipukalide C (**4.21**) in $CDCl_3$, 400 MHz

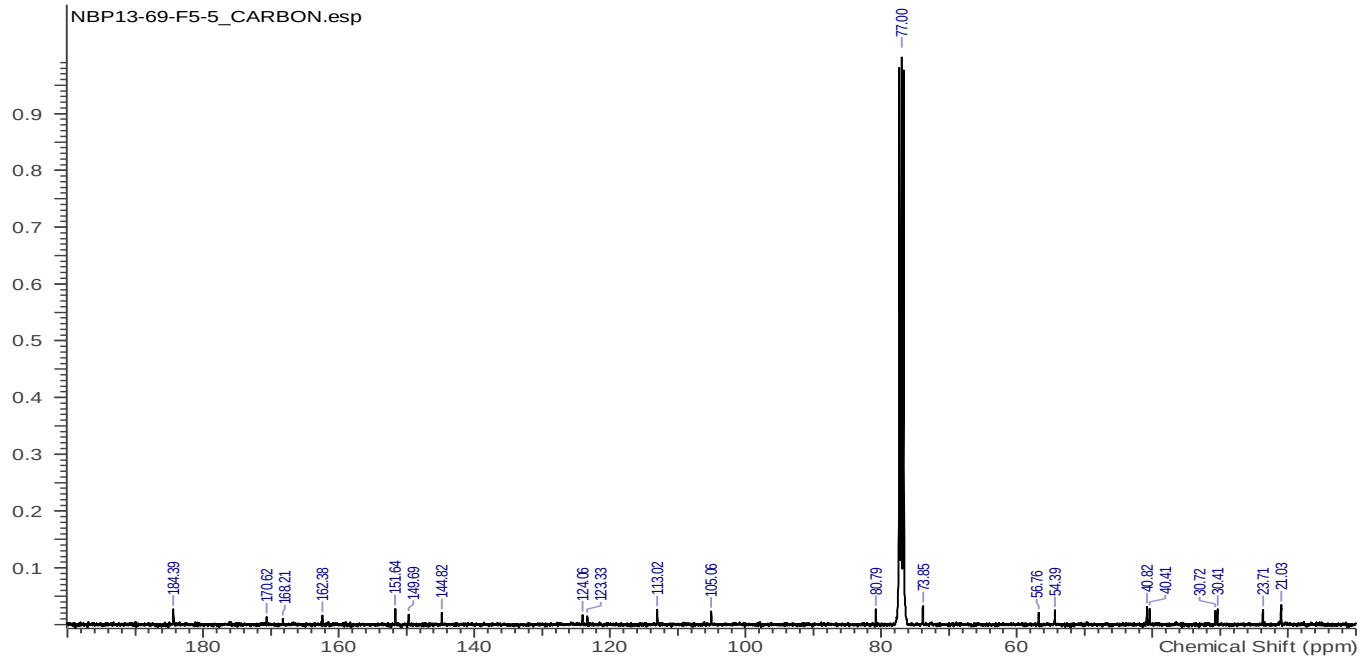

Figure Cxiv. ^{13}C NMR spectrum of keikipukalide C (**4.21**) in $CDCl_3$, 100 MHz

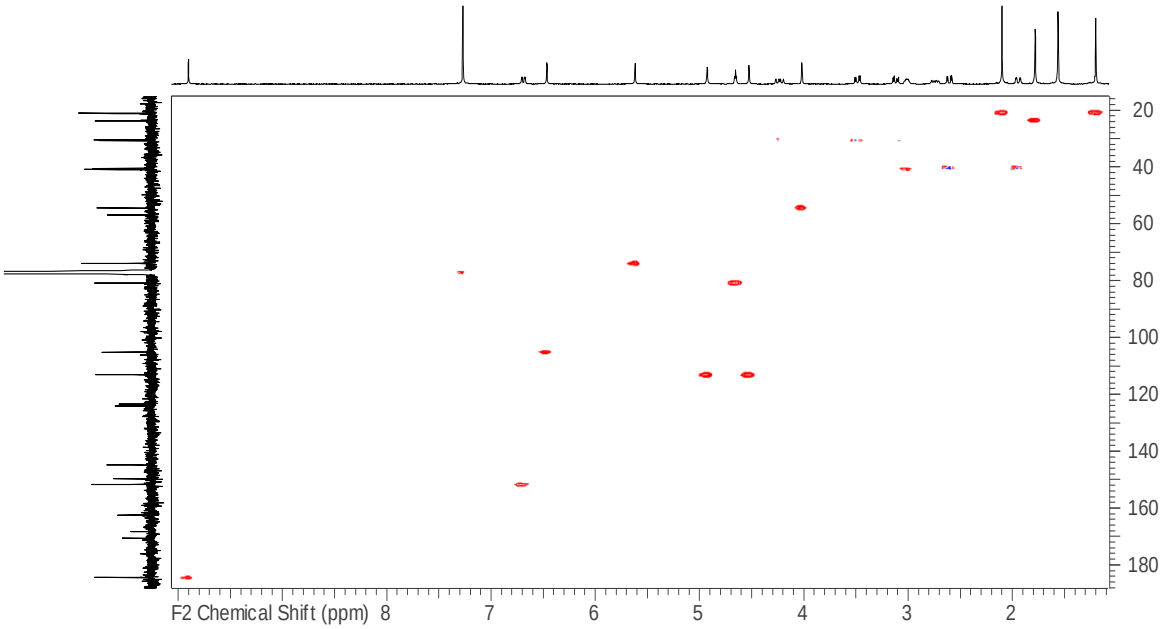

Figure Cxv. gHMQC of keikipukalide C (**4.21**) in $CDCl_3$, 400 MHz

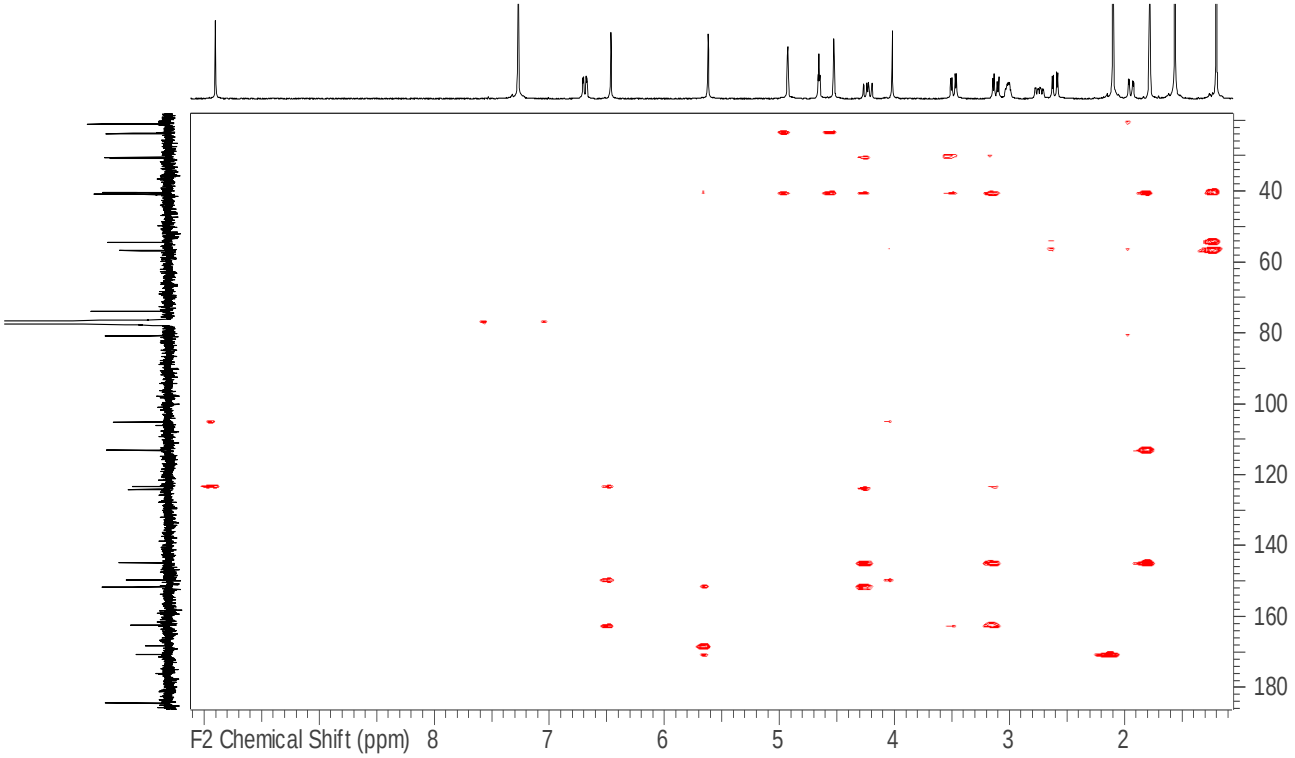

Figure Cxvi. gHMBC of keikipukalide C (**4.21**) in $CDCl_3$, 400 MHz

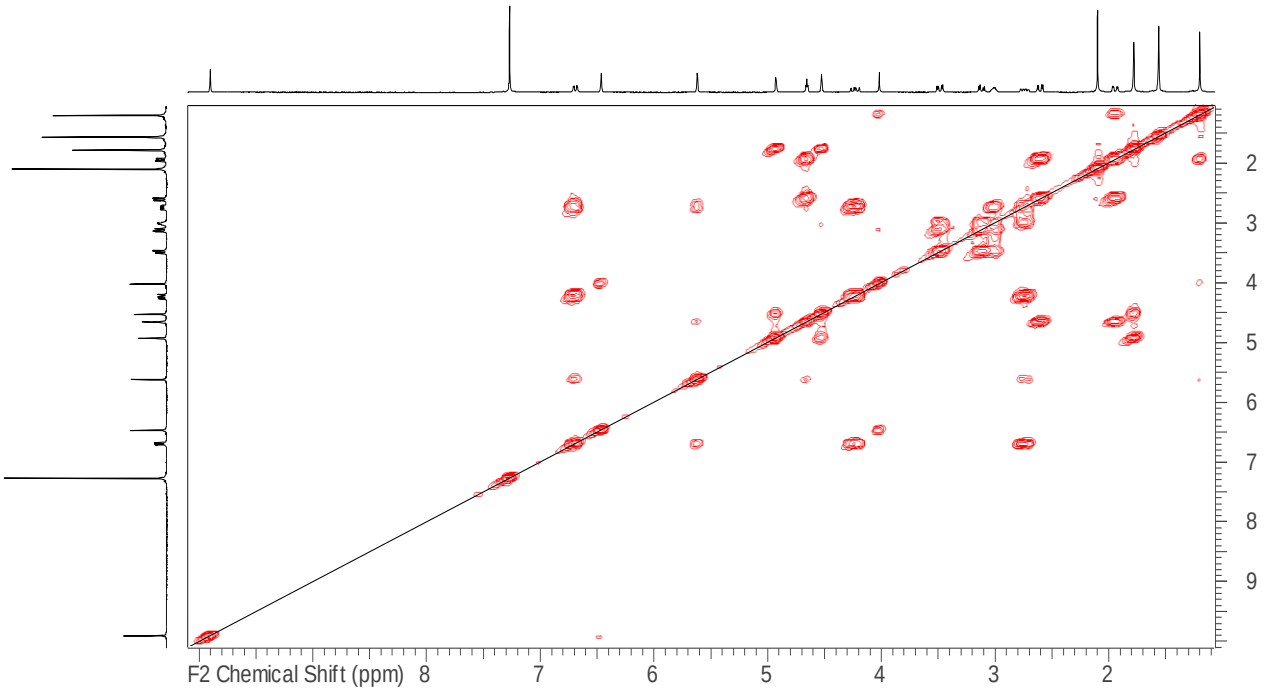

Figure Cxvii. gCOSY of keikipukalide C (**4.21**) in $CDCl_3$, 400 MHz

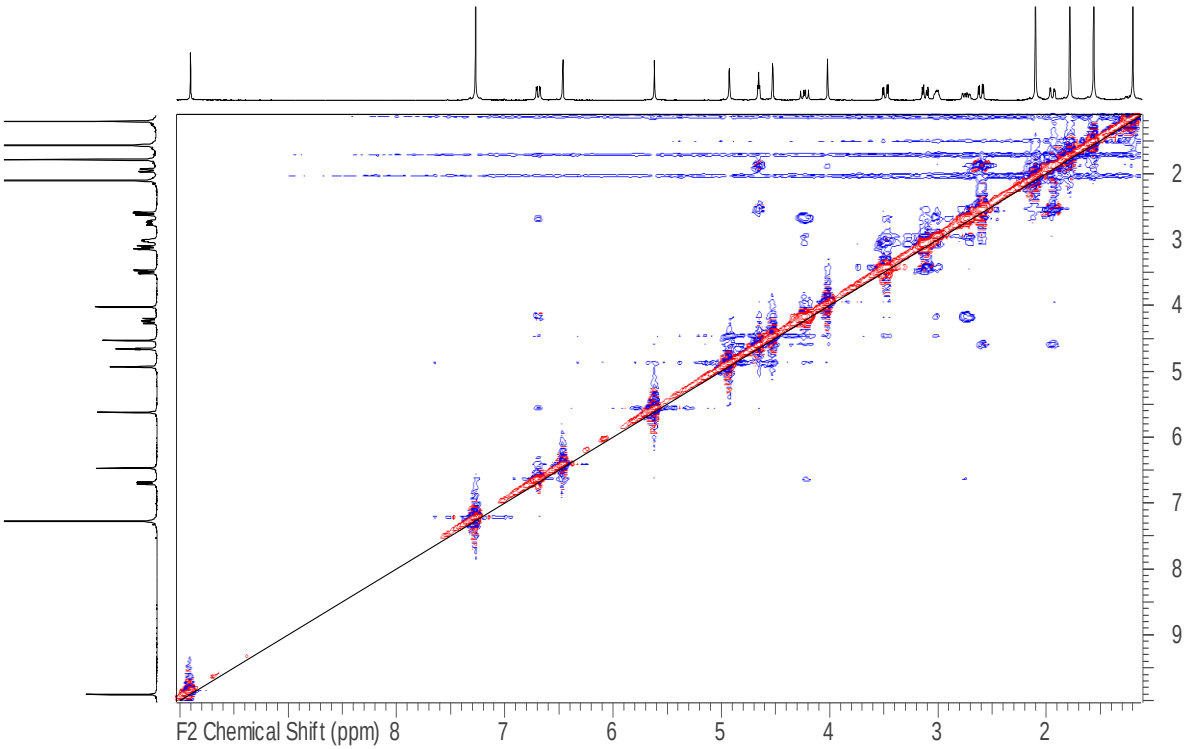

Figure Cxviii. NOESY of keikipukalide C (**4.21**) in $CDCl_3$, 400 MHz

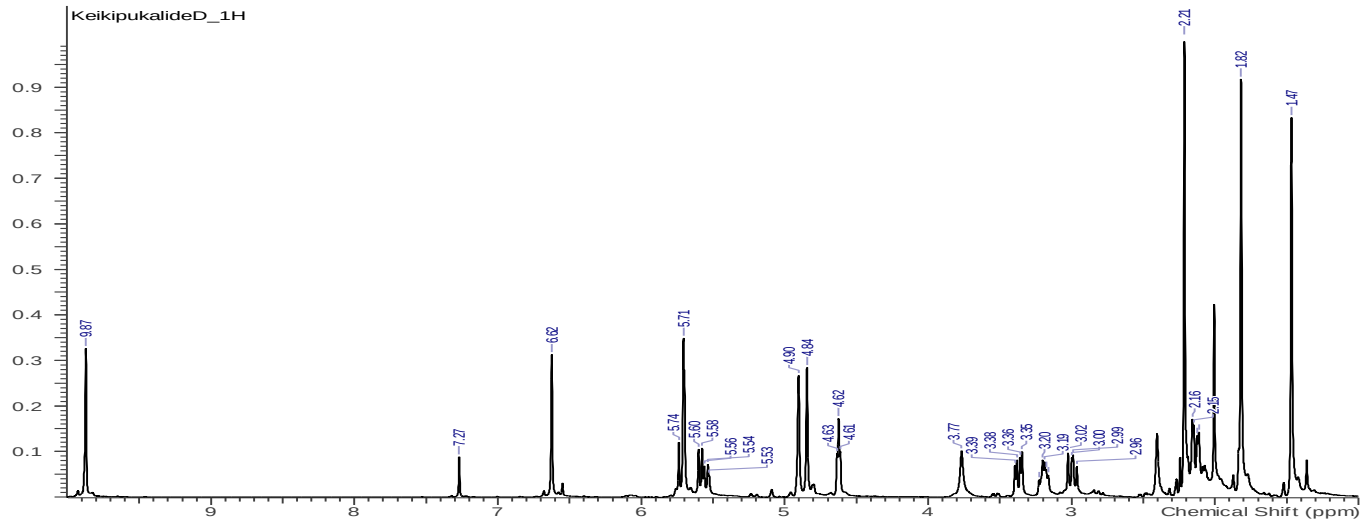

Figure Cxix. ^{1}H NMR spectrum of keikipukalide D (**4.22**) in $CDCl_3$, 400 MHz

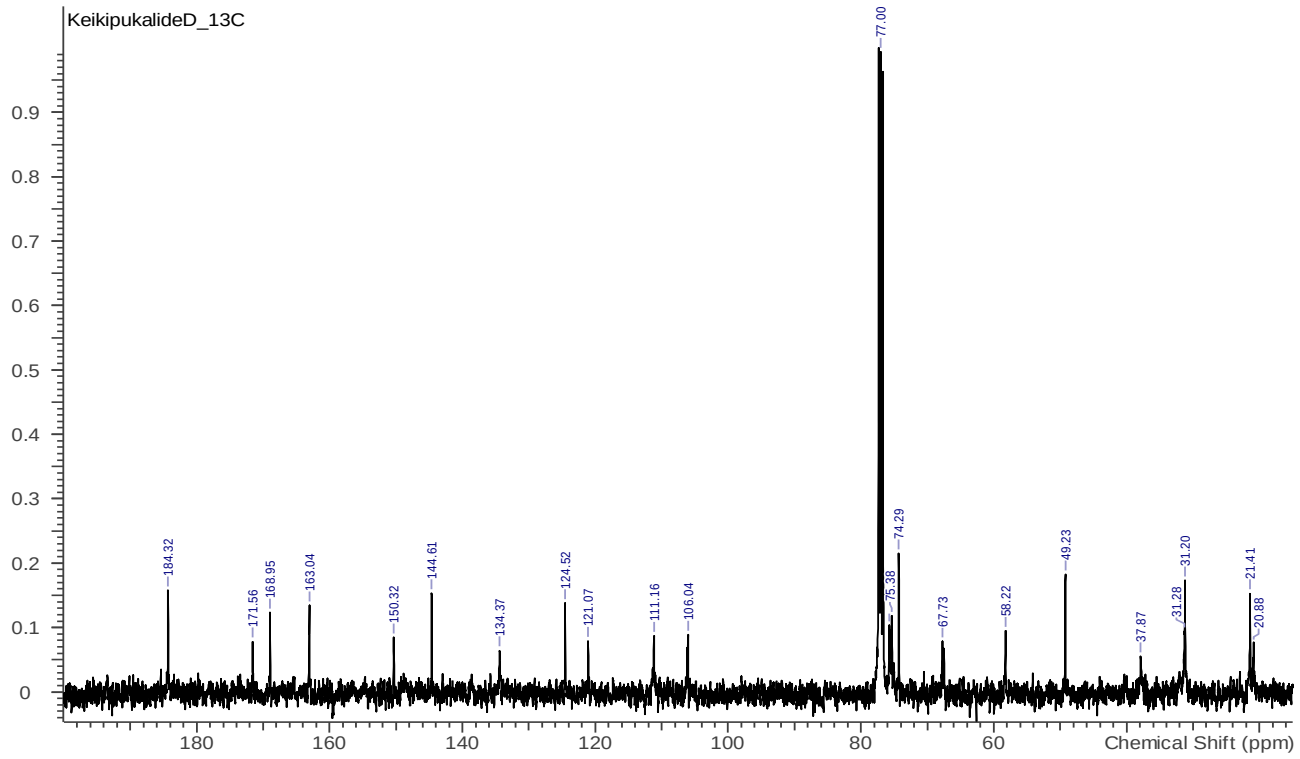

Figure Cxx. ^{13}C NMR spectrum of keikipukalide D (**4.22**) in $CDCl_3$, 100 MHz

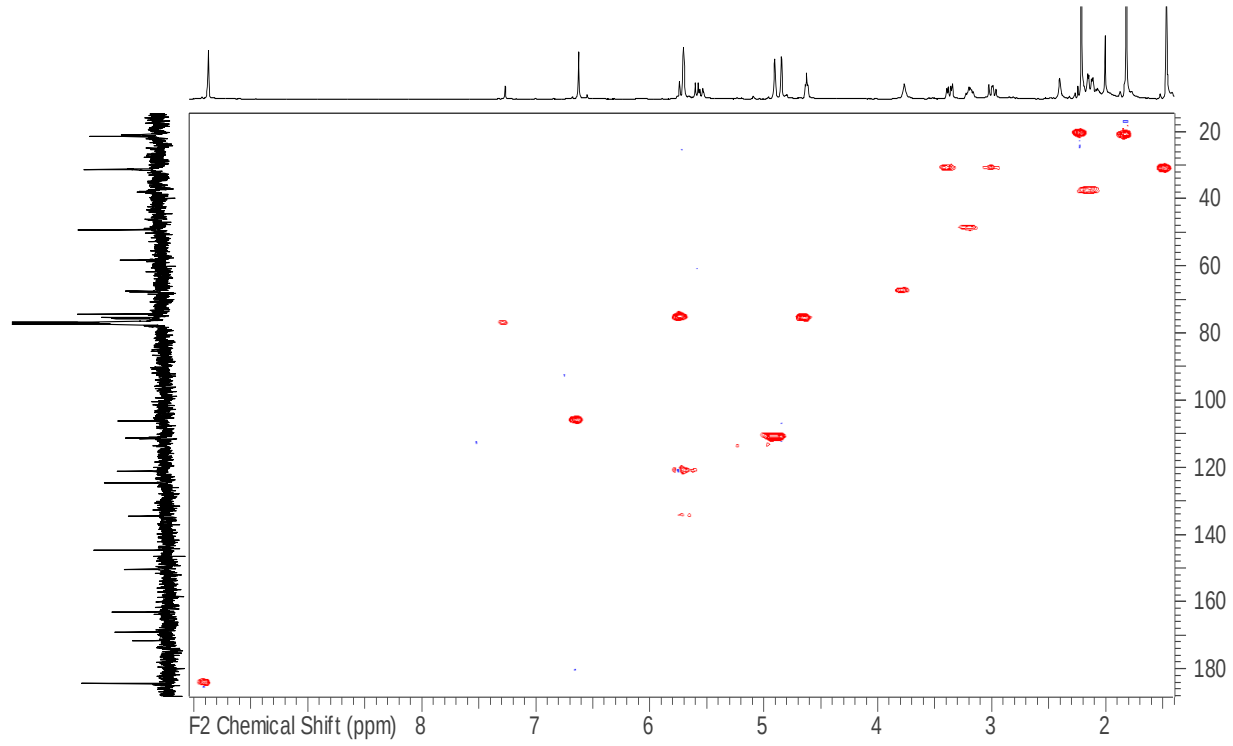

Figure Cxxi. gHMQC of keikipukalide D (**4.22**) in $CDCl_3$, 400 MHz

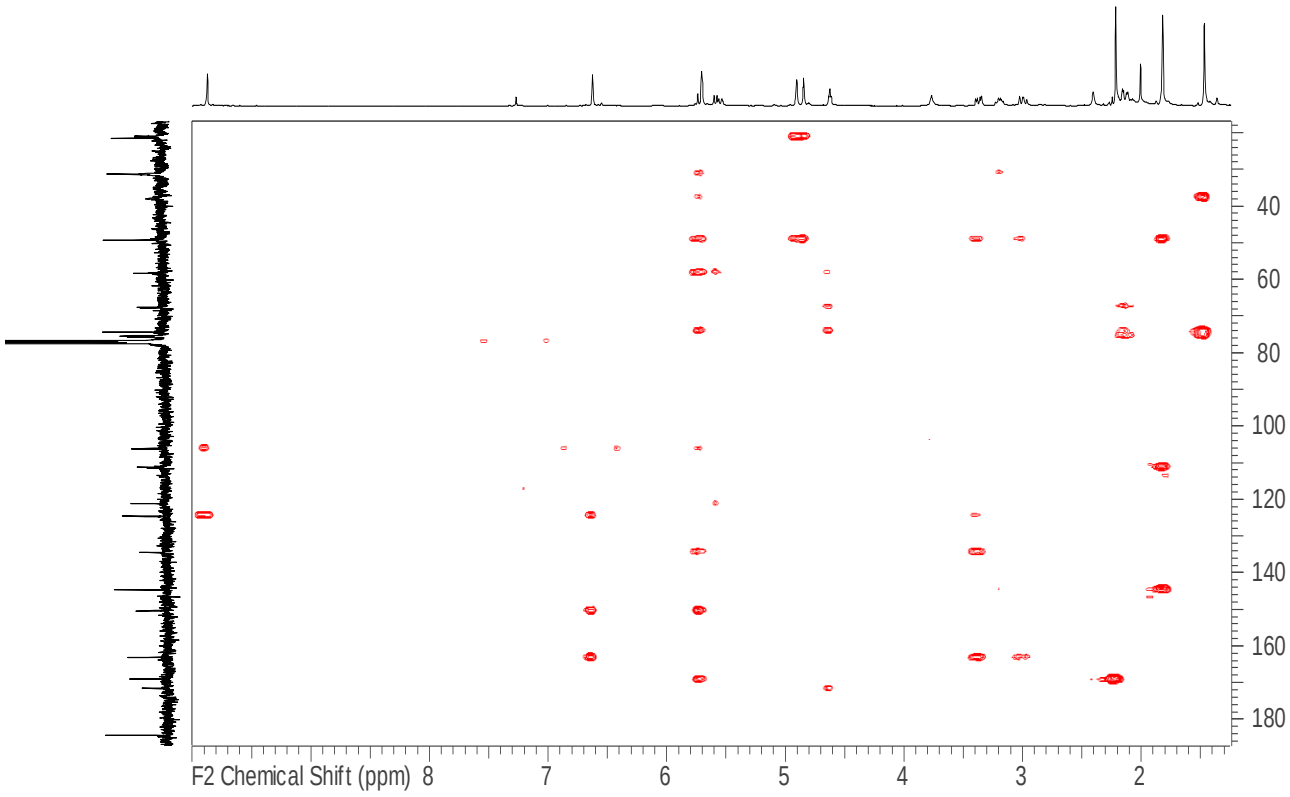

Figure Cxxii. gHMBC of keikipukalide D (**4.22**) in $CDCl_3$, 400 MHz

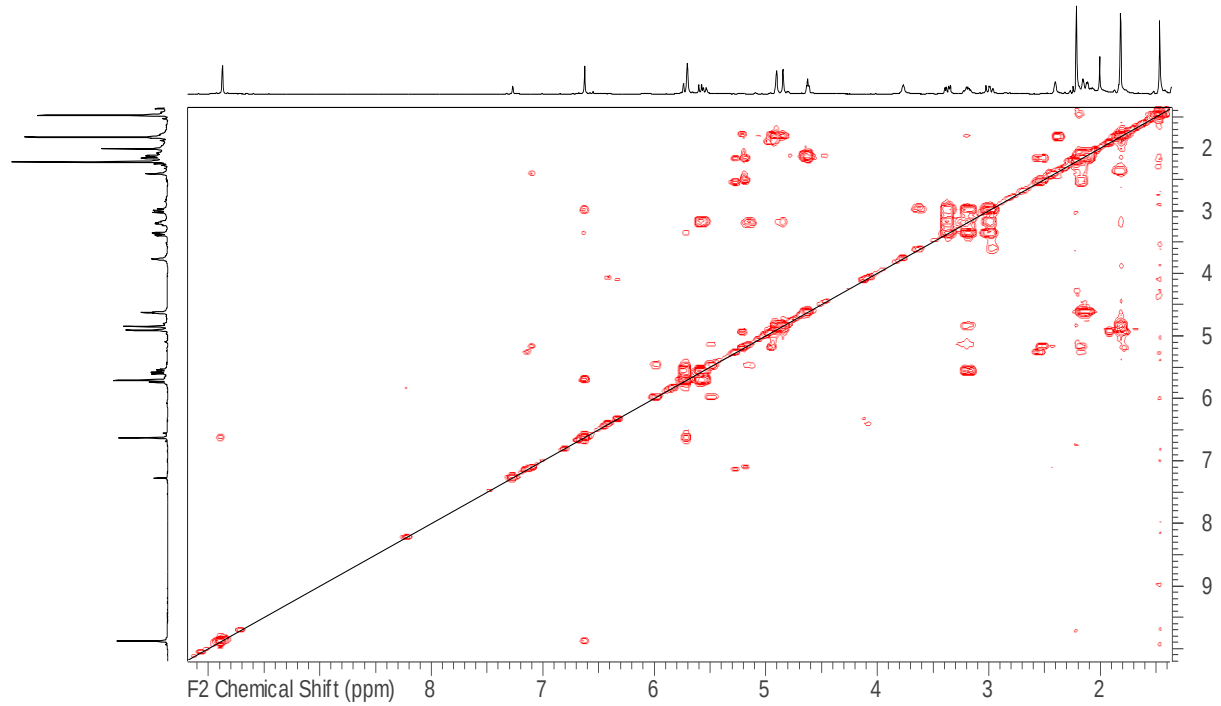

Figure Cxxiii. gCOSY of keikipukalide D (**4.22**) in $CDCl_3$, 500 MHz

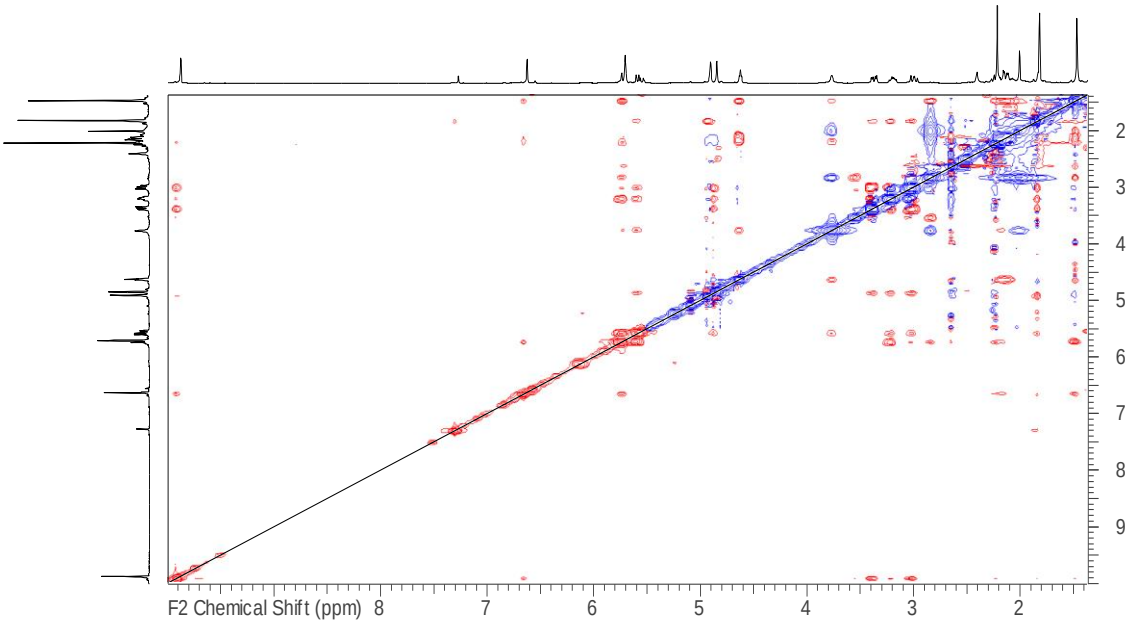

Figure Cxxiv. NOESY of keikipukalide D (**4.22**) in $CDCl_3$, 500 MHz

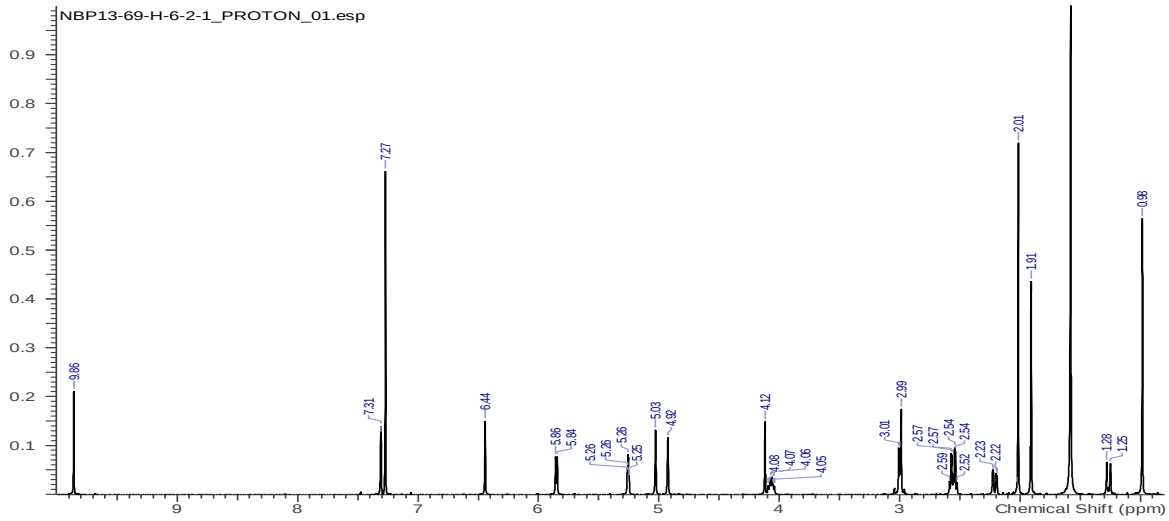

Figure Cxv. ^{1}H NMR spectrum of keikipukalide E (**4.23**) in $CDCl_3$, 500 MHz; 1.58 ppm is the water signal.

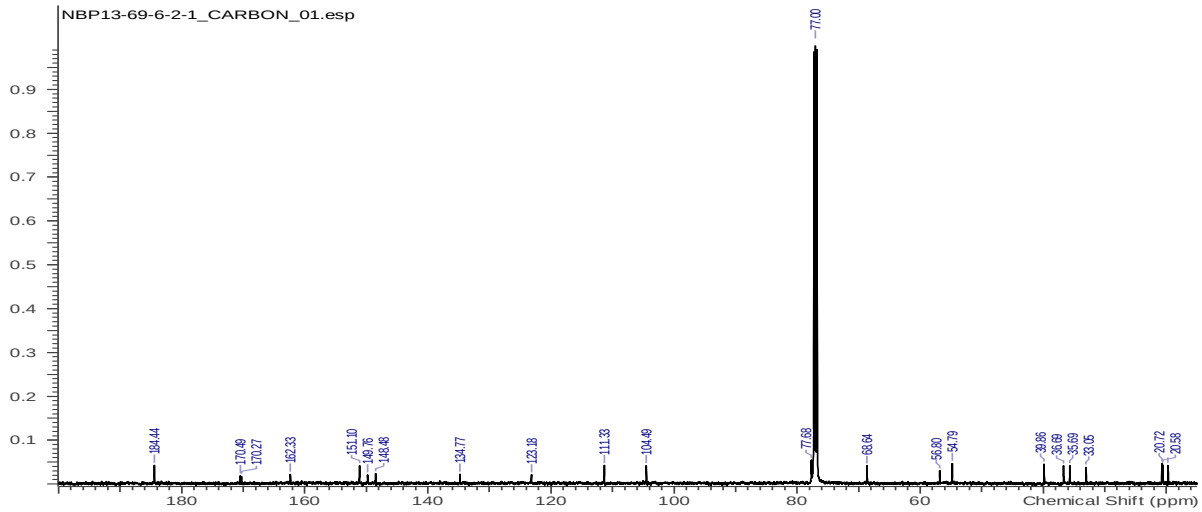

Figure Cxxvi. ^{13}C NMR spectrum of keikipukalide E (**4.23**) in $CDCl_3$, 125 MHz

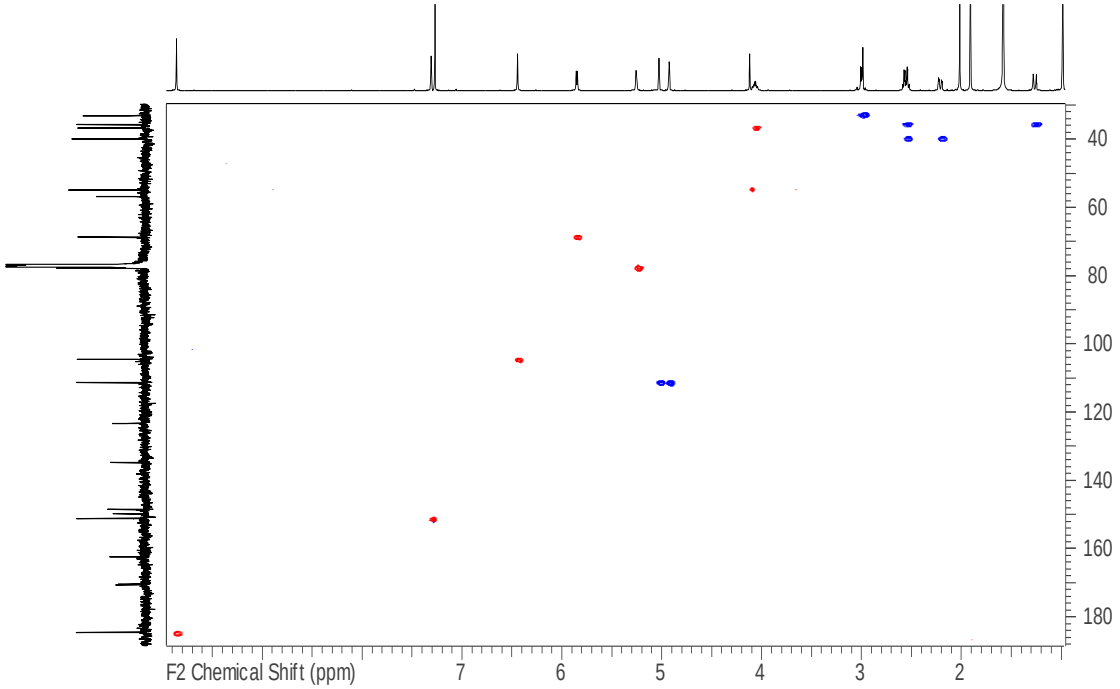

Figure Cxxvii. gHSQC of keikipukalide E (**4.23**) in $CDCl_3$, 600 MHz

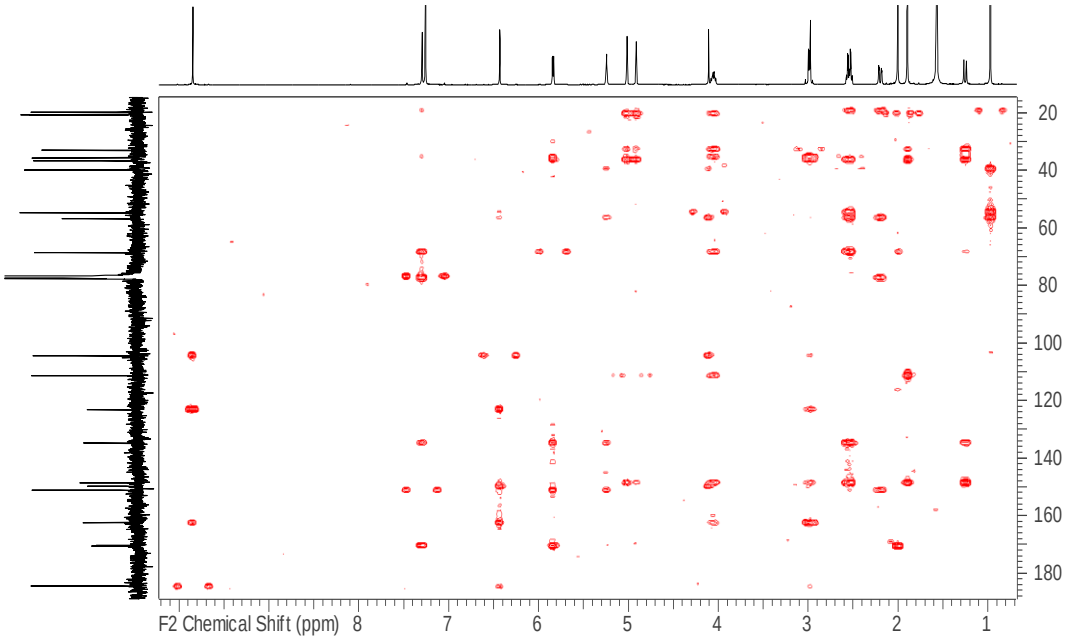

Figure Cxxviii. gHMBC of keikipukalide E (**4.23**) in $CDCl_3$, 500 MHz

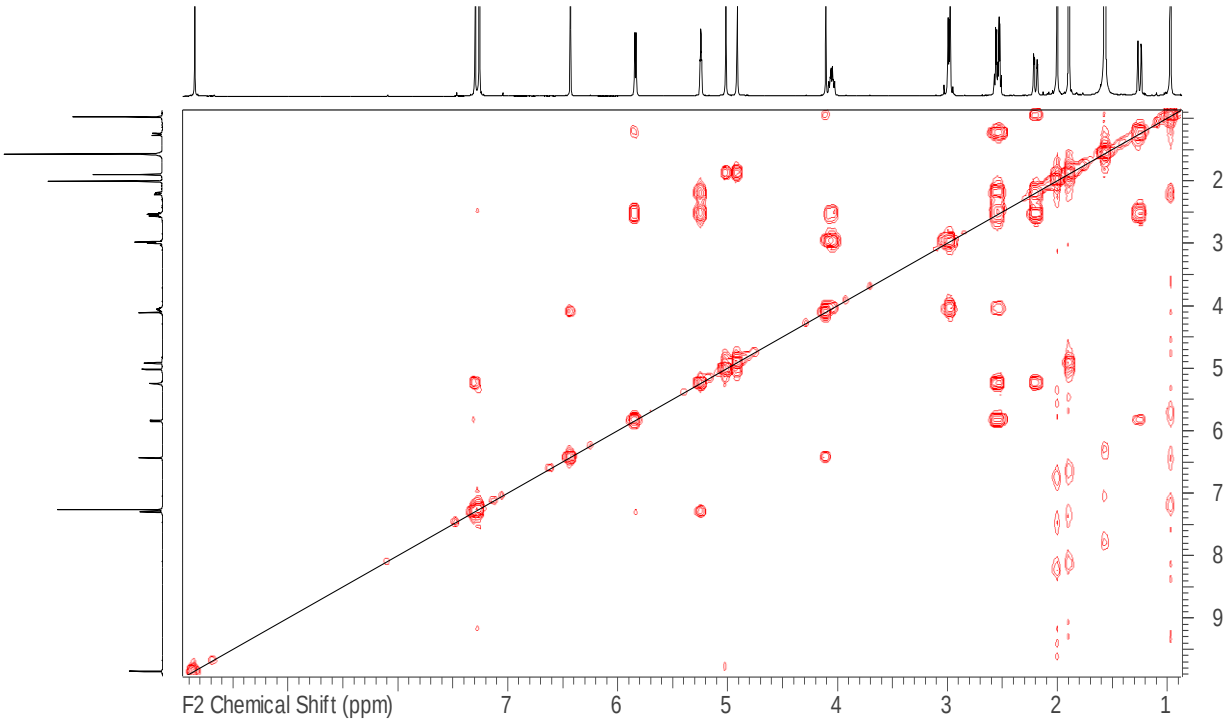

Figure Cxxix. gCOSY of keikipukalide E (**4.23**) in $CDCl_3$, 500 MHz

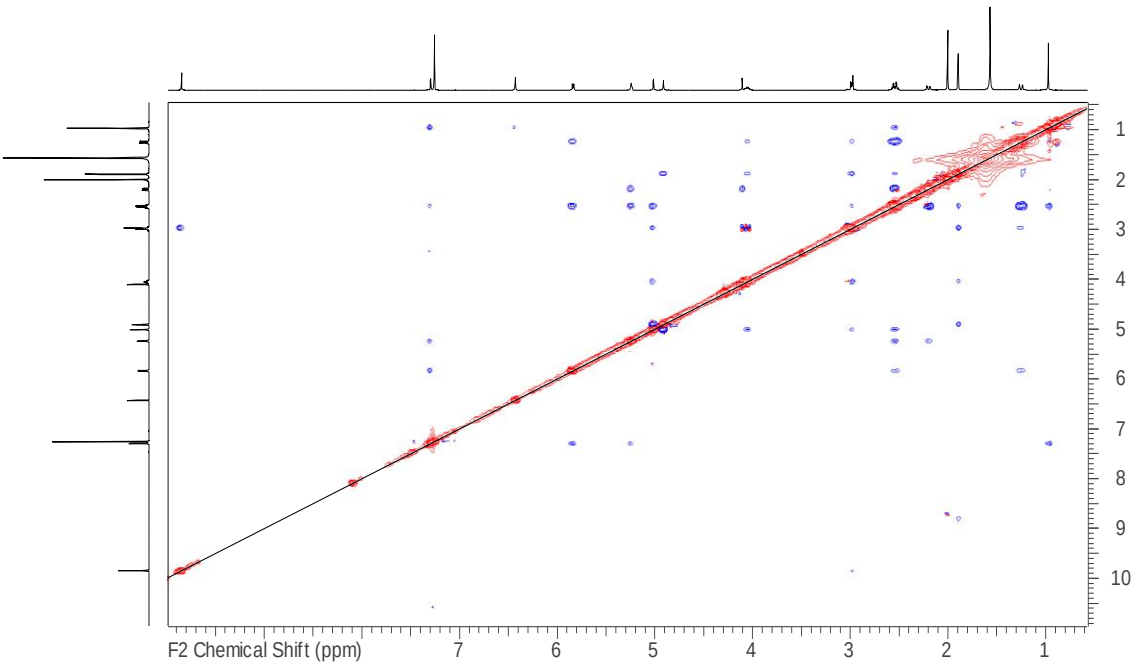

Figure Cxxx. NOESY of keikipukalide E (**4.23**) in $CDCl_3$, 500 MHz

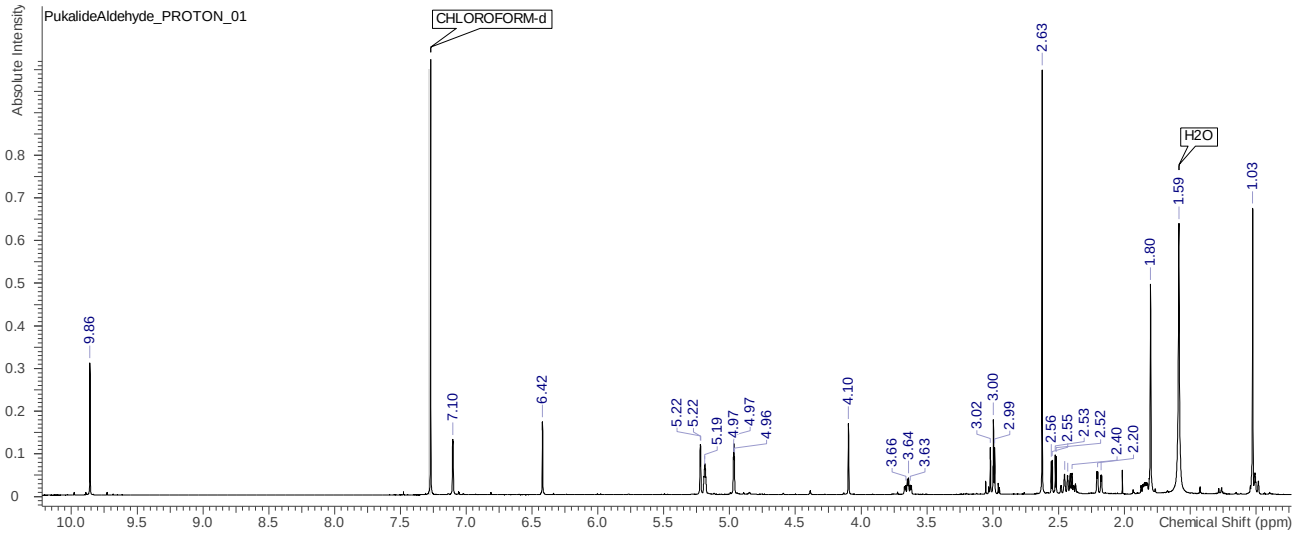

Figure Cxxxi ^{1}H NMR spectrum of pukalide aldehyde (**4.24**) in $CDCl_3$, 500 MHz

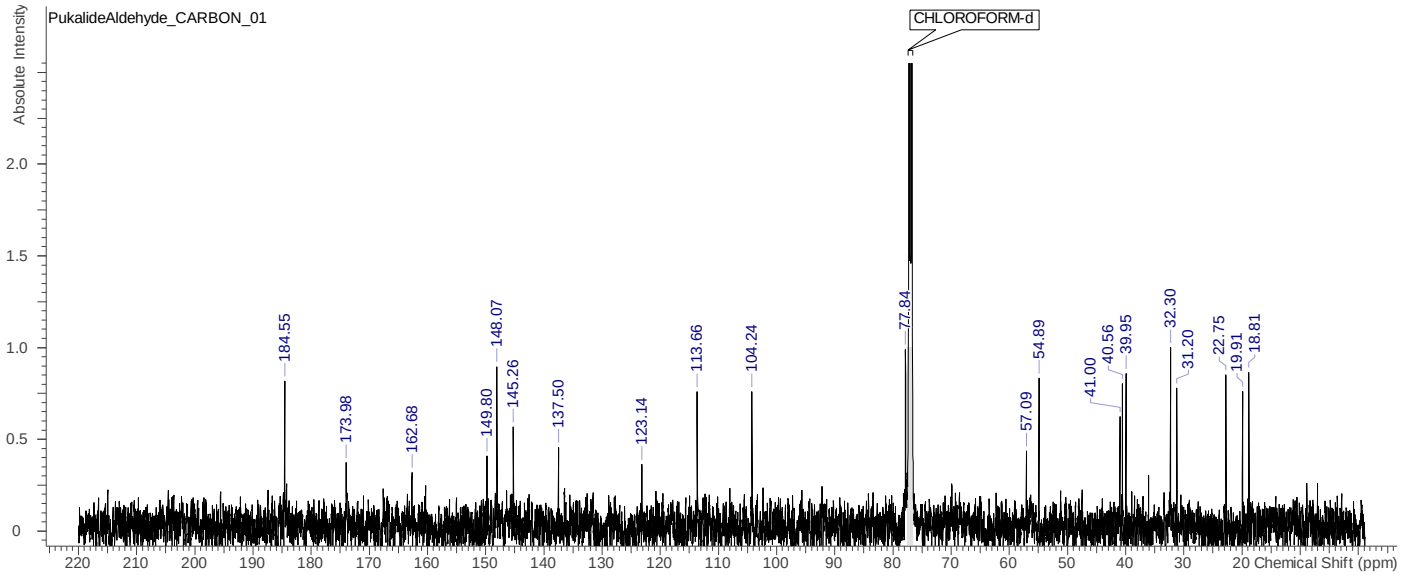

Figure Cxxxii^{13}C NMR spectrum of pukalide aldehyde (**4.24**) in $CDCl_3$, 125 MHz

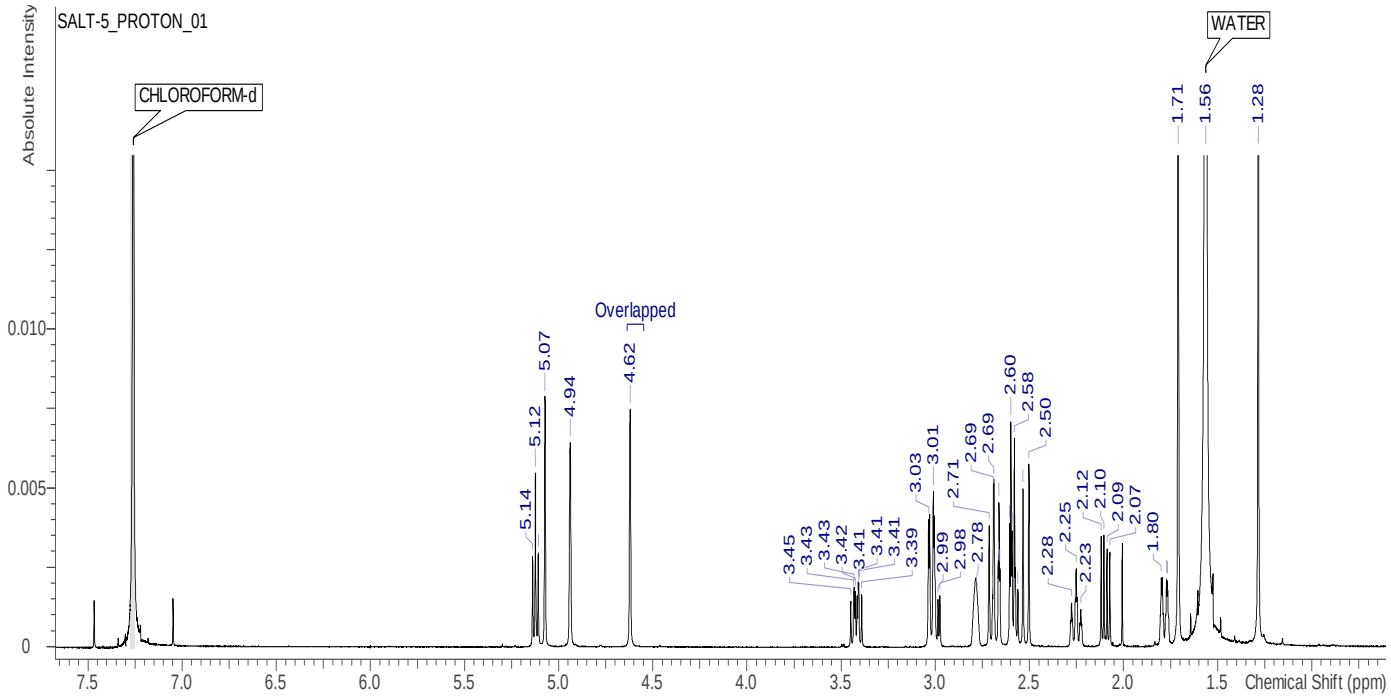

Figure C33^{1}H NMR spectrum of ineleganolide (**4.26**) in $CDCl_3$, 500 MHz

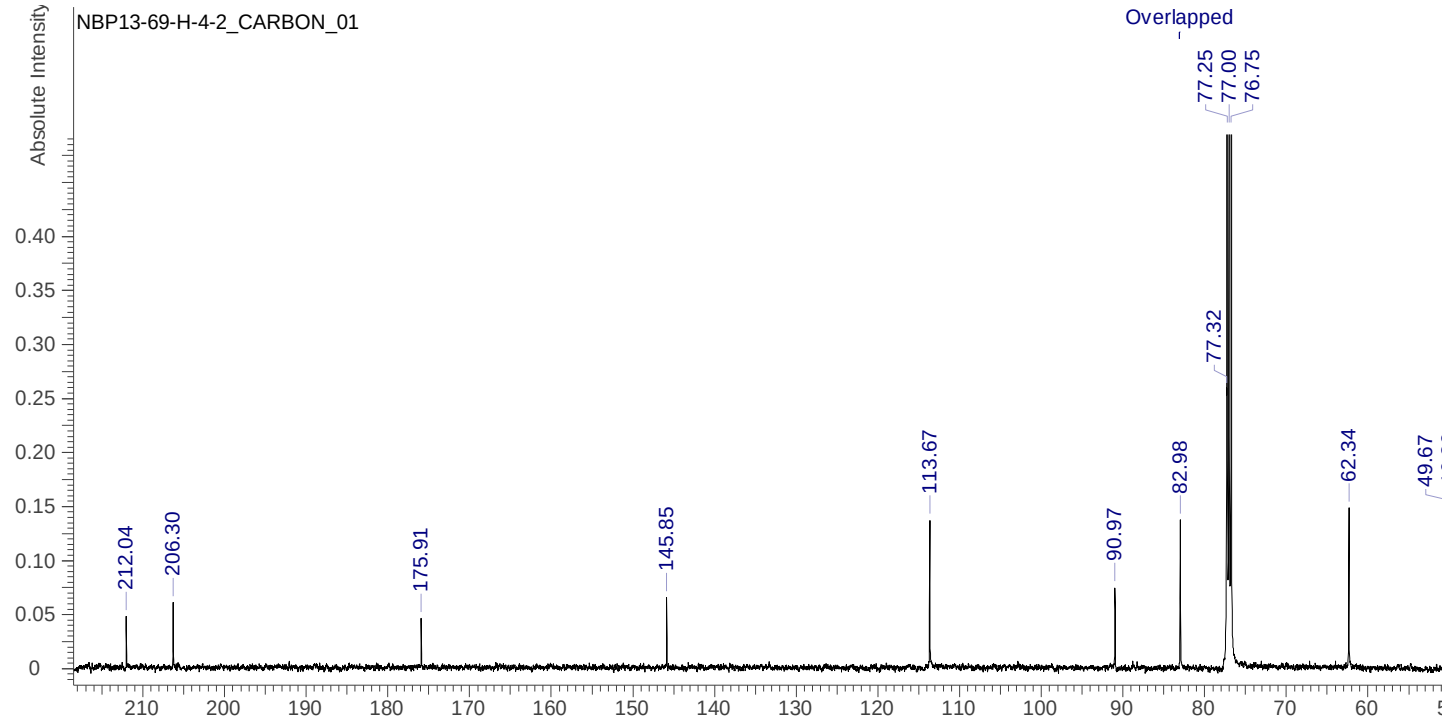

Figure Cxxxiv. ^{13}C NMR spectrum of ineleganolide (**4.26**) in $CDCl_3$, 125 MHz

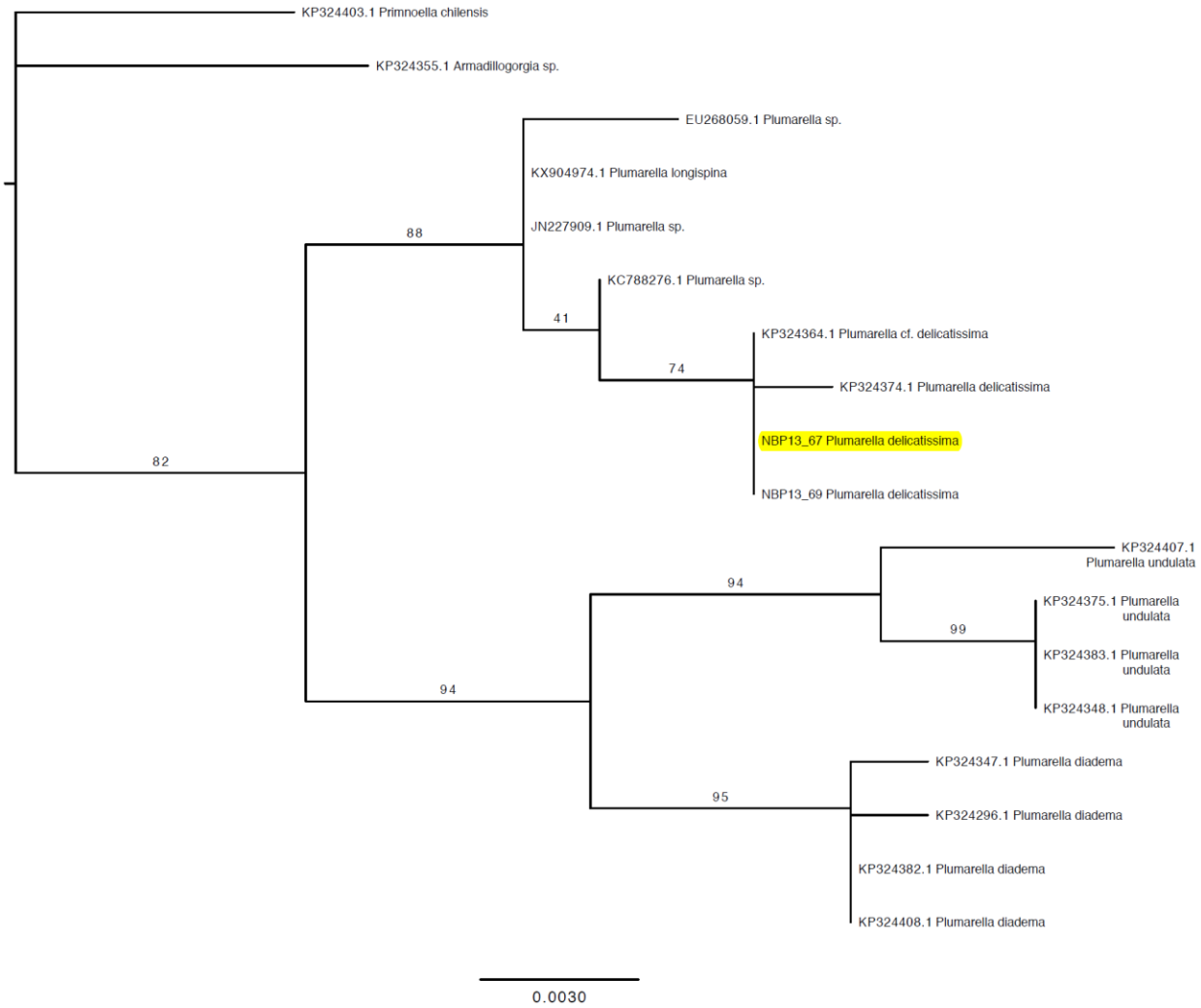

Figure Cxxxv. Maximum Likelihood tree topology comparing our *Plumarella* msh1 sequences with those available on Genbank

X-ray Crystallography Experimental

The X-ray diffraction data for keikipukalide A (**4.18**) and keikipukalide E (**4.22**) were measured on Bruker D8 Venture PHOTON 100 CMOS system equipped with a Cu K_α INCOATEC ImuS micro-focus source (λ = 1.54178 Å). Data integration and reduction were performed using SaintPlus 6.01 [2]. Absorption correction was performed by multi-scan method implemented in SADABS [3]. Space groups were determined using XPREP implemented in APEX3 [1]. Structures were solved using SHELXT and refined using SHELXL-2014 [4-7] (full-matrix least-squares on F^2) through OLEX2 interface program [8]. All non-hydrogen atoms were refined anisotropically. Hydrogen atoms of -CH,-CH_2 and -CH_3 groups were placed in geometrically calculated positions and were included in the refinement process using riding model with isotropic thermal parameters: Uiso(H) = 1.2(1.5)Ueq(-CH,-CH_2, (-CH_3)). The absolute configuration for each compound, has been established based on Flack parameter value and verified additionally with Bijvoet-Pair Analysis and Bayesian Statistics Methods [9,10] (Tables S2 and S4). P2 ≈ 1 for all cases and is the probability that the current model is correct assuming two possibilities – one out of two enantiomers present. Crystal data and refinement conditions are shown in Tables S1 and S3.

[1] Bruker (2016). *APEX3* (Version 2015.9). Bruker AXS Inc., Madison, Wisconsin, USA.
[2] Bruker (2016) SAINT V8.35A. Data Reduction Software.
[3] Sheldrick, G. M. (1996). *SADABS. Program for Empirical Absorption Correction.* University of Gottingen, Germany.
[4] G.M. Sheldrick (2015) "Crystal structure refinement with SHELXL", Acta Cryst., C71, 3-8
[5] Sheldrick, G.M. (1990) Acta Cryst. A46, 467-473
[6] Sheldrick, G. M. (2008) Acta Cryst. A64, 112-122.
[7] Sheldrick, G. M. (2015) Acta Cryst. A71, 3-8
[8] Dolomanov, O.V.; Bourhis, L.J.; Gildea, R.J.; Howard, J.A.K.; Puschmann, H., OLEX2: A complete structure solution, refinement and analysis program (2009). J. Appl. Cryst., 42, 339-341.
[9] A.L.Spek, Acta Cryst. 2009, D65, 148-155.
[10] R. W. W. Hooft, L. H. Straver , A. L. Spek J. Appl. Cryst. (2008), 41, 96-103

Table C1. Crystal data and structure refinement for keikipukalide A .	
Identification code	JAX_F2_3
Empirical formula	$C_{20}H_{20}O_6$
Formula weight	356.36
Temperature/K	100.0
Crystal system	orthorhombic
Space group	$P2_12_12_1$
a/Å	6.74700(10)
b/Å	13.2449(3)
c/Å	18.8700(4)
α/°	90
β/°	90
γ/°	90
Volume/Å^3	1686.29(6)
Z	4
ρ_{calc}g/cm^3	1.404
μ/mm^{-1}	0.862
F(000)	752.0
Crystal size/mm^3	0.14 × 0.07 × 0.02
Radiation	CuKα (λ = 1.54178)
2Θ range for data collection/°	8.156 to 154.438
Index ranges	-8 ≤ h ≤ 8, -15 ≤ k ≤ 16, -23 ≤ l ≤ 23
Reflections collected	25739
Independent reflections	3552 [R_{int} = 0.0710, R_{sigma} = 0.0356]
Data/restraints/parameters	3552/0/249
Goodness-of-fit on F^2	1.048
Final R indexes [I>=2σ (I)]	R_1 = 0.0352, wR_2 = 0.0698
Final R indexes [all data]	R_1 = 0.0433, wR_2 = 0.0731
Largest diff. peak/hole / e Å^{-3}	0.19/-0.18
Flack parameter	0.17(10)

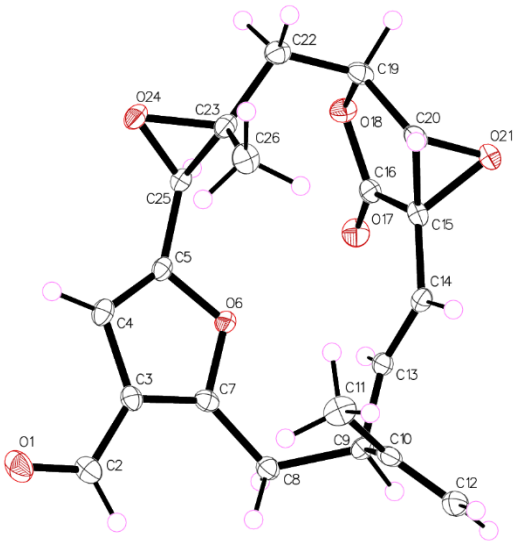

Figure Cxxxvi. Asymmetric unit of keikipukalide A (**4.18**). Anisotropic displacement parameters were drawn at 50% probability

Table C2. Results Bijvoet-Pair Analysis and Bayesian Statistics for keikipukalide A	
Space Group P212121	Student-T Prob. Plot
Wavelength 1.54178	Sample Size. 1478
Flack x .... 0.17(10)	Corr. Coeff. 0.999
Parsons z .. 0.20(10)	Intercept .. 0.016
	Slope 0.890
Bijvoet Pairs 1488	
Coverage ... 99	Bayesian Statistics
DiffCalcMax. 33.52	Student_T Nu 100
Outlier Crit 67.04	Select Pairs 1488
Scatter Plot	Theta_Min .. 7.73
Sigma Crit.. 0.25	Theta_Max .. 76.85
Select Pairs 106	**P2(true).... 1.000**
Number Plus 69	P3(true).... 0.981
Number Minus 37	P3(rac-twin) 0.019
Slope 0.902	P3(false) .. 0.4E-17
	G 0.6231
	G (su) 0.1761
	Hooft y ... 0.19(9)

Table C3. Crystal data and structure refinement for keikipukalide E	
Identification code	NBP13_69_H_6_3
Empirical formula	$C_{22}H_{24}O_7$
Formula weight	400.41
Temperature/K	100
Crystal system	orthorhombic
Space group	$P2_12_12_1$
a/Å	8.7671(2)
b/Å	11.4162(3)
c/Å	19.4875(4)
α/°	90
β/°	90
γ/°	90
Volume/Å^3	1950.44(8)
Z	4
ρ_{calc}g/cm^3	1.364
μ/mm^{-1}	0.845
F(000)	848.0
Crystal size/mm^3	0.31 × 0.116 × 0.03
Radiation	CuKα (λ = 1.54178)
2Θ range for data collection/°	8.978 to 154.788
Index ranges	-11 ≤ h ≤ 10, -14 ≤ k ≤ 14, -24 ≤ l ≤ 24
Reflections collected	29803
Independent reflections	4102 [R_{int} = 0.0664, R_{sigma} = 0.0323]
Data/restraints/parameters	4102/0/273
Goodness-of-fit on F^2	1.031
Final R indexes [I>=2σ (I)]	R_1 = 0.0344, wR_2 = 0.0782
Final R indexes [all data]	R_1 = 0.0401, wR_2 = 0.0812
Largest diff. peak/hole / e Å^{-3}	0.19/-0.18
Flack parameter	0.02(8)

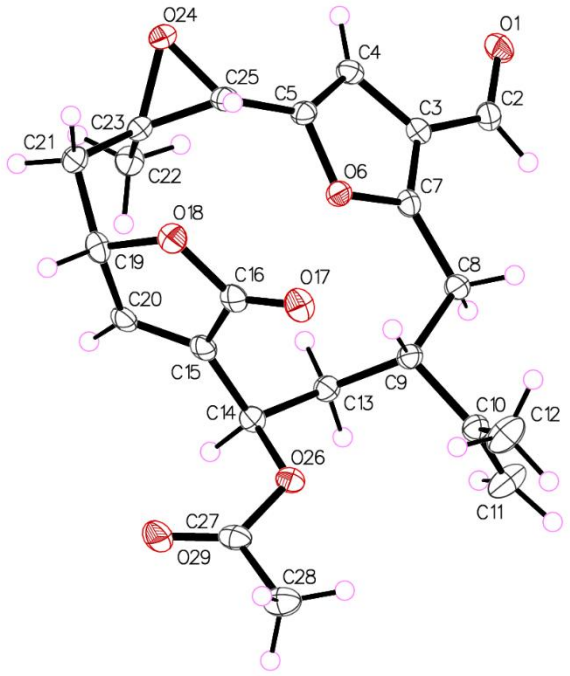

Figure Cxxxvii. Asymmetric unit of keikipukalide E (**4.23**). Anisotropic displacement parameters were drawn at 50% probability

Table C4. Results Bijvoet-Pair Analysis and Bayesian Statistics for keikipukalide E.	
Space Group P212121 Wavelength 1.54178 Flack x .... 0.02(8) Parsons z .. 0.04(8) Bijvoet Pairs 1744 Coverage ... 98 DiffCalcMax. 38.60 Outlier Crit 77.21 Scatter Plot Sigma Crit.. 0.25 Select Pairs 151 Number Plus 94 Number Minus 57 Slope 1.030	Student-T Prob. Plot Sample Size. 1734 Corr. Coeff. 0.999 Intercept .. -0.029 Slope ..... 0.890 Bayesian Statistics Student_T Nu 100 Select Pairs 1744 Theta_Min .. 6.76 Theta_Max .. 77.26 **P2(true).... 1.000** P3(true).... 1.000 P3(rac-twin) 0.9E-09 P3(false) .. 0.9E-38 G ..... 0.9530 G (su) ..... 0.1473 Hooft y ... 0.02(7)

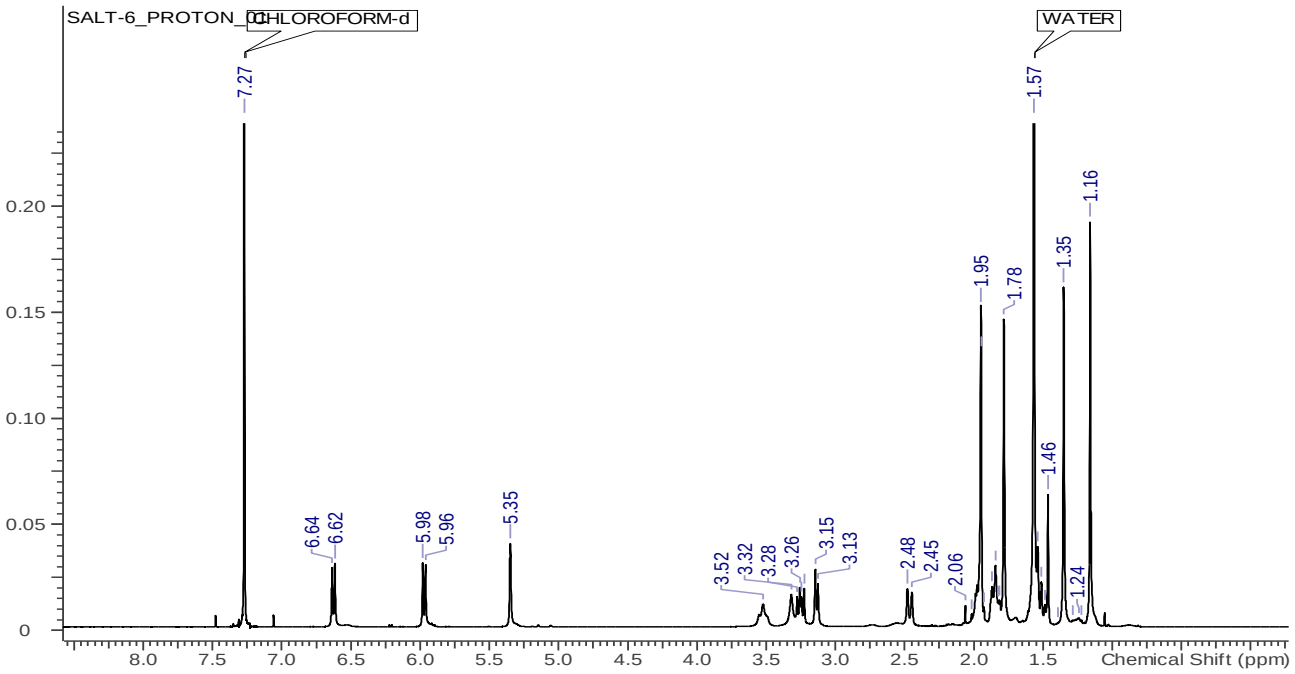

Figure Cxxxviii. ^{1}H NMR spectrum for bathyptilone A (**4.27**) in $CDCl_3$, 500 MHz

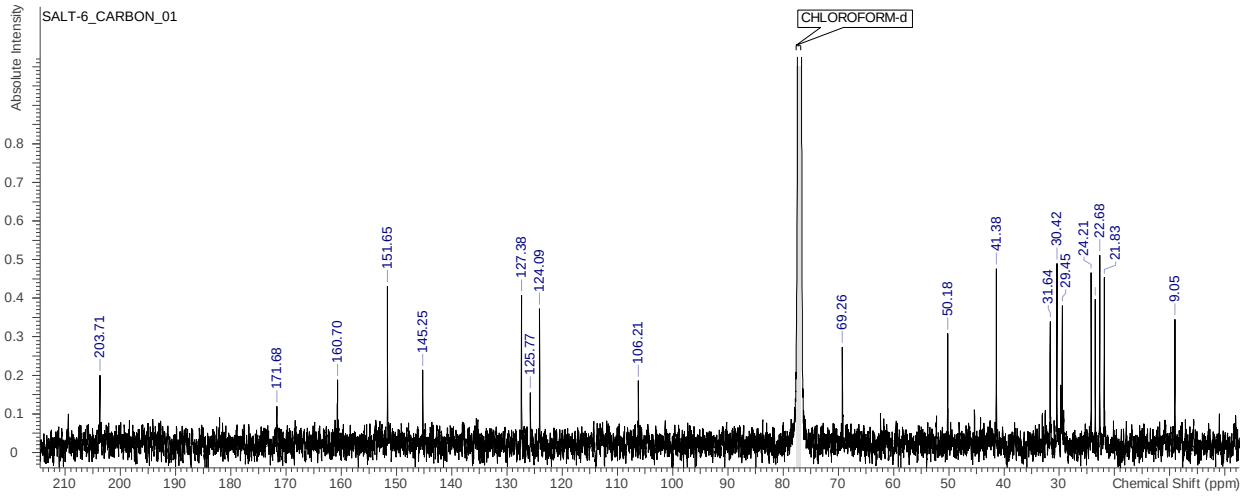

Figure Cxxxix. ^{13}C NMR spectrum for bathyptilone A (**4.27**) in $CDCl_3$, 125 MHz

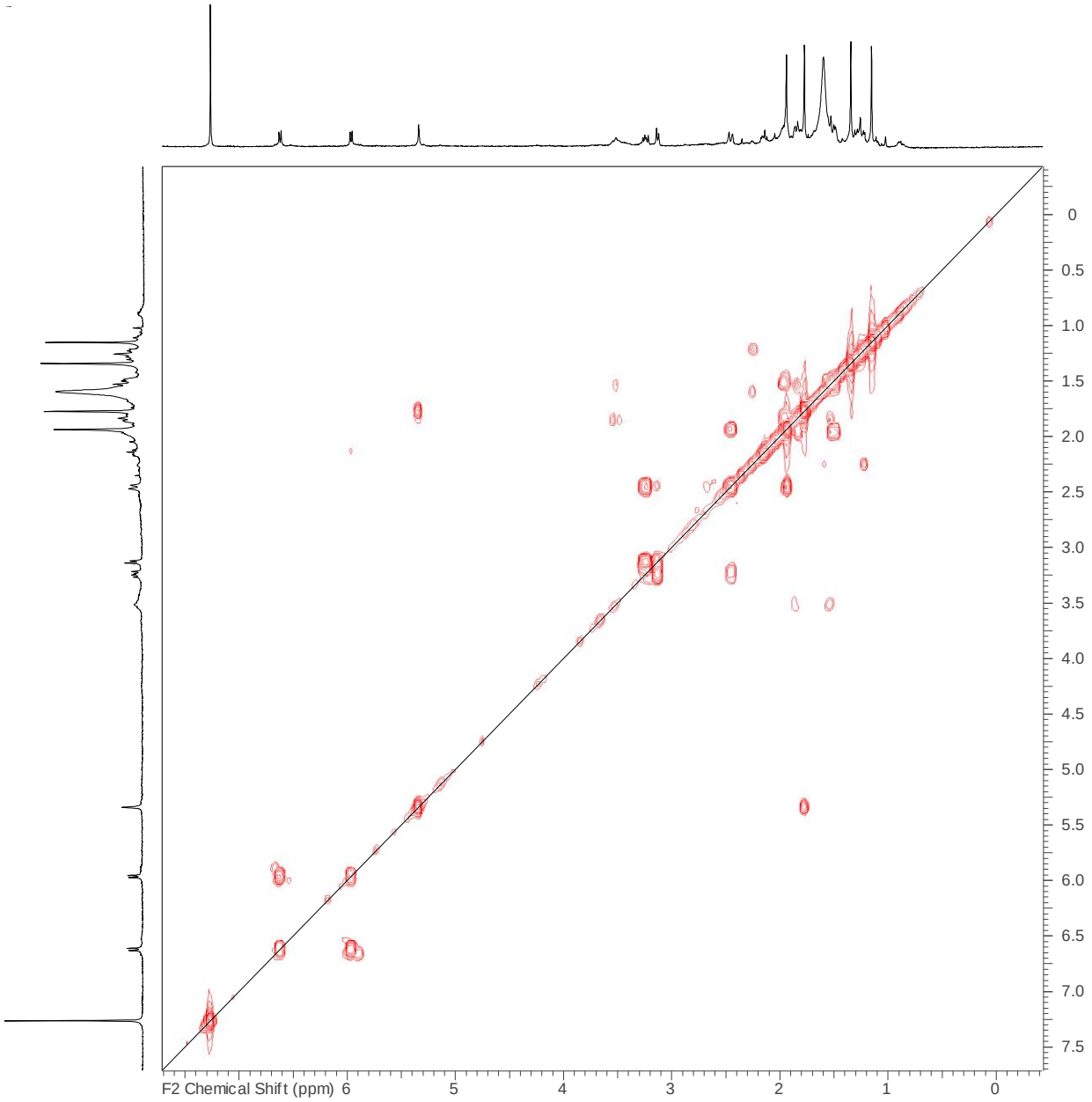

Figure CxI. ^{1}H-^{1}H COSY NMR spectrum for bathyptilone A (**4.27**) in $CDCl_3$, 500 MHz

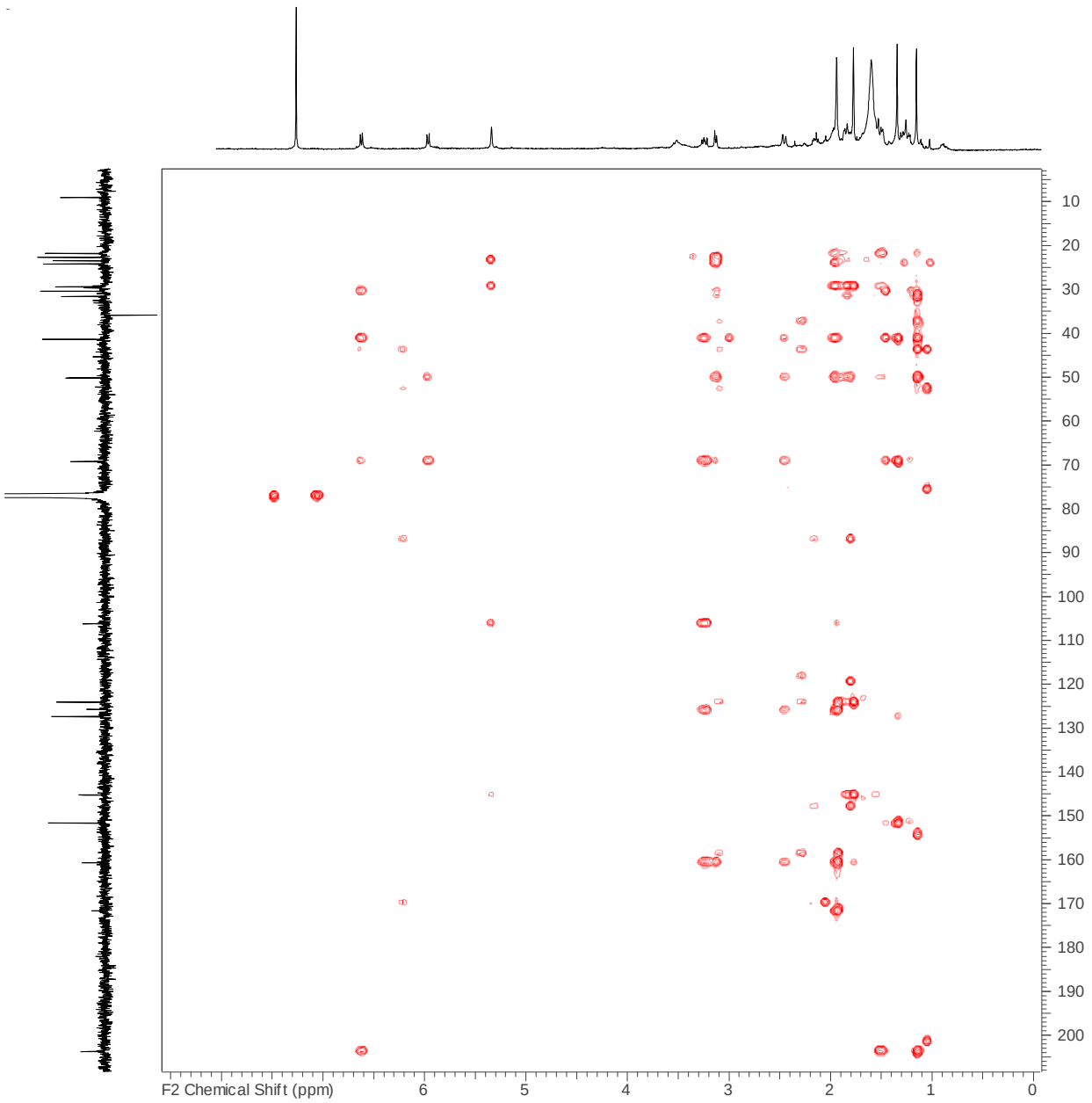

Figure Cxli. gHMBCAD NMR spectrum for bathyptilone A (**4.27**) in $CDCl_3$, 500 MHz

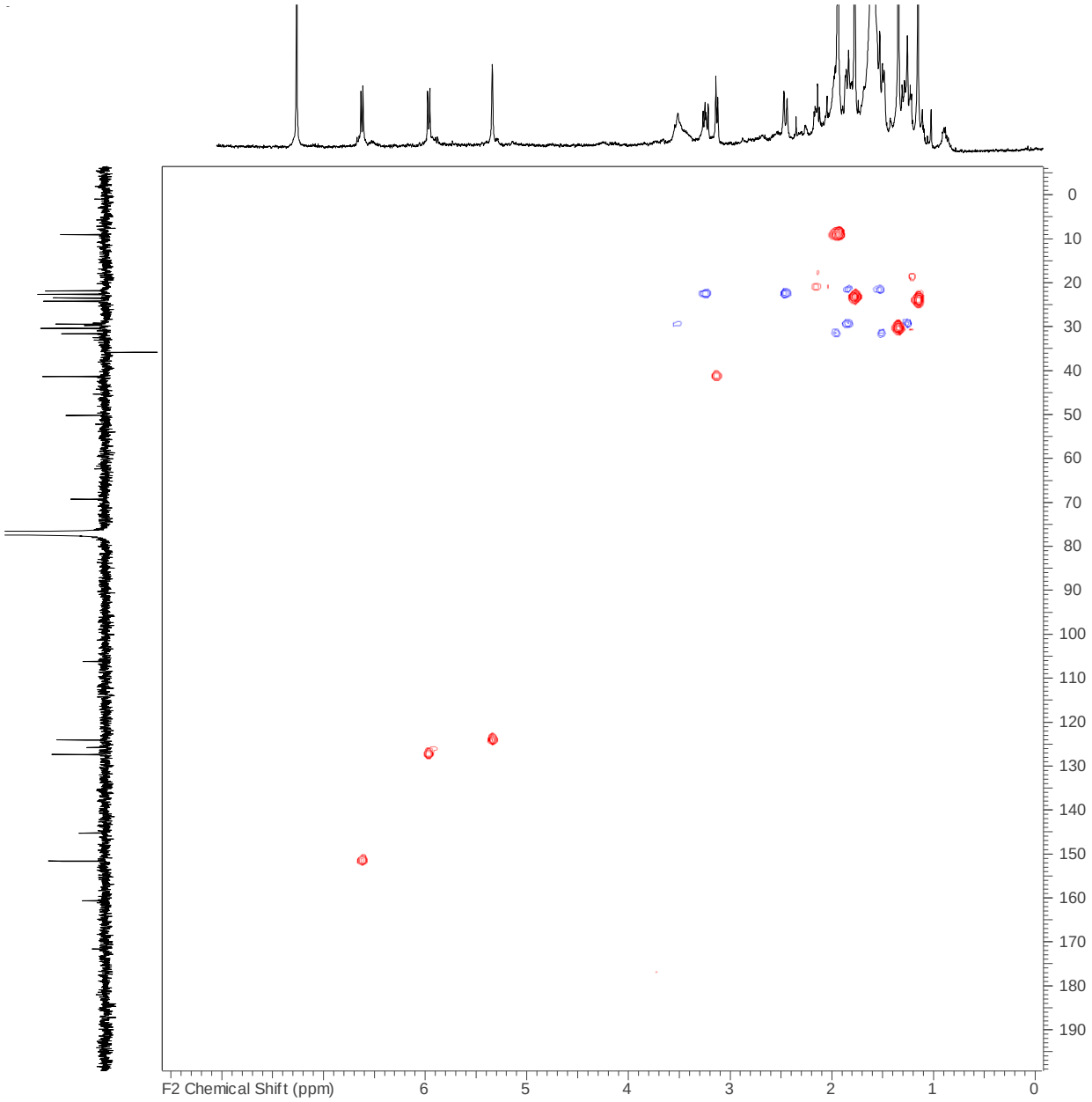

Figure Cxlii. gHSQCAD NMR spectrum for bathyptilone A (**4.27**) in $CDCl_3$, 500 MHz

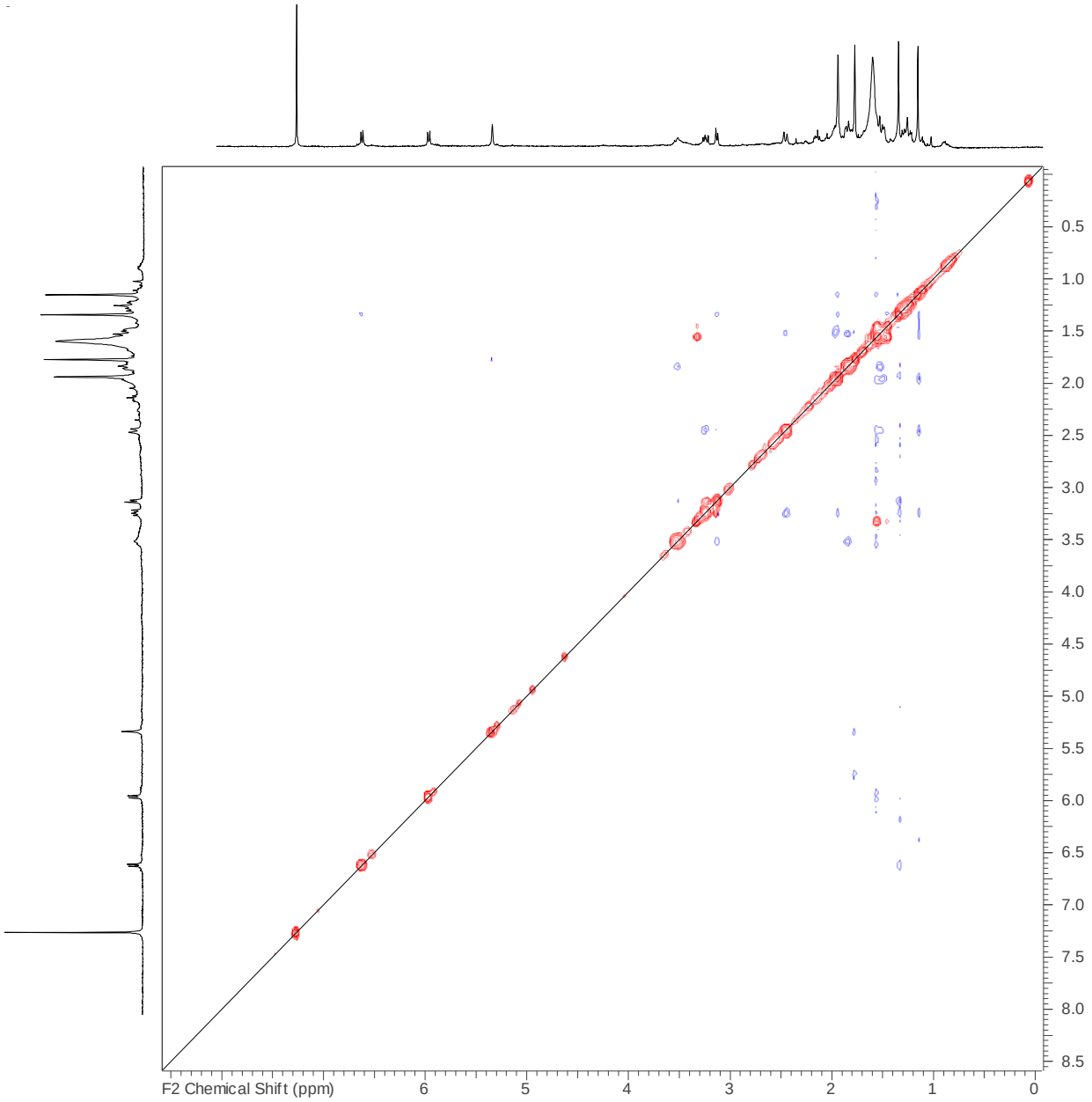

Figure Cxliii. NOESY NMR spectrum for bathyptilone A (**4.27**) in $CDCl_3$, 500 MHz

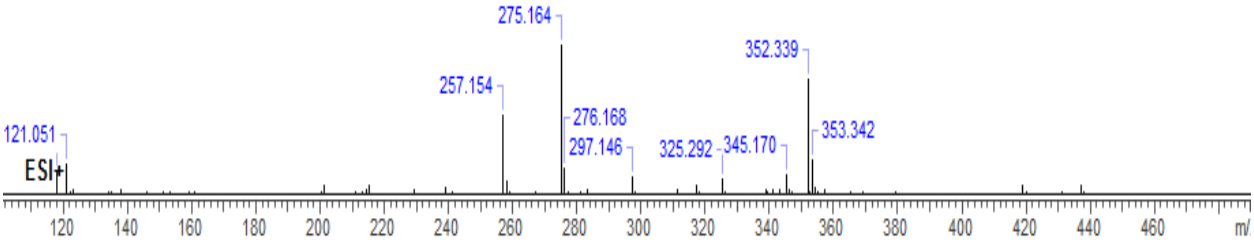

Figure Cxliv. HRESI-MS chromatograph and MS spectrum for bathyptilone A (**4.27**)

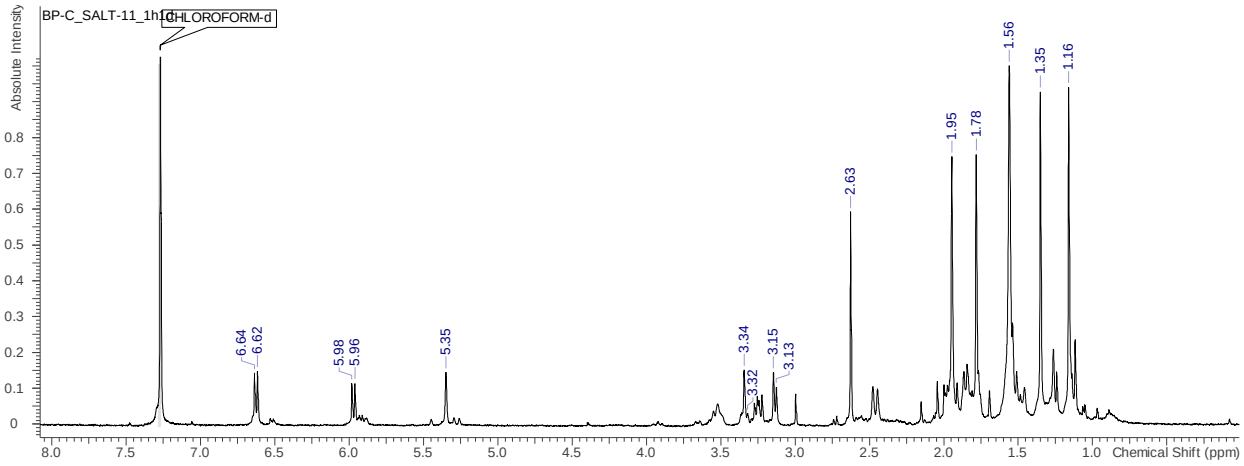

Figure Cxlv ^{1}H NMR spectrum for bathyptilone B (**4.28**) in $CDCl_3$, 500 MHz

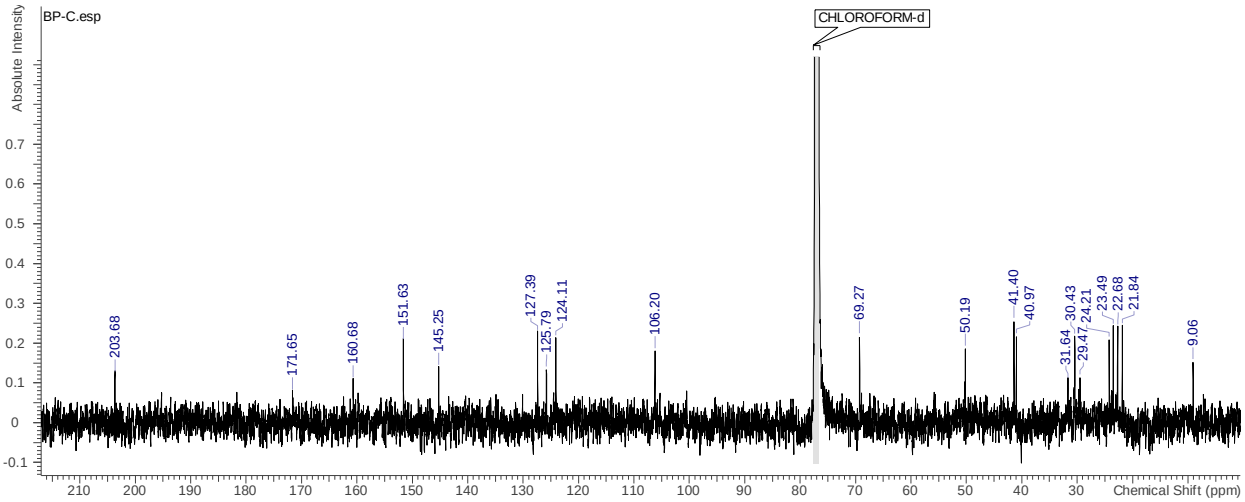

Figure Cxlvi ^{13}C NMR spectrum for bathyptilone B (**4.28**) in $CDCl_3$, 125 MHz

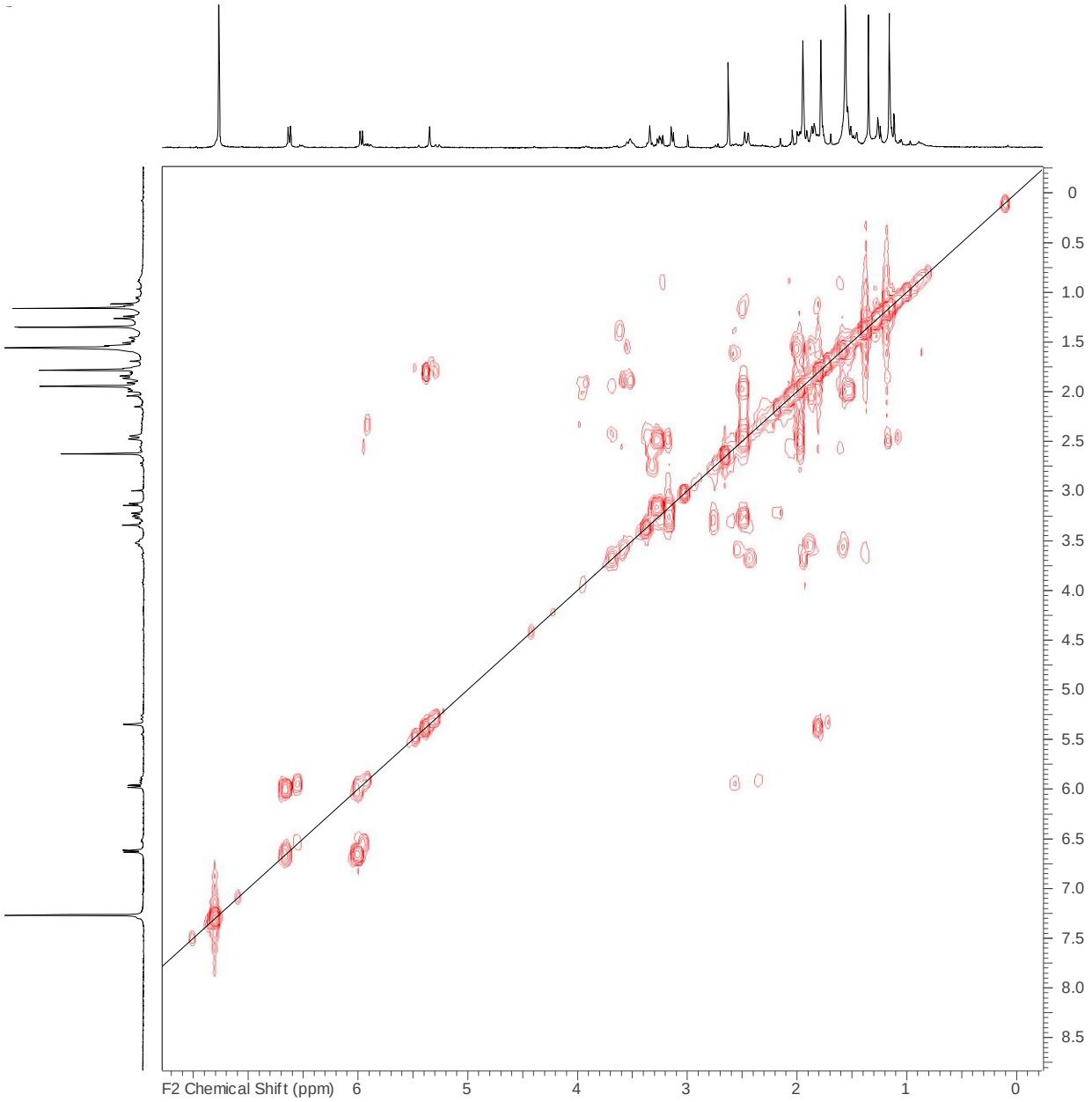

Figure Cxlvii gCOSY NMR spectrum for bathyptilone B (**4.28**) in $CDCl_3$, 500 MHz

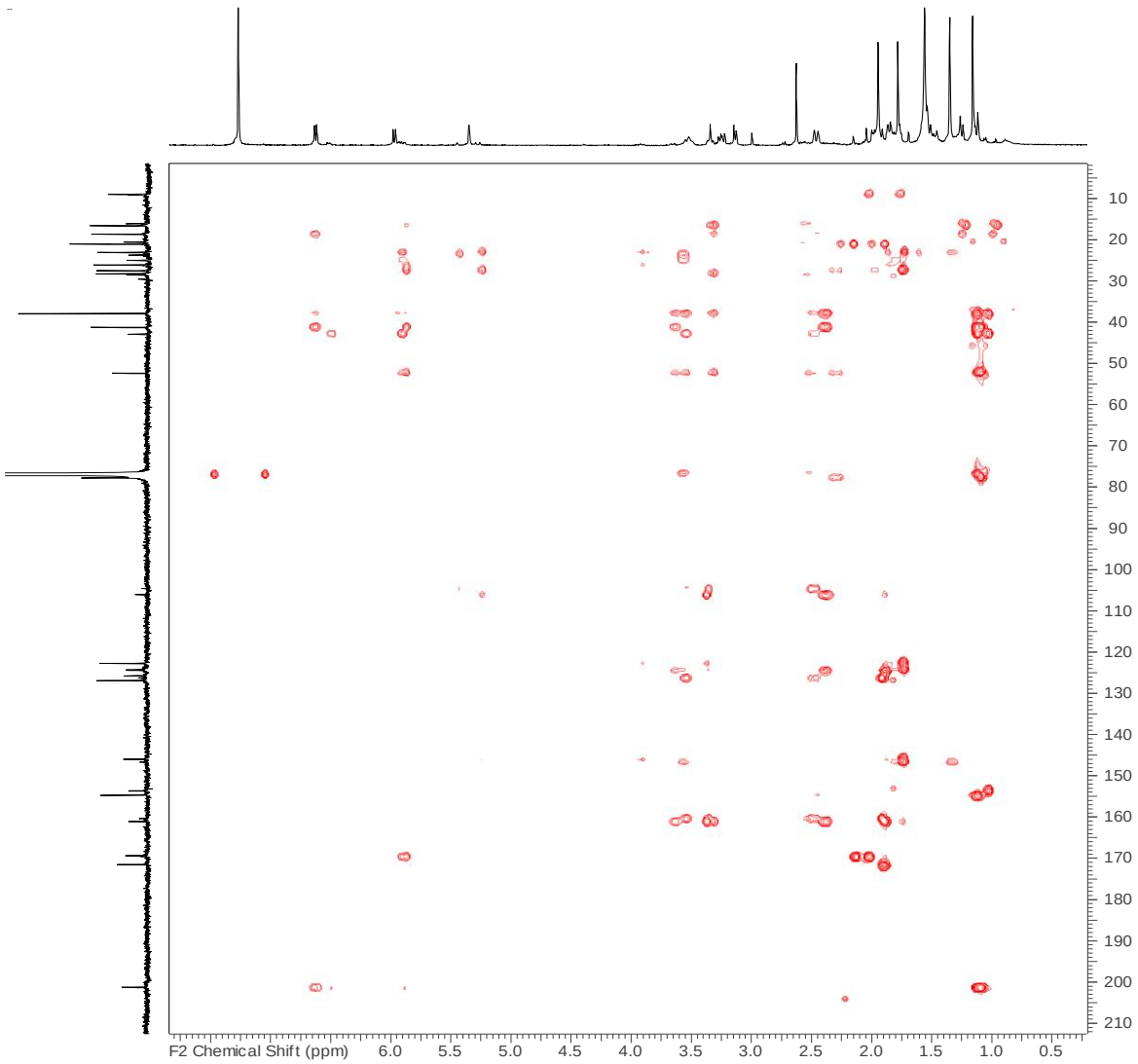

Figure Cxlviii gHMBCAD NMR spectrum for bathyptilone B (**4.28**) in $CDCl_3$, 500 MHz

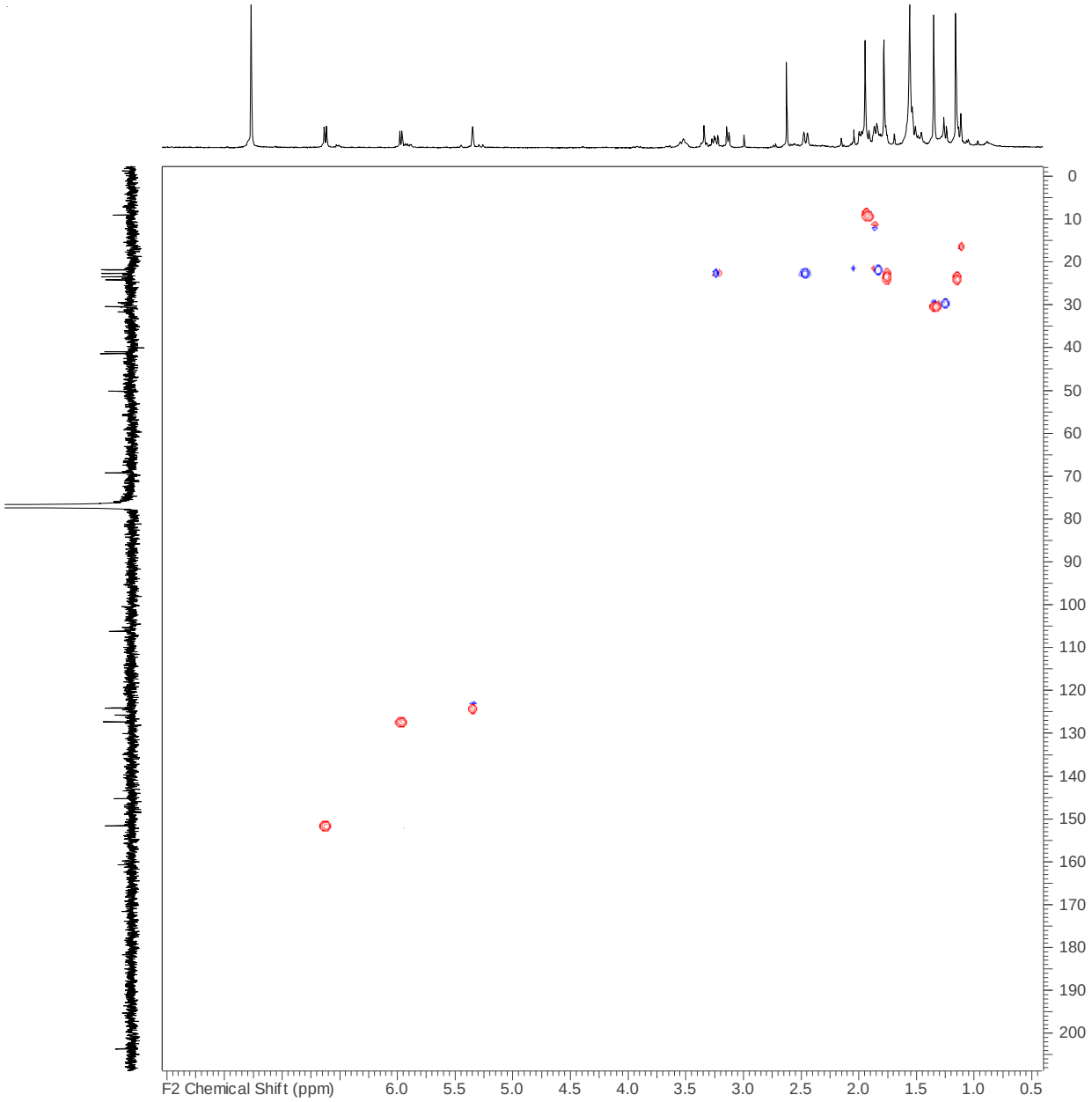

Figure Cxlix gHSQCAD NMR spectrum for bathyptilone B (**4.28**) in $CDCl_3$, 500 MHz

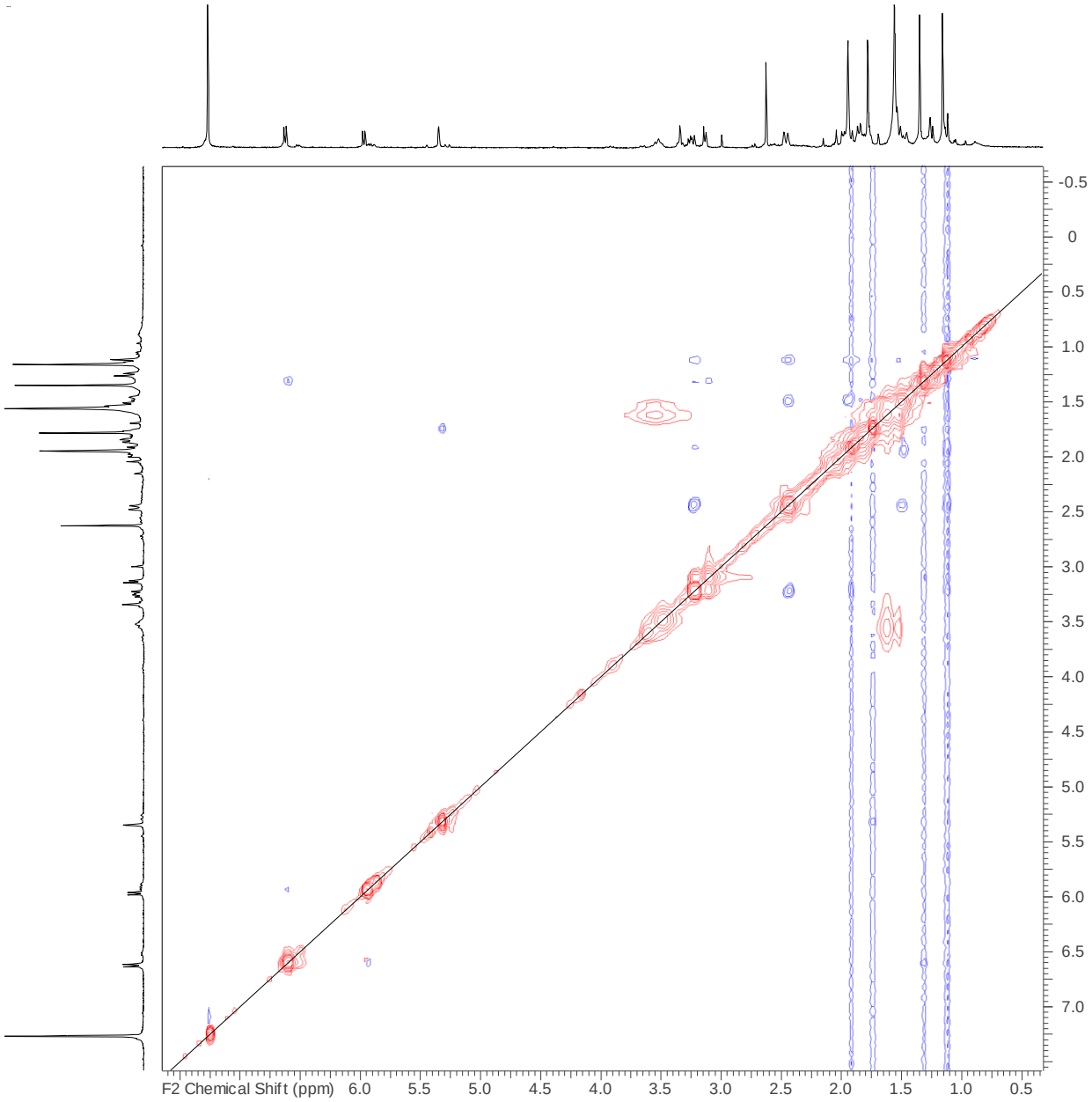

Figure CI NOESY NMR spectrum for bathyptilone B (**4.28**) in $CDCl_3$,500 MHz

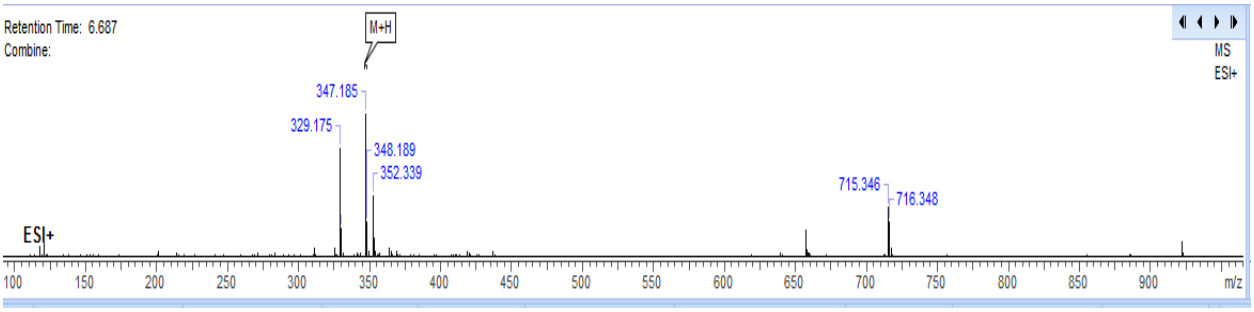

Figure Cli. High resolution ESI-MS spectrum for bathyptilone B (**4.28**) (150 mV)

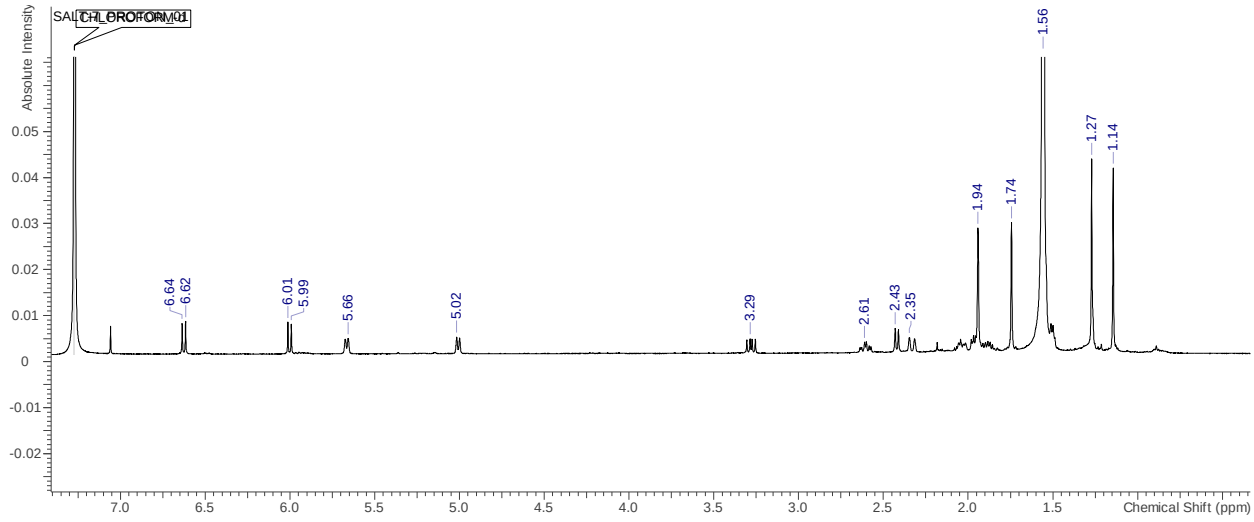

Figure Clii. ^{1}H NMR spectrum for bathyptilone C (**4.29**) in $CDCl_3$,500 MHz

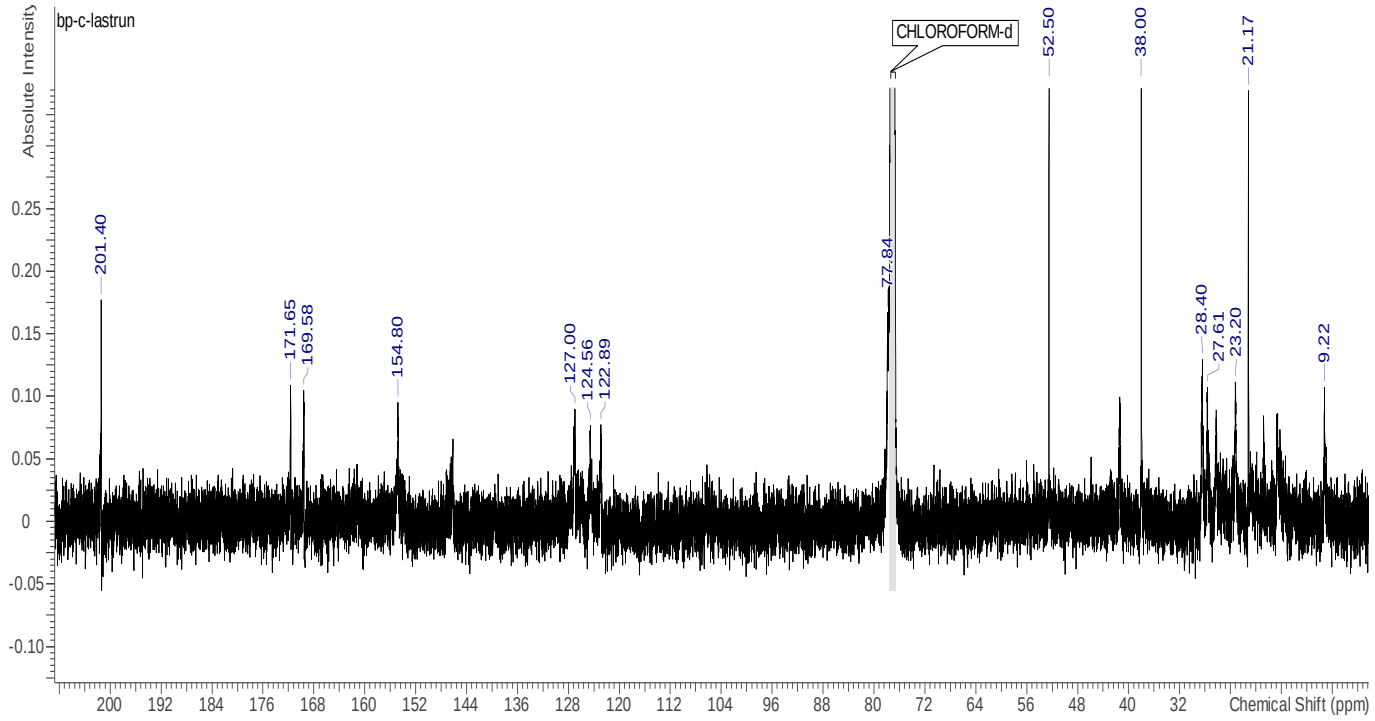

Figure Cliii. ^{13}C NMR spectrum for bathyptilone C (**4.29**) in $CDCl_3$,150 MHz

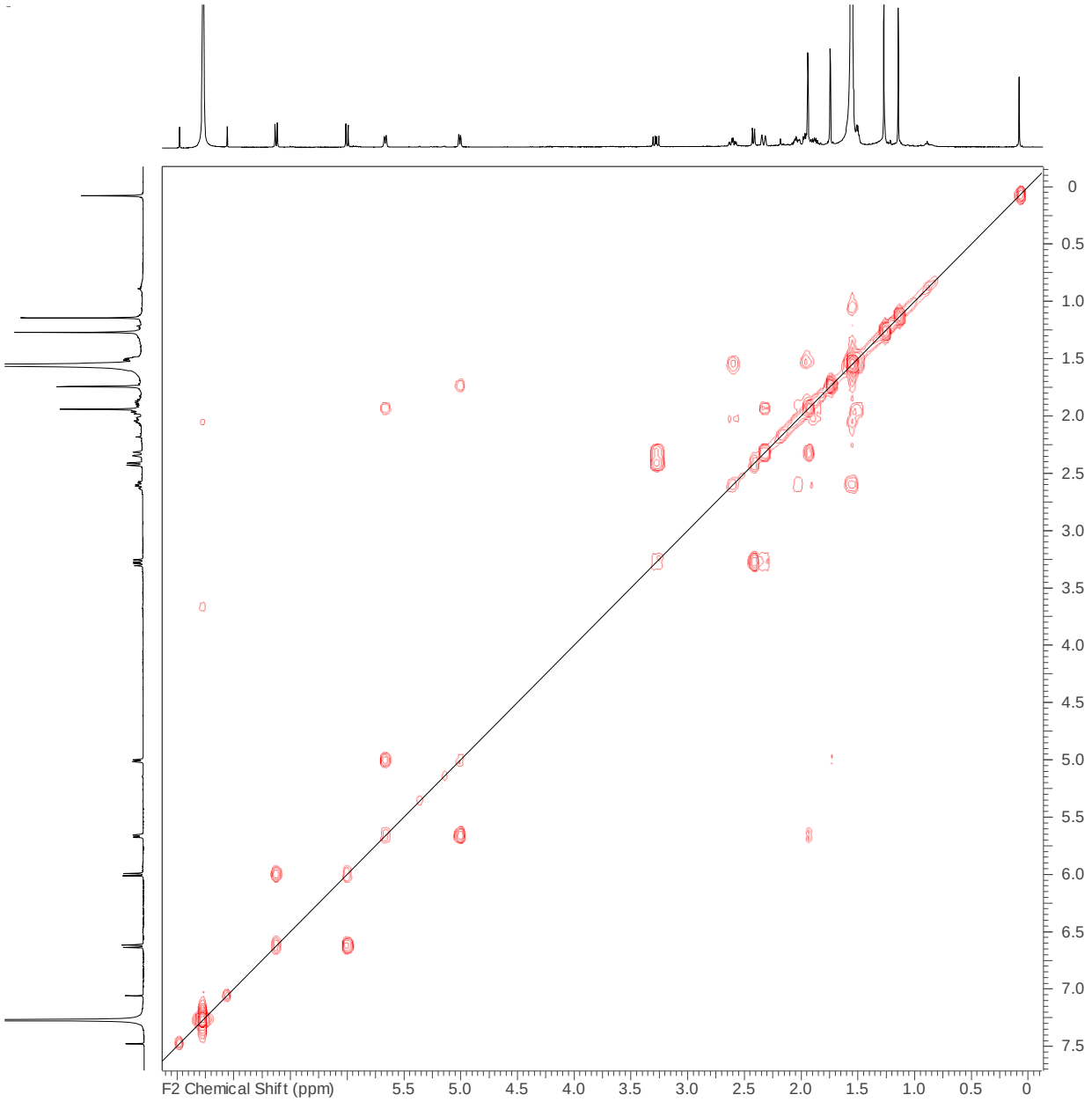

Figure Cliv. gCOSY NMR spectrum for bathyptilone C (**4.29**) (500 MHz, $CDCl_3$)

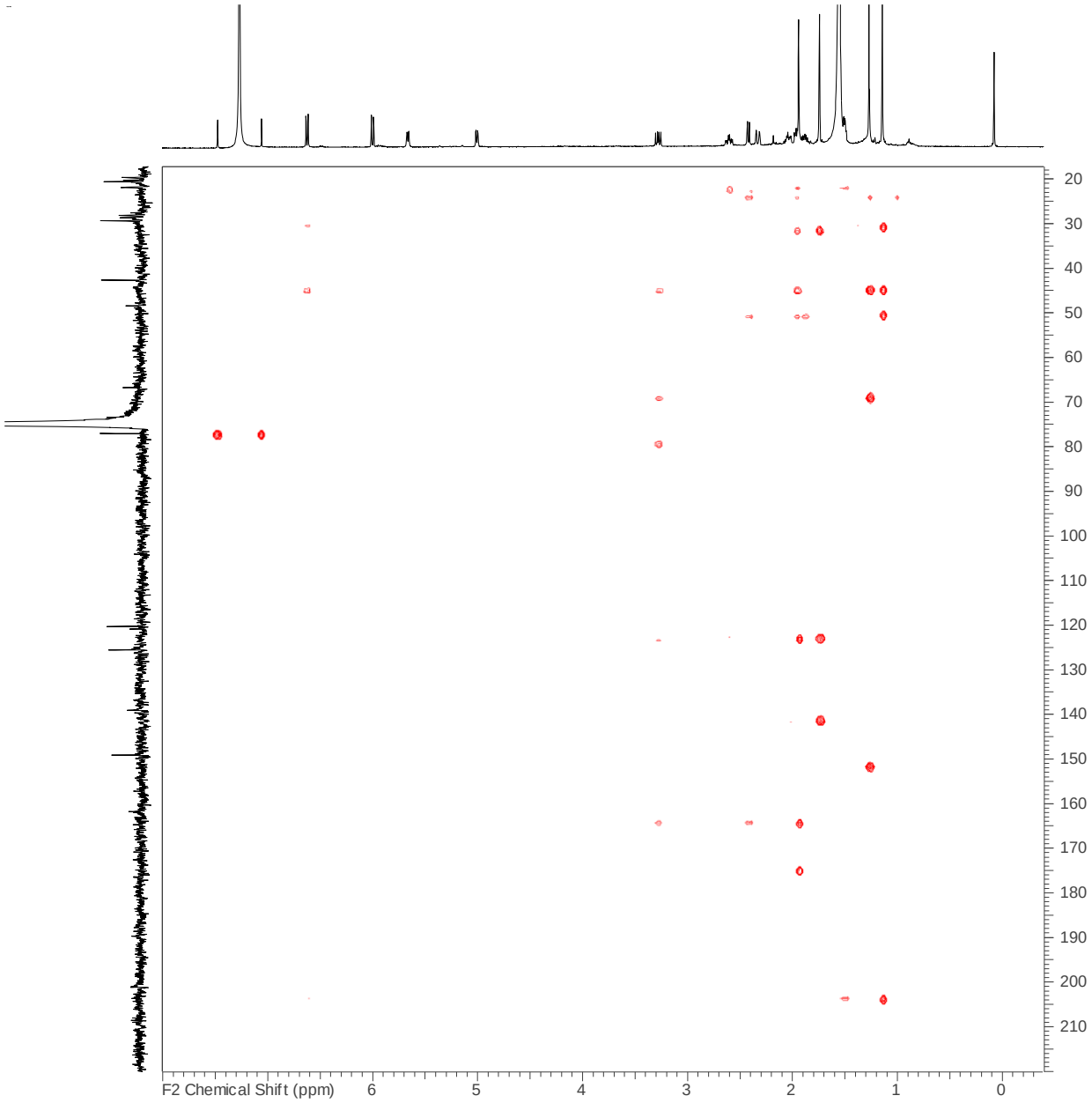

Figure CIv. gHMBCAD NMR spectrum for bathyptilone C (**4.29**) in $CDCl_3$, 500 MHz

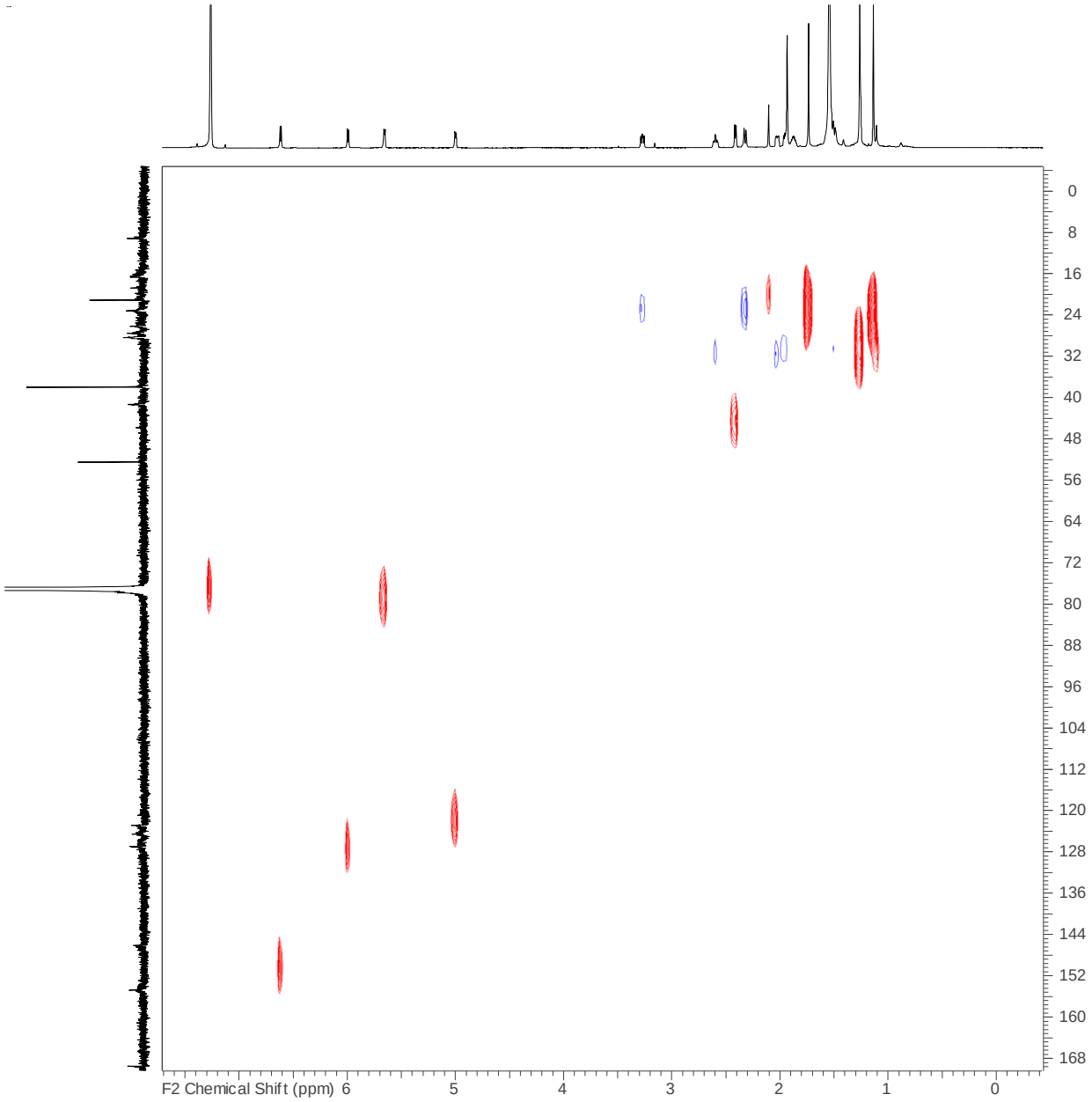

Figure CIvi. ^{1}H- ^{13}C HSQC NMR spectrum for bathyptilone C (**4.29**) in CDCl3, 800 MHz

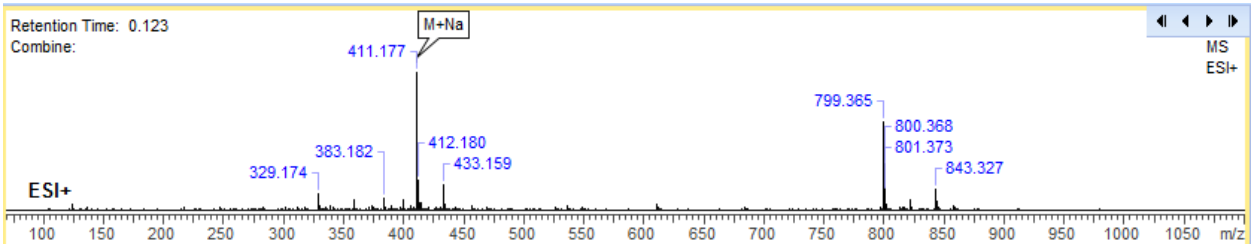

Figure CIvii. HREI-MS chromatograph and MS spectrum for bathyptilone C (**4.29**)

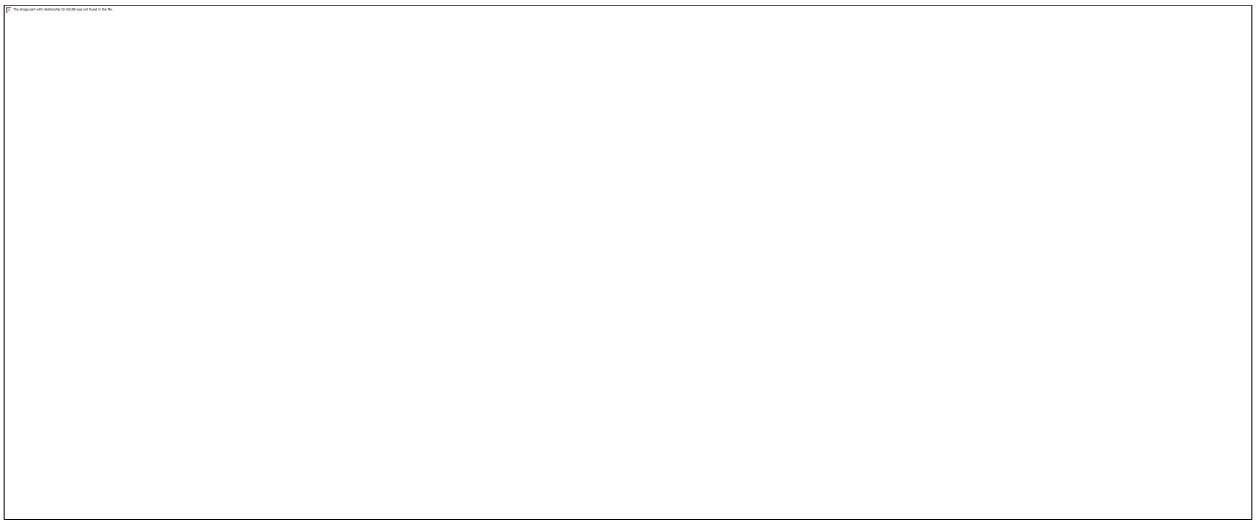

Figure Clviii. ^{1}H NMR spectrum for enbepenone A (**4.30**) in $CDCl_3$, 500 MHz

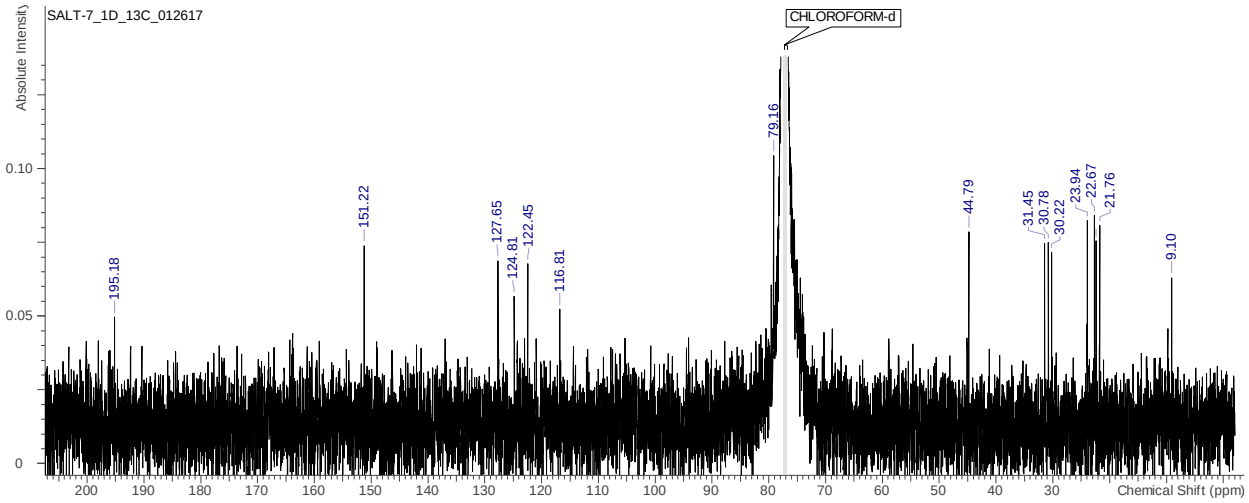

Figure Clix. ^{13}C NMR spectrum for enbepenone A (**4.30**) in $CDCl_3$, 200 MHz

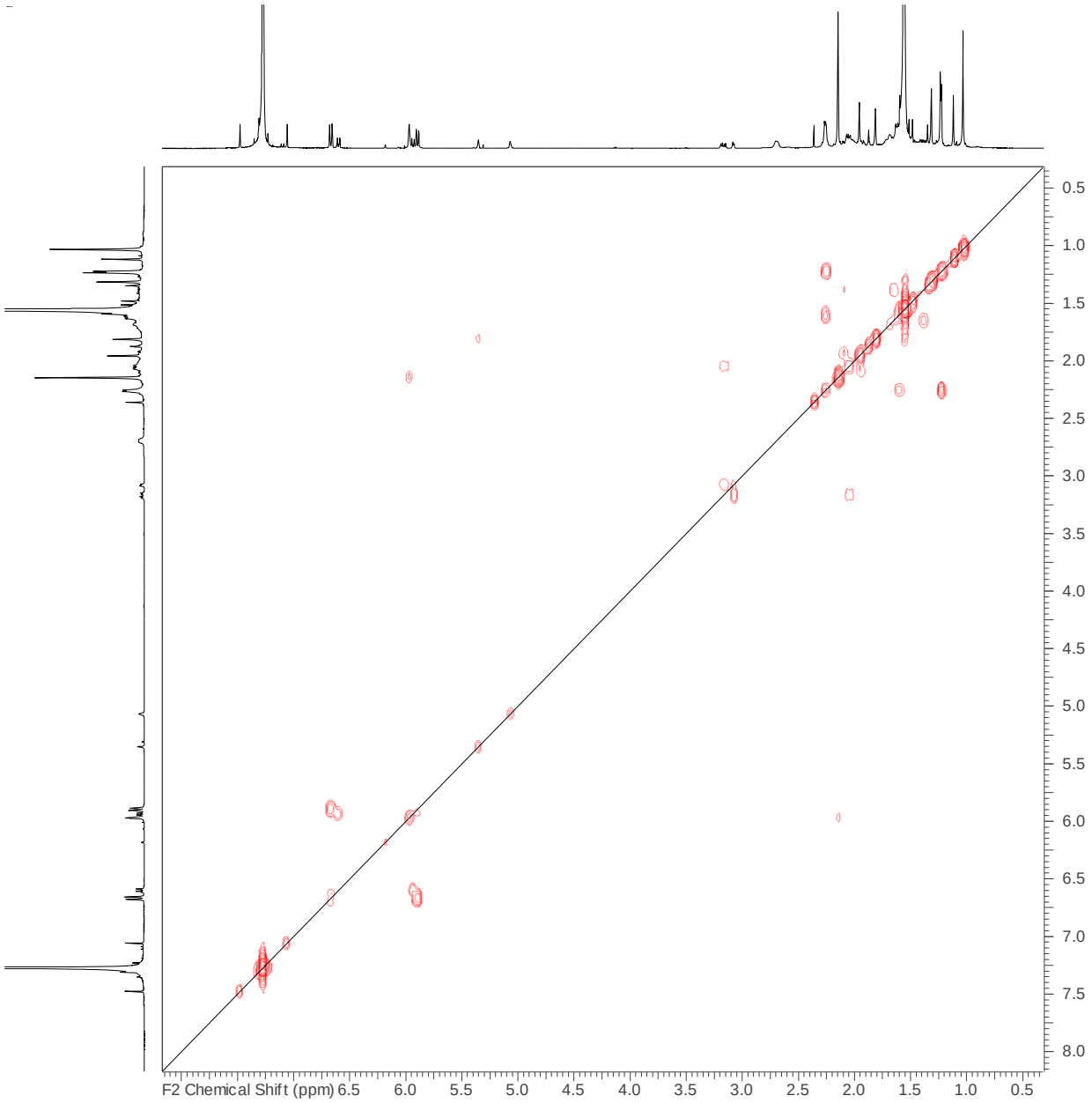

Figure CIx. COSY NMR spectrum for enbepenone A (**4.30**) in $CDCl_3$, 500 MHz

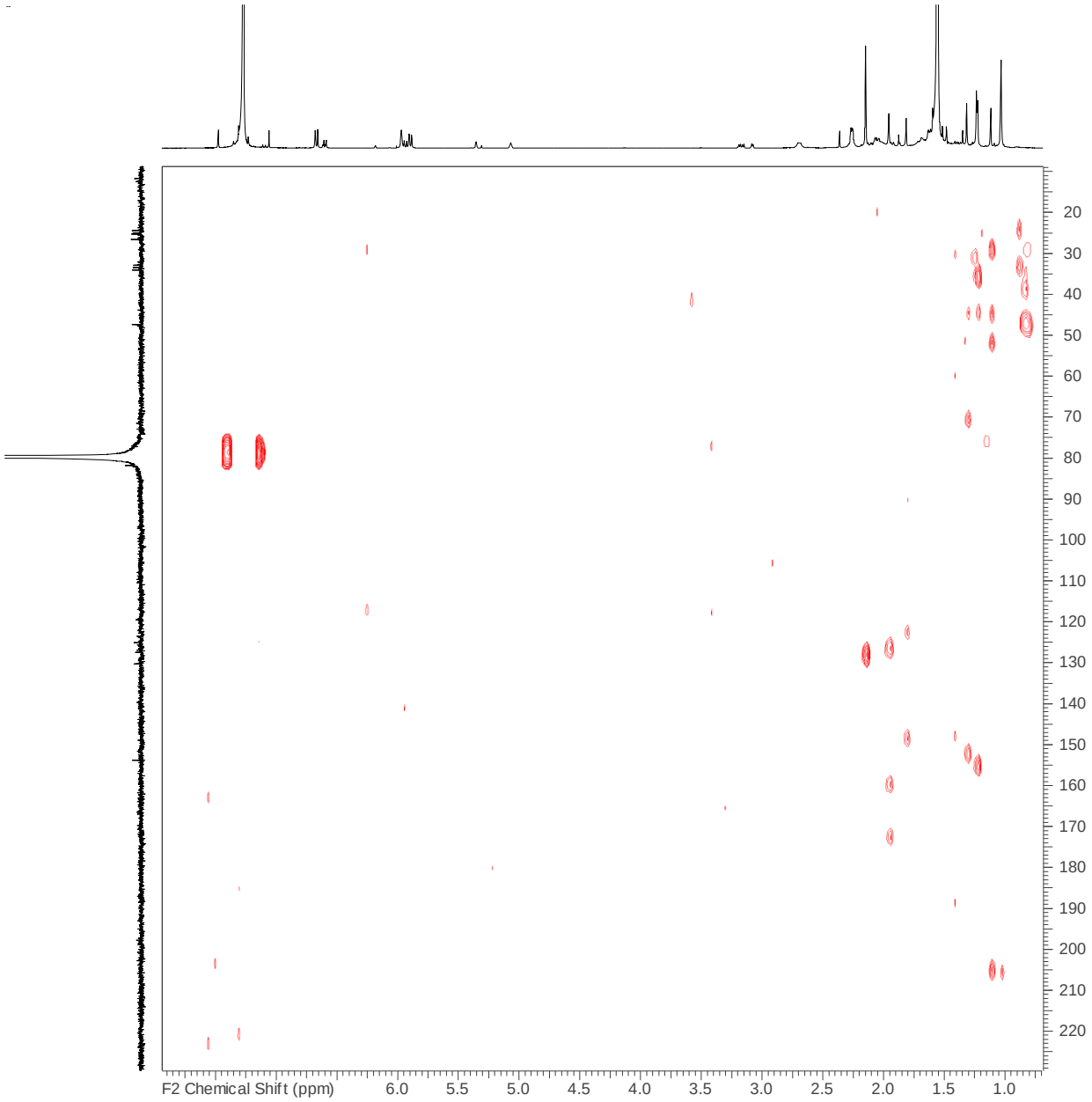

Figure Clxi. gHMBCAD NMR spectrum for enbepenone A (**4.30**) in $CDCl_3$, 800 MHz

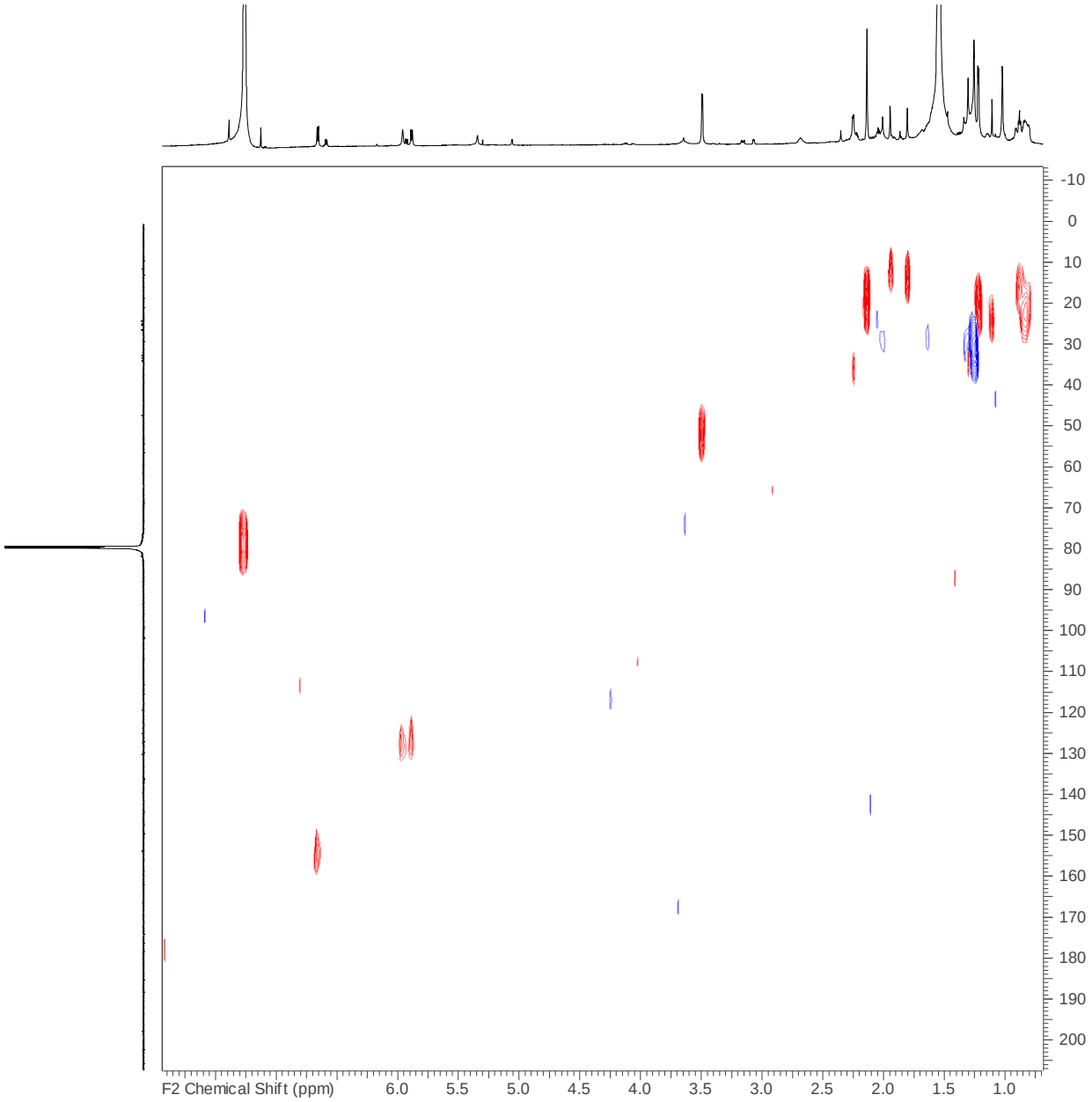

Figure CIxii. gHSQCAD NMR spectrum for enbepenone A (**4.30**) in $CDCl_3$, 800 MHz

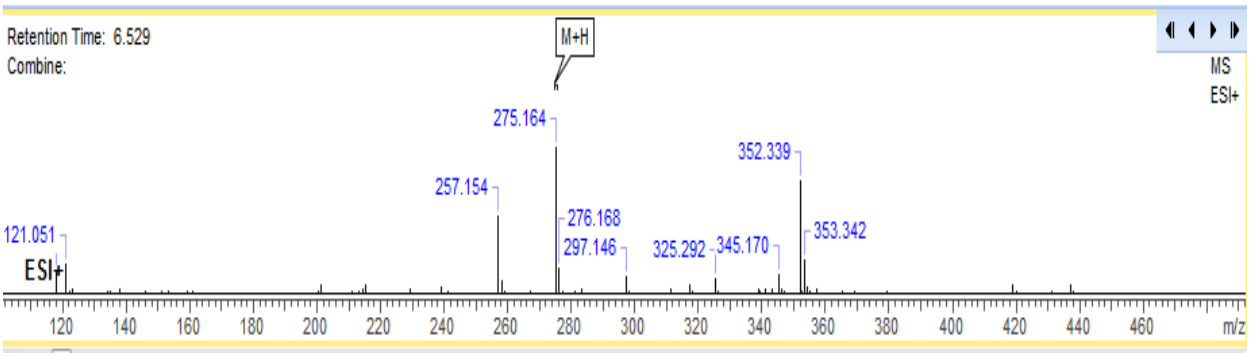

Figure Clxiii. HRESI-MS chromatograph and MS spectrum for enbepenone A (**4.30**)

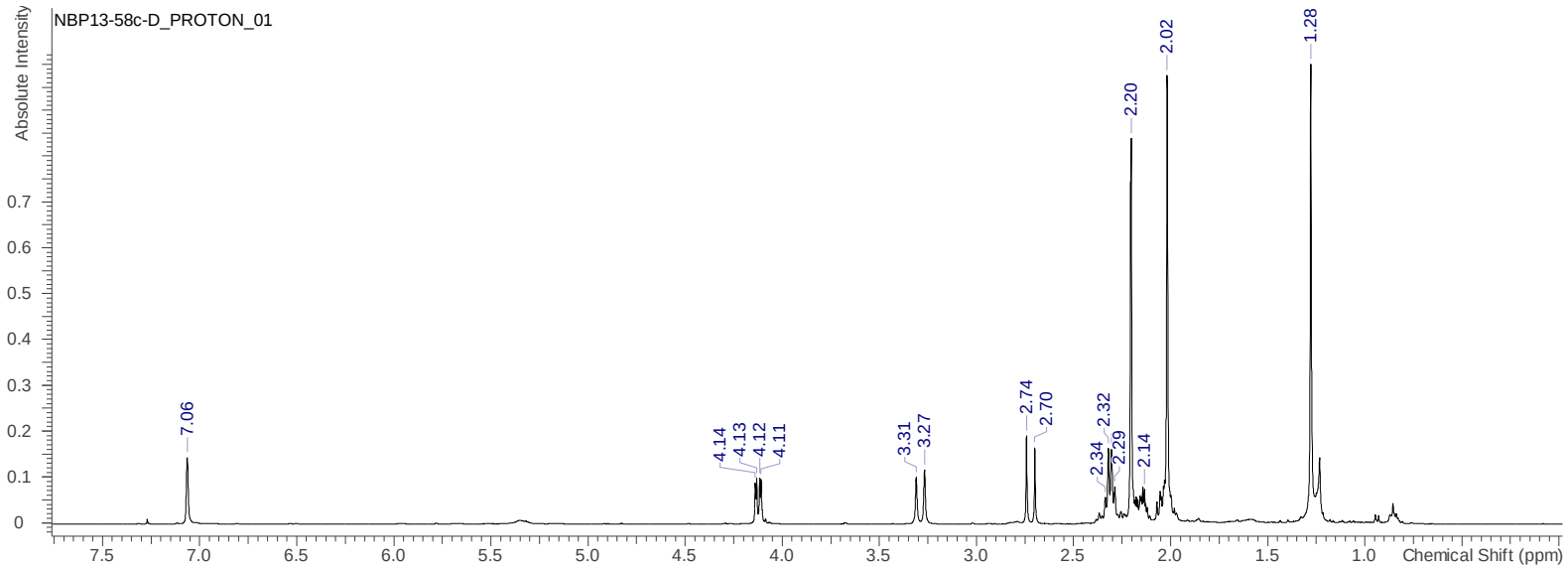

Figure Clxiv. ^{1}H NMR spectrum for scotianone A (**4.32**) in $CDCl_3$, 400MHz

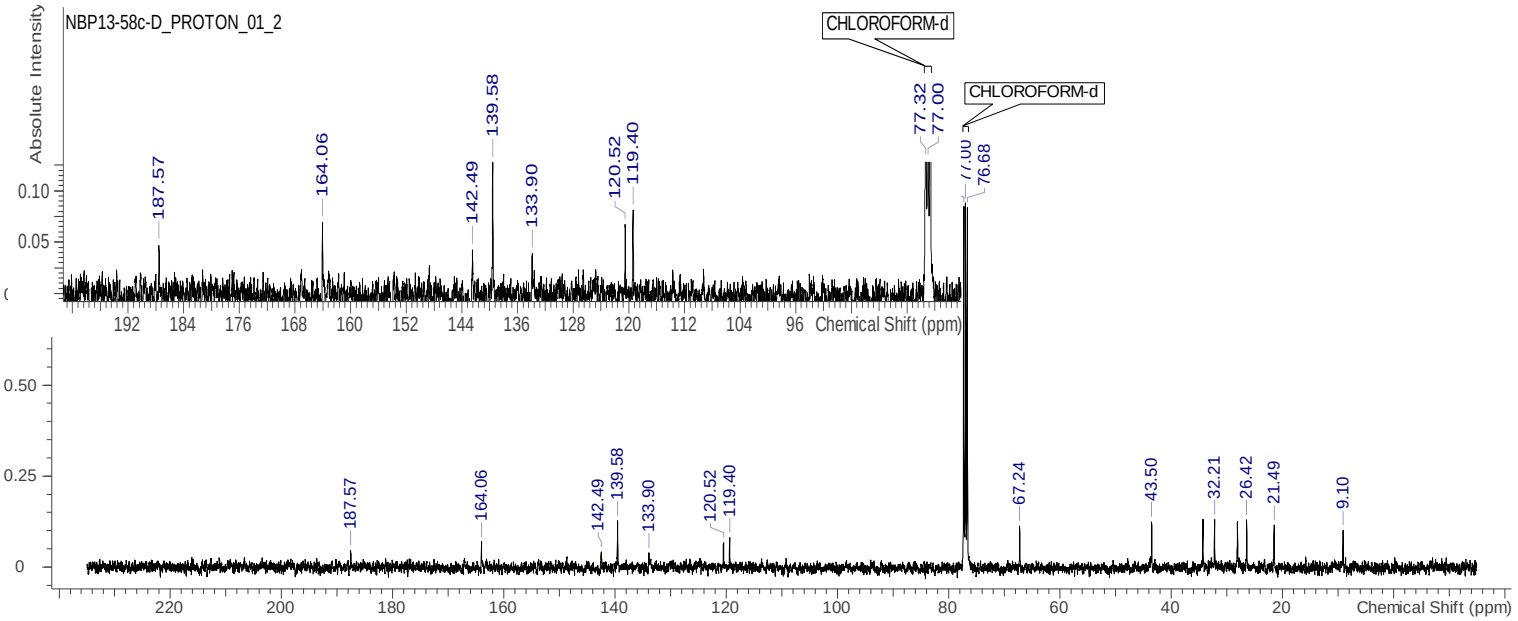

Figure Clxv. ^{13}C NMR spectrum for scotianone A (**4.32**) in $CDCl_3$, 100MHz

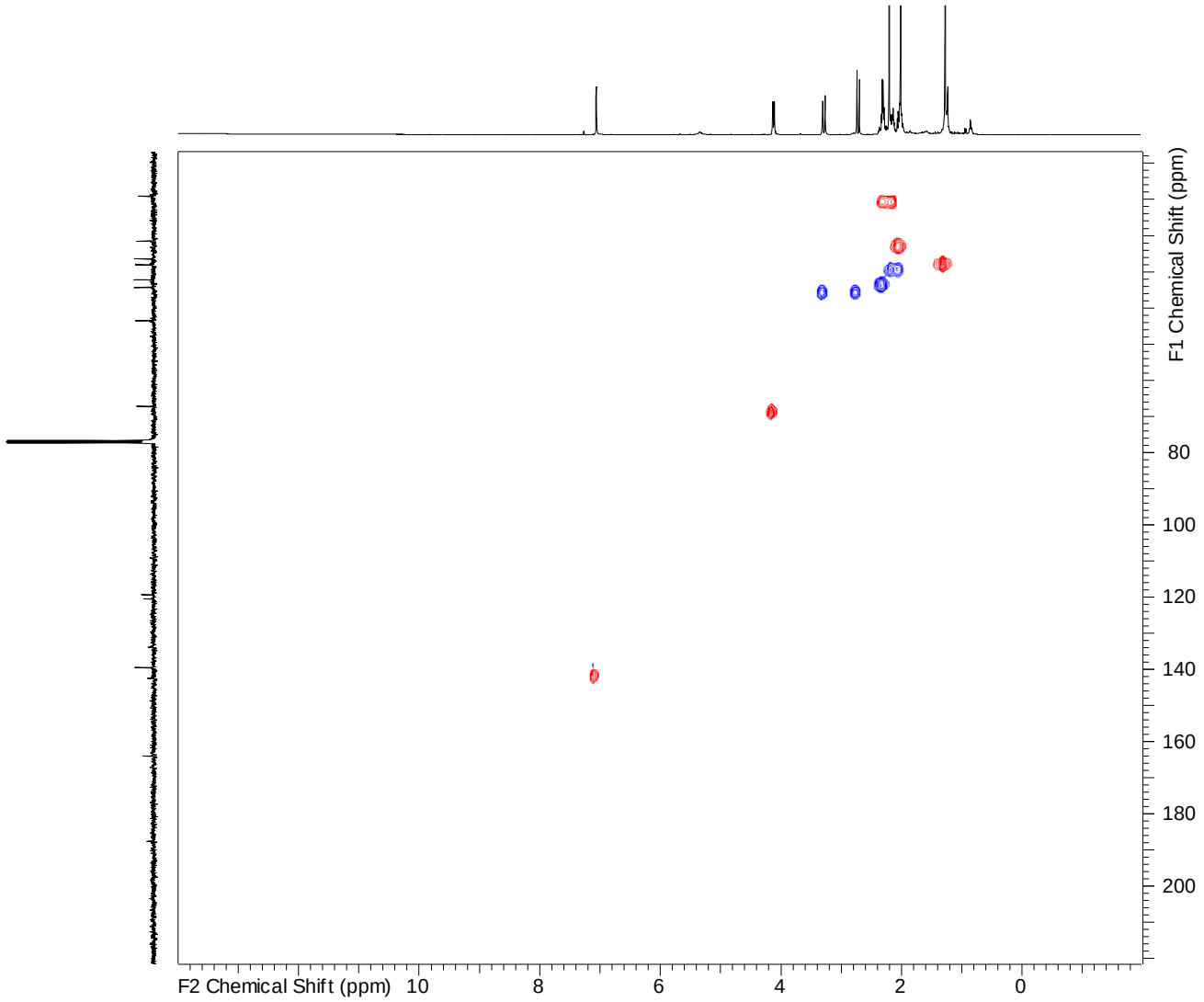

Figure Clxvi. gHSQCAD NMR spectrum for scotianone A (**4.32**) in $CDCl_3$, 600 MHz

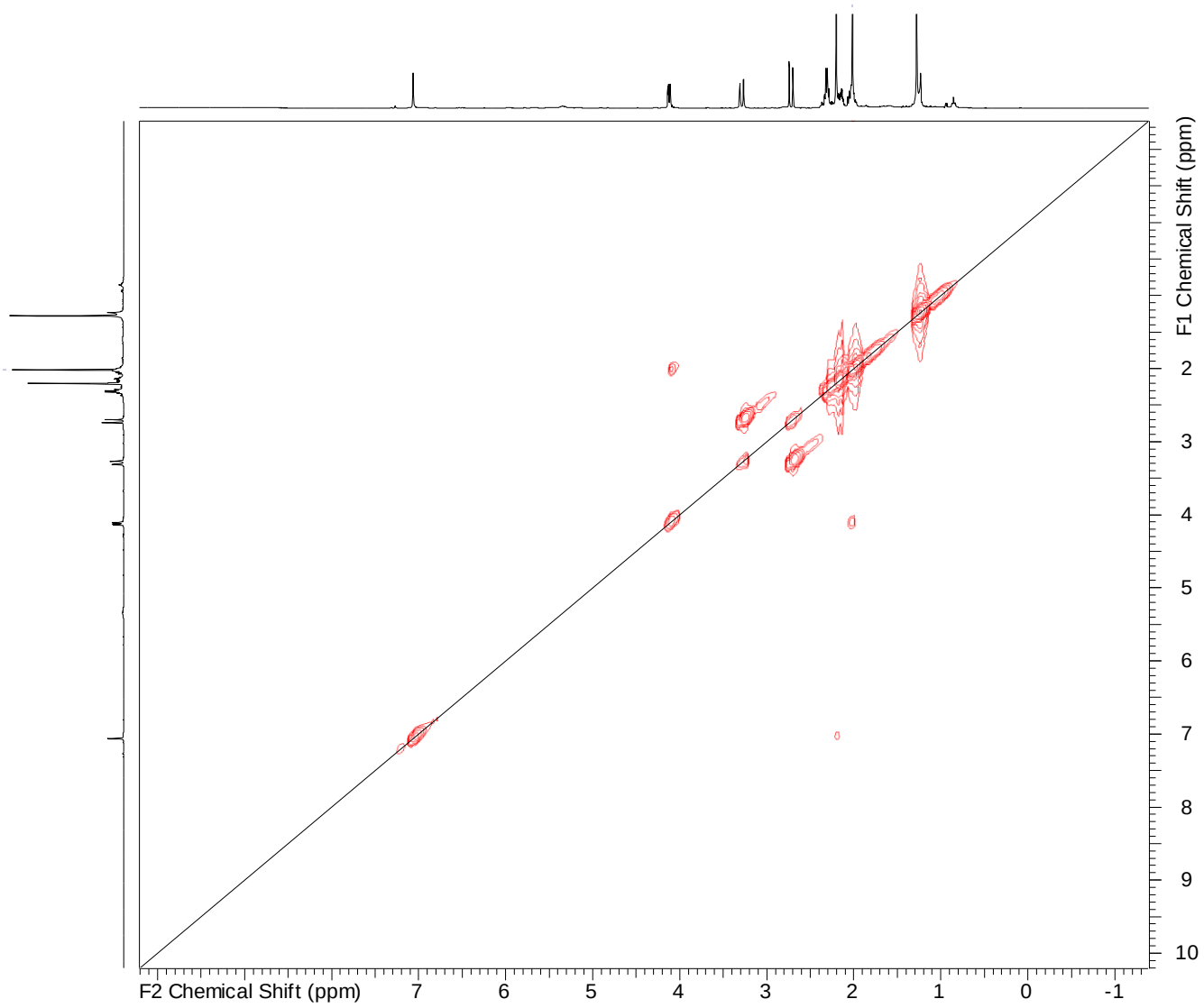

Figure Clxvii. gCOSY NMR spectrum for scotianone A (**4.32**) in $CDCl_3$, 600 MHz

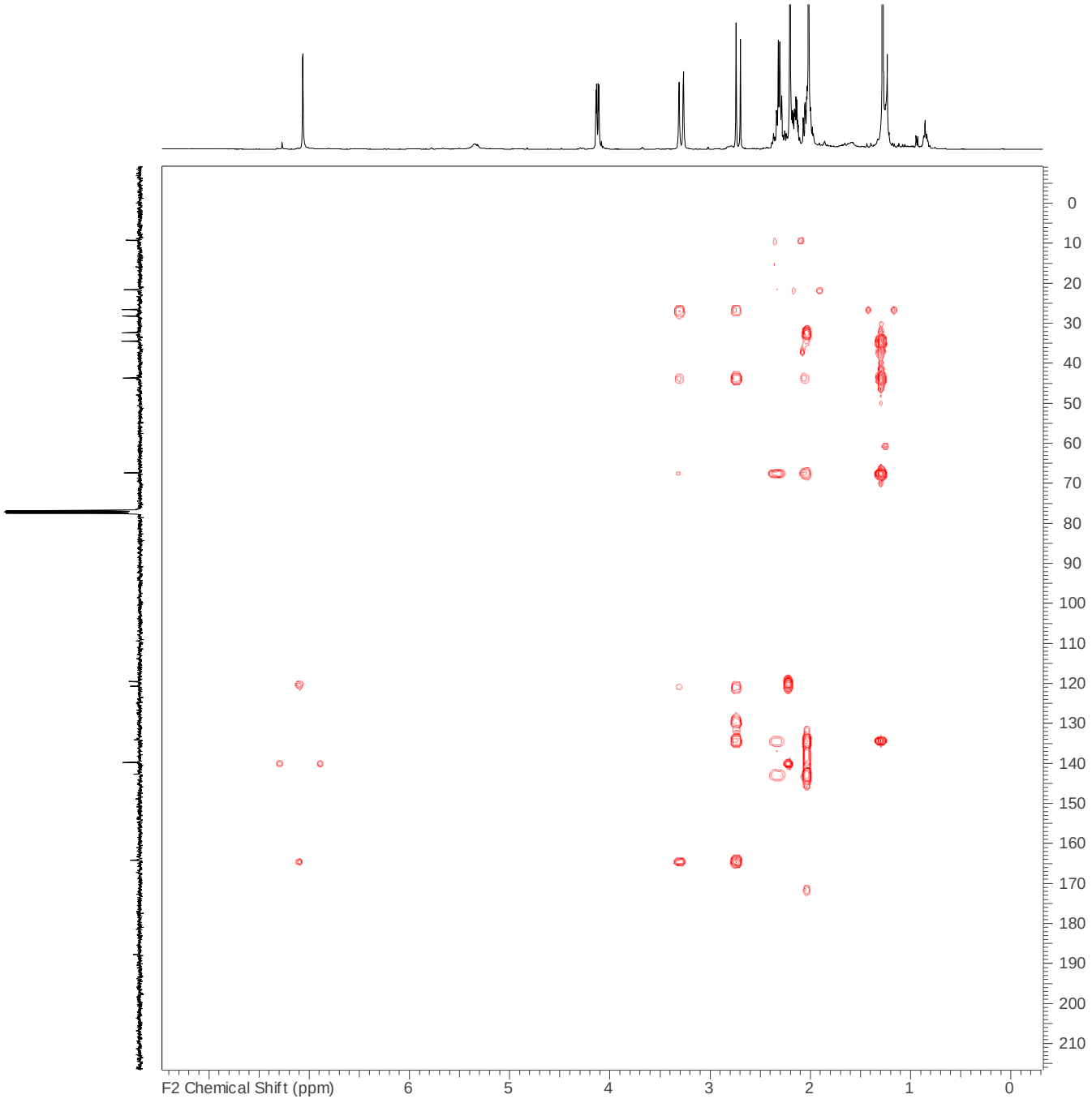

Figure Clxviii. gHMBCAD NMR spectrum for scotianone A (**4.32**) in $CDCl_3$, 500 MHz

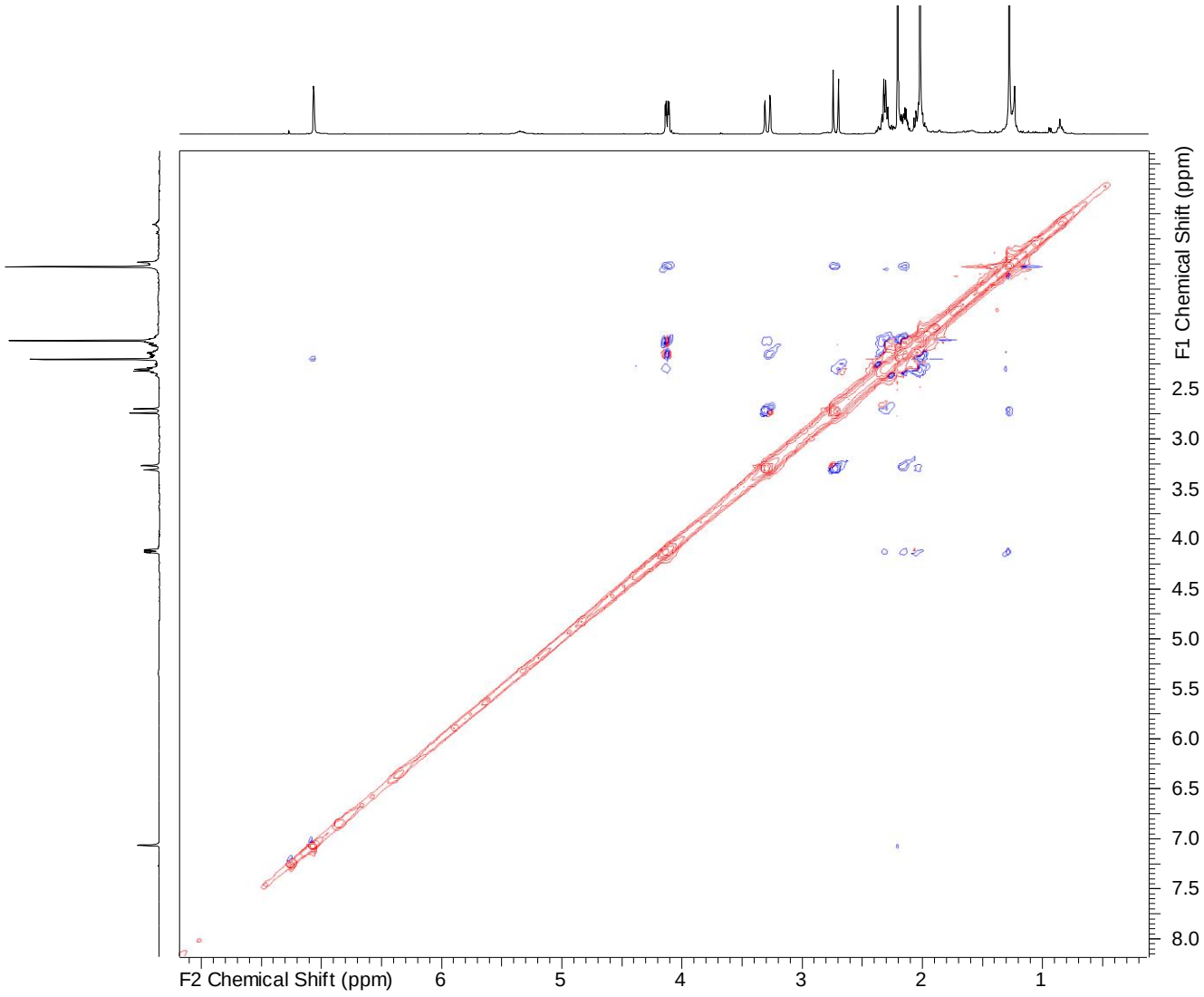

Figure Clxix. NOESY NMR spectrum for scotianone A (**4.32**) in $CDCl_3$, 500 MHz

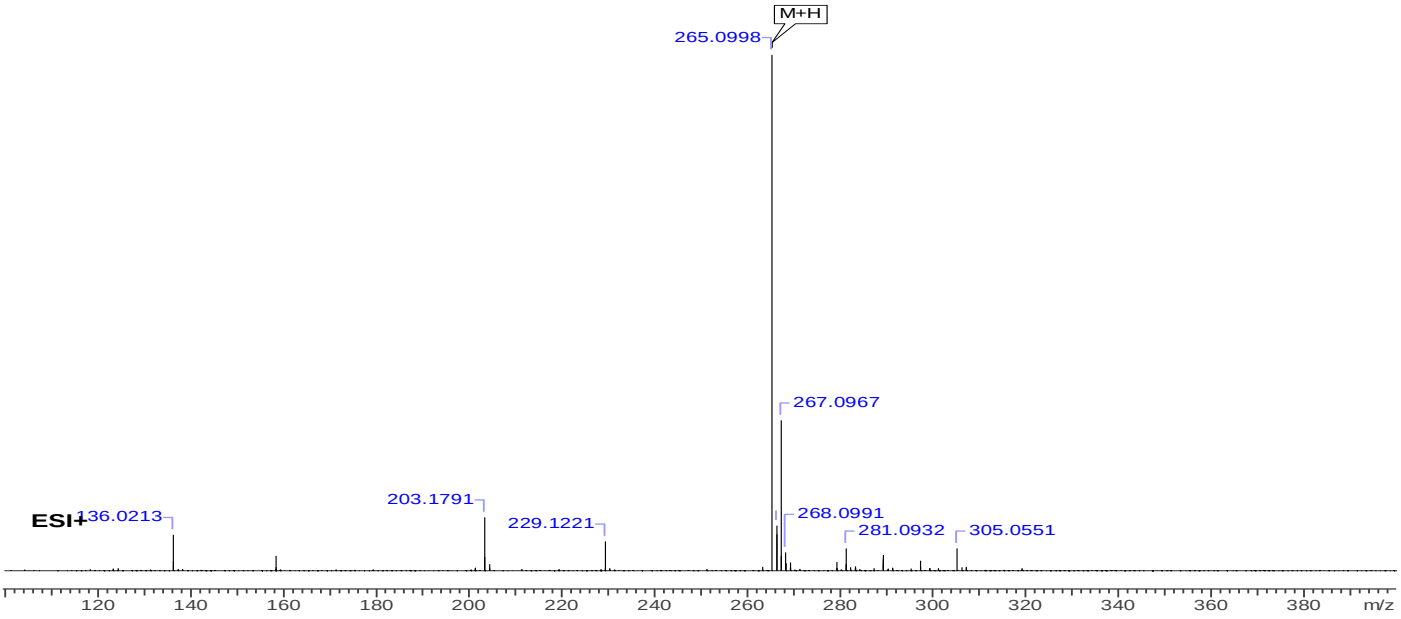

Figure Clxx. High resolution ESI- MS spectrum for scotianone A (**4.32**) (eV= 150V)

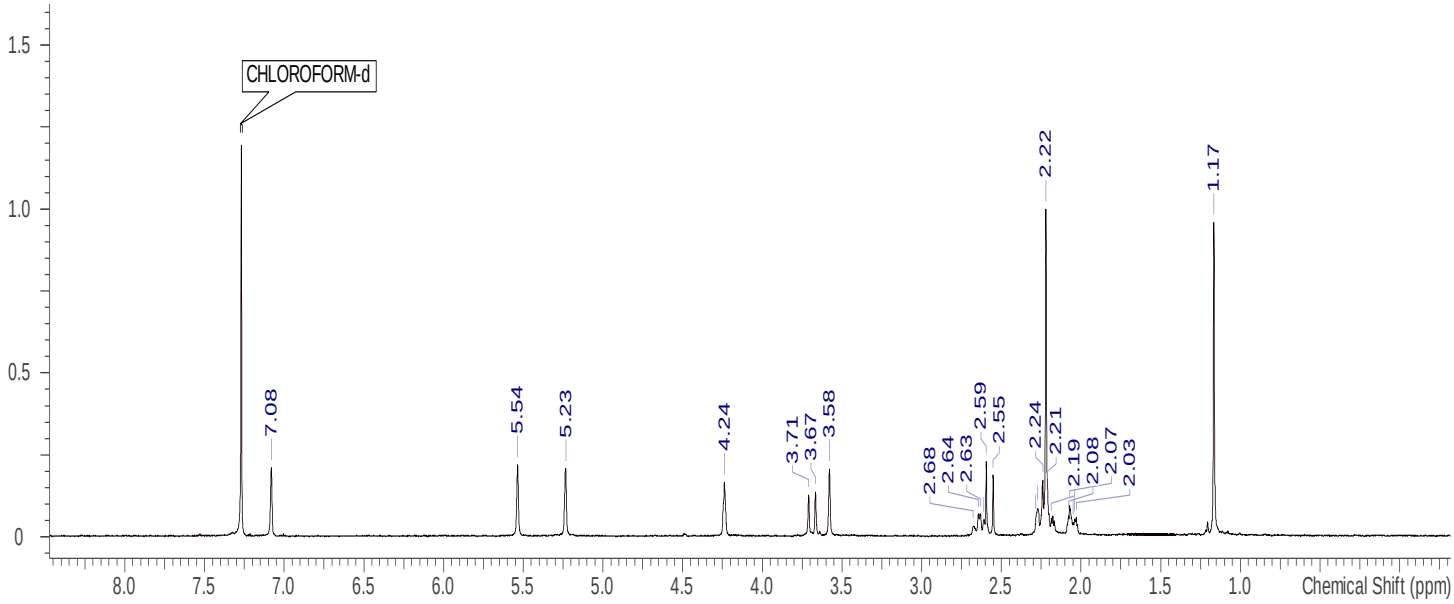

Figure Clxxi. ^{1}H NMR spectrum for scotianone B (**4.33**) in $CDCl_3$, 400MHz

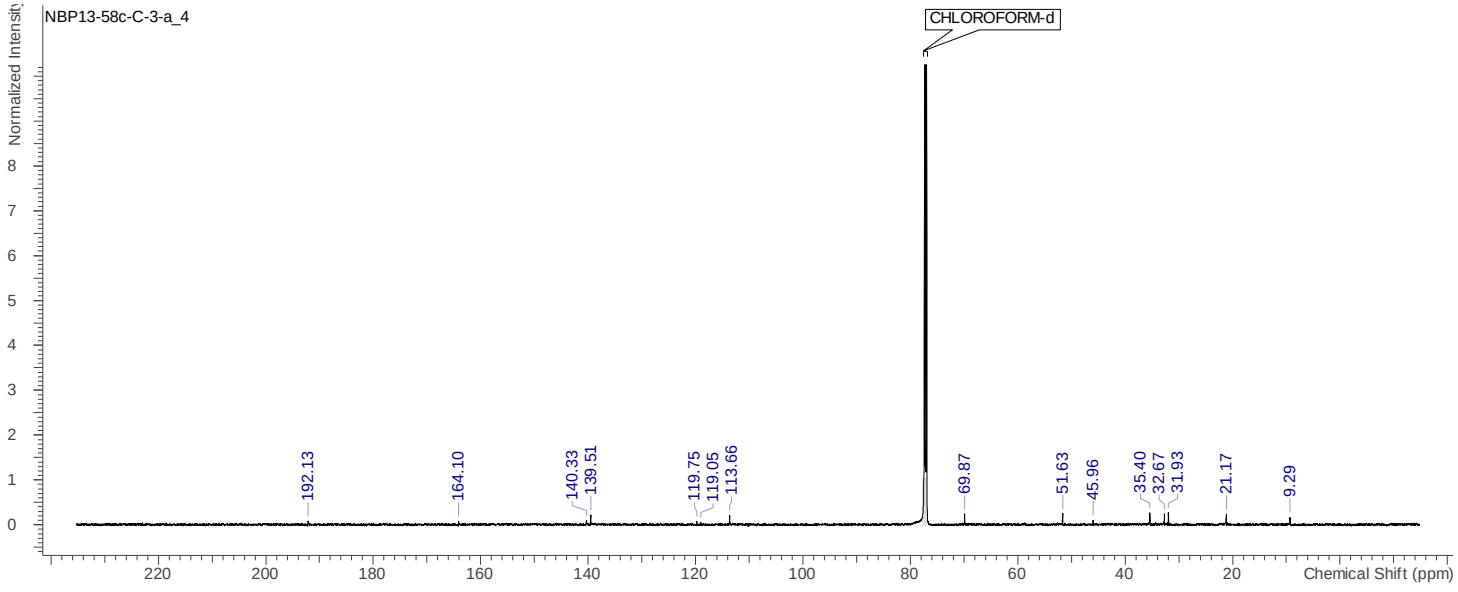

Figure Clxxii. ^{13}C NMR spectrum for scotianone B (**4.33**) in $CDCl_3$, 150 MHz

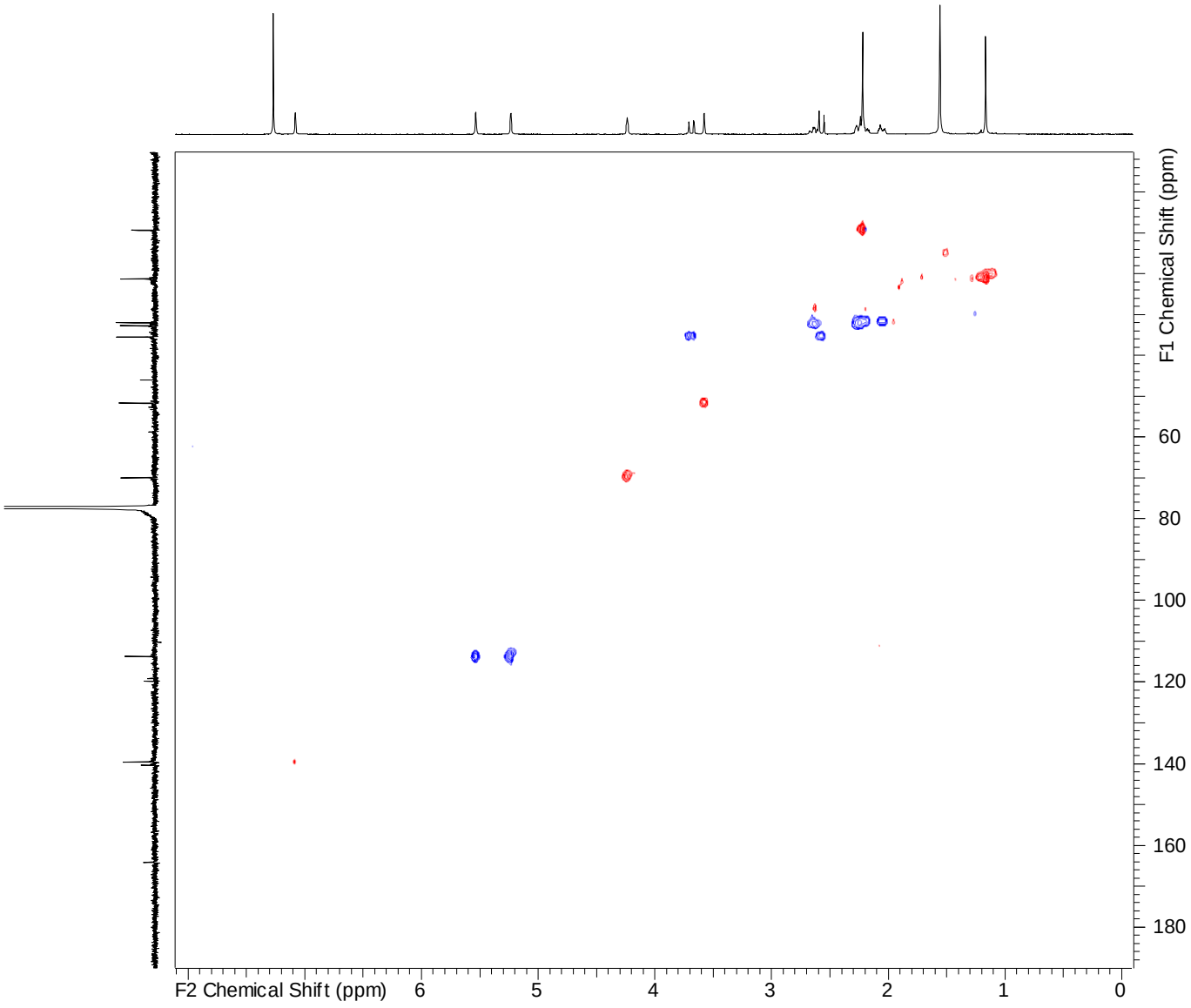

Figure Clxiii. gHSQCAD NMR spectrum for scotianone B (**4.33**) in $CDCl_3$, 500 MHz

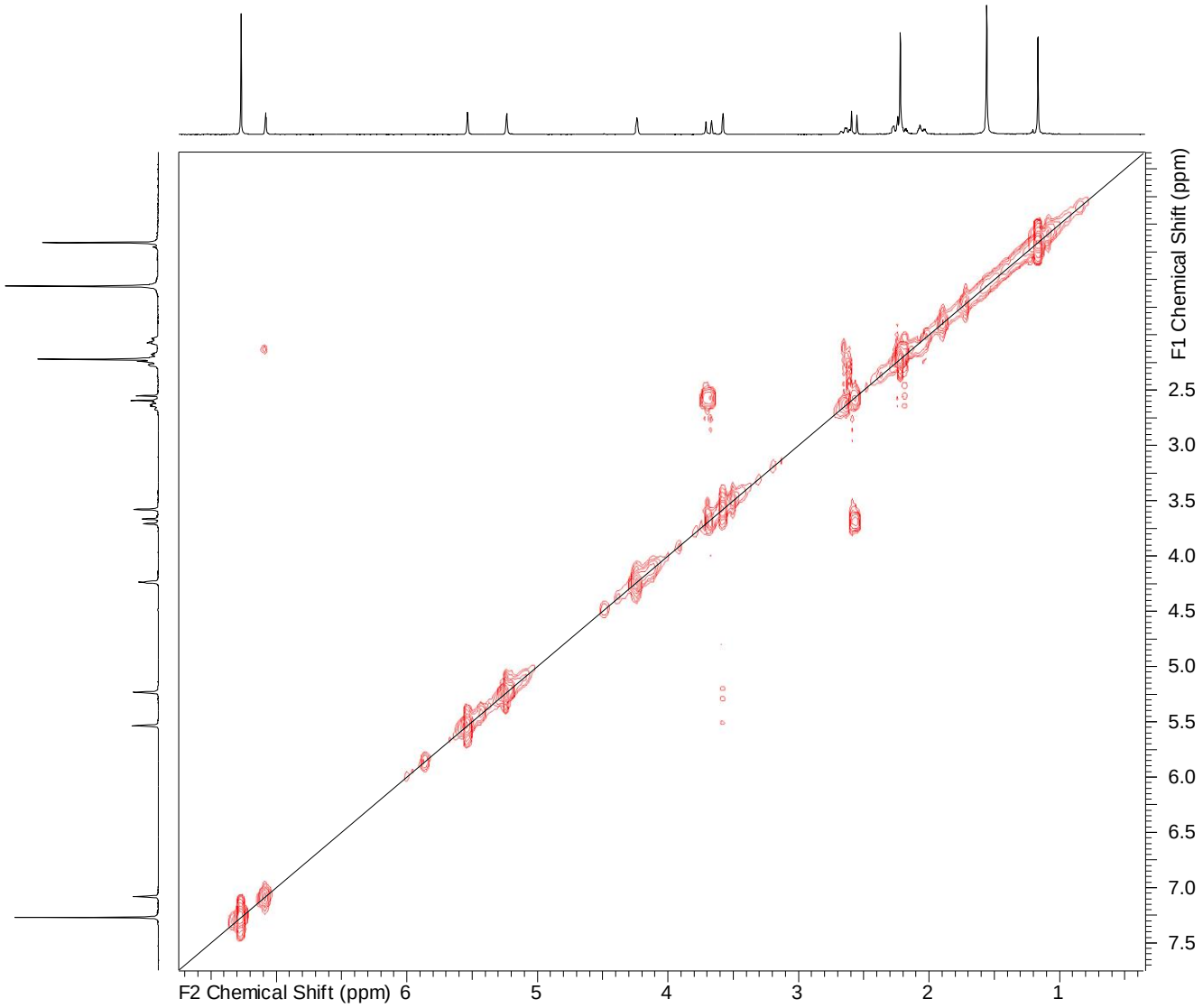

Figure Clxiv. gCOSY NMR spectrum for scotianone B (**4.33**) in $CDCl_3$, 600 MHz

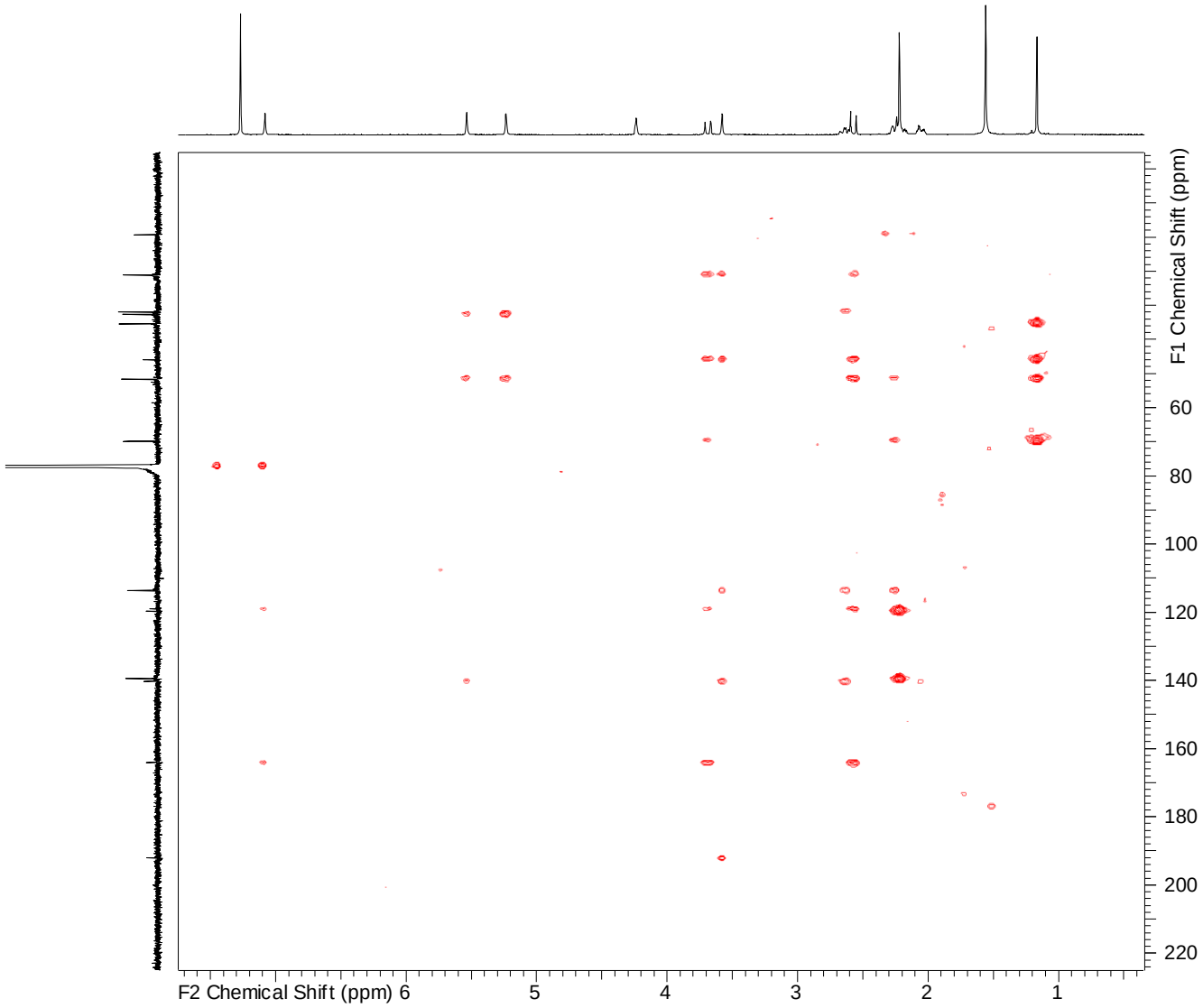

Figure Clxxv. gHMBCAD NMR spectrum for scotianone B (**4.33**) in $CDCl_3$, 600 MHz

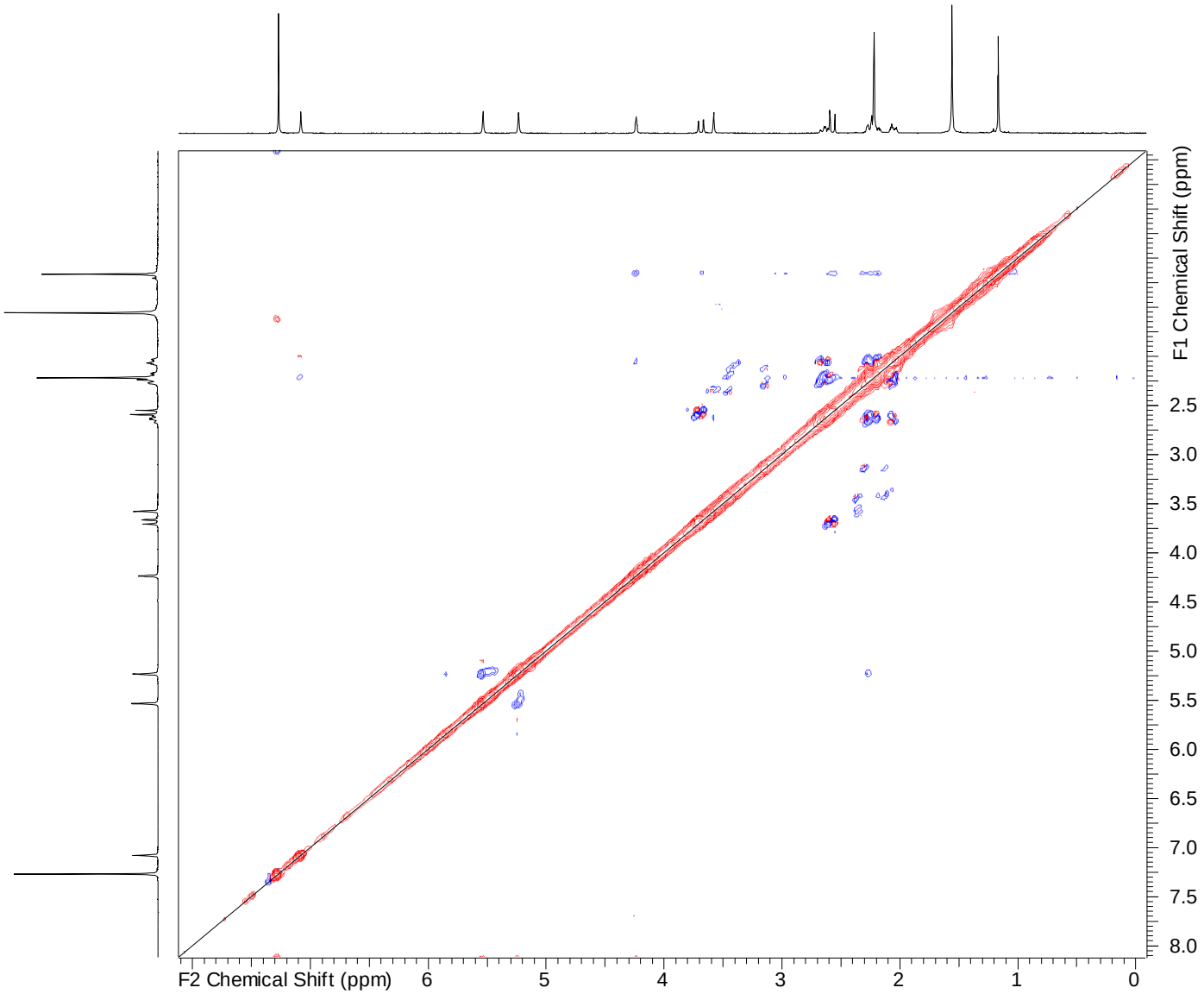

Figure Clxxvi. NOESY NMR spectrum for scotianone B (**4.33**) in $CDCl_3$, 500 MHz

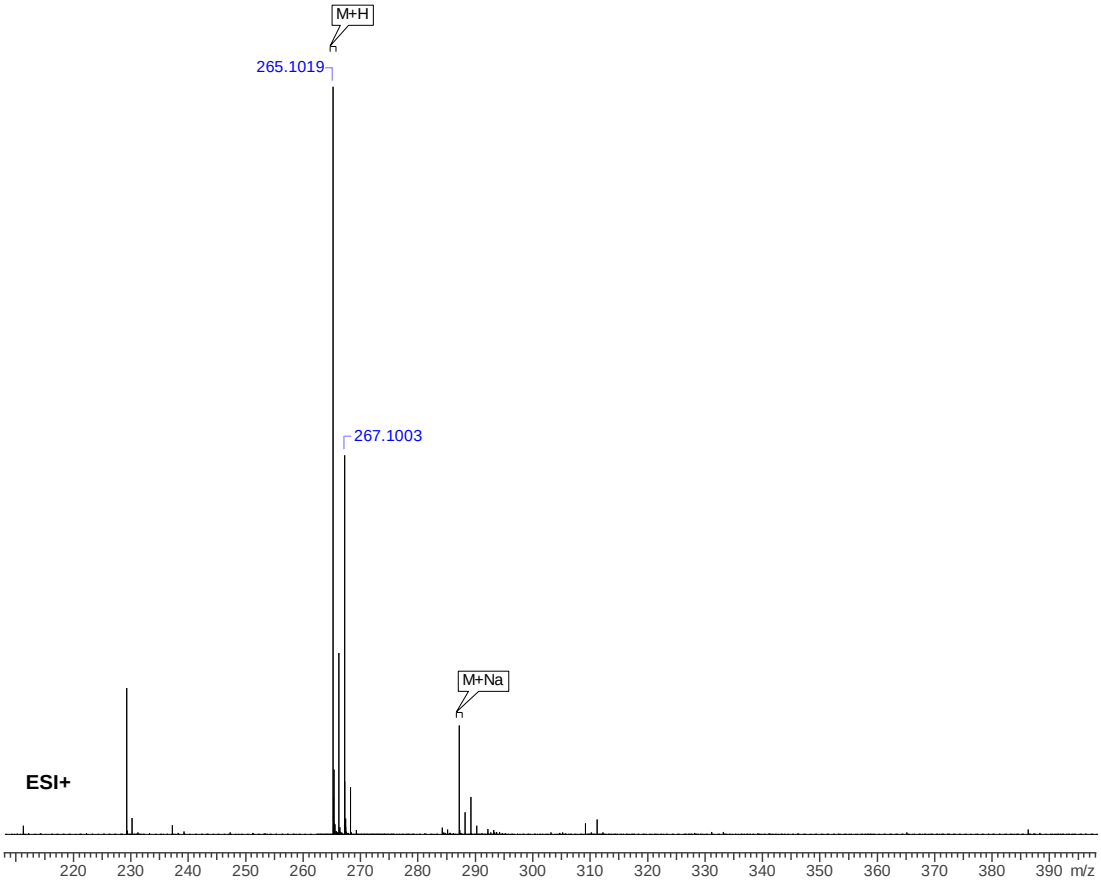

Figure Clxxvii. High resolution ESI- MS spectrum for scotianone B (**4.33**) (eV = 175V)

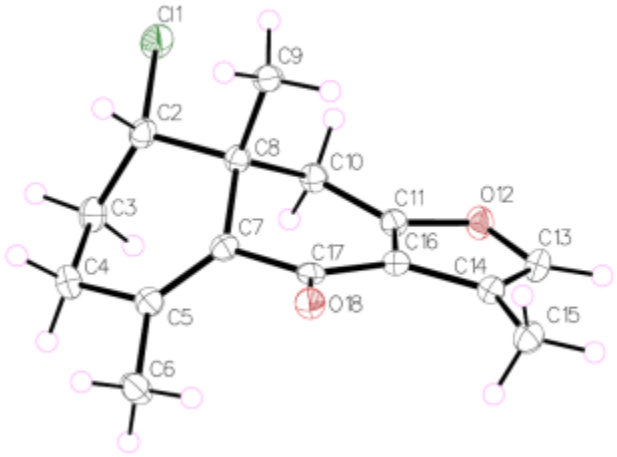

Figure Clxxviii. Asymmetric unit of scotianone A (**4.33**). Anisotropic displacement parameters were drawn at 50% probability.

Table C5. Crystal data and structure refinement for scotianone A .	
Identification code	NBP13_58c_D
Empirical formula	$C_{15}H_{17}ClO_2$
Formula weight	264.73
Temperature/K	100
Crystal system	monoclinic
Space group	$P2_1$
a/Å	7.0670(3)
b/Å	7.4533(3)
c/Å	12.6974(5)
α/°	90
β/°	100.4436(13)
γ/°	90
Volume/Å^3	657.72(5)
Z	2
ρ_{calc}g/cm^3	1.337
μ/mm^{-1}	2.496
F(000)	280.0
Crystal size/mm^3	0.071 × 0.052 × 0.014
Radiation	CuKα (λ = 1.54178)
2Θ range for data collection/°	7.078 to 137.43
Index ranges	-7 ≤ h ≤ 8, -8 ≤ k ≤ 8, -15 ≤ l ≤ 15
Reflections collected	7445
Independent reflections	2270 [R_{int} = 0.0256, R_{sigma} = 0.0344]
Data/restraints/parameters	2270/1/166
Goodness-of-fit on F^2	1.064
Final R indexes [I>=2σ (I)]	R_1 = 0.0260, wR_2 = 0.0659
Final R indexes [all data]	R_1 = 0.0264, wR_2 = 0.0661
Largest diff. peak/hole / e Å^{-3}	0.16/-0.20
Flack parameter	0.068(6)

USF

Santana Thomas <santanat@mail.usf.edu>

Regarding Incident 2315049 Request of permission to use published paper in dissertation

1 message

support@services.acs.org <support@services.acs.org> Tue, Oct 23, 2018 at 3:27 PM
To: santanat@mail.usf.edu

ACS Chemistry for Life®

Dear Santana,

Your permission requested is granted and there is no fee for this reuse. In your planned reuse, you must cite the ACS article as the source, add this direct link <https://pubs.acs.org/doi/abs/%2010.1021%2Facs.jnatprod.7b00732>, and include a notice to readers that further permissions related to the material excerpted should be directed to the ACS.

Please do not hesitate to contact me if you need any further assistance.

Regards,
Jawwad Saeed
ACS Customer Services & Information
https://help.acs.org

Incident Information:

Incident #: 2315049

Date Created: 2018-10-23T14:17:20

Priority: 3

Customer: Santana Thomas

Title: Request of permission to use published paper in dissertation

Description: Dear editor,

I am writing as a request of permission to use the contents of the current paper as a part of my dissertation to complete my requirements for my graduate degree. The paper that is published is entitled "Keikipukalides, furanocembrane diterpenes from the Antarctic Deep Sea Octocoral Plumarella Delicatissima".

Below is also the DOI for the publication in the Journal of Natural Products.

DOI: 10.1021/acs.jnatprod.7b00732

Thank you for your time and consideration. I look forward to your response.

Best regards,

--

Santana Thomas

Graduate Assistant

University of South Florida

4202 E. Fowler Ave, BSF 360

Tampa, Fl 33620

{CMI: MCID356525}